

THESIS

***Large scale dynamic molecular modelling of metal oxide
nanoparticles in engineering and biological fluids***

Adil Loya

Ph.D

A thesis submitted in partial fulfilment of the requirements of the University of
Hertfordshire for the degree of Doctor of Philosophy

The programme of research was carried out in the School of Engineering &
Technology, University of Hertfordshire, Hatfield, UK.

January 2015

Declaration Statement

I certify that the work submitted is my own and that any material derived or quoted from the published or unpublished work of other persons has been duly acknowledged (ref. UPR AS/C/6.1, Appendix I, Section 2 – Section on cheating and plagiarism)

Student Full Name: Adil Loya

Signed:Adil Loya.....

Date: January 2015

Abstract

Nanoparticles (NP) offer great merits over controlling thermal, chemical and physical properties when compared to their micro-sized counterparts. The effectiveness of the dispersion of the NP is the key aspect of the applications in nanotechnology. The project studies the characterization and modification of functional NPs aided by the means of large scale molecular thermal dynamic computerized dispersing simulations, in the level of Nanoclusters (NC). Carrying out NP functionality characterisation in fluids can be enhanced, and analysed through computational simulation based on their interactions with fluidic media; in terms of thermo-mechanical, dynamic, physical, chemical and rheological properties.

From the engineering perspective, effective characterizations of the nanofluids have also been carried out based on the particles sizes and particle-fluids Brownian motion (BM) theory. The study covered firstly, investigation of the pure CuO NP diffusion in water and hydrocarbon fluids, secondly, examination of the modified CuO NP diffusion in water. In both cases the studies were put under experiments and simulations for data collection and comparison. For simulation the COMPASS forcefield, smoothed particle hydrodynamic potential (SPH) and discrete particle dynamics potential (DPD) were implemented through the system. Excellent prediction of BM, Van der Waals interaction, electrostatic interaction and a number of force-fields in the system were exploited.

The experimental results trend demonstrated high coherence with the simulation results. At first the diffusion coefficient was found to be $1.7e-8m^2/s$ in the study of CuO NC in water based fluidic system. Secondly highly concurrent simulation results (i.e. data for viscosity and thermal conductivity) have been computed to experimental coherence. The viscosity trend of MD simulation and experimental results show a high level of convergence for temperatures between 303-323K. The simulated thermal conductivity of the water-CuO nanofluid was between $0.6—0.75W \cdot m^{-1} \cdot K^{-1}$, showing a slight increase following a rise in temperature from 303 to 323 K. Moreover, the alkane-CuO nanofluid experimental and simulated work was

also carried out, for analysing the thermo-physical quantities. The alkane-CuO nanofluid viscosity was found 0.9—2.7mpas and thermal conductivity is between 0.1—0.4W•m⁻¹•K⁻¹. Finally, the successful modification of the NPs on experimental and simulation platform has been analysed using different characterization variables. Experimental modification data has been quantified by using Fourier Transformation Infrared (FTIR) peak response, from particular ranges of interest i.e. 1667-1609cm⁻¹ and 1668-1557cm⁻¹. These FTIR peaks deduced Carboxylate attachment on the surface of NPs. Later, MD simulation was approached to mimic experimental setup of modification chemistry and similar agglomerations were observed as during experimental conditions. However, this approach has not been presented before; therefore this study has a significant impact on describing the agglomeration of modified NPs on simulation and experimental basis. Henceforth, the methodology established for metal oxide nanoparticle dispersion simulation is a novelty of this work.

Acknowledgements

In the name of Allah, The most beneficent and The most merciful, I bear witness that there is no deity worthy of worship except Allah without any partners or peers, all praise to Allah whom without His guidance and bounties won't reached this far in my life.

First of all thanks to Allah (SWT), Who supported me till this level of knowledge without Allah`s (SWT) help it would have not been possible. All the knowledge is given to us by Him. Then I will thank my parents and family in supporting me and motivating me for carrying out the research with having too many financial burdens still they did not back out. I will give sincere thanks to my kind and benevolent supervisor Dr. Guogang Ren for his utmost support of providing me knowledge, build my interest and guiding me on the track that is the future in my area of specialization. Thanks to Dr. Jacqueline Stair for generously supporting me in knowledge and understanding of the chemistry in greater detail. Finally thanks to all my friends and colleagues for their supports in kind suggestions and building my courage.

- ❖ Dr. Guogang Ren
- ❖ Dr. Jacqueline L. Stair
- ❖ Dr. Diogo Montalvao
- ❖ Dr. Andreas Chrysanthou
- ❖ Dr. Yong K. Chen (For the suggestion in improvement of report).
- ❖ Dr. Calvin Zhao
- ❖ Mr. Pete Thomson (For material and equipment support).

Table of Contents

Declaration Statement	ii
Abstract	iii
Acknowledgements	v
Table of Contents	vi
List of figures	xi
List of tables	xvii
Nomenclature	xix
Chapter 1 Introduction	1-1
1.1 Background Knowledge	1-1
1.2 Functionality of Nanoparticles in Fluids	1-3
1.3 Background Knowledge on Nanoparticle Dispersion	1-3
1.4 Objectives of the Thesis	1-4
Chapter 2 Literature Review	2-8
2.1 Nanofluids	2-9
2.1.1 Single-Step Procedure	2-10
2.1.2 Two-Step Procedure	2-11
2.2 Theory behind Dispersion of Nanoparticle	2-12
2.3 Stability of Dispersion	2-13
2.3.1 Derjaguin Landau Verwey & Overbeerk Theory	2-15

2.4	Heat Flow through Nanofluids	2-17
2.5	Parameters Related to Brownian Motion and DLVO	2-17
2.6	Dispersion of Nanofluids	2-18
2.6.1	Characterization Tools	2-20
2.7	Characterisation of Nanofluids/Nanoparticles	2-21
2.7.1	Characterizing Size, Shape and Zeta Potential of Nanoparticles	2-22
2.7.2	Surface Analysis	2-23
2.7.3	Chemical Structure Analysis	2-24
2.7.4	Analysis of Ion Concentration after Dispersion of Nanoparticles	2-25
2.7.5	Viscosity	2-27
2.8	Modification of Nanoparticles for Stable Nanofluids	2-30
2.8.1	Modification of CuO Nanoparticles	2-30
2.9	Historical Background and Need of Simulating Nanofluidic Systems	2-31
2.10	Stages of Simulation	2-34
2.11	Simulation Methodologies	2-36
2.11.1	Force Field	2-37
2.11.2	Pair Potentials	2-39
2.11.3	Ensembles and Velocity Theorem	2-42
2.11.4	Simulation Data Acquisition	2-43
2.11.5	Visualization Tools	2-43

2.12	Cases Investigated in This Work using MDS	2-43
2.12.1	Dispersion of CuO Nanoparticles in Aqueous Fluids	2-44
2.12.2	Dispersion of CuO Nanoparticles in Hydrocarbon Based Nanofluids	2-47
2.12.3	Dispersion of Surface Treated Nanoparticles in Aqueous Fluid	2-49
2.13	Summary Outlined	2-51
Chapter 3 Materials and Methodology		3-54
3.1	Experimentation	3-55
3.1.1	Materials/Tools	3-55
3.1.2	CuO Dispersion in Water	3-57
3.1.3	Surface Functionality of CuO Nanoparticles	3-59
3.1.4	CuO Dispersion in Alkanes	3-60
3.2	Characterization of Modified CuO Nanoparticles	3-61
3.3	Model and simulation methodology	3-61
3.3.1	Simulation of CuO in Water	3-64
3.3.2	Simulation of Nanoparticles in Alkanes	3-65
3.3.3	Simulating thermo-physical quantities	3-68
3.4	Summary Outlined	3-72
Chapter 4 Results		4-74
4.1	Dispersion of CuO Nanoparticles	4-74
4.2	Modification of CuO Nanoparticles	4-77
4.3	Detection of Cu Ion Release in Deionized Water	4-78

4.4	Comparison of Thermo-Physical Calculation of Simulation and Experiment of CuO Dispersion	4-80
4.4.1	Viscosity of CuO Dispersion in Water	4-80
4.4.2	Thermal Conductivity of CuO Dispersion in Water	4-81
4.4.3	Diffusion Coefficient of CuO Dispersion in Water	4-83
4.4.4	Radial Distribution Function of CuO Dispersion in Water	4-85
4.5	Comparison of Thermo-physical and Rheological Properties from Simulation and Experiment of CuO Nanoparticle Dispersion in Alkanes	4-89
4.5.1	Experimental and MD Viscosity Analysis of CuO Nanoparticle Dispersion in Alkanes	4-89
4.5.2	Viscosity of Alkanes	4-90
4.5.3	Diffusion Coefficient of Alkane and CuO Nanoparticle Dispersion in Alkanes	4-91
4.5.4	Thermal Conductivity of CuO Nanoparticle Dispersion in Alkanes	4-93
4.5.5	RDF of CuO Nanoparticle Dispersion in Hydrocarbon	4-94
4.6	Modification of CuO Nanoclusters Using Short Chain Functional Group	4-95
4.7	Summary Outline	4-97
Chapter 5	Discussions	5-99
5.1	Basic Dispersion Study	5-102
5.2	Experimental Modification of CuO Nanoparticles	5-103
5.2.1	CuO Modification for 2Hours Butyric Acid pH 5.5	5-104
5.2.2	CuO Modification for 2Hours Using Butyric Acid at pH 7.0	5-106

5.2.3	CuO Modification for 24Hours Using Butyric Acid at pH 7.0 -----	5-107
5.3	Simulation of Nanofluids-----	5-109
5.3.1	Drawback of Estimating the Thermo-physical Quantities by Particle Size- -----	5-126
5.3.2	Precise Approach to Approximate the Thermo-physical Quantities -----	5-126
5.4	Simulative Modification of Nanofluid-----	5-127
5.5	Summary Outline-----	5-133
Chapter 6	Conclusion-----	6-136
6.1	Future Work-----	6-139
6.2	Recommendations -----	6-140
6.3	List of Publication -----	6-141
References	-----	142
Appendix A	– Dynamic and static model of nanoparticle dispersion -----	156
1)	Equation and formulation -----	156
	Static particle model -----	156
	Dynamic particle model -----	159
Appendix B	– ICP methodology -----	165
Appendix C	– LAMMPS input script -----	166
Appendix D	– Published Study 1 -----	173
Appendix E	– Published Study 2 -----	180

List of figures

Figure 1-1 Dimension and time scale used in various types of simulations; QM/MM is quantum mechanics and molecular mechanic simulation that runs at 10^{-15} - 10^{-12} time scale with dimensions of less than nanometre; MDS is molecular dynamic simulation that runs at 10^{-12} - 10^{-9} scale with dimensions of from angstrom to micrometre; MSS is mesoscale simulation that runs at 10^{-6} - 10^{-3} with dimensions of micro to millimetre and FEAS is finite element analysis simulation that runs at actual time i.e. seconds with dimensions in metres.1-2

Figure 1-2 Flowchart of thesis experimental and simulation work1-4

Figure 2-1 Colloidal stability mechanism of nanoparticles in fluids.....2-14

Figure 2-2 DLVO theory mechanism2-16

Figure 2-3 Mechanism of ultrasonic device2-19

Figure 2-4 Mechanical dispersing devices; a) mechanical mixer and b) shear mixer.....2-20

Figure 2-5 Dynamic light scattering mechanism for measuring the nanoparticles size and potential2-23

Figure 2-6 FTIR spectroscopy mechanism and results display2-24

Figure 2-7 ICP-OES mechanism2-26

Figure 2-8 TA1500Ex rheometer; flat plate mechanism for measuring fluid viscosity2-27

Figure 2-9 TA1500Ex rheometer; cone plate mechanism for measuring fluid viscosity.....2-29

Figure 2-10 Flow chart of molecular dynamics simulation.....2-35

- Figure 2-11** Schematic show representing research design and simulation mechanism of the CuO-water nanofluid MD research work2-46
- Figure 2-12** Schematic illustration of CuO nanoclusters in Paraffin.....2-48
- Figure 2-13** Schematic chart of surface treated CuO nanoclusters in water. Step by step visualization of the nanoclusters with functional group in water system; a) Green particles are the alkyl chain; b) Dark navy blue colour represents carboxylate group attachment to the surface of nanoclusters; c) Yellow-Red particles bonded together are CuO nanoclusters...2-50
- Figure 3-1** CuO NPs image observed by TEM. The average size of nanoparticle is approximately 50 nm. The CuO crystal structure is shown in the up-right corner (Ren et al., 2009).....3-56
- Figure 3-2** Dispersion tools used for the research work; a) Ultrasonic (Sonics VC 750), b) Disperlux Shear mixer, and c) Polytron Homogenizer.....3-58
- Figure 3-3** Step-by-step demonstration of visualising nanoparticle dispersion in water on OVITO; a) Initial step after opening OVITO, b) how to launch LAMMPS trajectories, c) opening the dump file and d) visualized screen dump of simulation.3-63
- Figure 3-4** Molecular system comparison of without and with CuO nanoparticles: a) simulation results (control) of pure water molecules in an orthogonal box of 40 Angstrom x 25 Angstrom x 40 Angstrom, the box contained 463 TIP3P water molecules, where white is oxygen and blue is hydrogen. b) The simulation box containing CuO nanoparticles and with the TIP3P water molecules in an orthogonal box sized by 40 Angstrom x 40 Angstrom x 25 Angstrom with 463 water molecules; where red is copper, yellow oxygen bonded in CuO nanoparticle. The blue is hydrogen and the white is oxygen.....3-65
- Figure 3-5** CuO nanoparticles in alkane fluid; the cyan blue balls are representing n-Eicosane ($C_{20}H_{42}$) and red is the Cu and yellow is the oxygen connected to Cu.....3-67

Figure 3-6 Radial distribution function peak connection with atomic movement3-71

Figure 4-1 The comparison of hydrodynamic particle sizes of varied concentrations in 500 ml beaker and 60 ml beaker for 15 minutes of dispersion at concentrations of 0.001%, 0.01% and 0.1%4-75

Figure 4-2 The variation of 0.1% CuO nanofluid hydrodynamic particle size due to the change in sonication time and sonication power4-76

Figure 4-3 Effect on hydrodynamic particle sizes of CuO nanoparticles by using different dispersion methods4-77

Figure 4-4 Modified CuO nanoparticles by using butyric acid as the reagent; a) CuO nanoparticle original particles; b) CuO nanoparticle modified using BA (Reaction time 2 hours and pH5.5); c) CuO nanoparticle modified using BA (Reaction time 2 hours and pH7); d) CuO nanoparticle modified using BA (Reaction time 24hours and pH7)4-78

Figure 4-5 ICP results of Cu ion release in deionized water4-79

Figure 4-6 Comparison of experimental and MD simulation viscosity results of CuO nanosuspension and water4-81

Figure 4-7 Thermal conductivity of water and CuO Nanosuspension, measured using MD simulations and experimental thermal conductivity was obtained by literature (Karthik et al., 2012).....4-82

Figure 4-8 Diffusion coefficient of the water at ---298K, ---308K and ---318K and CuO nanosuspension at ---298K, ---308K and ---318K.....4-83

Figure 4-9 Radial distribution function of the water system4-86

- Figure 4-10** The comparison of RDF of CuO nanoclusters in water under different temperatures.....4-87
- Figure 4-11** Experimental and simulation viscosity of pure alkanes (purple) and alkane with CuO nanoclusters (red) additives against temperature rise4-90
- Figure 4-12** Diffusion coefficients; a) diffusion of alkanes at different temperatures. b) diffusion of alkanes with CuO nanoclusters. Values are mostly in the region of $1\text{E}-8$ to $1\text{E}-14$ m^2/s4-92
- Figure 4-13** Thermal conductivity of alkane with CuO nanoclusters; red line with diamond button is thermal conductivity for CuO with alkane and purple line with square button is for thermal conductivity for pure alkanes4-93
- Figure 4-14** RDF figure of alkane CuO nanosuspension and alkane4-94
- Figure 4-15** Diffusion coefficients; a) diffusion coefficients of CuO nanoclusters in water with butyric acid ($1.517\text{e}-09\text{m}^2/\text{s}$); b) diffusion coefficients of CuO nanoclusters in water ($2.73\text{e}-08\text{m}^2/\text{s}$)4-96
- Figure 5-1** Hydrodynamic nanoparticle size.....5-100
- Figure 5-2** Schematic illustration of equilibration convergence of heat autocorrelation ...5-101
- Figure 5-3** Butyric acid surface modified CuO nanoparticles using reagent at pH5.5 and reaction time of 2 hours5-105
- Figure 5-4** Butyric acid surface modified CuO nanoparticles prediction of chemical composition; a) bi-dentate attachment structure; b) uni-dentate attachment structure.....5-105
- Figure 5-5** Butyric acid Surface modified CuO nanoparticles using reagent at pH7 and reaction time of 2 hours5-106

- Figure 5-6** Butyric acid surface modified CuO nanoparticles predicted chemical composition; a) bi-dentate attachment structure; b) uni-dentate attachment structure.....5-107
- Figure 5-7** Butyric acid surface modified CuO nanoparticles using reagent at pH7 and reaction time of 24 hours5-108
- Figure 5-8** Butyric acid surface modified CuO nanoparticles predicted chemical composition; a) bi-dentate attachment structure; b) bridging attachment structure.5-108
- Figure 5-9** Comparison between experimental and MD achieved viscosities for water (blue coloured bars); comparison between experimental and MD achieved viscosities for CuO-water nanofluid (red coloured bars)5-110
- Figure 5-10** A Log diffusion coefficient of simulation and the log diffusion coefficient of calculated by using Stoke-Einstein method.....5-111
- Figure 5-11** The Radial distribution function (RDF) of CuO nanoclusters in water in this work: a1) RDF for 298K; b1) RDF for 308k; c1) RDF for 318k; a2) RDF simulated representation at 298k; b2) RDF simulated representation at 308k; and c2) RDF simulated representation at 318K; a3) RDF simulated representation at 298k; b3) RDF simulated representation at 308k; and c3) RDF simulated representation at 318K; a4) RDF simulated representation at 298k; b4) RDF simulated representation at 308k; and c4) RDF simulated representation at 318K.....5-115
- Figure 5-12** HACF for pure alkanes; a) 303K alkane with CuO nanofluid heat autocorrelation convergence result. b) 313K alkane with CuO nanofluid heat autocorrelation convergence result. c) 323K alkane with CuO nanoparticle nanofluid heat autocorrelation convergence result5-119
- Figure 5-13** Stress autocorrelation function of molecular dynamic simulations of alkanes with CuO nanoclusters (Loya et al., 2015)5-120

Figure 5-14 Stress autocorrelation function of alkanes at different temperatures; (a) 303K SACF of alkanes; (b) 313K SACF of alkanes; (c) 323K SACF of alkanes (Loya et al., 2015)5-122

Figure 5-15 % increment of viscosity of nanofluid from original alkane.5-124

Figure 5-16 Discrepancies between alkane and CuO-alkane nanofluid.....5-125

Figure 5-17 Simulated visualization of the surface modification of CuO nanoclusters using butyric acid functional group in water system; a) Green particles are the alkyl chain; b) Dark navy blue colour represents Hydrogen group and white ones represent oxygen particles; c) Yellow and red particles bonded together are CuO nanoclusters.....5-129

Figure 5-18 Radial distribution function of CuO nanoclusters with butyric acid in water system.....5-131

Figure 5-19 Radial distribution function of butyric acid functional group moieties attachment to CuO nanoclusters in a water system.....5-132

List of tables

Table 2-1 Nanoparticle dispersing devices	2-18
Table 2-2 Dispersion devices for different characterizing parameters	2-20
Table 2-3 Nanoparticle dispersion simulation's historical background (Loya et al., 2014b)...	2-33
Table 2-4 Topics covered throughout this research	2-44
Table 4-1 Highest RDF of CuO nanoclusters in water under simulated temperatures.....	4-87
Table 4-2 Viscosity of alkanes from our work and comparison with the work of others.....	4-91
Table 5-1 Water diffusion blocks	5-112
Table 5-2 Water + CuO diffusion blocks.....	5-113
Table 5-3 Alkane diffusion blocks.....	5-116
Table 5-4 CuO-Alkane diffusion blocks.....	5-117
Table 5-5 Time taken by each simulation to evaluate viscosity of alkanes.....	5-123
Table 5-6 BA-CuO-water diffusion blocks	5-128
Table A-0-1 Variables of equation (A-2)	157
Table A-0-2 Variables of equation (A-15)	161
Table A-0-3 Variables of equation (A-16)	161

Table A-0-4 Description of variables on total potential energy for equation (A-19) 162

Table A-0-5 Dimension and their state space values 164

Nomenclature

Symbols	Meanings
OVITO	Open visualisation tool
σ	$\sqrt{2K_b T \omega}$
E_{UB}	$E_{\text{crossterms}} + E_{\text{Nonbond}} + E_{\text{H-Bond}}$
AD	Anno domini
q	Atomic charges
Kb	Boltzmann constant
BD	Brownian dynamics
BM	Brownian motion
BET	Brunauer–Emmett–Teller
BA	Butyric acid
COO^-	Carboxylate
$(\text{COOH})\text{-CuO-H}_2\text{O}$	Carboxylate-Copper oxide-water (Butyric acid modified copper oxide in water sysetm)
CNS	Central nervous system
CeO_2	Cerium oxide
CVD	Chemical vapour deposition
CHARMM	Chemistry at HARvard Macromolecular Mechanics
COMPASS	Condensed-phase Optimized Molecular

	Potential for Atomistic Simulation studies
F^c	Conservative force linked to momentum
Cu	Copper
$\text{Cu}(\text{OH})_2$	Copper hydroxide
Cu^{++}	Copper ion
CuO	Copper oxide
CuO	Copper Oxide
CuO-O-M	Copper oxide – Oxygen – metal group
CuO NPs	Copper Oxide Nanoparticles
$\text{CuO-C}_n\text{H}_{2n+2}$	Copper oxide with alkane system
CuO-NC	Copper oxide-Nanocluster
CuO-H ₂ O	Copper oxide-water system
Cu-AR	Copper-Argon
$[\text{Cu}(\text{C}_2\text{O}_2)_2(\text{H}_2\text{O})_2]^{-2}$	Copper-carboxylate-water interconnection
CuO-H ₂ O	Copperoxide-Water
$E_{\text{Crossterms}}$	Cross interacting terms include the dynamic variation among the bond stretching, bending, and torsion angle rotation
E_{Nonbond}	Deals with Vander Waals forces and Columbic electrostatic force
K	Degree Kelvin
P	Density

DLVO	Derjaguin and Landau, Verwey and Overbeek
\bar{D}	Diameter of the crystallites
ε	Dielectric constant
φ	Dihedral torsion angle
DECM	Direct electric chemical method
DPD	Discrete particle dynamics
F^D	Dissipative force
DLS	Dynamic light scattering
$C_{20}H_{42}$	Eicosane
EAM	Embedded atom method
EDX	Energy-dispersive X-ray spectroscopy
EMD	Equilibrium molecular dynamics
EtOH/water	Ethanol/Water
FEAS	Finite element analysis simulation
FENE	Finitely extensible nonlinear elastic
\hat{r}_j	Force in particular directions
FTIR	Fourier transmission Infrared
α	Gaussian number
GANN	Genetic algorithm neural networks
μ PT	Grandcanonical ensemble
HACF	Heat Autocorrelation Function

HACF	Heat autocorrelation function
C_v	Heat capacity at constant volume
$D = \frac{K_m}{C_v \rho}$	Heat diffusion coefficient
$\text{Cu}_2\text{SO}_4 \cdot 5\text{H}_2\text{O}$	Hydrated Copper sulphate
$\text{Zn}_2\text{B}_6\text{O}_{11} \cdot \text{H}_2\text{O}$	Hydrated Zinc Borate
$E_{\text{H-Bond}}$	Hydrogen bonding term
r_{ij}	i-j atomic separation distance
ICP-OES	Inductive couple plasma-Optical emission spectroscopy
ICP	Inductive coupled plasma
LAMMPS	Large-scale Atomic/Molecular Massively Parallel Simulator
L-J	Leonard-Jones
Ltd	Limited
MSS	Mesoscale simulation
mPas	Milli Pascal second
ml	Millilitre
MD	Molecular dynamics
MDS	Molecular dynamics simulation
NC	Nanocluster
nm	Nanometer

NP	Nanoparticle
NEMD	Non-Equilibrium molecular dynamics
NPT	Number of atoms, pressure and temperature (Isotherm-Isobaric ensemble)
NVE	Number of atoms, volume and energy (Microcanonical ensemble)
NVT	Number of atoms, volume and temperature (Canonical ensemble)
OPLS-FF	Optimized Potentials for Liquid Simulations- Force field
x	Out of plane angle
PCM	Phase change materials
PEO	Polyethyleneoxide
QM/MM	Quantum mechanics/Molecular mechanics
RDF	Radial distribution Function
F^R	Random force
h	Range of Lucy kernel function
RPM	Revolutions per minute
RK	Runge-Kutta
SEM	Scanning electron microscopy
SCI	Science citation index
SPC-E	Simple point charge-extended
SPH	Smoothed particle dynamics

NaOH	Sodium hydroxide
NaH ₂ PO ₂ H ₂₀	Sodium hypophosphite
STP	Standard temperature and pressure
SACF	Stress autocorrelation function
$\sum \theta$	Summation of all angles (The bond angle bending energy terms)
Σ bond	Summation of All bonds (The covalent bond stretching energy terms)
\sum_x	Summation of all out of plane angles (This is a harmonic function)
$\sum \varphi$	Summation of all torsions (The torsion angle rotation energy terms)
T	Temperature
R _c	The cut-off
TA	Thermal analysis
TC	Thermal conductivity
K _m	Thermal conductivity of medium
d _t	Time step size
$E_{total} = \sum bond + \sum \theta + \sum \varphi + \sum x + E_{UB}$	Total energy
\vec{f}	Total force

$E_{Non\ bond} = \sum_{i>j} \left[\frac{A_{ij}}{r_{ij}^9} - \frac{B_{ij}}{r_{ij}^6} \right] + \sum_{i>j} \left[\frac{q_i q_j}{\epsilon r_{ij}} \right] + E_{H-Bond}$	Total non-bonded energy
TIP3P	Transferable intermolecular potential 3P
TEM	Transmission electron microscopy
θ	Two bond angle
UV	Ultraviolet
R_{ij}	Unit vector in direction of $R_i - R_j$
UFF	Universal Force field
V_{ij}	Vector difference of velocities
V	Volumetric concentration
$Wm^{-1}K^{-1}$	Watt per meter per Kelvin
\hat{w}	Wavelength of the incident beam
WCA	Weeks-Chandler-Andersen
$\omega(r)$	Weighting factor
XRD	X-ray diffraction
XPS	X-ray photoelectron spectroscopy
$Zn(OH)_2$	Zinc hydroxide
ZnO	Zinc Oxide

Equation Symbols	Meanings
\cap	The distance between the particle
dp	The diameter of particle
V	V is the volume fraction.
π	Pie
τ	Torque
η	Viscosity
$\dot{\gamma}$	Shear rate
v	velocity
$F_{\dot{\gamma}}$	Force due to shear rate
ω	Angular velocity
F_{σ}	Force due to shear stress
M	Moment
α	Gap angle
R	Radius of rotational disc.
\vec{f}	Chemical vapour deposition
F^C	Conservative force linked to momentum
F^D	Dissipative force
F^R	Random forces
r_{ij}	The influence of the forces in particular directions
λ	Thermal conductivity

C_v	Heat capacity at constant volume
ρ	Density
K_B	Boltzmann Constant
J	Heat autocorrelation function
$J(0)$	Heat flux at start of simulation
$J(t)$	Heat flux at time period t simulation
e_i	Site energy
v_i	Velocity of particle i
f_{ij}	The force on atom i due to its neighbor j
$P_{xy}(0)$	P_{xy} refers to an independent component of the stress in the x - y direction (at initial position)
$P_{xy}(t)$	P_{xy} refers to an independent component of the stress in the x - y direction (at initial position t)
x_{ij}	The distance between particle i and j .
N	Number of particles
$r_i(t)$	The position of the particle at time t
$r_i(0)$	The distance from initial position of the particle
D_{S-E}	Stoke and Einstein Diffusion Coefficient
D_{Sim}	Simulation of Diffusion Coefficient
δ	Gap between two plates

i	The relative percentage increment of viscosities
ν_0	The viscosity of basefluid.
ν_i	The viscosity of nanofluid.
Q	Total heat flow
qm	Heat flow of medium
qp	Heat flow of particle
λ_m	Thermal conductivity of medium
λ_p	Thermal conductivity of particle
A_m	Area of medium
A_p	Area of particles
$\left(\frac{dT}{dx}\right)_m$	Temperature gradient of medium
$\left(\frac{dT}{dx}\right)_p$	Temperature gradient of particle
S_p	Surface area of particle
S_m	Surface area of medium
n_m	Number of atoms of medium
n_p	Number of atoms of particle
r_m	Radius of medium particle
r_p	Radius of nanoparticle
λ_{eff}	Effective thermal conductivity

q^*	Rate of heat transfer in dimensionless form
$K.E_p$	Kinetic energy of particles
m_p	Mass of the particle
v_p	Velocity of the particle
\bar{V}_p	Average particle velocity
c	Constant of thermal conductiveness
\bar{c}_v	Specific heat per particle
l	Mean free path
E_{Total}	Total energy
$\sum bond$	Summation of All bonds The covalent bond stretching energy terms
$\sum \theta$	Summation of all angles The bond angle bending energy terms,
$\sum \phi$	Summation of all torsions The torsion angle rotation energy terms
$\sum x$	Summation of all out of plane angles This is a harmonic function.
E_{UB}	$E_{crossterms} + E_{Nonbond} + E_{H-Bond}$
$E_{crossterms}$	Cross interacting terms include the dynamic variation among the bond stretching, bending, and torsion angle rotation.
$E_{Nonbond}$	Deals with Vander Waals forces and Columbic electrostatic force.
E_{H-Bond}	Hydrogen bonding term.
A_{ij}, B_{ij}	All are from quantum mechanics
$\sum \theta$	Summation of all angles (The bond angle bending energy terms)

Σ bond	Summation of All bonds (The covalent bond stretching energy terms)
$\sum x$	Summation of all out of plane angles (This is a harmonic function)
$\sum \varphi$	Summation of all torsions (The torsion angle rotation energy terms)
T	Temperature
R_c	The cut-off
K_m	Thermal conductivity of medium
d_t	Time step size
$E_{total} = \sum_{bond} + \sum \theta + \sum \varphi + \sum x + E_{UB}$	Total energy
\vec{f}	Total force
$E_{Non\ bond} = \sum_{i>j} \left[\frac{A_{ij}}{r_{ij}^9} - \frac{B_{ij}}{r_{ij}^6} \right] + \sum_{i>j} \left[\frac{q_i q_j}{\epsilon r_{ij}} \right] + E_{H-Bond}$	Total non-bonded energy
θ	Two bond angle
R_{ij}	Unit vector in direction of $R_i - R_j$
V_{ij}	Vector difference of velocities
V	Volumetric concentration
$Wm^{-1}K^{-1}$	Watt per meter per Kelvin
$\omega(r)$	Weighting factor

Chapter 1

Introduction

Chapter 1 Introduction

1.1 Background Knowledge

The journey of nanotechnology started from 1959, the time when Nobel Laureate Richard Feynman stated that “*There’s Plenty of Room at the bottom.*”(Feynman, 1959). Nanotechnology, a phrase that describes itself; nano meaning “*small particles with dimensions of nearly 1×10^{-9}* ” as shown in **Figure 1-1**, and technology stands for “*use of tools or devices*”, thereby nanotechnology stands for “*making use of small particles*”(Eyett, 1990, Flanagan, 1990, Kennell and Robinson, 1990). The most common method being used to implant nanoparticle (NP) in any system with effectiveness is to firstly disperse the nano sized particles in the fluids of choice; and then applying it for application. The nanosized particles dispersion can be carried out in many different ways. However, to achieve a long lasting effect or a stable dispersion of the NP, it can be achieved using surface modification of those particles, or by attaching some functional group to the surface of the NP. This attachment is mostly achieved using an organic solvent or surfactant i.e. surface active agents.

The real use of the nanotechnology goes back to many years in history. It can be traced back to the gold NPs that were used in medieval times. During the era of the Roman civilisation it was used to decorate glass objects (Giljohann et al., 2010). Colloidal suspensions were created by melting gold and silver NPs for medicinal purposes. Lead sulphide nanocrystals were used as a hair dying formula developed during times of the Greek and Romans (Giljohann et al., 2010). During the 4th century AD; Romans used gold and silver as colloidal NPs to develop a colour-shifting effect, this was used to decorate the cups known as Lycurgus Cup.

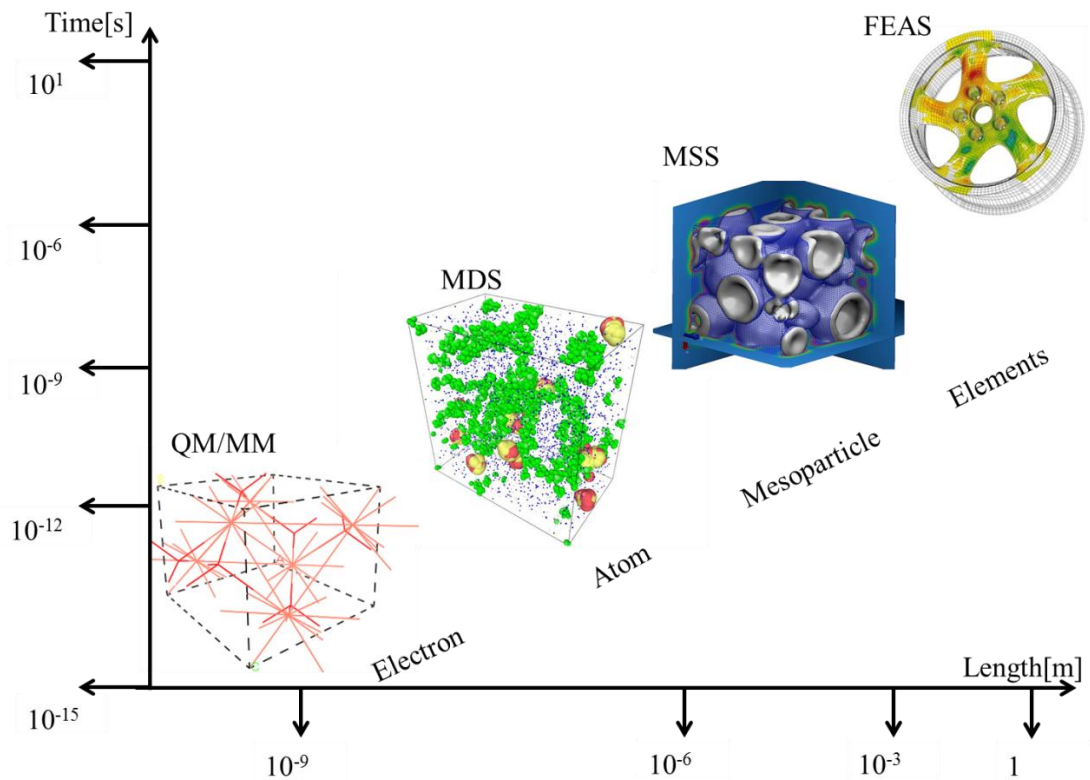


Figure 1-1 Dimension and time scale used in various types of simulations; QM/MM is quantum mechanics and molecular mechanic simulation that runs at 10^{-15} - 10^{-12} time scale with dimensions of less than nanometre; MDS is molecular dynamic simulation that runs at 10^{-12} - 10^{-9} scale with dimensions of from angstrom to micrometre; MSS is mesoscale simulation that runs at 10^{-6} - 10^{-3} with dimensions of micro to millimetre and FEAS is finite element analysis simulation that runs at actual time i.e. seconds with dimensions in metres

For the last 2 decades i.e. from 1995 onwards there has been an extensive number of research articles on nanotechnology. Science Citation Index (SCI) journals during 2009, recorded around 300-320 research publications. Today the topmost goal is to achieve the functionalized nanofluids for various applications (Leuba et al., 2013, Iijima and Kamiya, 2009, Murthy et al., 2011).

1.2 Functionality of Nanoparticles in Fluids

NPs are the core element of this research, which play a great role due to their capabilities of enhancing and changing the properties of the different substances when mixed together, such as in our case dispersion in fluid, aqueous solution, hydrocarbon fluids and biological liquids (Leuba et al., 2013, Giljohann et al., 2010, Murthy et al., 2011).

This thesis elucidated the dispersion processes of NCs and NPs in different fluids, which is the first step of using NPs for many engineering applications (Reia da Costa and Skordos, 2012), such as drug delivery (Giljohann et al., 2010), tribology (Wu et al., 2007), lubrication (Hernández Battez et al., 2008), the heat transfer application (Shin and Banerjee, 2011), chemical industry, oil lubrication applications (Wu et al., 2007, Hernández Battez et al., 2008), and polymer industry.

1.3 Background Knowledge on Nanoparticle Dispersion

The NPs dispersion deals with various phenomena and applications of this system are vast. Various parameters that control the dispersion technique are related to the fields of chemistry, physiochemical and physical sciences. These fields of science are used for interpreting interactions due to the physical nature of liquids and the chemical interactions between NP and fluid particles (Aqil et al., 2008, Mudunkotuwa and Grassian, 2011). Parameters such as particle size, zeta potential, viscosity and thermal conductivity inform us about the dispersion of NPs and its stability properties in base fluids.

1.4 Objectives of the Thesis

This thesis entails a systematic investigation on the preparation, characterization and modification of nanofluids. Their physiochemical, thermal, and rheological properties are investigated by experimental and simulation approaches. Flowchart in **Figure 1-2** informs briefly about the three major studies carried out through this thesis. However, where the research with CeO₂ NPs in aqueous solution is a case study, which results are presented in Appendix D.

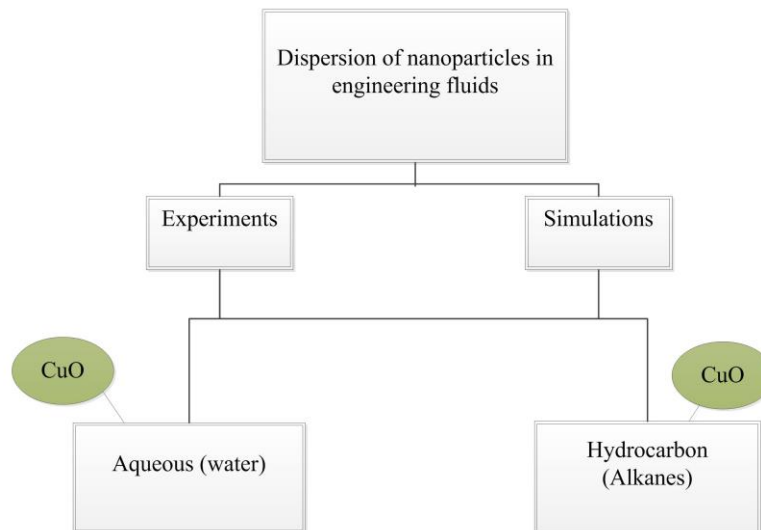


Figure 1-2 Flowchart of thesis experimental and simulation work

There are 6 chapters in this thesis. Below is the summary of each chapter:

Chapter 1: This chapter gives an introduction to nanotechnology, nanomaterials, nanofluids and their characterization techniques, applications and simulative approach of the dispersed nanofluids. The objectives and the motivation for the present work are also mentioned in this chapter.

Chapter 2: Detailed discussion on CuO NPs dispersion in different fluids is presented. A literature survey on characterization, modification, and application of nanofluids has been accomplished in this section of the thesis. Further physiochemical, thermal and rheological properties of nanofluids have been considered for the literature review, providing a more detailed understanding of the nanofluidic systems.

Later, the literature on the use and application of MD for nanofluid simulation has also been presented in this particular chapter. Finally, different studies carried out in this thesis have also been elaborated before establishing the methodology and procedure.

Chapter 3: Materials, methodology and experimental work performed during the research period have been described in this chapter. CuO NPs and water are the main “ingredients” used in this study. In further experiments, Hydrocarbon fluids have also been considered. Experimental work and simulative set up on MD have been conveyed. Software and source codes used for simulations are also discussed.

Chapter 4: The results of simulations and experiments have been conveyed in this chapter. Results are of a) initial dispersion study, b) characterization analysis achieved from experimental instruments, c) surface modification of NPs and d) simulation data analysis.

Chapter 5: Discussion of the results and experiments are presented in this chapter. This chapter contains the contrasts on two different studies a) simulation of NPs in fluids and b) the experimentation of NP dispersion. Furthermore, this chapter discusses the dispersion of CuO NP in water and hydrocarbon fluids. More emphasis has been spared on the Brownian motion (BM) that is entangled with dissipative particle dynamics potential (DPD). A comparative study has been conducted among diffusion constant, thermal conductivity, and viscosity. Later, radial distribution function (RDF) has been discussed in detail to understand the agglomeration of the nanofluid system.

Chapter 6: Conclusion of the whole thesis is compiled in this chapter. Chapter 6 states the outcomes and benefits that this research has brought about. Summary of the overall outcomes have been compared based on simulations, experimental and reference studies. Future works and the further applications have also been discussed. Recommendations have been suggested by the final outcomes and their analyses.

Chapter 2

Literature Review

Chapter 2 Literature Review

Dispersing NPs in fluids provides enhancement to the fluidic properties. These enhancements are related to the physiochemical and thermo-physical properties. The application of these modified fluids can alter performance of the system. Such systems are heat transfer, drug delivery, heat plate exchanger, lubrication and tribology. Nanofluids enhance properties such as viscosity, diffusion coefficient and thermal conductivity of fluids.

The viscosity improvement is mostly achieved by the additional concentration of NPs. Nevertheless for thermal conductivity improvement; volume fraction is also responsible, but at the same time, factors like NP shape and crystallographic properties are also accountable. Throughout this research, most of the criteria of the literature survey are carried out over the use of nanofluids as thermal conductivity and viscosity enhancer. The nanofluids of metal oxide NPs (i.e. CuO, CeO₂, TiO₂, and ZnO), other metals and ceramic NPs considerably enhance the fluid properties.

Alkane as water immiscible organic solvent has shown rapid cultivation of *M.trichosporium* OB3b biological system. Furthermore, 4-days after cell growth, improvement was noticed by Han et al., (2009). This effect was due to the change in system viscosity. For dielectric property improvement, metal oxide NPs in paraffin oil can improve rheological and thermal properties that play role in enhancing the dielectric properties of the nanofluid. Further, the use of CuO NPs in paraffin/alkanes demonstrated, high dielectric losses around 1 MHz, has been concluded by Mergos et al. (2012). This could be of the importance to control at the time of overvoltage spikes (Mergos et al., 2012).

Additionally this could further be correlated with the study of the TiO₂ NPs and the gold NPs capped by n-dodecane-1-thiol dispersed in hexane water interface that showed high dielectric losses as investigated by Ferdous et al. (2012).

2.1 Nanofluids

Preparation of nanofluids is the foremost important step in the applications of nanofluids for example; antiviral, antifungal, lubrication, thermal energy storage and heat transfer. The success of all the applications related to nanofluids depends on the consistent techniques for creating homogeneously dispersed and stable nanofluids. However, to investigate the thermal properties, heat transfer characteristics of nanofluids, and physiochemical properties it is necessary to take robust planning steps. The way of combining NPs and base liquids is immense. Diverse NPs of oxides, nitrides, metals, metal carbides, non-metals and nanotubes could be dispersed into distinctive base liquids. Examples of these is water (Fedele et al., 2011), ethylene glycol (Kanaras et al., 2002) and lubricating oils (Li et al., 2011) to produce useful nanofluids. Different applications may have its most suitable NP-liquid mixture.

Analysts have advanced diverse synthesis procedures for NP generation and scattering, which can be ordinarily partitioned into two classes, to be specific “single-step” strategy and “two-step” technique by Eastman and U.S Choi et al. (L. Xue, 2004). Different nanofluid arrangements or combination have its own particular application zone. The technique of synthesizing nanofluids may also guarantee fitting NP size, scattering uniformity, physical and synthetic security and low agglomeration. To make a nanofluid, the particles ought to be made modest enough to be suspended by Brownian movement and be ensured in opposition to accumulation. BM is naturally dispersive and without aggregative forces, shows diffusion of NPs in miscible fluids. Still, the need of subduing aggregation methods for NP agglomeration in base fluid is highly required.

Luckily many of the operative secondary techniques such as controlling pH values, zeta potential charges, surface modification, use of surfactant and ultrasonic vibrations are capable to achieve and maintain the stability of nanofluids in contradiction of sedimentation. All these techniques tend to change the formation of particle clusters to acquire stable suspensions. However, the utilization of these techniques depends on the particular application. The most

common approach is to add surfactant, which are normally oleic acid, thiols, silanes and laurate salts. Xuan (Xuan, 2000) also investigated four possible means of enhancing the thermal properties of nanofluids a) increase of surface area due to the suspension of NPs, b) the thermal conductivity increment, c) increase in colloidal system of suspension, and d) dispersion capability is enhanced. Choosing the appropriate dispersants depends on the properties of the specific particle-liquid fluid.

2.1.1 Single-Step Procedure

Single-step system has been utilized successfully to prepare nanofluids holding dispersed high thermal conductive metal NPs (Eastman et al., 1997). Yatsuya et al. (1978) suggested one of the first successful method; called the direct evaporation, and later improved by Wagener and Gunther (1999). As with the latent gas–condensation method, the system includes vaporization of an origin material under vacuum conditions. However, the build-up of the vapour to form NPs happens through contact between the vapour and a fluid. NP agglomeration is avoided by flowing the fluid constantly. The requisition of this system needs critical confinement. The fluid must have a low vapour pressure, normally less than 135 Pa. The mixture vapour build-up system is a different method, in which NPs are framed by the thermal disintegration of a bulk material, entrained in a bearer gas passing through a heater.

In the immediate-dissipation procedure, synthetic vapour build-up seems to accord favourable circumstances as far as control of molecule size, simplicity of adaptability, and the plausibility of transforming novel core-shell nanostructures are concerned. Zhu et al. (2004) generated copper-ethylene glycol nanofluids by altering the polyol process for copper NPs by decreasing copper sulphate penta-hydrate ($\text{CuSO}_4 \cdot 5\text{H}_2\text{O}$) with sodium hypophosphite ($\text{NaH}_2\text{PO}_2 \cdot \text{H}_2\text{O}$) in ethylene glycol under the microwave irradiation. Decent sizes of 20nm Cu NPs were formed. It was discovered to be a speedy and proficient single-step system for arranging stable and non-agglomerated copper nanofluids. Moreover, it was needed that this strategy might be augmented to different metallic nanofluids. The single-step method can help in diminishing the agglomeration and enhancing the stability of nanofluid. In contrast to the

two-step method, at present, the amounts of nanofluids that could be prepared by using this technique are relatively lower, even though, it is probable that single-step methods might be scaled to a cost effective run for the extensive preparation of nanofluids.

The chemical vapour condensation (CVD) technique is another efficient choice, in which NPs are formed by thermal decomposition of a metal-organic precursor entrained in a carrier gas passing through a furnace. It has recently been modified to synthesize and disperse non-agglomerated NPs into fluids in a single step (L. Xue, 2004). Comparing with the direct-evaporation method, chemical vapour condensation appears to offer advantages in terms of control of particle size, ease of scalability, and the possibility of producing novel core-shell nanostructures.

The NPs dispersion methods currently being used are a) single-step method, i.e. direct evaporation condensation method (DECM), b) submerged-arc NPs synthesis system (SANSS), c) laser ablation method and d) wet chemical method (Namburu et al., 2007, Zhu et al., 2007, Wu et al., 2009, Choi, 2009, Li et al., 2009).

2.1.2 Two-Step Procedure

In a two-step procedure, firstly dry powder is produced then the NP powder is dispersed in a base liquid. The liquid that is formed is known as nanofluids. NPs are formed by different techniques. Bulk material is transformed to particles consisting of 1-100nm. The gas condensation system is a typical method of synthesizing NPs (Granqvist and Buhrman, 1976), the process consist of initial vaporization of the original bulk material in a vacuum chamber and formation of vapours into NPs by collision with a regulated force of an inert gas.

Ashly in 1994 carried out a study of spray transformation process. This process begins with water soluble salts of bulk material. Then this solution is vaporised and then later dried by a spray drying method. Further this vaporised solute is subjected to fast precipitation method in fluidized mattress reactor to disperse equitably the mixture; this causes the major volatile

constitutes to be removed from the mixture and at last it yields permeable NP with a uniform structure. Moreover, Chen et al. (1995) suggested an electro hydrodynamic cone-fly method to prepare NPs from monodispersed colloidal solution.

More developments have helped to produce high number of NPs possibly between 2-100nm. This was possible by subjecting condensed metal vapours in a supersonic spout. Hill et al. (1963) suggested this system and later advanced by Bowles et al. (1981) and Brown et al. (1992). One small drawback of this method was that after the vaporization period, the NPs might agglomerate but by low cost dispersion method it was possible to break that agglomeration during dispersion. The best part of using these NPs was that these agglomerated particles showed enhancement in different properties of fluids. Two-step procedure works in an excellent manner for non-metallic and metal-oxide NPs to disperse them in water or ethylene glycol. Metallic NP gives high thermal properties in fluids as investigated by Eastman et al. (1996). Additional use of modifying agent may be required for nanofluid stability (Xuan and Li, 2000).

2.2 Theory behind Dispersion of Nanoparticle

Dispersion of NPs is a process in which the NPs are diffused in a dispersing medium like fluids. These fluids can be of any different grade such as biological grade, aerospace fuel grade, automotive fuel grade, aqueous solutions and buffering solutions. According to kinetic theory of molecules, as the molecule interacts with other molecules heat is generated due to kinetic molecular movement of the particle. This concept approaches the dispersion of NPs in different solvents; thereby this model causes anomalous increase in the heat transfer of the nanofluids. Furthermore, this model depends on four major effects produced by nanofluids i.e. a) BM of NP b) liquid layering at liquid particle interface c) Nature of heat transport between NPs and d) the clustering effect of NPs in fluid. These factors cause the particles to undergo a random motion. This is due to BM as this motion effects the NP and liquid interaction. From this interaction heat is evolved and the NP starts to cluster and agglomeration takes place as

the particle are left to settle in the solvent. To overcome this, modification of the particles is necessary, this will help in seizing agglomeration behaviour and the stable suspension can be maintained.

2.3 Stability of Dispersion

There are many different factors that affect the stable dispersion of NPs in fluids such as chemical composition, physical conditions and the use of a surfactant (surface active agents). For example, to homogeneously disperse $Zn_2B_6O_{11} \cdot 3H_2O$ NPs the oleic acid modification technique can be used (Tian et al., 2008). Modification can be carried out in many ways with different NPs, since chemical composition and their reaction circumstances vary due to the molecular attachment, functional group, charge condition and physical conditions. Therefore, to improve the particle dispersion, a functional group attachment is necessary. The BM and colloidal mechanism stability is related to each other, this is shown in **Figure 2-1**. The colloidal suspension that exhibit's the BM, is controlled using two major forces; attractive and repulsive forces. These forces later cause the chemical and physical interaction. During the domination of attractive forces the NPs try to agglomerate with one another, however when the repulsive forces dominate the NPs exhibits stability.

The attractive forces cause coalesces between particles due to Van der Waal forces of attraction, which in turn cause instability in the suspension. This is composed of three sub-forces of attraction i.e. a) London dispersion forces, b) Keesome forces and c) Debije permanent dipole induced forces. The London dispersion forces are long range forces of attraction whereas Keesome and Debije are short range interaction forces.

The repulsive forces drive the system to stability by counteracting the Van der Waal forces of attraction and removing coalesces between the particles. This repulsive force that helps in stabilization are further subdivided into 3 major forces; a) Electrostatic stabilization b) Steric stabilization and c) Depletion stabilization. The combination of electrostatic stabilization and steric stabilization together causes electrosteric stabilization, whereas, when steric and

depletion stabilization are connected together they cause the system to move towards polymeric stabilization.

Colloidal stability of nanoparticles divided into two categories:

1. Attractive forces
2. Repulsive forces

Due to “Attractive forces” the NPs start to agglomerate in the colloidal system. A coalesce forms and different forces that exhibit this nature of attraction in colloidal system are Van der Waal forces. The repulsive forces are the part of the colloidal stability mechanism. Repulsive forces are responsible for making NPs stable inside the fluid and to overcome agglomeration of NP as shown in **Figure 2-1**.

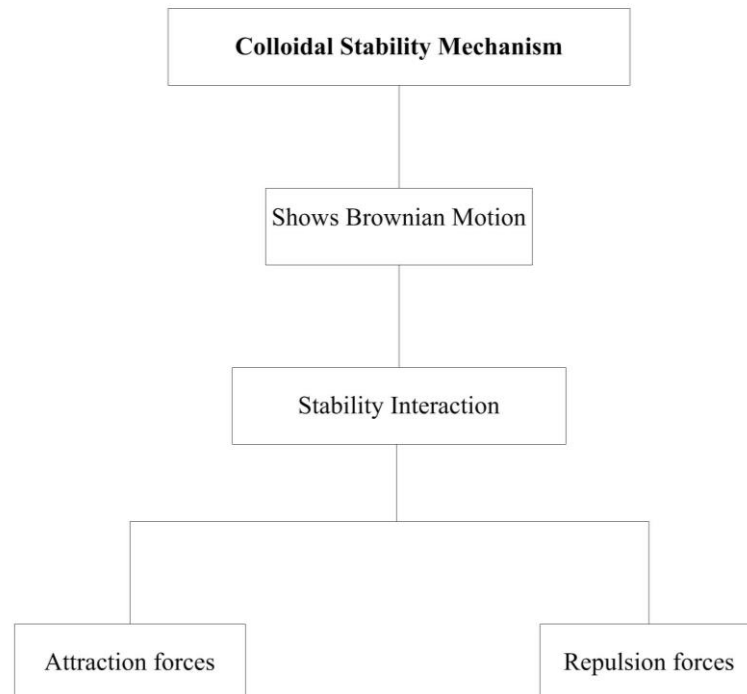


Figure 2-1 Colloidal stability mechanism of nanoparticles in fluids

2.3.1 Derjaguin Landau Verwey & Overbeerk Theory

The phenomena of stable dispersion can be understood by establishing the factors and parameters affecting the dispersion stability. Thereby, colloid is the first branch of dispersion science to understand, since they are the particles which undergo dispersion and imparts the phenomenon of colloidal stability. This is dependent on the interaction of the molecules and the chains of atoms. This is better understood with the help of Derjaguin & Landau (1941) / Verwey & Overbeerk (1948) (DLVO) theory. This theory explains the potential barrier between the NPs.

Figure 2-2 is the flow chart that explains the colloidal stability behaviour. The colloidal stability is related to the particle dispersion. Colloids are the particles that are dispersed homogeneously through the fluids.

The stability of colloids counts on two contributions of the total energy;

- 1) Repulsion of the ionic double layers U_R
- 2) Van der Waals attraction between the colloidal particles U_A

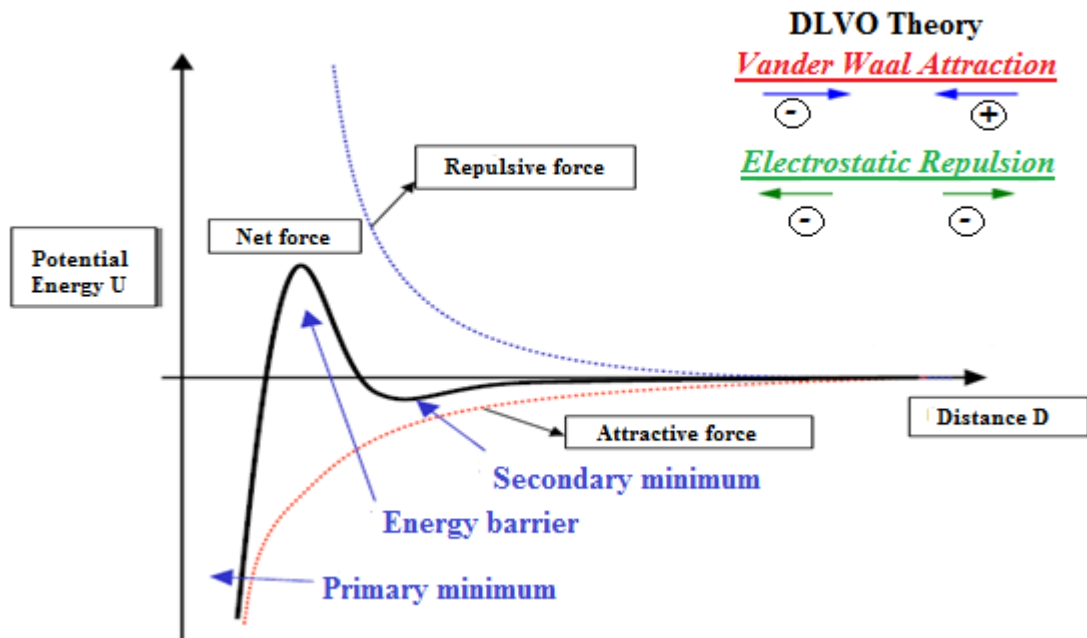


Figure 2-2 DLVO theory mechanism

Figure 2-2; illustrates the values of net force of potential energy generated by the electrical double layer should be greater enough to avoid the attraction barrier otherwise it will form aggregates. Further, this attraction and formation of aggregates causes instability of the colloidal NP in the suspension giving an unstable dispersion. Therefore, it is much more favourable for a system to keep its net force potential energy generated by the electrical double layer attracted to repulsive region, so that the aggregation can be overcome, and hence forming a stabilized suspension of colloidal NPs. DLVO theory estimates the required surface potential to allow the colloidal NP in dispersed state.

For high concentration NP suspensions (i.e. 30 – 60 %) with submicron size particles, surface distance between the two particles demonstrates the maximum surface potential between them causing the mean distance to increase about 1 -10 μm (Iijima and Kamiya, 2009). This is due to the particles being surrounded in Van der Waal forces. However, this surface distance between the particles can be calculated by **equation 2-1**,

$$\cap = dp \left(\sqrt{\frac{1}{3\pi V} + \frac{5}{6}} - 1 \right) \quad (2-1)$$

Where \cap is the distance between the particle, dp is the diameter of particle, and V is the volume fraction.

2.4 Heat Flow through Nanofluids

The heat flow through the system of nanofluids is determined by two models. These models are necessary for estimating the BM and the velocity of the particle inside the fluid i.e. related to Stoke-Einstein's particle model:

1. Static particle model
2. Dynamic particle model (Kumar et al., 2004)

These models are further explained in **Appendix A**. The static and dynamic particle model equations were derived to obtain different quantities, which are; particle sizes, surface area, thermal conductivity and diffusion constant. They are mentioned in **Appendix B**.

2.5 Parameters Related to Brownian Motion and DLVO

There are some basic parameters that are entangled with BM and DLVO phenomena. These parameters are used for computation of both phenomena. These computations are carried out using pair potential on a simulation platform.

There was significant work carried out on the particle sizing and zeta potential for BM. The mimicking of BM mainly depends on the particle sizes. Without knowing the particle sizes of NP the Brownian phenomena cannot be simulated. The zeta potential has also considered having a high impact on the Brownian phenomena; since it provides the charge between the

particle and the particle-particle spacing. It can be replicated by the work done by Zhu et al., (2007) to characterize the zeta potential of NPs in low concentrated solution. This parameter is being used to change the environment, health hazards and other commercial prospects of NPs. This is the reason zeta potential is considered as one of the important parameter in the study of nanotoxicology (Monteiro-Riviere and Tran, 2007, Zhu et al., 2007). This parameter also undermines the stability phenomena of dispersion system. Thus by doing different analysis, safety and precaution need to be considered for NPs study (Karakoti et al., 2006). There is less systematic information available regarding, reproducing the readings of zeta potential measurement of the dispersed NPs in different mediums.

2.6 Dispersion of Nanofluids

The basic dispersion tools of nanofluids are rarely known by people. The common tool for dispersing NPs is ultrasonicator. However, there are further ways to disperse NPs. One way to disperse NPs perfectly in any solution or fluid is necessary that the dispersion tool is ideal according to the base fluid and NP properties. The most common dispersion tools used are shown in **Table 2-1**.

Table 2-1 Nanoparticle dispersing devices

Disperser	Applicability
1. Ultrasonic Probe disperser	Good disperser for most liquids
2. Mechanical Mixer	Good disperser for most liquids
3. Shear Mixer	Only feasible for high viscous liquids

After dispersion is carried out correctly, it is important to characterize the stability of dispersion of NP in the suspension. To find nanofluid physiochemical properties, it is necessary to characterise them using state of art characterising tools as mentioned in section 2.7.1.

There are two basic methods to disperse nanoparticles in fluids for example; by using ultrasonic probe and mechanical mixer.

- 1) The ultrasonic probe disperses NPs with the help of acoustic ultrasonic forces that generate sound waves to break down the agglomeration.

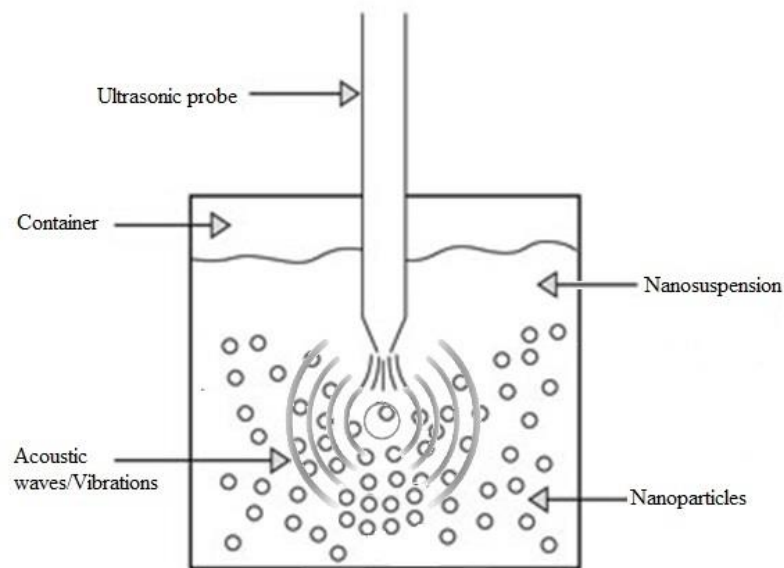


Figure 2-3 Mechanism of ultrasonic device

- 2) The second method disperses the NPs using the mechanical shear force. There are two types of mechanical shear force mixer a) Mechanical mixer and b) shear mixer as shown in **Figure 2-4**. The shear mixing technique uses high or low speed shear force to break down the agglomeration and to homogeneously disperse the particles.

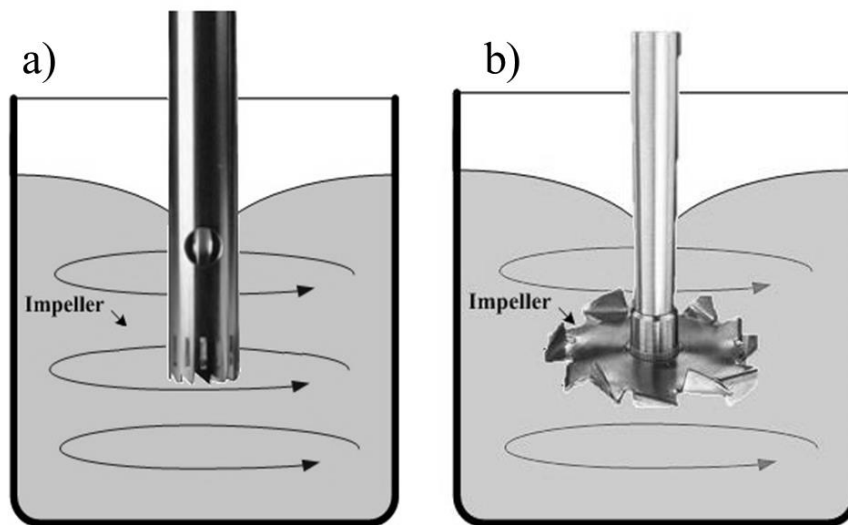


Figure 2-4 Mechanical dispersing devices; a) mechanical mixer and b) shear mixer

The methods shown in **Figure 2-4** helps in dispersing the nanoparticles in different base fluids. Further, in the section 2.7.1 effect of dispersion was characterized using different tools.

2.6.1 Characterization Tools

Instruments used mostly for characterizing the nanoparticle or nanofluid samples are mentioned in **Table 2-2**.

Table 2-2 Dispersion devices for different characterizing parameters

<i>Parameter</i>	<i>Techniques</i>
Dispersion Stability	Visual observation, Dynamic Light Scattering (DLS), Zeta potential
Agglomeration/ Aggregation	Transmission Electron Microscope (TEM), Scanning Electron Microscope(SEM), Dynamic Light Scattering, Zeta potential

Size	SEM,TEM, DLS, Scanning Mobility Particle Sizer
Shape	SEM,TEM, X-ray Diffraction (XRD)
Surface Charge	Zeta potential measurement using Doppler micro electrophoresis
Surface Area	Brunauer, Emmett and Teller (BET)
Surface Chemistry and Contamination	Contamination X-ray Photoelectron Spectroscopy (XPS), Energy Dispersive X-ray Spectroscopy (EDX), Secondary ion mass spectrometry (SIMS), Electrochemistry redox potential
Solubility/Dissolution	Conductivity, UV-vis spectroscopy, Ion exchange chromatography.

The **Table 2-2** explains how to disperse the particles and to characterize them. To make a suspension that can meet all the requirements of the application, it is first vital to understand different characterization tools and their methodologies as given in section 2.8.

2.7 Characterisation of Nanofluids/Nanoparticles

The fluid that is achieved with dispersion of NPs need to be characterised to understand the physiochemical, surface morphology, rheological and thermal properties. To characterize these properties different ways have been established. The first most important physical quantity that has a high impact on nanofluid properties is the size and shape of the NPs (Zhao et al., 2009, Pastoriza-Gallego et al., 2011). Later, surface coverage, surface morphology and chemical composition, ions release factor and rheological properties are also of importance for characterizing nanofluids (Zhao et al., 2009, Pastoriza-Gallego et al., 2011).

2.7.1 Characterizing Size, Shape and Zeta Potential of Nanoparticles

Zeta potential as already noted above is a major parameter to measure the stabilization of the NPs in the solution. This is independent from the sonication power or dispersion techniques. However, zeta potential can be varied using couple of other major parameters such as pH of the suspension and concentration. As the pH is changed, the zeta potential can be varied easily. The change in pH has a major effect on stabilizing the particles, as investigated, Rutile-TiO₂ NPs can be stabilized by using pH > 4.5 and for Anatase by using pH > 7 (Mandzy et al., 2005). Later, it was investigated that the variation of pH from 5 to 7 of silicon dioxide water nanofluid with particle size of 20nm; affects the viscosity of the fluid (Zhao et al., 2009). Further, zinc NPs in aqueous suspension show instability at pH 7.2 – 12, due to formation of unstable colloids of Zn(OH)₂ (Degen and Kosec, 2000).

CuO NPs aqueous solution was also examined at different pH giving a stability from pH < 6 (Pastoriza-Gallego et al., 2011). Therefore, these various studies on pH variation show that nanofluid suspension stability can significantly be altered using pH level. From these studies, it can also be concluded that most suspensions show stability either at zeta potential higher than 30mV or less than -30mV.

To investigate the correct size of the NPs there are many ways that have been established. The most common method is to use either TEM or SEM to analyse the size or shape of the NPs. Second most common approach is DLS technique. This method scatters light onto the particles and the reflected light gives the size of the NPs within the liquid. However, this is not the true size of the particle; instead it is the hydrodynamic size of the particle.

DLS has a laser source that emits a beam on particles in a confined cell known as zeta cell. This laser beam penetrates through the transparent body of the cell and strikes on the particle. This striking of beam causes deflection in the intensity of laser light as shown in **Figure 2-5**; further this intensity helps in interpreting the size of the particles and also their zeta potential.

However, for zeta potential, there are two electrodes on both sides of the cell that inducts small current through the suspension for analysing zeta potential.

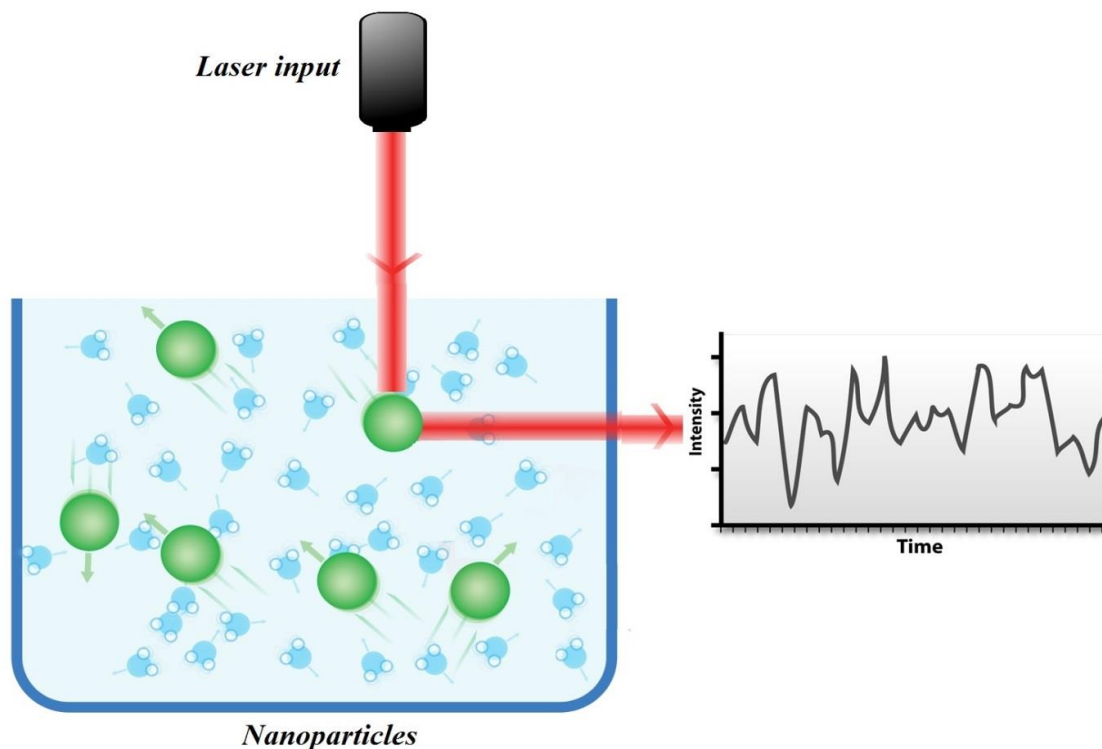


Figure 2-5 Dynamic light scattering mechanism for measuring the nanoparticles size and potential

2.7.2 Surface Analysis

To analyse the surface area of the NP BET technique is common available method (Hwang and Barron, 2011). BET was developed by Stephen Brunauer, Paul Emmett and Edward Teller in 1938, where BET is their abbreviated surnames. This technique uses nitrogen gas in a partial vacuum chamber. The nitrogen gas adheres to the surface of atom or molecules of the gas. The quantity of gas adsorbed depends on the exposed area and on the physical conditions like pressure of the gas, temperature and interaction strength between molecules. Running BET on STP (Standard Temperature and Pressure) conditions helps the analysis of sample surface area.

2.7.3 Chemical Structure Analysis

Analysing the chemical composition, structure infrared and Raman spectroscopy are commonly used and easy to handle techniques (Zhang and Yan, 2010). The infrared spectroscopy can be used to analyse the surface modification of NPs after the attachment of the surfactant (Zhang and Yan, 2010). This technique helps to understand the chemistry behind the modification of the NPs using different groups of attachments such as 1) carboxylate group 2) amine group and 3) silane group. FTIR uses infrared laser beam to detect the functional groups within the compound by the help of vibrational movement caused by atoms/phonon due to light excitation at different wavenumbers. These wavenumbers give an idea about the attachment group because different compounds act in different manner to the emitted infrared light.

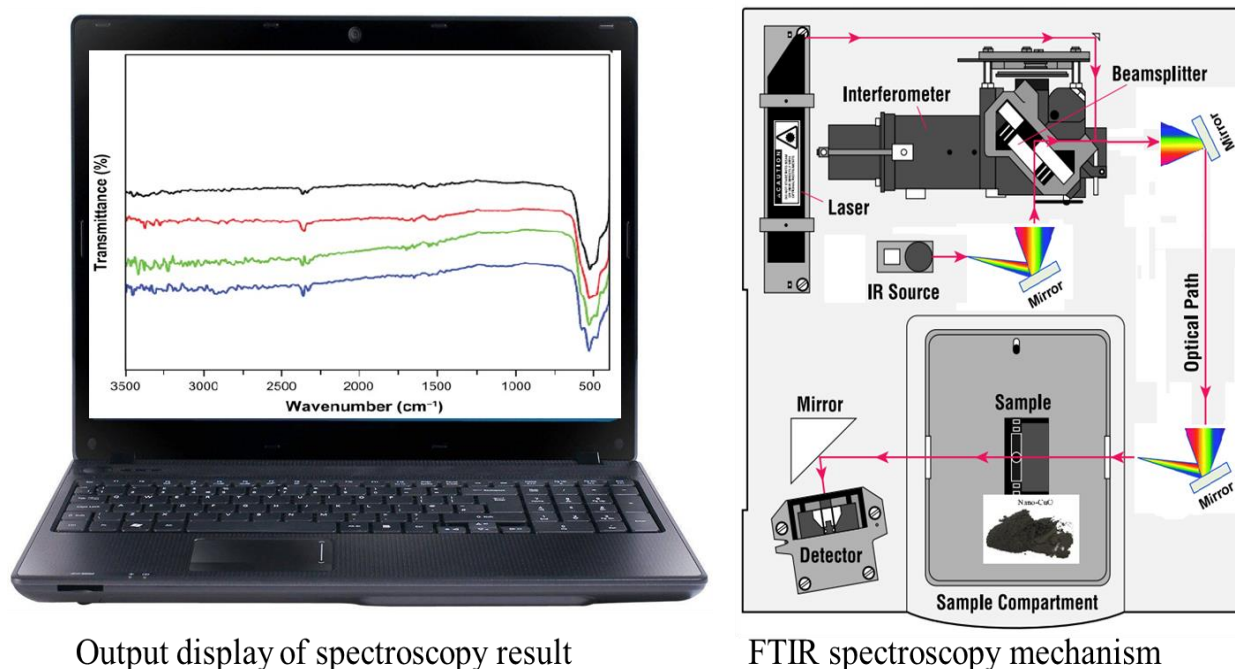


Figure 2-6 FTIR spectroscopy mechanism and results display

Shining dark body source shown in FTIR spectroscopy mechanism of **Figure 2-6** emits infrared energy in the form of a beam. This passing infrared beam can be controlled through an opening to measure the spectroscopy of the specimen. The beam then proceeds in the interferometer, where the "spectral encoding" takes place. The resultant interferogram signal then exits the interferometer. The beam is then excited on the compartment where it is transmitted through or reflected off of the specimen surface. Here the frequencies of energy, which are interestingly normal for the sample, are retained. The infrared beam goes to the detector for final estimation. The detector measures and signifies unique exceptional interferogram signs. Finally, the measured indicated result is digitized and sent to the machine where the Fourier transformation takes place. The final infrared range is then displayed to the client for translation and any further analysis. The illustrated **Figure 2-6** shows the FTIR spectroscopy mechanism.

2.7.4 Analysis of Ion Concentration after Dispersion of Nanoparticles

Ions released can also be analysed with the help of inductively coupled plasma – optical emission spectroscopy (ICP-OES). ICP-OES uses hot plasma to excite the ions in the liquid or the gas state. This technique uses high energy plasma spark from an inert gas like argon over the sample that is sprayed in a vacuum chamber. This excitation releases different colours and these colours help to analyse the ionic concentration within the system. ICP is a helpful technique to analyse the ionic release of NPs since NPs are used for drug delivery to central nervous system (CNS). It is very crucial to analyse the ion release of NP dispersion in different fluids. This ion release at that stage can be harmful if it is in high concentrations. For this purpose, ICP can be the appropriate way to analyse ion release. The Orbaek and Barron (2009) formulation is already out there to calculate the NP ionic concentration.

Moreover, ICP is a spectral method used to undermine very precisely the elemental composition of samples. It can also be used to quantify the elemental concentration within the sample.

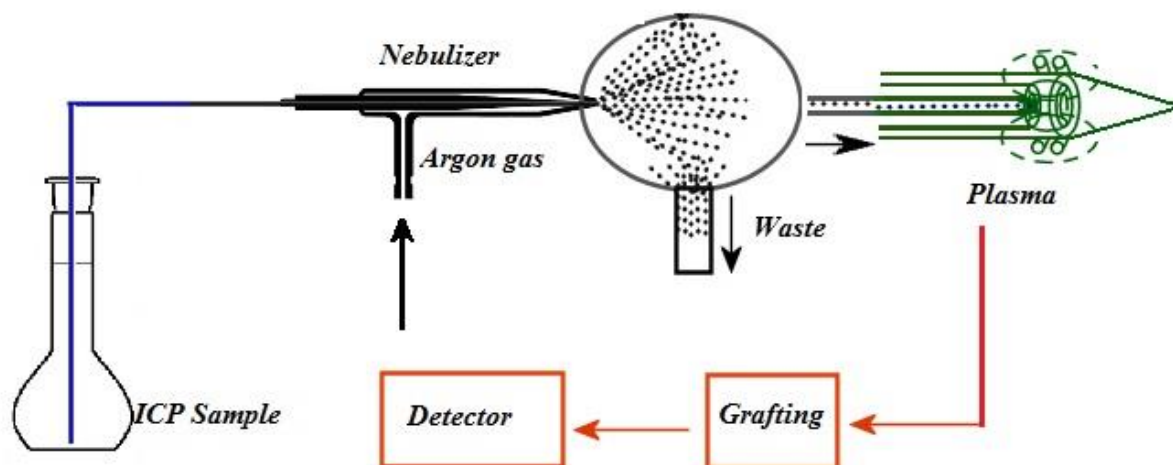


Figure 2-7 ICP-OES mechanism

ICP-OES is one of the most popular tools in analytical chemistry for trace elemental analysis. This device works on a spontaneous emission of photons from atoms and ions that releases excited radio frequency discharge. Liquid and gas samples can be directly tested, while solid sample needs digestion using acid wash or microwave digestion.

After the digestion of the solid sample, it is converted into aerosol using nebulizer either pneumatic or ultrasonic nebulizer. Aerosol formed by nebulizer is fed into plasma chamber. The temperature at plasma chamber core is approximately 10000K; therefore the sample rapidly changes into vapours. Analyte elements are liberated in ion and atomic forms. These ions and atoms release different photons, where the number of photons is directly related to the concentration of the sample. Further, these photons are generated from the gain of additional excitation energy due to the plasma interference. Later, this excitation is relaxed to ground state by releasing photonic energy. Each photon releases different levels of energy. Consequently, this energy is translated to wavelength form for data quantification.

A lens or a concave mirror is used to collect these emitted photons. This lens forms a subsequent image of the ICP using a monochromator. Monochromator decodes the plasmonic wavelength signal into electrical signal by a photo detector. Finally, photo detector process

this signal, which can be then visualized on computer screen. The mechanism is also shown in **Figure 2-7**.

2.7.5 Viscosity

Rheological analysis is also a necessary parameter that analyse viscosity, shear rate and shearing stress of nanofluid. The viscosity is a drag force that exists between molecular layers of the fluid. This property is important for lubrication as well as for drug delivery applications. As already known that pH affects the viscosity of the nanofluid (Zhao et al., 2009), in similar manner viscosity is also effected by other parameters of nanosuspension for example, the size of NPs, concentration of particles and diffusion rate of particles in the suspension. The rheometer is a device that helps in analysing these rheological properties of fluid.

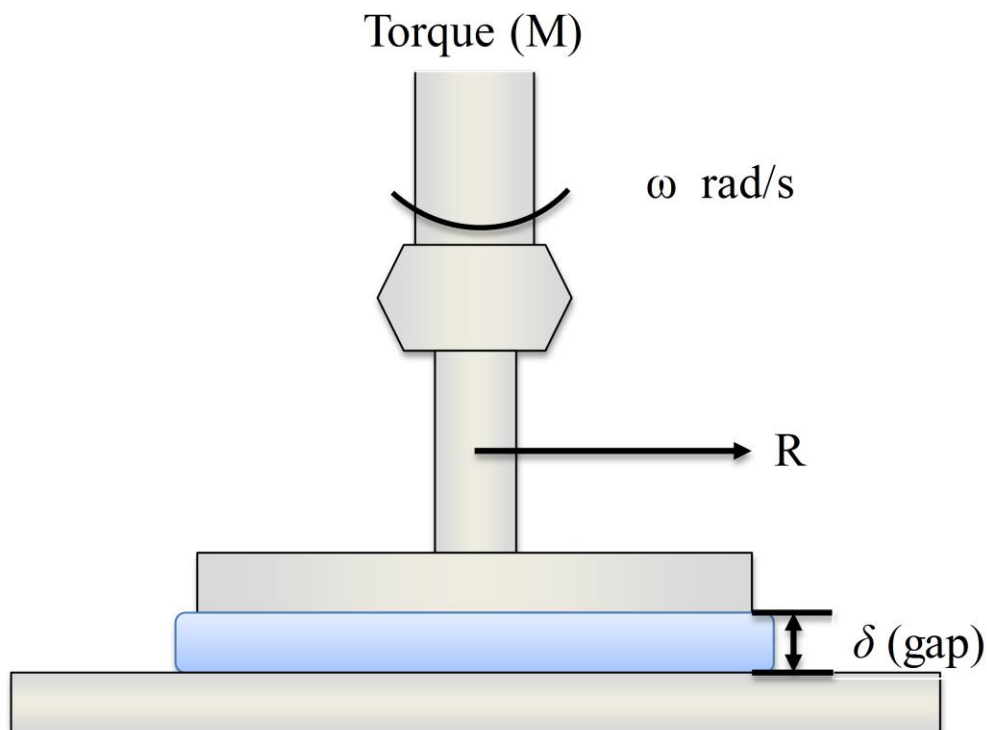


Figure 2-8 TA1500Ex rheometer; flat plate mechanism for measuring fluid viscosity

The rheometer is used for dynamic mechanical analysis to analyse the viscosity of a material, whereas, rheology is the study of flow and deformation of matter. The mechanisms used in a rotational rheometer are related to shear stress that is produced by the force per unit area that causes the material to move against the surface on which it is settled as shown in **Figure 2-8**. Therefore, this shear stress moves with a rotational speed of ω , this is related to shear rate. This shear stress is directly related to the viscosity of the fluid being measured. The parallel plate mechanism for measuring viscosity is simple and commonly used technique. The fluid is placed between the two parallel plates, where the upper plate is rotating with rotational speed of ω , however, the base is fixed on which the sample is placed. This rotation of the fluid using the upper plate causes the fluid to deform with respect to the base, causing the torque or shearing force to generate i.e. τ . Where, τ is directly related to the applied shear rate and the viscosity of the material. Hence this can be put through as shown as **equation 2-2**.

$$\tau = \dot{\gamma} \eta \quad (2-2)$$

Further, where $\dot{\gamma}$ is the shear rate and its related with the velocity V and “ δ ” is the height between two Plates is given by **equation 2-3**,

$$\dot{\gamma} = \frac{V}{\delta} \quad (2-3)$$

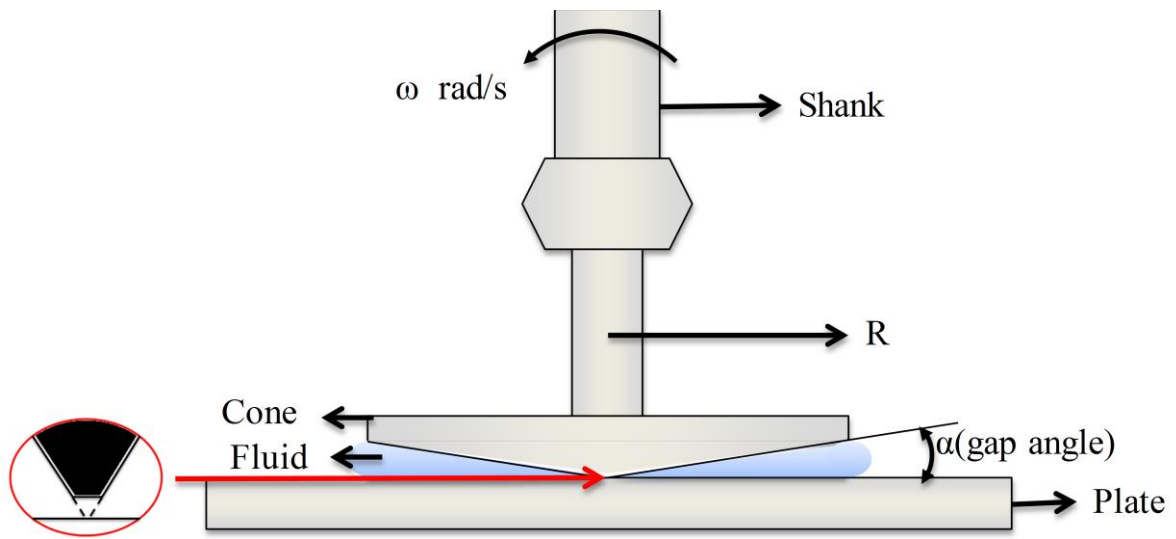


Figure 2-9 TA1500Ex rheometer; cone plate mechanism for measuring fluid viscosity

The cone plate geometry is used for measuring the viscosity as presented in **Figure 2-9**; however, this geometry is more useful for creep measuring test. The gap angle α is from 0° - 4° increment. The plate and cone geometry are organized in a parallel mode, in theory the tip of the cone is aligned with the plane of the plate. Further, the equations related to this methodology are given from **equation 2-4** to **2-7**.

$$\text{Shear rate}(s^{-1}) = F_{\gamma} \omega \quad (2-4)$$

$$\text{Shear stress}(Pa) = F_{\sigma} M \quad (2-5)$$

$$F_{\gamma} = \frac{1}{\tan \alpha} \quad (2-6)$$

$$F_{\sigma} = \frac{3}{2\pi R^3} \quad (2-7)$$

R, in equation 2-7 is the radius of the rotational disc.

2.8 Modification of Nanoparticles for Stable Nanofluids

The necessity of the modification of NPs comes from altering the properties of the particles in a particular fluidic system. The NPs are modified using different modifying dispersants also known as surface active agents or surfactants. These surfactants are chemical modifying groups. They modify the NPs by chemical attachment to their surfaces. The metal oxide NPs are mostly modified using the carboxylic group (Leuba et al., 2013) or silanes (Zhao et al., 2014) to make these NPs hydrophobic to the aqueous fluid. This causes them to become compatible with non-polar solvents. Furthermore, this gives a high dispersive property in non-polar solvent. However, the homogeneous dispersion of the NPs in polar solvents, requires the modification that depends on the stability of ions and functional group charge transfer to the NPs (Iijima and Kamiya, 2009, Kraynov and Müller, 2011). The basic polar stabilizer or modifying agents are amine groups (Kumar et al., 2003) and sorbates (Kraynov and Müller, 2011, Zhao et al., 2013).

2.8.1 Modification of CuO Nanoparticles

NPs have a high surface area to volume ratio which enhances diffusion properties. However, controlling this diffusion is a challenging task (Iijima and Kamiya, 2009, Kida et al., 2007). Several studies have focused on NP dispersion and stabilization in a base fluid to establish an effective methodology for dispersed NPs in fluids (Anandan and Rajan, 2012, Fedele et al., 2011, Palabiyik et al., 2011). CuO NPs are widely used and investigated metal oxides due to their atomic structure and thermal stability, however the dispersion properties of these particles are not widely reported (Anandan and Rajan, 2012, Fedele et al., 2011).

Further, CuO is a multipurpose NP due to its variety of applications from engineering to the biomedical field. This NP is far better than other counterparts of the metal oxide NPs since

CuO is more stable than other NPs (Pike et al., 2006). Further, implementation of CuO in different engineering fields is high. However, mostly before applying NPs in any system of interest, the NPs are widely converted into nanofluids by dispersing the NP in fluids. The CuO NPs are being used for the improvement of thermal conductivity for lubricants, as well as for tribological properties (Wu et al., 2007). CuO NP's are also being used in electrochemical cells (Morales et al., 2005), magnetic disks (CuO nanowire have low ferromagnetism behaviour (Vila et al., 2010)), inkjet printers, electrospinning (Xiang et al., 2011), and heat transfer fluid (Wu et al., 2007).

Short chain carboxylate attachments and amine group's attachment are not widely being used for the modification chemistry of CuO NPs. However, there are few studies which have reported that the modification of the CuO NPs using amine group can be beneficial for biological systems (Satish et al., 2012). Modifying the NPs enhances optical properties, such as fluorescence and fluorescence decay as reported by El-Trass et al., (2012).

2.9 Historical Background and Need of Simulating Nanofluidic Systems

The main drawback of experimental data is that the equipment is expensive and not generally easy to use. In addition, for a complex nanofluid material to be tested some of the thermal properties of test samples are hard to determine; until the sample is homogeneously dispersed in which the status is incomprehensible. Therefore, it is necessary to proceed from the experimental mechanism of dispersion as a base level; and then approach mathematical simulations to get the thermo-physical parameters of the system for supporting design of the materials compositions.

Implementation of the MD method is an effective way to analyse material microscopic and nanoscopic properties. Although, experimental studies are vast, there is a rapid increase in MD studies since last decade, and is currently on developing stages. Nevertheless, MD simulations have also made a great progress in studying the thermal properties of the material, isothermal crystallization process of the metal NPs (Hu et al., 2010), nanowires melt

behaviour (Vila et al., 2010), and nanomaterial's thermal conductivity (Sun et al., 2011), rheological analysis (Cheng and Grest, 2012), protein biological liquids, etc.

MD simulation techniques have been carried out by Rao et al., (2013) to determine the thermal capacity of n-alkanes systems and the self-diffusion coefficient of fluids. Que et al., (2010) have also used mechanical MD simulation results to investigate the binding system (heptadecane and pentadecane), the self-diffusion coefficient and the ratio of volume with mutation relationship of temperature over heptadecane and pentadecane fluidic systems. Therefore, simulations are becoming more common practice in the modern day world. Simulation saves material, money and time.

In comparison to literature, MD simulations can be approached to replicate the nanofluids. Simulations are not an old technique and they are being used since the start of computer era. Currently, simulation that is used for replicating the real phenomena of NPs dispersion is through its initial stages, nevertheless, nanofluid dispersion simulations existed since last decade. Initially these simulations were mostly focused on colloidal particle system simulated using Leonard –Jones (L-J) potential. Later, Argon gas as a base fluid with Cu NPs were simulated using L-J potential and embedded atom method (EAM) potential, this was a simulation related to dispersion in condensed gaseous phase system (Sarkar and Selvam, 2007, Li et al., 2008). Later as the technology advanced, researchers started simulating dispersion of NPs in liquid molecular system such as Cu NPs that were simulated in water based system (Rajabpour et al., 2013). Furthermore, list of last decade work carried out by several researchers for simulating different NPs in base fluid system have been collected in **Table 2-3**. On the other hand, studies are being conducted on simulating metal oxide NPs in various fluids due to their capabilities of improving the base fluid. This has already been investigated by Loya et al., (2014c) in the study of CuO dispersion in aqueous fluid. Before moving to the simulations, it is crucial to understand dispersion and interaction mechanism of NPs with fluids. Simulating NPs dispersion requires understanding of the compilation of force field, pair potentials and ensembles. Furthermore, one should know how to simulate this system, which has been presented in section 2.11.

Table 2-3 Nanoparticle dispersion simulation's historical background (Loya et al., 2014b).

S No.	Referenced work	On What	Forcefield/ potentials used	Year
1	Loya et al., (2014c)	CuO in water	COMPASS forcefield, DPD potential and SPH potential	2014
2	Rajabpour et al., (2013)	Cu water simulation	L-J potential and Lorentz-Berthlot	2013
3	Kang et al., (2012)	Cu-Ar Ar-Ar	L-J Potential	2012
4	Mohebbi, (2012)	Beta-Si ₃ N ₄ in argon system	L-J Potential, Morse function and Charm FF	2012
5	Lin et al., (2012)	Ethylene Glycol-Cu	L-J Potential, Morse potential, Lorrentz Berthelot mixing rule and JR FF	2012
6	Lv et al., (2011)	Cu in argon liquid	L-J Potential	2011
7	Rudyak et al., (2011)	General Np in dense fluid	L-J potential and R-K Potential	2011
8	Sun et al., (2011)	Cu-Ar nanofluid	L-J Potential and EAM potential	2011
9	Cheung, (2010)	Nanoparticle-solvent	L-J potential	2010
10	Sankar et al., (2008)	Pt-water and pt-pt	L-J potential, Morse potential and FENE potential	2008

Table 2-3 continued

11	Lu and Fan, (2008)	Alumina-water or C ₂ H ₅ OH or C ₂ H ₄ (OH) ₂	L-J potential	2008
12	Li et al., (2008)	Cu-Ar	L-J potential	2008
13	Sarkar and Selvam, (2007)	Cu-Ar	EAM and Potential	L-J 2007
14	Luo et al., (2006)	Hydrocarbon- water- polymer Np	Gromos force field and L-J potential	2006
15	Barbier et al., (2004)	PEO Oligomers melts with silica nanoparticles	L-J potential, UFF and OPLS FF	2004
16	Starr et al., (2002)	Polymer melt with np	L-J potential and FENE model	2002
17	Malevanets and Kapral, (2000)	Nanocolloidal model	L-J potential	2000
18	Heyes et al., (1998)	Colloidal model	WCA and potential	L-J 1998

2.10 Stages of Simulation

First initial parameters for force field and potential are set, after this, the system velocity is fixed and then ensembles are implemented to mimic the real thermo-physical conditions. Later, in comparison to the chemical and thermo-physical parameters, the system is then equilibrated for certain time steps. These simulations are processed until the converging results are obtained to the actual system. Time step is the major dependent factor. This accounts for equilibrating the kinetics of the system that takes place; and the system moves

from un-equilibrated condition to equilibrium conditions. The above explained method has been compressed to a flowchart for better understanding as shown in **Figure 2-10**.

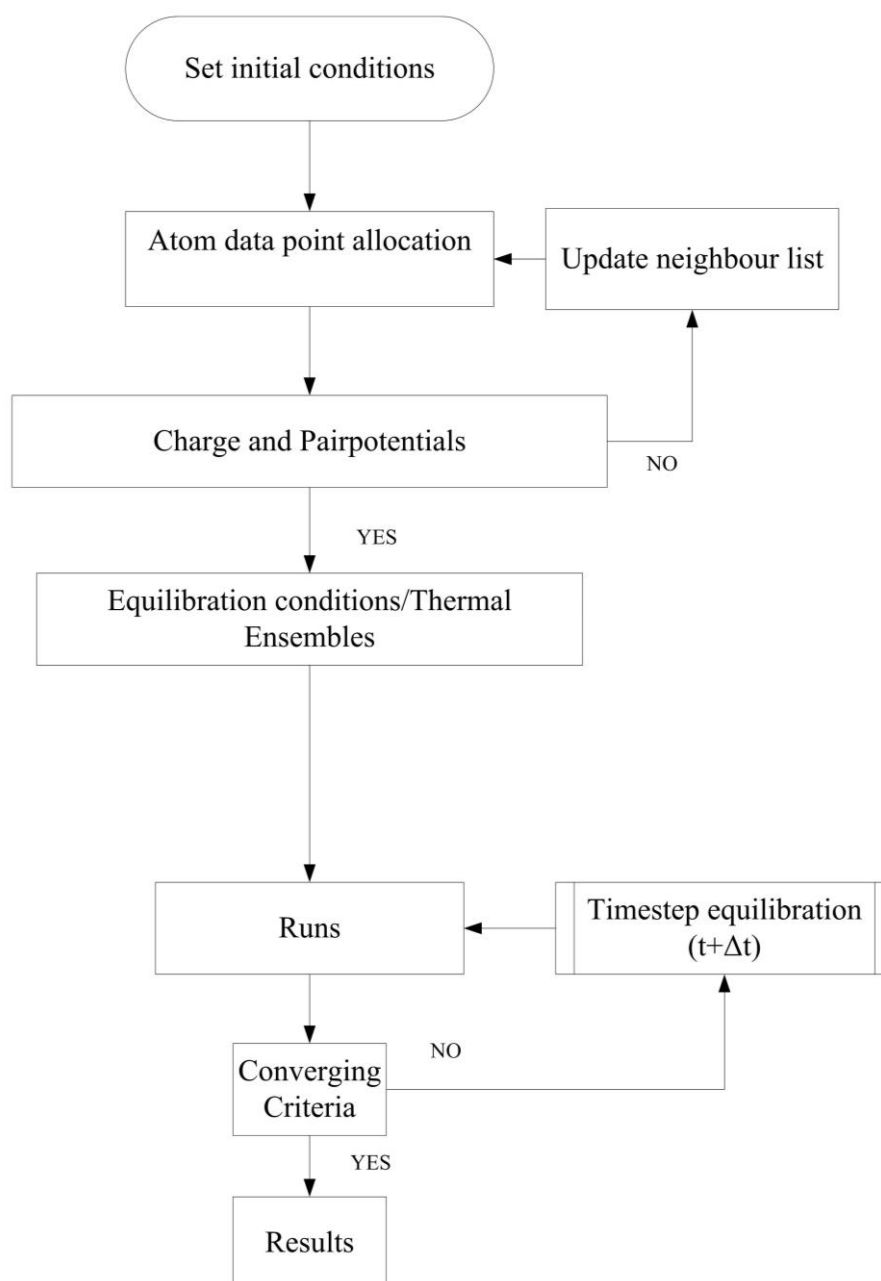


Figure 2-10 Flow chart of molecular dynamics simulation

2.11 Simulation Methodologies

Simulations are becoming crucial techniques to gather information on different experimental procedure. The necessity of using simulation nowadays is increasing due to its cost effective nature and time saving capabilities. Nanofluids simulations are mostly performed using MD. For this, software packages selection was based on the criteria of the conditions that were needed to be simulated. The flexibility was also a major concerning factor for the applicability of different systems.

The Large-scale Atomic/Molecular Massively Parallel Simulator (LAMMPS) was the best means of simulating the design criteria. This is the code generated by the Sandia Laboratories by S.Plimpton (1995). This MD prospective software has high viability over other available software of MD like Monte Carlo and Gromacs. A desired experimental system was replicated on LAMMPS MD simulation package. There are two different types of dispersion simulations 1) Non-equilibrium MD simulations and 2) Equilibrium MD simulations.

1) Non equilibrium Molecular Dynamics

The Muller-Plathe algorithm is used to describe the exchange momenta between two particles in distinctive regions of the simulation box every N steps. The shear velocity profile in the system is induced using this algorithm. This algorithm calculated the viscosity of the fluid using Non-Equilibrium MD (NEMD) technique. Further, this algorithm is also known as reverse non-equilibrium MD (reverse NEMD), that helps in computing the viscosity. NEMD method imposes a shear velocity profile on the system and calculates the off-diagonal component of the stress tensor to analyse the response, which is proportional to the momentum flux. In contrast to equilibrium MD, this technique is time consuming due to off-diagonal stress calculations.

2) Equilibrium Molecular Dynamics

Equilibrium MD (EMD) can be studied using micro-canonical ensemble. This dynamic directly solves Newton's equation of motion, and hydrodynamics is inbuilt in it. Further, the accuracy of results obtained using EMD in contrast to experimental ones for analysing thermo-physical quantities are not convincing, likewise, that of NEMD (Chen et al., 2010).

2.11.1 Force Field

Within the simulation system, force field plays an important role since it provides charges on atoms for interaction. The force field is a mathematical parameter that governs the energies and potentials between interactive atoms. The physiochemical settings of the system refer to the thermal, chemical and physical properties such as initial temperature settings, charges and dynamics of the system.

The macroscopic MD simulations mimic the molecular interactions between different molecules of various elements; in compound form or ionic form. These different thermo-physical types of interactions of MD quantities can be tailored and analysed by true boundary conditions. These boundary conditions are related to the physical conditions, chemical interactions, charges, viscosity of the system, and motion exhibition of the particles. Furthermore, these initial conditions for the dispersion of NCs are also related to the atomic charge within the system for interaction, molecular bonding, forces of attraction (i.e. Van der Waal or electrostatic coulombs interactions), force fields, pair potentials (i.e. molecular mechanics constants) and molecular weight.

The MD simulations of NP dispersion in fluids are performed by initially setting these major parameters to replicate actual dynamics that exist in a real system. Likewise, these molecular interaction parameters are controlled by different force fields such as universal, OPLS, Gromos, CHARMM and COMPASS (Condensed-phase Optimized Molecular Potential for

Atomistic Simulation studies). However, out of these force fields, COMPASS force field was used to simulate metal oxides (Bunte and Sun, 2000, Sun, 1998, Sun et al., 1998, Zhao et al., 2007). This is an ab-initio force field that has confirmed the usage of condensed-phase properties. This force-field has helped a wide range of molecular calculations of structural, vibrational, conformational, thermo physical and other physiochemical properties in the condition of isolation and condensed phases.

The implementation of this force field is wide covering from organic molecules, inorganic molecules, polymers, metals and metal oxides (Bunte and Sun, 2000, Sun, 1998, Sun et al., 1998, Zhao et al., 2007). COMPASS force field has already been carried out on metal oxide molecules in an organic environment (Zhao et al., 2007). Coulombs law is used to calculate electrostatic interactions and Morse function is utilized for covalent/ionic attachment between metal-oxide bonds. Previous works show that this force field can also be applied to chemical species such as alkanes, aliphatic chains, organic molecules, benzene rings, and esters (Sun, 1998, Zhao et al., 2007, Sun et al., 1998, Bunte and Sun, 2000). For calculation and parameterization, COMPASS forcefield uses two major common techniques in molecular mechanics a) Ab-initio parameterization and b) Empirical parameterization.

Ab-initio is used on potential energy surfaces to derive partial charges and valence parameterization as the first process. Van der Waal parameters can also be set by Ab-initio. To achieve a considerable comparison with experimental work, the force field is upgraded; so that valance parameter in gas phase experimental data can be analysed comprehensively. At the very end, the Van der Waal parameters are optimized to overcome the condensed phase parameters. The COMPASS force field terms that are used for energy calculations (Sun, 1998) are computed by **Equations given in (A.1)** also the abbreviations of the terms are given in **Equations (A.1)** and defined in **Table A.1**.

2.11.2 Pair Potentials

After applying force field on the molecular system of NPs with fluid, pair potential or algorithms that run the MD are applied. Force field helps in molecular interaction using quantum and molecular mechanics, however, diffusion of the NP is necessary after molecular interactions. The diffusion of NP in a realistic mode demonstrates BD.

The interaction between the molecules exhibits BM, as this mimics the random forces in the system. The system is equilibrated using different algorithms behind the scene to design a virtual NPs dispersion fluid. Computer simulations were used to analyse the trajectory of dispersion of hydrodynamic dispersed particle system by Ermak (1975). Later MaCammon (1978) also worked on the hydro-dynamically concentrated system. The hydro-dynamical system exhibits the inter-particle distance is much greater than the range of hydrodynamic interactions. However, the BD implementation by Ermak was highly probable to give concurrent results with the experimental values achieved.

The hydrodynamics of the system display combinations of Coulomb interactions; i.e. long range interactions as well as the Van der Waal interactions; i.e. short range interactions. Furthermore, the dynamics of the system is more convincing after applying the DLVO (Kruyt, 1952) factor in the system to mimic the charges to enhance the realistic intermolecular attractions and repulsions. This hydrodynamic effect in the system is further achieved and enhanced using Smoothed Particle Hydro-dynamic's (SPH) potential.

After hydrodynamic effect is replicated in nanofluidic system, random diffusion needs to be applied. Several studies about simulation work were reported on the diffusion of polymeric, ionic and mineral NPs (Cooke and Elliott, 2007, Hoang, 2007, Kowsari et al., 2008). An example of this is calcite NPs; which have been simulated in water for salt MD for thermal energy storage nano-fluidic simulations (Cooke and Elliott, 2007). Such Simulations are mostly conceiving diffusions of the polymeric NPs or di-block polymers represented by spheres. The major diffusion phenomena that have been implemented on the NPs or the

polymer dispersion are with the help of BD (targeting the random motion of the particles in a solvent or any solution system). Further surveys show that the best way to simulate dispersion of the metal oxide NPs in the water system can be carried out using the discrete particle dynamic (DPD) potential (Spaeth et al., 2011, Symeonidis et al., 2005, Gao et al., 2007). This potential has the power to disperse NPs as well as replicating the phenomena of the BD (Hoogerbrugge and Koelman, 1992). DPD was first carried out on nano-water systems (Hoogerbrugge and Koelman, 1992, Koelman and Hoogerbrugge, 1993). Moreover, the work was carried out by P. Esponal and P.B Warren for implementing the DPD technique using statistical mechanics. DPD technique imparts stochastic phenomena on particle dynamics (Español and Warren, 1995). This is how BD was integrated into DPD technique.

However, the random forces will only be in pairwise interaction since DPD at the same time imparts the hydrodynamic effect on the system. Many studies of DPD for complex fluidic systems (Spaeth et al., 2011, Symeonidis et al., 2005, Gao et al., 2007) show that the dispersion of NPs in water exhibits complex properties and to simulate this, initial selection of boundary conditions are important to replicate the real scenario. Thereby, the best way to simulate, is to acquire the boundary conditions of the existing experimental system and then use the MD simulator to further implement it (Cheng and Grest, 2012). The considerations of the boundary conditions are particle sizes, force field for particle-to-particle interactions, solvent in which the particles will be diffused, and physiochemical nature of the system (Bunte and Sun, 2000, Zhao et al., 2007).

The governing parameters for the fluidic system simulation are entangled with two major criteria's DPD and SPH (Monaghan, 2005). DPD and SPH in this study are two major potentials to simulate the model of CuO NPs in water. First formulated by (Monaghan, 2005, Gingold and Monaghan, 1977) used SPH on non-spherical stars and later they worked on implementing particles in hydrodynamics with Lucy on kernel estimation (Gingold and Monaghan, 1982, Lucy, 1977). To implement stochastic effect DPD was executed with hydrodynamic effect (Spaeth et al., 2011, Symeonidis et al., 2005, Gao et al., 2007). Conservation of momentum forces governing DPD is F^c , dissipation of energy through the

system is represented by dissipative forces F^D . F^R , this is another parameter governing the random forces related to the random stochastic motion of particles within the system. These three forces are the part of the DPD pair-style that is carried out as a command to execute the DPD actions. Through combining the above mentioned forces DPD's total force \vec{f} can be executed to perform the desired motion. The influence of the forces in particular directions is handled by \widehat{r}_{ij} .

The equations related to DPD phenomenon are **equation 2-8** and **equation 2-9**, further elaborated in **Appendix A-1**.

$$\vec{f} = (F^C + F^D + F^R)r_{ij} \quad (2-8)$$

To define the hydrodynamic heat conduction through the desired system, SPH pair-style was used. The governing phenomena behind SPH is to control the particles. These particles are defined by i and j parameters. Heat diffusion coefficient governed this system that is an **equation (2-9)**.

$$D = \frac{\lambda}{C_v \rho} \quad (2-9)$$

D is the heat diffusion coefficient, λ is the thermal conductivity, C_v is the heat capacity constant volume and ρ is the density. The final parameter that is related to SPH is “ h ” which is the range of the Lucy kernel function to estimate of momentum quantities that are related with velocities, energy and densities by approaching an interpolation function to transform a set of partial differential equations into integral equations (Lucy, 1977). Discrete points are used to evaluate the vectors and scalar quantities between particle to particle interactions. Therefore, there is no need of estimating through grid (Liu and Liu, 2003) since interpolation function is approached to simulate the interaction between neighbouring particles, which are Kernel functions as stated by Lucy in 1977 (Canor and Denoël, 2011, Lucy, 1977). It is a continuous polynomial function derivable over its compact support with $k=1$.

2.11.3 Ensembles and Velocity Theorem

Subsequently, after mimicking interaction potentials and forces between the atoms and molecules, the velocity verlet theorem is used. The velocity verlet theorem is a time dependent movement of the atoms from one position to another using an algorithm movement which is based on BD. Later, these velocities or positions are controlled using the thermal ensembles i.e. canonical NVT (Number of particles, Volume and Temperature), grand canonical μ PT (Chemical potential, Pressure and Temperature), isobaric and isothermal NPT (Number of particles, Pressure and Temperature) and micro canonical NVE (Number of particles, Volume and Energy). These ensembles carried out the thermal and physical perturbation to change the dynamical position of the system. This causes the system to move to a un-equilibrium state. After moving to a un-equilibrium state the system then easily converges to the equilibrium state to acquire the smoothness of temperature and physical quantity fluctuations. Finally this helps with the convergence of running simulation. Later, this can be altered by varying the time steps to achieve the real convergence results.

1) Micro canonical Ensembles NVE

NVE ensemble is applied for equilibration of conservation of energy throughout the system.

2) Canonical Ensembles NVT

NVT ensemble is applied for equilibrating system with varied pressure input, however, the volume and temperatures are kept constant.

3) Isothermal-Isobaric NPT

NPT ensemble is applied for equilibrating system with varied volume input, it mean the lattice boundary of the system can vary either in x, y, or z directions, whereas, the pressure and temperature are kept constant during equilibration.

In this work the MD viscosity and thermal conductivity of the system is determined using the Green Kubo's viscosity relation (Kubo, 1957), that is carried out by LAMMPS MD package.

2.11.4 Simulation Data Acquisition

Running the simulations is not just a process of exhibiting the real conditions, but also post-processing is essential. Further, analysing the data output from the simulative runs is the main task. Without post-processing the output data, the study is invalid and the coherence of the simulation work to that of experiment cannot be understood. The MD simulation data acquisition is not simple due to the lack of visualization software for visualising trajectories as well as the transparency of the results cannot be met until the results are quantified properly. The data acquisition packages are many and the output data is analysed by help of these. The best mean to interpret the results output from the simulation run; is to make the acquisition on Matlab or excel. Visualization tools are used to visualize the output dumps of the LAMMPS to display the MD motions exhibited by the trajectories output.

2.11.5 Visualization Tools

The visualization tool used for post-processing the simulation trajectory outputs through this study; is Ovito. This software was developed by Alexander Stukowski that helps in displaying the trajectory output of LAMMPS (Stukowski, 2010). Using this software, the dump output files can be run to visualize the performance.

2.12 Cases Investigated in This Work using MDS

In this thesis, three major studies are investigated under the topic of NP dispersion in engineering fluids as shown in **Table 2-4**. Major part of the research is based on the dispersion dynamics of NCs in fluids through modelling and simulation.

Table 2-4 Topics covered throughout this research

<i>Nanoparticle dispersion in engineering fluids</i>	
<i>Studies</i>	<i>Formulation</i>
CuO-NC in Aqueous fluids	CuO - H ₂ O
Modified CuO-NC in Aqueous fluids	(COOH)-CuO - H ₂ O
CuO-NC in Hydrocarbons	CuO -- C _n H _{2n+2}

In this study, simulation of Copper oxide NC (CuO NC`s) in water (CuO-H₂O) suspension system has been presented at a molecular scale in a dynamic fluidic system as schematically shown in **Figure 2-11**. Later, the dispersion of CuO NC`s in hydro-carbon based fluids was also carried out as shown in **Figure 2-12** and experimental work has been presented. Finally, these CuO NC`s were modified using butyric acid (BA) and their simulation as shown in the **Figure 2-13**.

2.12.1 Dispersion of CuO Nanoparticles in Aqueous Fluids

Dispersion simulation on CuO NPs in water was carried out on LAMMPS MD package. Further, water acts as a constitute material for dispersion, in comparison with other fluids. The CuO NPs were chosen due to their stability in water. Moreover, the CuO nanofluid holds high demand for various applications when dispersed in water. The applications associated with CuO NPs dispersion in water are a) waste water treatment, b) heat transfer application, c) antibacterial, and d) coolant.

CuO is used for treating contamination of arsenic materials from water by the help of its absorbent capabilities because pH adjustments are not required for oxidation of As (III) to As (V), also it inhibits the presence of anions. Cao et al., (2007) produced CuO NCs with high

surface area through a two-step process. These NCs hold high removal capability for As (III), which can be easily separated and digested during water treatment processes.

Furthermore, CuO NPs can be used for heat transfer applications due to their ability of improving the thermal conductivity by 15-18% (Karthik et al., 2012, Manimaran et al., 2014). Moreover, these NPs are also used as coolant material as investigated by Anandan and Rajan,(2012), since they help in modifying the thermal conductivity of base fluid. The CuO NPs antibacterial properties can be understood by Hassan et al., (2012), they concluded that CuO nanocrystals demonstrate the capability of inhibition at concentration of 2.5 µg/ml and later it was also seen by TEM analysis that CuO nanocrystals ruptured the cell wall, which caused irreversible damage to the cell envelope finally leading to cell death.

Therefore, these concerns and importance necessitate the use of CuO NPs dispersion simulation in water. The initial setup of how the experiment and simulation were conducted for this case study is shown in **Figure 2-11**.

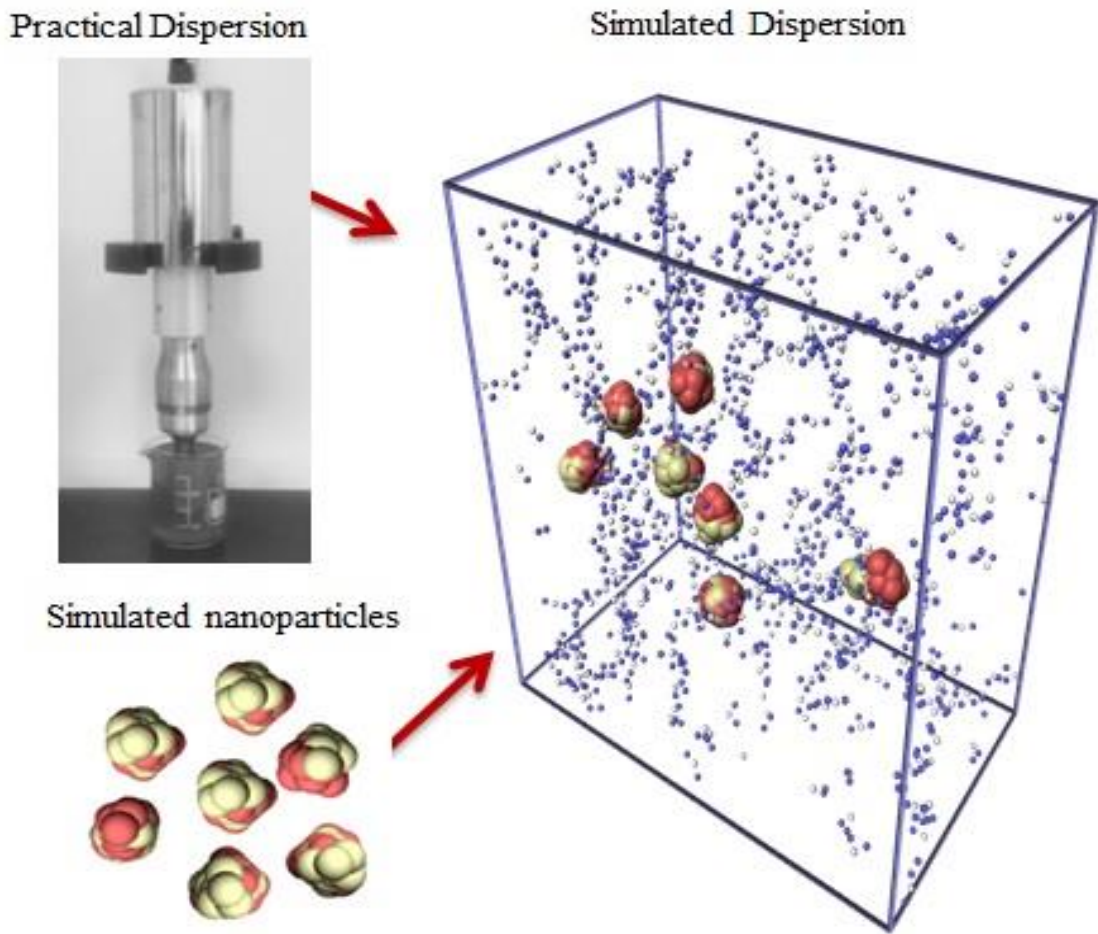


Figure 2-11 Schematic show representing research design and simulation mechanism of the CuO-water nanofluid MD research work

2.12.2 Dispersion of CuO Nanoparticles in Hydrocarbon Based Nanofluids

For biological and thermal transformation applications, the uses of long chain hydrocarbons have become a focus in terms of materials resistance to thermal conduction, wear, and durability. Nanomaterials can be beneficial in broadening their perspectives by improving the thermal capability and conductivity either as Phase Change Materials (PCM) for energy storage applications or biological applications (Shin and Banerjee, 2011, Li et al., 2011). The straight chain alkanes such as paraffin have shown a high usage of material like micro and NPs as additives with high applicability on reducing wear out, and improving the thermal transfer properties.

The preparation and characterization of NPs in fluids as additives demonstrated the system's thermal transferring and di-electric enhancements, physiochemical stability, and rheological smoothness (Mergos et al., 2012, Han et al., 2009, Hosseini et al., 2012, Jesumathy et al., 2012, Sonawane et al., 2012). Before the use of NPs, heat transfer fluids suspensions properties were improved using micrometre particles. They did improve thermal properties, however the suspensions had a high level of aggregation and instability due to the bigger particle sizes, which caused clogging (Boothroyd, 1971, Sohn and Chen, 1981, Ahuja, 1982, Kurosaki et al., 1986).

CuO NPs were investigated in API-SF engine oil and base paraffin oil, that proved enhancement in the wear capabilities of the material by reducing the worn scar depth by 17%-78% and helped in reducing the friction by 6% (Wu et al., 2007). During the last decade, some NPs have been used as a basic surface active agent i.e. surfactant for lubricants. It is approved that CuO NP's led a big leap in enhancing the wear properties and reducing friction as known from several different studies (Wu et al., 2007, Hernández Battez et al., 2008).

Experimental researches have been carried out to understand the underlying capabilities of the nanofluidic materials (Sonawane et al., 2012, Hosseini et al., 2012). Nevertheless, by carrying out numerical simulation, it will be more convincing in targeting the chemical and physical

conditions that are hard to be performed experimentally within the fluidic system. In contrast to all this, in this work, paraffin based fluid was simulated with CuO NPs to analyse the thermo-physical and rheological properties of this nanofluidic system. The designed system is shown in **Figure 2-12**.

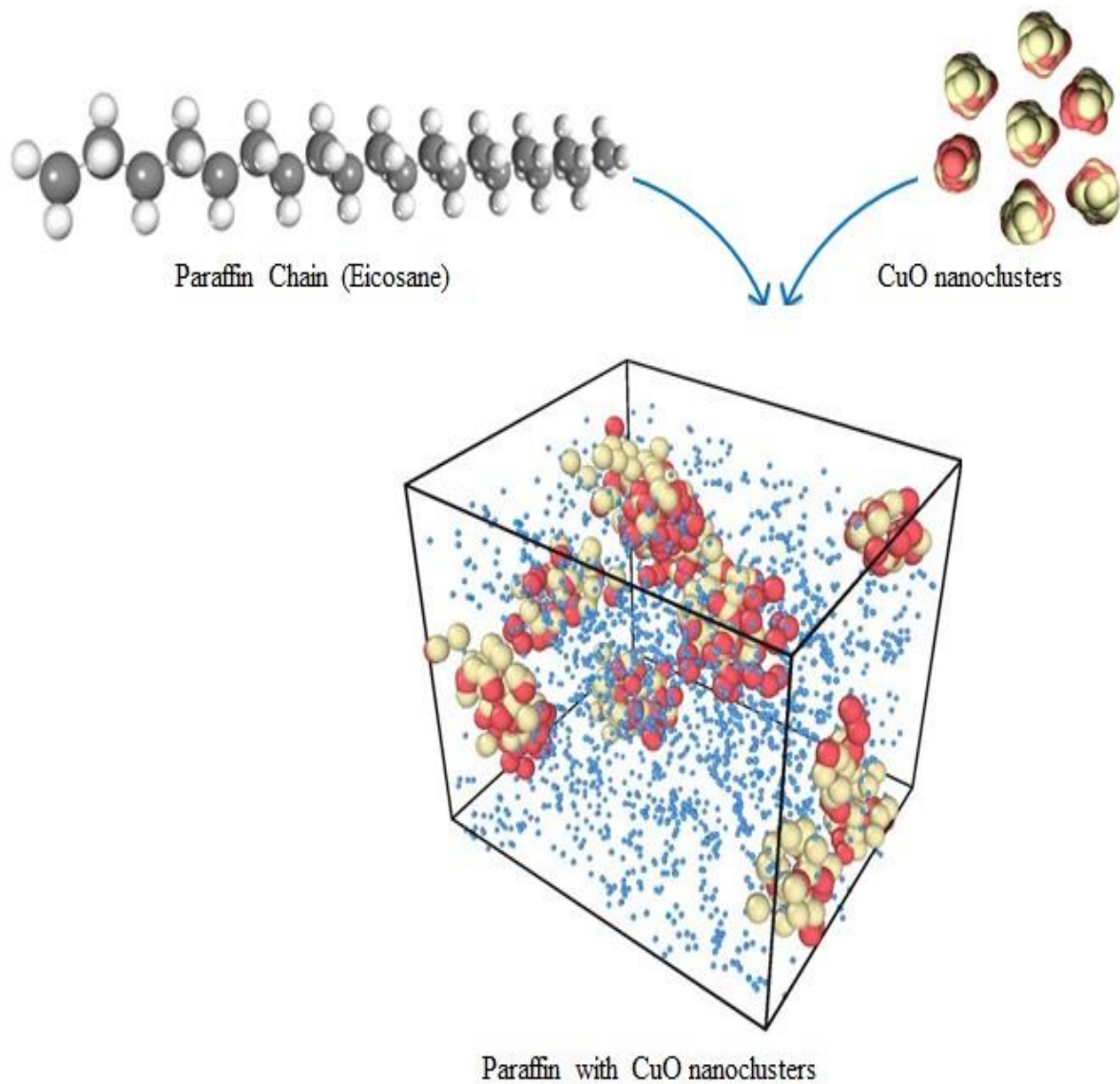


Figure 2-12 Schematic illustration of CuO nanoclusters in Paraffin

2.12.3 Dispersion of Surface Treated Nanoparticles in Aqueous Fluid

The final study on simulation work is by modifying the CuO NCs using surface treatment. Later, these surface treated NPs were dispersed in water. This study will suggest how the NCs can be surface treated in simulation to replicate the realistic mechanism that exists in dispersing these particles. The surface treatment of the CuO NCs were carried out using BA, since BA is a small chain carboxylate group, that attaches to the CuO NCs easily, and further by doing so, we can identify three different mechanism of carboxylate attachment over the NCs. Moreover, the application of this attachment can be used for inhibiting cancerous cells.

It has been found that the butyrate or short chain fatty acids help as a source of energy for colon mucosa by stimulating fluid and electrolyte absorption. Moreover, it helps in preventing colon inflammation, carcinogenesis and oxidative stress, regulates the colon's defence barriers (Gonçalves et al., 2009). However, the absence of butyrate of short chain fatty acids is linked with death of colon cells and mucosal atrophy.

Butyrate group also acts as a chemo preventive agent (Wollowski et al., 2001), since it is in-vitro exposure of tumour cells shows induce apoptosis and inhibition of proliferation. Therefore, due to these factors BA was chosen as a modifying agent. Further, NC just serves as a carrier particle for drug-delivery (Minelli et al., 2012). Hence, in our case CuO NCs already act as an antibacterial agent, but surface treating them using BA enhances their further capabilities of inhibiting tumour cells and bacteria. The simulation schematic chart of surface treated CuO NPs is shown as **Figure 2-13**.

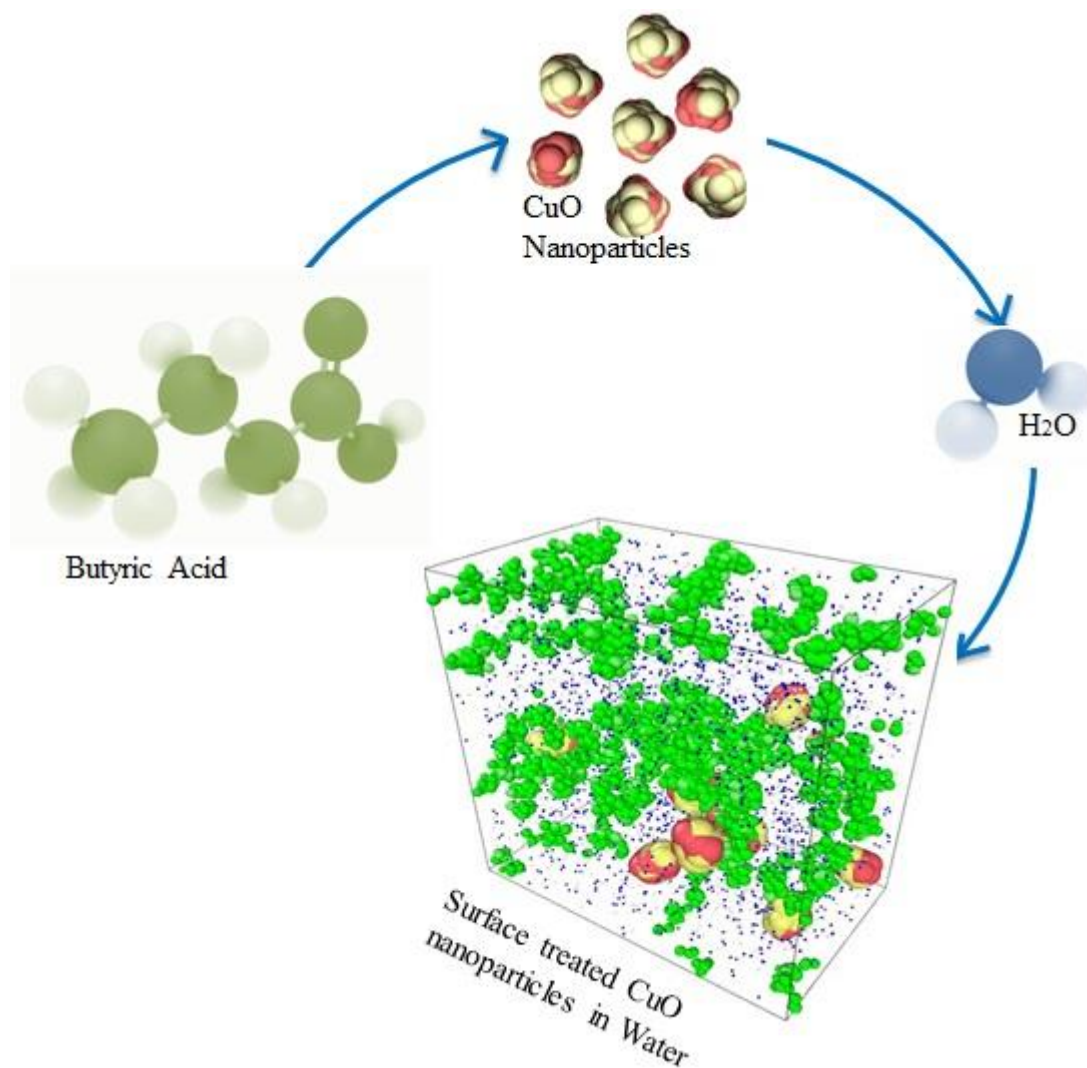


Figure 2-13 Schematic chart of surface treated CuO nanoclusters in water. Step by step visualization of the nanoclusters with functional group in water system; a) Green particles are the alkyl chain; b) Dark navy blue colour represents carboxylate group attachment to the surface of nanoclusters; c) Yellow-Red particles bonded together are CuO nanoclusters

2.13 Summary Outlined

This chapter elucidates the background knowledge and in-depth overview on the topic of research; below are the points that have been clarified in this chapter, few points are also used to elaborate the upcoming chapter briefing.

1. The chapter presents the background knowledge on the nanoparticle and nanofluids; in which the nanoparticle and nanofluid formation has been discussed in detail.
2. Dispersion mechanism and its theory has been elaborated; that explains four major dispersion phenomena that are connected with dispersion mechanism that are
 - a) BM of NP
 - b) Liquid layering at liquid particle interface
 - c) Nature of heat transport between NPs
 - d) The clustering effect of NPs in fluid
3. The stability of dispersion is elaborated and background knowledge on this has elucidated that dispersion stability can be controlled by DLVO factor and forces of attraction (i.e. Van der Waal forces) and repulsion.
4. The heat flow through the system consists of two models a) static particle model and b) dynamic particle model.
5. Zetapotential and particle size are the two major parameters underpinned; which are related to BM and DLVO.
6. Different ways of dispersing nanoparticle in fluid has been presented and further characterizing devices are discussed. The dispersing devices help in de-agglomerating the nanofluid and avoiding sedimentation of particles. However, characterizing devices are used for analysing different properties of the nanoparticles and nanofluids.
7. When the pH of the suspension is not capable of altering the properties required; hence the surface modification of nanoparticles is essential. Hydrophobic surface modification of nanoparticles can be conducted using various surface active functional

groups such as short chain carboxylate group (i.e. butyric acid, beta alanine and etc.) and long chain carboxylate groups(i.e. oleic acid, silanes and etc.).

8. It is known that the molecular dynamics simulation can be utilized for simulating nanoparticle dispersion in fluids. Furthermore, detailed background knowledge on molecular dynamic simulation of nanofluid has been established; through which various techniques and easy to use methodology has been underpinned.
9. The reason LAMMPS package has been chosen for simulating nanofluids is due to the versatility for calculating the .various thermo-physical quantities.

Chapter 3

Materials and Methodology

Chapter 3 Materials and Methodology

This section contains information regarding the materials and techniques used to perform the experiments. It is subdivided into two major sections; a) experimentation setup and b) simulation setup.

- a) In the first section, the basic studies on dispersion of NPs in fluid that were carried out using different dispersing methods are explained. CuO NPs were modified by the chemical surfactant (i.e. BA) for investigation of dispersion and aggregation phenomena between the pure NPs–water suspension and modified NPs water suspension.

Two different nanofluids were prepared by dispersing CuO NPs in the base fluids a) CuO in water and b) CuO in Alkanes. CuO NPs were dispersed in these base fluids to increase their viscosity and decreases their diffusion values.

- b) The second and the third sections of this chapter discuss the methodology of performing the simulations that were carried out for analysing the viscosity and diffusion coefficient of the nanofluids. Simulations were performed using MD software LAMMPS. The trajectories of the simulation were used on OVITO for visualization.

Three simulations were performed during this research: Rheological and thermo-physical analysis of a) CuO NPs in water and b) in alkanes. c) Diffusion analysis of surface modified CuO NPs in water.

3.1 Experimentation

3.1.1 Materials/Tools

Nanoparticles: The CuO NPs were produced by using thermal plasma process (TescmiaTM) by QinetiQ material Ltd (Farnborough, UK) as shown in **Figure 3-1** (Ren et al., 2009). The process guarantees a very high purity of NPs production. These NPs were with a density of 6.3-6.49 g/cm³ (Xu et al., 2009) and size of 20-70 nm. For dispersion; three different devices were employed: 1) ultrasonic probe (Sonics VC750) 2) Mechanical mixer and 3) Goldrich Shear mixer. Malvern Nano Zetasizer (ZS) was used for particle sizing and charge analysis. For Cu ion release ICP (Varian ICP-OES) analyser was used.

The crystal structures of CuO were analysed using XRD. The measurement of CuO NP's crystal size or the average of the particle size is 22.6 nm, and CuO content is 78.1% ($X_{\text{CuO}} = 78.1\%$). This is due to the reaction of CuO with the environment to produce Cu₂O:



Average sizes of these NPs have been primarily reported to be in the range of 23-32 nm and the density of bulk copper being 6300Kg/m³ (Ren et al., 2009).

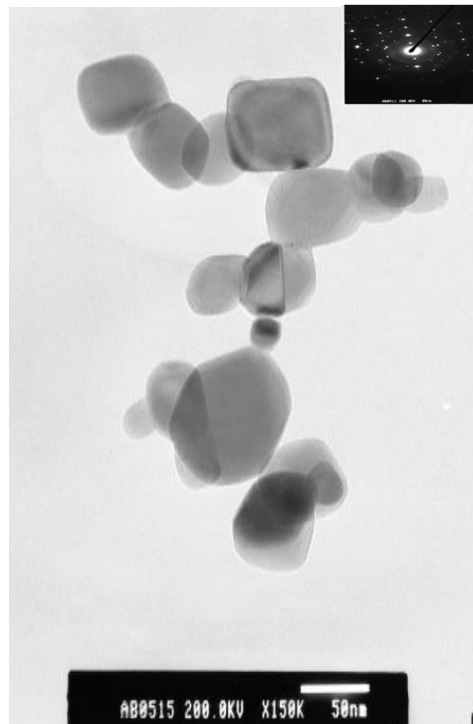


Figure 3-1 CuO NPs image observed by TEM. The average size of nanoparticle is approximately 50 nm. The CuO crystal structure is shown in the up-right corner (Ren et al., 2009)

For CuO modification, 0.2 g CuO NPs was used for all three experiments. 1.5 g of butyric acid was used which was obtained from Sigma Aldrich. NaOH was also obtained from Sigma Aldrich and 1 M solution was used for experimentation. For sonication; the ultrasonic probe from Sonic VC750 was used for sonicating the mixture before refluxing. The surface modification of CuO NPs was carried out with BA for comparing the reference CuO dispersion properties with modified ones.

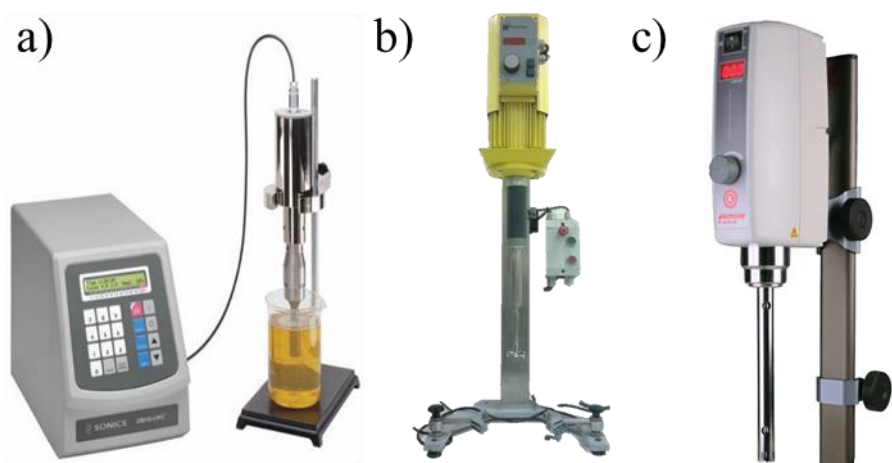
After surface modification of CuO NPs, the characterization was carried out using characterization tools to quantify the modified surface and to identify the modification style. To characterise the modified NPs, Perkin Elmer's FTIR spectrometer was applied. The range of this device is from 350-4000 cm^{-1} .

Fluids used were De-ionized water and Alkane (i.e. Dodecane and Decane) purchased from Sigma Aldrich.

3.1.2 CuO Dispersion in Water

The CuO NPs dispersion is carried out by ultrasound and mechanical mixer using the equipment's shown in **Figure 3-2**. The mechanism of an ultrasound is that the ultrasonic device generates sound waves to break down the agglomeration of NPs. The mechanism of a shear and mechanical mixer uses high or low speed shear force to break down the agglomeration and to disperse homogeneously the particles.

The second phase of the research in this thesis is focusing on the characterization of surface modified CuO NPs by using a short carboxylate chain attachment.



All the three equipment are available at University of Hertfordshire.

Figure 3-2 Dispersion tools used for the research work; a) Ultrasonic (Sonics VC 750), b) Disperlux Shear mixer, and c) Polytron Homogenizer

3.1.2.1 Cu^{+2} Ion release from CuO-water nanofluid

Cu^{+2} ion release from CuO NPs in nanofluid suspension was investigated to determine its dispersion factor and saturation in water. Furthermore, the ion release information is also useful for MD representation on the basis of chemical composition and elemental analysis of the amount of Cu and oxygen present in the NPs.

Cu^{+2} ion release from CuO NPs in nanofluid suspension was investigated using Inductive Coupled Plasma-Optical Emission Spectroscopy (ICP-OES) method. For our research Varian ICP-OES was used. Before carrying out the experiments on ICP, it is necessary to acid wash the apparatus. This takes into consideration all glass pipettes, containers and volumetric flasks that will be used.

ICP pre-examination steps for release of the Cu^{+2} ions in water based nanofluid (repeated experimentally 3 times):

0.1% of NPs will be dispersed and then let them sediment, then take the solution into an acid wash centrifuge tube for centrifuging.

Centrifuge the sample @ 8000 RPM for 1hour.

After centrifuge, transfer the supernatant to another acid wash centrifuge and then filter the solution and finally transfer to another clean acid wash centrifuge.

Now solution is prepared for ICP examination.

3.1.3 Surface Functionality of CuO Nanoparticles

CuO was modified using BA. BA was used as the reagent for surface modification of CuO NPs. Three different modification experiments were carried out which are:

- 1) CuO NPs modification by using BA with pH 7 for 2 hours.
- 2) CuO NPs modification by using BA with pH 7 for 24 hours.
- 3) CuO NPs modification by using BA with pH 5.5 for 2 hours.

3.1.3.1 CuO Nanoparticles Modification Using BA with pH 7 for 2Hours

CuO NPs were modified with BA. Initially NPs were dispersed with BA in de-ionized water using magnetic stirrer. While the stirring was carried out, the pH was altered to 7. Later the solution was sonicated for 10 minutes and then refluxed for 2 hours, also 1.5 g of BA was neutralized to pH 7 using 1 Molar NaOH and 0.2 g of CuO NPs was added and sonicated for 10 mins with vigorous stirring to form stable suspension. The pH was re-checked using pH paper. The suspension was heated for 2Hrs at 90°C while stirring. The molar equivalence for the above situation was 1:1000.

The modified NP mixture was cooled to room temperature. Thereafter, it was centrifuged at 8000 RPM for 20 min with the addition of ethanol (approx. 10-20% v/v of reaction

mixture) to aid settling of the modified particles. The supernatant was then discarded. The obtained solid (i.e. modified NP) was first re-dispersed in 10-20% ethanol/water solution with the aid of 3 min sonication, and then centrifuged in the same manner as described above. Three replicates of initial washing and centrifuging on modified CuO NPs with water/EtOH and 100% EtOH washes were carried out. The solid was dried using vacuum oven for 3-4 Hrs at 40° C.

3.1.3.2 CuO Nanoparticles Surface Treatment Using BA with pH 7 for 24 hours

The same procedure from section 3.1.3.1 was followed for the second experiment but the refluxing condition was changed to 24 hours.

3.1.3.3 CuO Nanoparticles Modification Using BA with pH 5.5 for 2 hours

The same steps from section 3.1.3.1 were followed for the third experiment, with an exception of pH that was altered to 5.5 using 1 M NaOH.

3.1.4 CuO Dispersion in Alkanes

The dispersion of NP was carried out in hydrocarbon based fluid Dodecane and Decane. This part of the study investigated the viscosity of the nanofluid, i.e. Dodecane with CuO NPs. The device used to analyse viscosity was the TA AR1500Ex rheology instrument. These readings were used for comparing results obtained with MD for CuO NPs dispersion in alkanes.

3.2 Characterization of Modified CuO Nanoparticles

Surface modification of CuO NPs was analysed using a Perkin Elmer's FTIR instrument in transmission mode under air. FTIR spectra were used to analyse the chemical change on the surface of the modified CuO NPs. The base reference was taken as the original CuO NPs, and then the difference between the modified NPs was checked with the original CuO NPs spectrum. Different characteristic peaks and range formation showed the successful attachment over the NPs surface. The resolution and range used for characterising the samples was 350– 4000 cm^{-1} respectively.

3.3 Model and simulation methodology

For performing MD simulation it is necessary to have state of art and high end computational power. In this research to simulate MD of nanofluid system the computational power used for this purpose were;;

The system that was used for simulation was of following specification; a) Core i7 processor vpro @ 3.5 GHz, 1GB NVIDIA GT520 Card, 8GB RAM, and cluster computer was also used for processing the simulation. Cluster configuration was 48 Xeons (E5520s) 2 socket x 4-core (no hyperthreading) with 24 Gb RAM and DDR Infiniband form part of the Main cluster (chassis 1, 2 and 3).

The simulation of dispersing nanoparticles in engineering fluids was performed in a systematic way.

1. First the nanoparticle is formed on the Material studio software. The Material studio is a versatile software used for molecular designing and molecular arrangement.

2. After forming the nanoparticle on the material studio; the fluid system is established around the nanoparticles. Now from here the COMPASS forcefield parameters are implemented on the system using Discover module of the Material studio software. This module implements charges on the atoms.
3. Next, the (atomic coordination, charges and configuration) established system is exported from material studio in a LAMMPS readable format, which is then used by LAMMPS read command for establishing atomic configuration and pair potential settings.
4. From here, after establishing a desired system (initial configurations or boundary conditions) it is now the task of the LAMMPS script to execute the particular functions and commands for simulating the desired system.
5. After the initial configuration is read by the LAMMPS package, it executes the pair potential and charges on the atoms; doing this enables the atoms to interact in actual way.
6. After setting all the initial boundary conditions, pair potentials and charges, the system is then equilibrated from its original position by ensembles. These ensembles are of different types, enabling the user to equilibrate according to desired conditions.
7. Computes and fixes commands are used for executing and analysing properties from this equilibrated system.
8. Dumps command is implemented for achieving the output trajectory of the simulation.
9. Finally running parameters are set for equilibrating for a certain time limit specified by user.

The above mentioned steps described how to perform nanofluid dispersion simulation using LAMMPS package. Furthermore, in Appendix E nanofluid simulation script and use of different commands within the script has been briefed out.

The output is visualized on the Ovito and its explain in **Figure 3-3**.

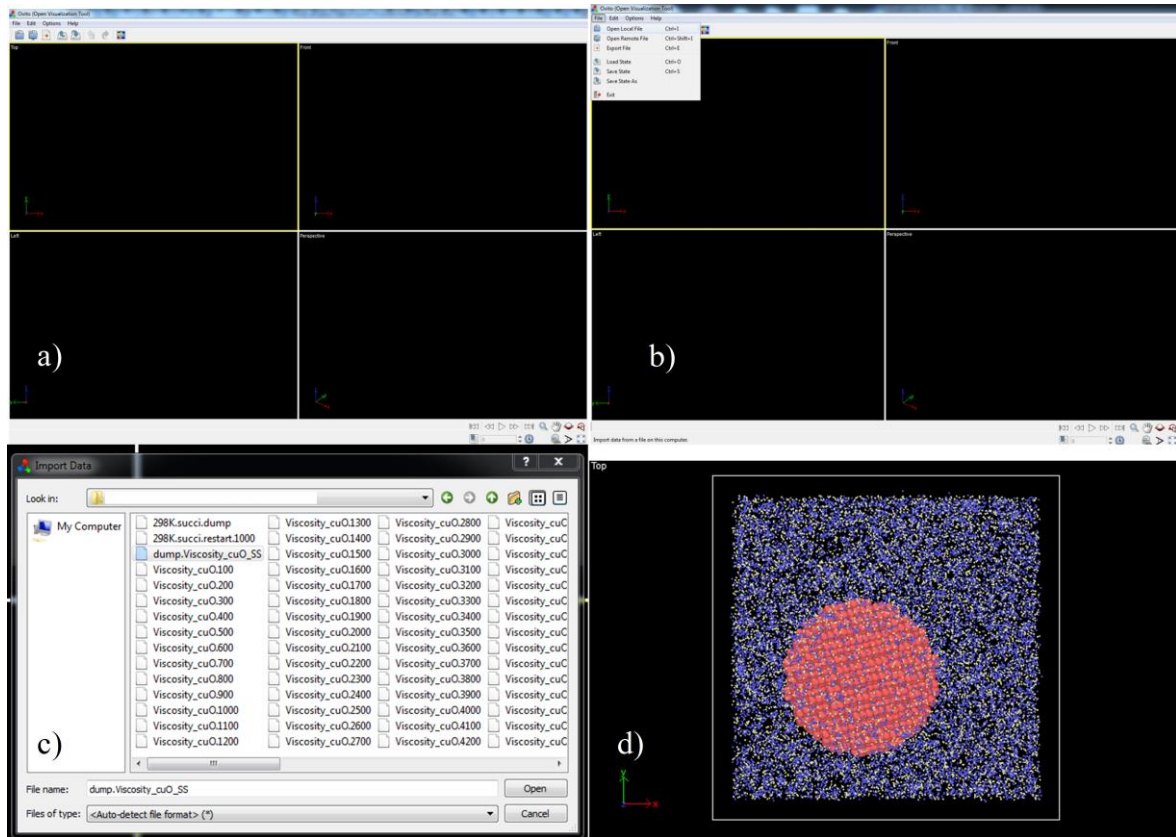


Figure 3-3 Step-by-step demonstration of visualising nanoparticle dispersion in water on OVITO; a) Initial step after opening OVITO, b) how to launch LAMMPS trajectories, c) opening the dump file and d) visualized screen dump of simulation.

After performing different dispersion simulations convergence of thermo-physical quantities was required. For validating convergence of different quantities; different convergence techniques were used. The viscosity was validated by monotonic convergence of stress autocorrelation function, for validation of thermal conductivity monotonic convergence of heat autocorrelation function was used; finally for validating convergence of diffusion coefficient multiple slope of mean square displacement was used, further the obtained values were compared with the literature values.

3.3.1 Simulation of CuO in Water

The CuO NPs used for this MD simulation was generated on Material studio Accryles Inc, USA. Simulation of NPs dispersion in water was carried out using Large-scale Atomic/Molecular Massively Parallel Simulator (LAMMPS) which is a free source code provided by the Sandia group (Plimpton, 1995, Thompson, 2012, Petersen et al., 2010). The first system was composed of 463 transferable intermolecular potential 3P (TIP3P) water molecules (Jorgensen et al., 1983) and simulated with SPH and DPD potential in an orthogonal box (40 Angstrom x 25 Angstrom x 40 Angstrom) and is shown in **Figure 3-4a**.

The second simulation initial system setup used 252 CuO molecules represented by 7 NPs, each carrying 36 molecules bonded by COMPASS force field. The NP size was 0.4 nm in a 463 TIP3P water molecular system in an orthogonal box (40 Angstrom x 25 Angstrom x 40 Angstrom) and their molecular system comparison is shown in **Figure 3-4b**.

The system was equilibrated for approximately 147 picosecond under NPT ensemble; this ensemble enables the system to keep the pressure constant at a varied volume. Pressure of 1 bar at the temperature of 303K was used. Van der Waals and electrostatic forces were imparted on the non-bonded interaction for dispersion. COMPASS force field was employed to put charges on the system.

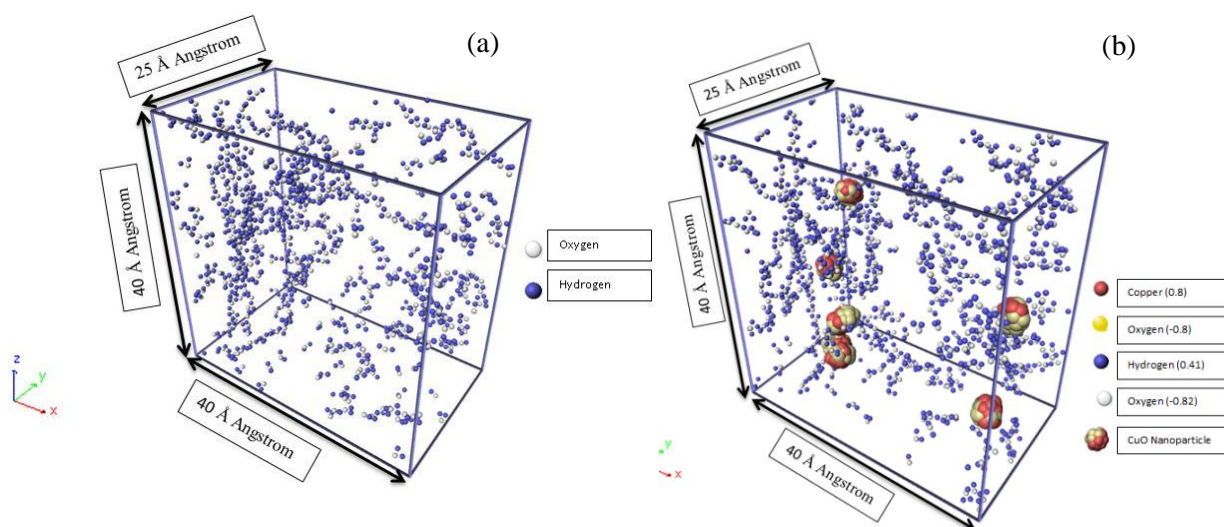


Figure 3-4 Molecular system comparison of without and with CuO nanoparticles: a) simulation results (control) of pure water molecules in an orthogonal box of 40 Angstrom x 25 Angstrom x 40 Angstrom, the box contained 463 TIP3P water molecules, where white is oxygen and blue is hydrogen. b) The simulation box containing CuO nanoparticles and with the TIP3P water molecules in an orthogonal box sized by 40 Angstrom x 40 Angstrom x 25 Angstrom with 463 water molecules; where red is copper, yellow oxygen bonded in CuO nanoparticle. The blue is hydrogen and the white is oxygen

3.3.2 Simulation of Nanoparticles in Alkanes

MD simulation of alkane (Eicosane i.e. $C_{20}H_{42}$) has also acted as a constitute fluid and was used as a control medium in the whole system. Amount of CuO used in alkane's simulation was calculated to be 3% according to their weight ratio. This CuO NP's was generated and assigned in the base fluid system i.e. Paraffin oil. Then COMPASS forcefield was incorporated into the generated particles fluid system (Sun, 1998). As it is already been used for alkanes and benzene based system, this force field proved to be a right approach for the fluidic system in this work because it can simultaneously apply charges for alkane and CuO nanoparticles (Sun, 1998). For the simplicity of understanding simulation operation, the paraffin used for the MD simulation was a straight chain alkane molecule, later simulated on the LAMMPS platform. This system was equilibrated from 303 K to 323 K, with degree intervals of 10 K. All the above simulations were carried out under atmospheric pressure.

The system configuration in the simulations was controlled using NPT ensemble. Pair potentials were applied using SPH and DPD potentials. These two potentials (SPH and DPD) were employed because they give a realistic effect on the system configuration, further giving hydrodynamic and random Brownian effect in the system.

The system was equilibrated for different iteration levels until the stress and heat auto correlation was converged for viscosity and thermal conductivity calculations respectively. COMPASS force field was established in material studio. The system with NP and alkanes has been shown in **Figure 3-5**. For clearer alkane visualization, the alkane radius has been decreased so that NPs can be illustrated clearly.

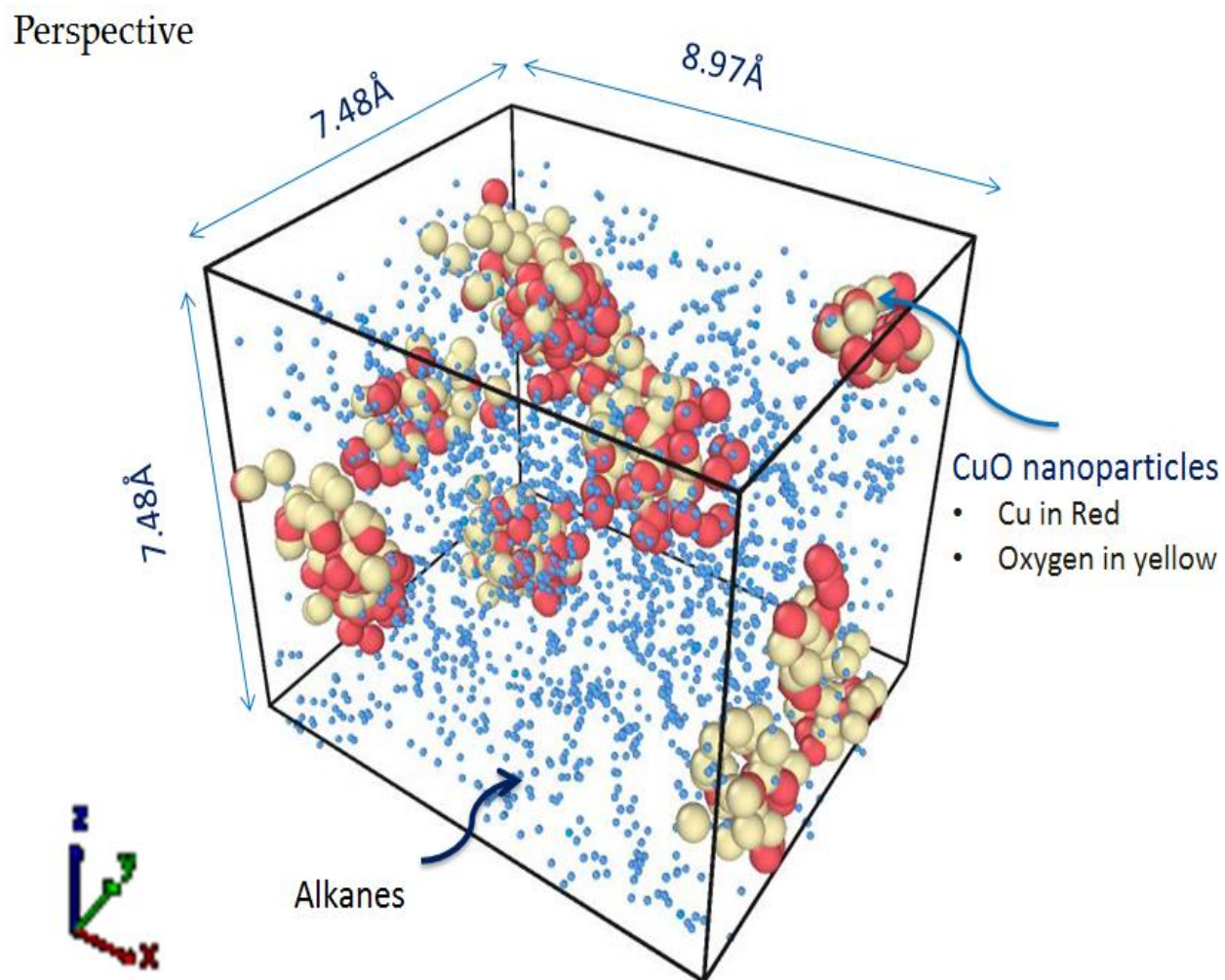


Figure 3-5 CuO nanoparticles in alkane fluid; the cyan blue balls are representing n-Eicosane ($C_{20}H_{42}$) and red is the Cu and yellow is the oxygen connected to Cu

3.3.3 Simulating thermo-physical quantities

1) Thermal conductivity

The thermal conductivity of the system was analysed with the help of Green Kubo technique used with LAMMPS platform. The approach used, was equilibrium molecular dynamics (EMD). The selection of EMD was due to its flexibility with periodic boundary conditions. The non-equilibrium molecular dynamics (NEMD's) depends on the Fourier's Law of conduction whereas, a counterpart, the EMD uses fluctuation dissipation theorem and the simulation outputs is highly sensitive with expensive computational cost (Esfarjani et al., 2011). Moreover, the EMD is normally applied to a system by first making a system equilibrium conditions to a desired temperature and then a constant energy can be applied to the system for calculating or computing the thermal conductivity tensor by using Green–Kubo (Green, 1952, Kubo, 1957) relation.

Simulation can run under various statistical ensembles, that are canonical (NVT), grand canonical (μ PT), isobaric and isothermal (NPT) and micro canonical (NVE). It is known that Green-Kubo's derivative relation have been used on all the mentioned ensembles (Green, 1952, Kubo, 1957). Lepri assessed micro canonical ensemble for acquiring the thermal conductivity but with a diverging and non-trivial results. This was further explained, that if the velocities of the centre of mass is set to zero so some proportion of parametric heat flux will be subtracted from the system then subsequently it might converge (Lepri et al., 2003). However, to achieve a higher accuracy, a better computing methodology such as the canonical ensemble or isobaric ensemble with the Green–Kubo formula needed to be selected for calculating thermal conductivity.

The thermal conductivity is calculated through inducing additional thermal forces to all the atoms confined in the system (Maeda and Munakata, 1995). The equation used to calculate the heat flux and thermal conductivity (Tretiakov and Scandolo, 2004) is **equation 3-2 and 3-3:**

$$\lambda = \frac{V}{3K_B T^2} \int_0^\infty \langle J(0) \cdot J(t) \rangle dt \quad (3-2)$$

Where λ is the thermal conductivity variable that depends on the K_B Boltzmann constant, T is the temperature and V is the volume, J is the heat flux, and t is the time period.

J denotes the heat current function (Tretiakov and Scandolo, 2004):

$$J = \sum_i e_i v_i + \frac{1}{2} \sum_{i < j} (f_{ij} (v_i + v_j)) x_{ij} \quad (3-3)$$

Where is the v_i velocity of particle i and f_{ij} is the force on atom i due to its neighbour j from the LJ potential and e_i is site energy and x_{ij} is the distance between particle i and j .

2) Viscosity

Viscosity was calculated with help of Green-Kubos viscosity measurement method in the same way as thermal conductivity. To measure viscosity, the stress tensor was applied to analyse the shearing viscosity. **Equation 3-4** was used to implement the stress tensor (Kubo, 1957):

$$\eta = \frac{V}{K_B T} \int_0^{\infty} \langle P_{xy}(0) \cdot P_{xy}(t) \rangle dt \quad (3-4)$$

Where η is the viscosity, V is the volume of the system, T is the temperature, K_B is the Boltzmann constant and P_{xy} refers to an independent component of the stress in the x-y direction.

The viscosity validation is carried out by integrating the stress tensor with respect to time correlation. The stress tensor calculates the stress in xy direction, which is denoted by P_{xy} . Further, there are three major stress tensors that are considered in the calculation of stress autocorrelation function a) P_{xy} ; b) P_{yz} ; and c) P_{xz} . These stress tensors compute the shearing stress between the atomic deformation and the resistance between the particles.

3) Diffusion coefficient

Diffusion coefficient was measured to investigate the effect of diffusion rate with the system. The diffusion was measured using two different approaches (Allen and Tildesley, 1989, Alder et al., 1970), a) Diffusion by simulation **equation 3-5** and b) Diffusion by Stokes-Einstein formula **equation 3-6** :

$$D_{Sim} = \lim_{t \rightarrow \infty} \frac{1}{6N} \frac{d \langle |r(t) - r(0)|^2 \rangle}{dt} \quad (3-5)$$

Where $r(0)$ is the distance from initial position of the particle and $r(t)$ is the position of particle at time t .

$$D_{S-E} = \frac{K_B T}{6\pi\eta r_p} \quad (3-6)$$

Where K_B is the Boltzmann constant, T is the temperature, η is the viscosity and r is the radius of the particle.

4) Radial distribution function

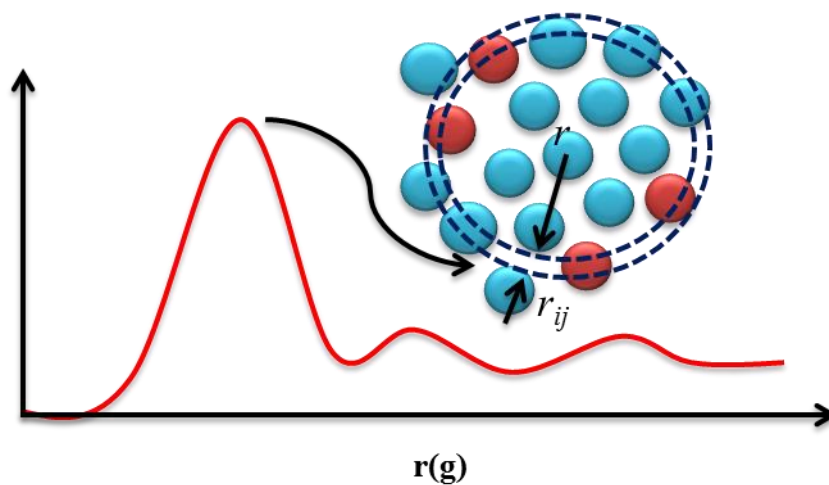


Figure 3-6 Radial distribution function peak connection with atomic movement

Radial distribution function (RDF) explains the atom to atom interaction and by this the aggregation status can be known. This is related to aggregation, because the interaction kinetics between atoms gives characteristic peaks. These peaks are used for analysing the distance between two consecutive atoms. RDF is also related to pair distribution function. The mechanism of RDF is shown in the **Figure 3-6**.

For a better understanding of the aggregation phenomenon, RDF is introduced on the basis of pair distribution function of molecules and equations for averaging densities were established by John G. Kirkwood, Born, and J.E Mayer to describe the diffusion between the cut-off distance among molecules (Kirkwood, 1935, Born and Green, 1946, Kirkwood et al., 1950).

3.4 Summary Outlined

This chapter presented the method of performing experiments and simulations. The experiments were performed on dispersion and characterizing of NPs and nanofluids. Furthermore, simulations were performed using molecular dynamics. After performing experiments and simulations the results were compared and discussed.

1. First, initial dispersion experiments were carried out to examine the basic properties of dispersion. The basic properties that were examined are a) particle size, b) sonication power, c) zetapotential and d) sonication time. These properties examined were dependent on one another.
2. Surface modification of CuO nanoparticles using short chain carboxylate group was performed, these were the second set of experiments accomplished for analyzing the change in the aggregation and dispersion performance.
3. Dispersion characterization was performed using devices that were able to measure specific parameters for calculating nanoparticle dispersion and modification. The surface chemical characterization was performed using FTIR, particle size and zetapotential was measured using Zetasizer, ICP was used to measure the ion release from CuO nanoparticle when in suspension and finally, rheometer was used to measure the viscosity of the nanoparticle suspension.
4. Simulations were also performed for mimicking the rheological experiments. MD was used to suspend nanoparticles in fluids. Material studio was used as molecular modelling software to create nanoparticle of desired shape and size. Furthermore, the modelled system was scripted on LAMMPS source code package to perform the simulation. Trajectories achieved from simulation outcomes were visualized on OVITO.

Chapter 4

Results

Chapter 4 Results

This chapter presents results of different studies of dispersion of CuO NCs in water and alkane base fluids. Moreover, the chapter informs about the outcomes of experimental surface modification of the CuO NCs and their simulations under different environmental conditions in water based fluids.

4.1 Dispersion of CuO Nanoparticles

Dispersion studies of the NPs dispersion were performed to exam the effects of NPs dispersion properties under varying physical and chemical conditions. The variations of parameters also have a considerable impact on the size change of the NPs. On the other hand, with theoretical prospect, the concentration has also proved definite effect on the size of the particles as they agglomerated (Zhao et al., 2009).

It can be proposed that the concentration of NPs affects the particle size due to the attractive and repulsive forces existing between the particles. It means more volume fraction of particles will show bigger particle size than the lower volume fraction of NPs; because if the system is instable it will show more aggregation and coalesces of particles, consequently, causing an increase in the particle size. Furthermore, this particle size is not the actual size of the particle rather it is a hydrodynamic particle size. The hydrodynamic particle size is the size of the outside liquid layer being formed over the NP or NC.

The attractive and repulsive forces existing between the particles help to determine the stability of the particle dispersion. However, if there are attractive forces between the particles; the agglomeration is likely to arise, leading to a potential rise to the size of particles, due to the formation of NPs into lumps (Rosicka and Sembera, 2013). However the repulsive forces have an opposite effect (Rosicka and Sembera, 2013). If there is a

repulsive force between particles, it causes stability. A NP size is reduced due to less agglomerations as stated by Yang et al., (2010).

To determine if the size of beaker impacts CuO NPs dispersion when sonicated, two beakers of different sizes were chosen, a) 60 and b) 500 ml. CuO NPs concentrations in water ranged from 0.001%w/w and 0.01%w/w and the results are shown in **Figure 4-1**. For the 60 ml beaker, particle sizes ranged from 244.4 to 160.4 nm. The particle sizes achieved using the 500 ml beaker were larger ranging from 2432 to 712.3 nm. Nevertheless, as already stated, the sizes of the NPs are also affected by the changing physical conditions. It was determined by changing the beaker sizes; as they had a considerable effect on the particle sizes as represented in **Figure 4-1**.

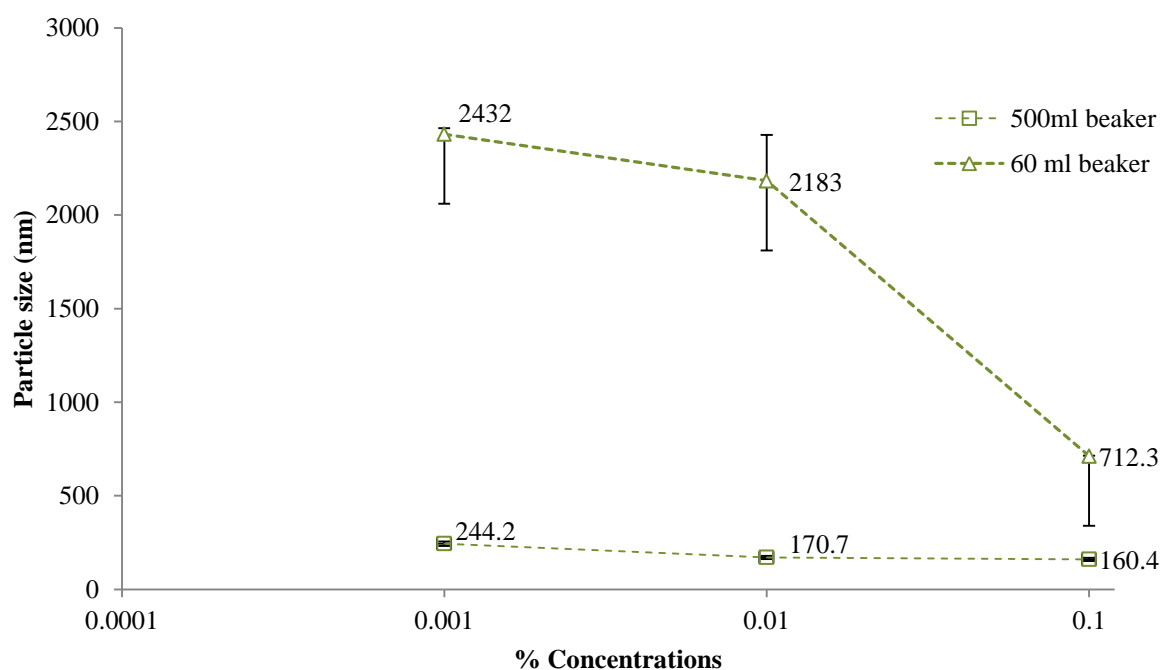


Figure 4-1 The comparison of hydrodynamic particle sizes of varied concentrations in 500 ml beaker and 60 ml beaker for 15 minutes of dispersion at concentrations of 0.001%, 0.01% and 0.1%

Sonication power and sonication time both affect the particle sizes as shown in the **Figure 4-2**. However, the sonication time is inversely related to the particle size. This can be seen from the **Figure 4-2** that shows when the sonication time is increased to 10 minutes, for any specific level of the power input the particle size decreases. This experiment was not carried out for 0.01% and 0.001% concentrations, since the change in the particle size variation was not appreciable enough.

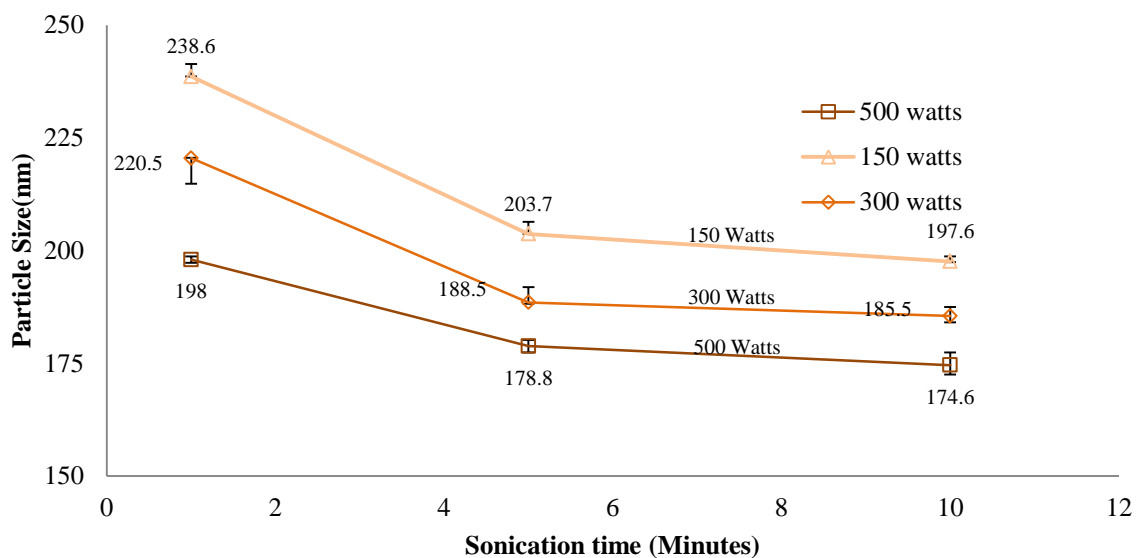


Figure 4-2 The variation of 0.1% CuO nanofluid hydrodynamic particle size due to the change in sonication time and sonication power

Later, the effect of concentration on particles was also gathered with the use of different dispersing devices that can be seen from the **Figure 4-3**. The lowest particle size was obtained using Sonic's Ultrasonic device. The largest particle size was recorded using Goldrich Shear mixer.

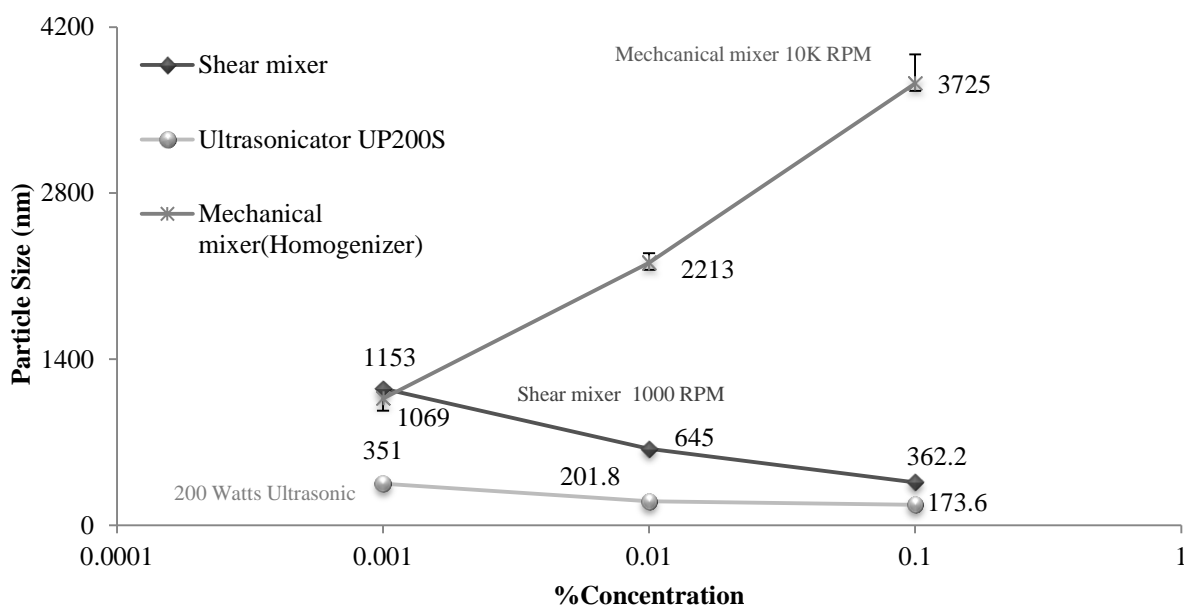


Figure 4-3 Effect on hydrodynamic particle sizes of CuO nanoparticles by using different dispersion methods

4.2 Modification of CuO Nanoparticles

FTIR analysis of the modified NPs showed chemically bonded carboxylate attachments on the surface of the NP. The FTIR results of the different modified CuO NPs are shown in **Figure 4-4**, which indicates the modification due to the carboxylate attachment of either uni-dentate or bi-dentate chain on the CuO NP. Different reaction conditions were used demonstrating these surface attachments of functional group to the CuO NP.

Surface treated NP samples show attachments of carboxylate from range of 1300-1750 cm^{-1} . This is a range showing three different methods of carboxylate attachment groups a) uni-dentate, b) bi-dentate and c) bridging that is also stated by Jiang et al., (2010).

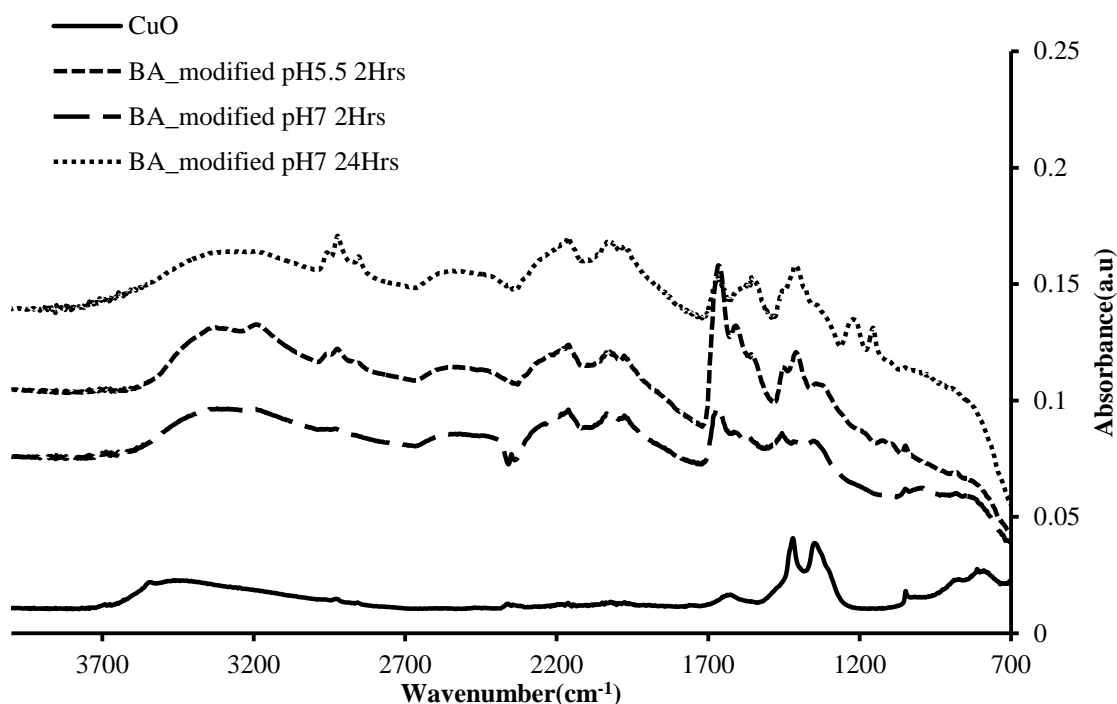


Figure 4-4 Modified CuO nanoparticles by using butyric acid as the reagent; a) CuO nanoparticle original particles; b) CuO nanoparticle modified using BA (Reaction time 2 hours and pH5.5); c) CuO nanoparticle modified using BA (Reaction time 2 hours and pH7); d) CuO nanoparticle modified using BA (Reaction time 24hours and pH7)

4.3 Detection of Cu Ion Release in Deionized Water

The CuO NPs ion release was measured by dispersing NPs in water. First the sedimentation of NPs was carried out over a three days period. The ion release in water over this period of days discharged significant amount of Cu⁺⁺ ions. This discharge was measured using ICP-OES. The release of copper ions in water is shown in **Figure 4-5**. The release of Cu⁺⁺ ions seems substantially high, since the released amount has shown a logarithmic trend of increment. The productive data of ion release can help in analysing the release rate of ions for metal oxide NPs. In the case of CuO ions, the release rate can be estimated by the simple logarithmic chart as shown in **Figure 4-5**.

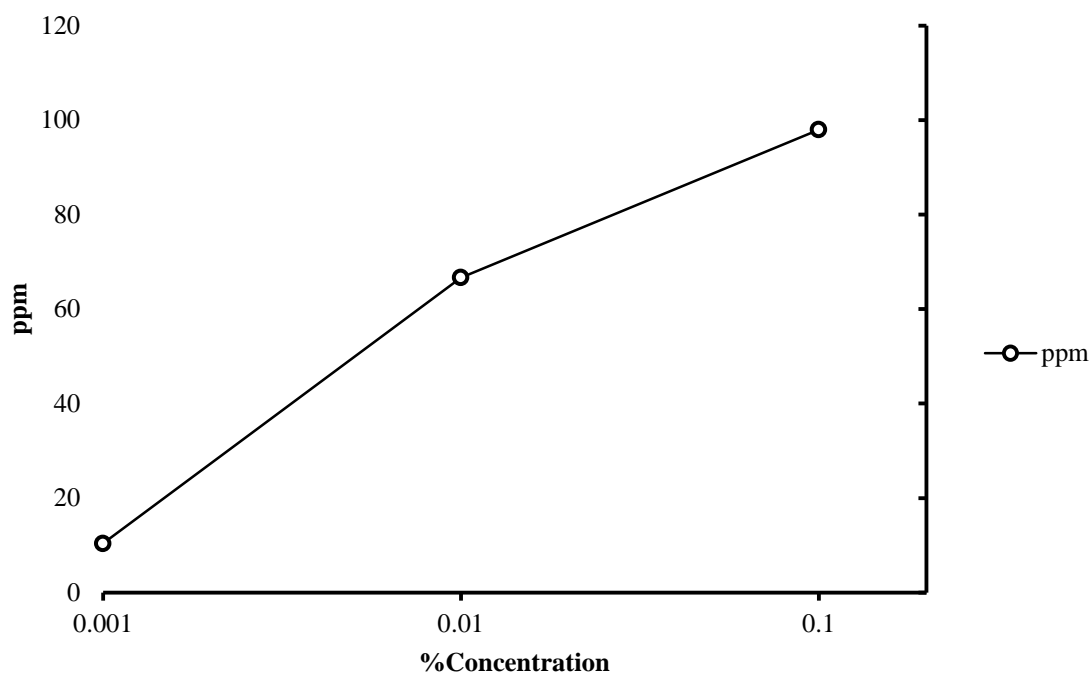


Figure 4-5 ICP results of Cu ion release in deionized water

Further, the microwave digestion of the raw CuO NP`s was also carried out and later ion release of these particles was recorder to be 80ppm, this was done to compare with the sediment particle`s ion release. It was found that the ion release of raw CuO NPs is higher than the two concentrations i.e. 0.001% and 0.01%, whereas 0.1% concentrated CuO NPs suspension demonstrated higher rate of ion release to that of microwave digested particles.

4.4 Comparison of Thermo-Physical Calculation of Simulation and Experiment of CuO Dispersion

Contrast of experimental and simulation thermo-physical quantities have been explored in this section. The comparison between two different procedures; simulation and experiment is carried out; however, the volume fraction was kept as a constant parameter in both procedures.

4.4.1 Viscosity of CuO Dispersion in Water

The simulated viscosity of CuO NCs dispersed in water is coherent to the experimental trends reported in the literature. The viscosity of the TIP3P water model is decreasing with increasing environmental temperature as shown in **Figure 4-6**. These simulated trend values are highly correlated with achieved results (Wu et al., 2006, Gonzalez and Abascal, 2010). The simulations carried out from temperatures around 298-300K, gave the viscosity of TIP3P model as 0.321-0.311 mPas. Whereas, the experimental value obtained in this work was around 0.59 mPas, these values can also be compared with Shen and Freed (2002) achieved viscosity of 0.5 mPas at 300K using simulation technique of Langevin dynamics. The viscosity values obtained in this work were higher, because of the higher heat conduction through the system and the use of the DPD potential. A decrease was observed for the viscosity of the TIP3P water model with the increasing temperature of the system. This is a usual phenomenon for any liquid, as the temperature is increased the molecules start to expand, which leads to anomalous decrease in viscosity.

Experimental viscosity results of dispersing CuO NPs in deionized water were gathered using TA AR1500Ex rheology instrument and compared to the data of Nguyen et al., (2007), and the viscosity obtained from genetic algorithm-neural network (GANN) method (Karimi et al., 2011), which are shown in **Figure 4-6**.

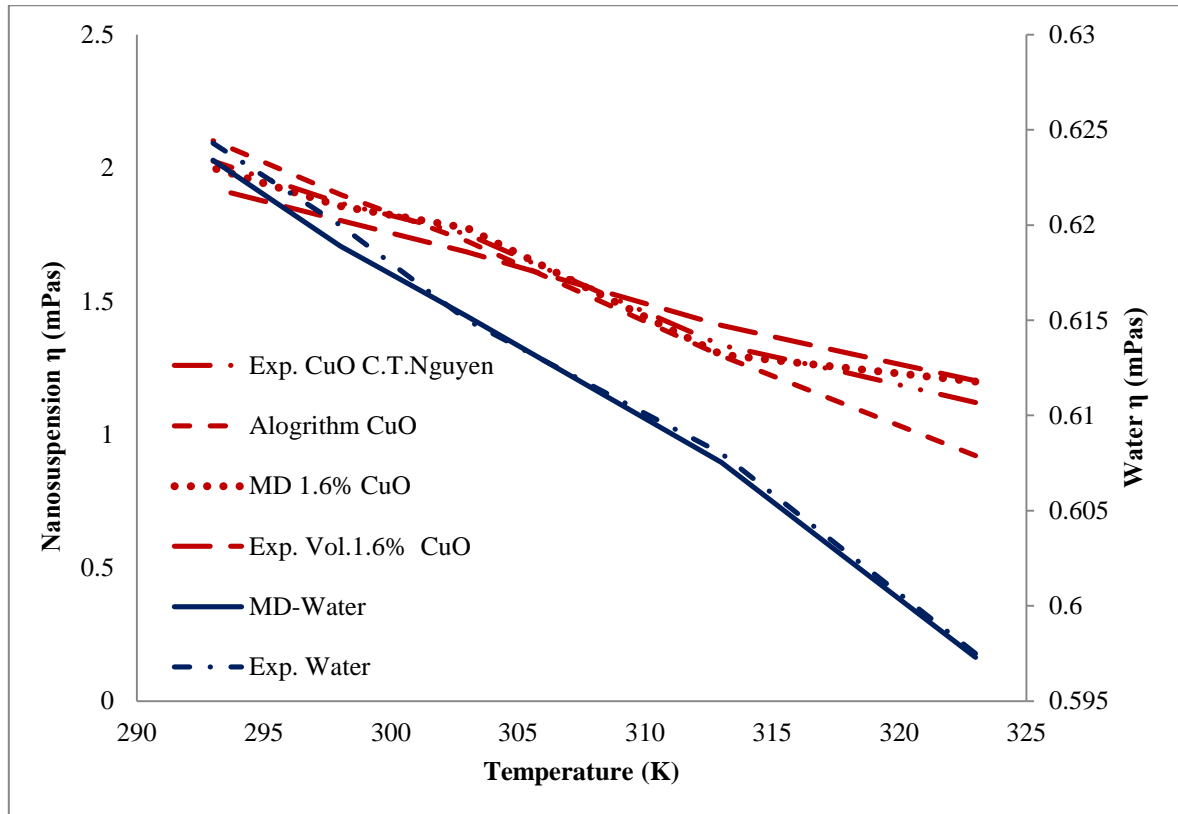


Figure 4-6 Comparison of experimental and MD simulation viscosity results of CuO nanosuspension and water

4.4.2 Thermal Conductivity of CuO Dispersion in Water

The thermal conductivity was simulated and compared with literature (Karthik et al., 2012); further results are shown and compared in **Figure 4-7**.

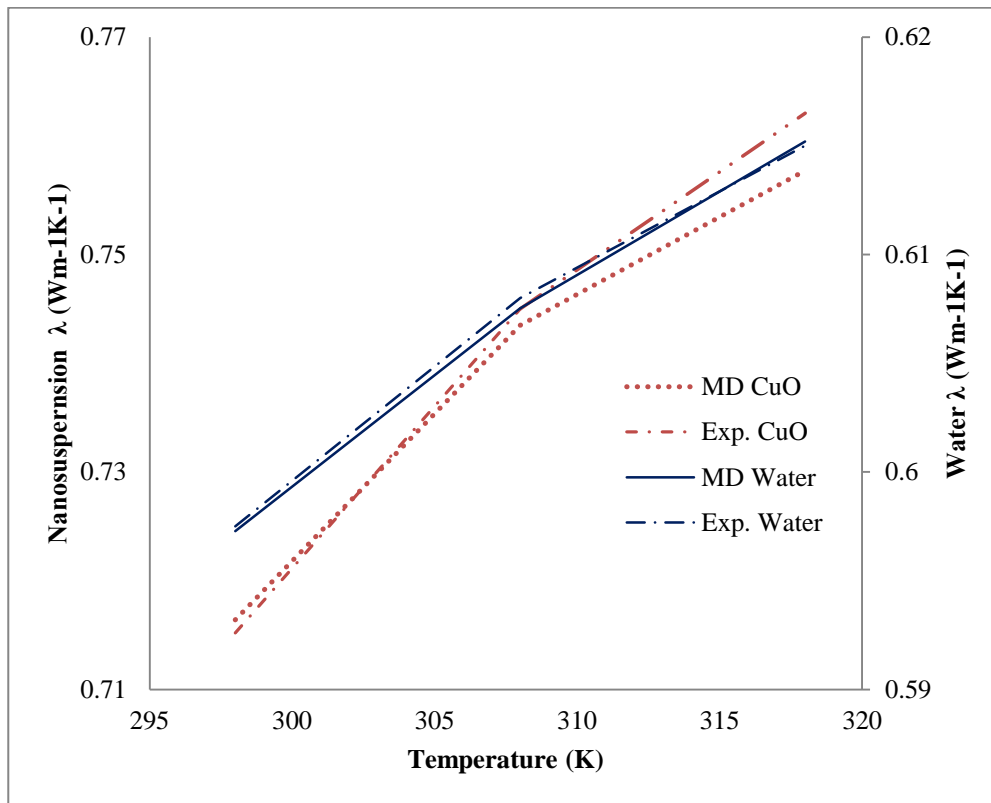


Figure 4-7 Thermal conductivity of water and CuO Nanosuspension, measured using MD simulations and experimental thermal conductivity was obtained by literature (Karthik et al., 2012)

Experimental results of thermal conductivity were obtained from Karthik et al. (2012) and compared with the results recorded from the simulations as demonstrated in **Figure 4-7**. A simulative thermal conductivity value of $0.712 \text{ Wm}^{-1}\text{K}^{-1}$ at 298 K, was in good coherency with the results obtained experimentally, which was $0.710 \text{ Wm}^{-1}\text{K}^{-1}$. The 3- ω experimental methodology was used by Karthik et al. (2012) to find the thermal conductivity of CuO nano-fluid. Whereas, simulations were performed and equilibrated for different time steps to obtain the desired results coherent to the experimental data. Furthermore, for different temperatures, the study was compared with the experimental data results with Karthik et al., (2012).

4.4.3 Diffusion Coefficient of CuO Dispersion in Water

Establishment of water self-diffusion coefficient was carried out initially, and then CuO NCs diffusion in water was modelled to extend further analysis as shown in **Figure 4-8**.

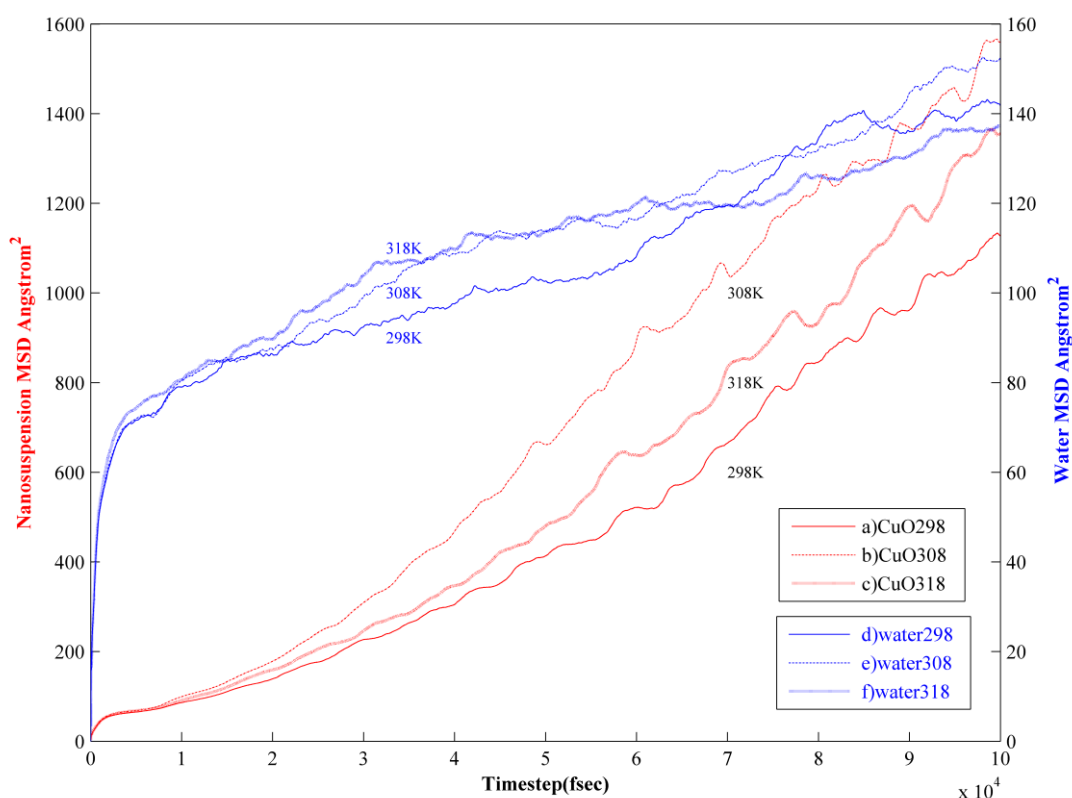


Figure 4-8 Diffusion coefficient of the water at ---298K, ---308K and ---318K and CuO nanosuspension at ---298K, ---308K and ---318K

The blue line results shown in **Figure 4-8** are the self-diffusion coefficient of water molecules simulated at different temperatures. From **Figure 4-8** the calculated diffusion coefficient shows a linear increase in the diffusion of the water with temperature increment and this can be correlated by TIP3P water molecules carried out by Markovitch and Agmon (2008); from which it was found the TIP3P water molecules at 320 K results are in good agreement with this study result of water molecule's self-diffusion coefficient

and other experimental data value as $2.272E10^{-9}$ m²/s (Eisenberg and Kauzmann, 1969). In comparison to reference work, in this work values obtained are higher, due to the simultaneous implementation of two different potentials of dispersion; DPD and SPH. It is also known that implementation of DPD potential helps in decreasing computation time steps for equilibrium convergence and higher accuracy results are achieved apart from pure BD (Español and Warren, 1995). Moreover, another difference may arise due to the use of different simulative packages and their different routes of calculation. However, while considering these discrepancies the results obtained are in a good correlation with others.

With establishment of the initial water model's self-diffusion coefficient as a reference study, practical simulative model design of CuO NCs diffusion has been initiated in water fluid. However, the reported comparative study can be novel in itself; since there is no available data on the simulation of CuO-NC in water. The results obtained for the diffusion coefficient of the CuO NP model are shown in **Figure 4-8**.

The diffusion coefficients found in **Figure 4-8** are at different temperature correlations; from 298K to 318K. The diffusion interaction of CuO NC particles was simulated in the water molecular system. For 298 K, obtained value is low when compared to higher temperatures, which reflects that the power of diffusion is increased with temperature input and this is the same for the water based model. In contrast to, CuO NC's diffusion coefficient achieved in this work that was concurrent to the work of CuO Nano-rod diffusion coefficient in water by Cheong and Grier (2010), in which he measured the diffusion coefficient with holographic video microscopy and obtained the value of $2.31E-7$ m²s⁻¹ at 298K.

4.4.4 Radial Distribution Function of CuO Dispersion in Water

For a better understanding of the aggregation phenomenon, radial distribution function (RDF) was introduced because it informs about pair distribution function of molecules and different researchers (Kirkwood, 1935, Born and Green, 1946, Kirkwood et al., 1950) established equations for averaging densities to describe the cut-off distance between molecules. The calculated RDF in this work was used to estimate the aggregation of the CuO-NC water system. The RDF contrast between different temperature levels for simulation with and without NCs was carried out. As shown in **Figure 4-9**, the water simulation RDF showed much less aggregation since the peaks are smooth rather than being intense. Further detailed description appeared from the **Figure 4-9**, that the peaks are not dominating the cut-off distance for water system; which were presented mostly within the range of 0-0.5nm. This could be due to the movement of molecules in the system, but not caused by the effect of agglomeration.

Similar data have been found in other studies for radial distribution function (RDF) of water and cut-off distance, similar to the results in **Figure 4-9** achieved in this study, which is between the distance of 0.1-0.5 nm, based on the water TIP3P model and SPC-E model (Wang et al., 2009). However, water models investigated by Wang et al., (2009) showed the difference among their RDF between two different styles of simulation in terms of coarse graining level and atomistic level. Clearly their results of atomistic level are in excellent agreement with those achieved in this work, including the diffusion coefficients that are presented at different temperatures.

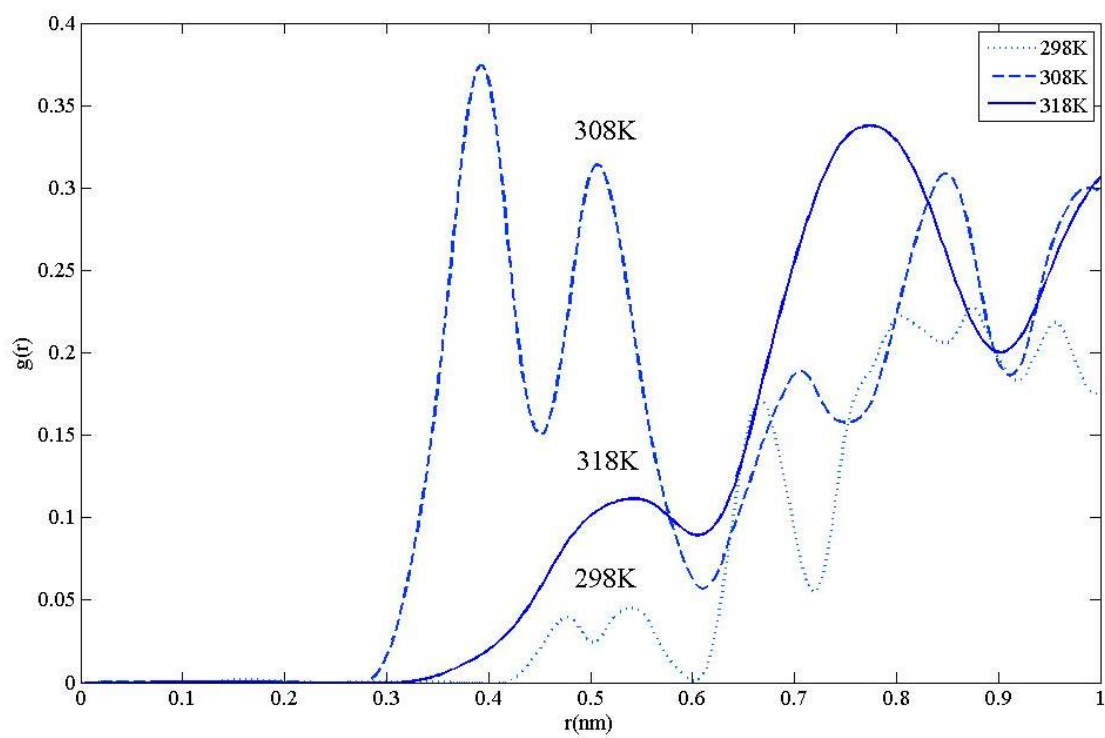


Figure 4-9 Radial distribution function of the water system

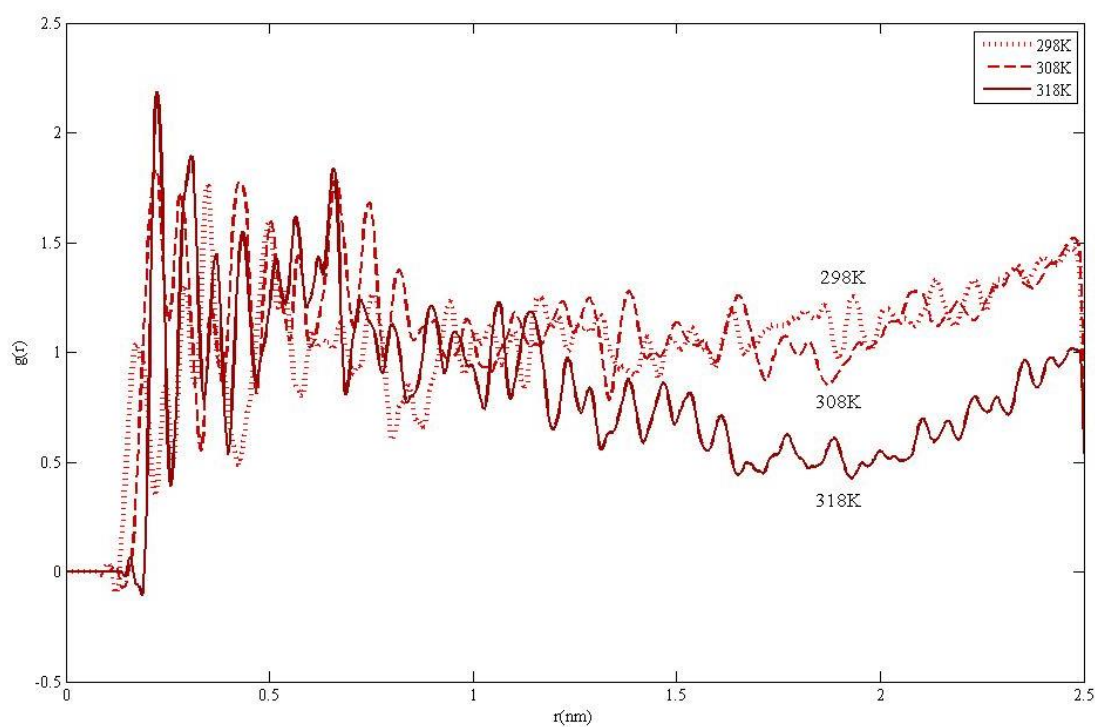


Figure 4-10 The comparison of RDF of CuO nanoclusters in water under different temperatures

Table 4-1 Highest RDF of CuO nanoclusters in water under simulated temperatures

Temperature (K)	Highest intensive signal g(r) water	Highest intensive signal g(r) CuO in water
298	0.325	1.600
308	0.370	1.800
318	0.210	2.200

The RDF's of CuO NCs water system is presented in **Figure 4-10**. Some further results of RDF analysis had shown simulative approach in more details. It can be seen from the **Figure 4-9**, that simulation of the TIP3P water model does not have any aggregation since the peaks are not strong but smooth. Whereas, the RDF results of **Figure 4-10**, have strong peaks representing aggregation of CuO NCs in water under different temperatures. **Table 4-1** gives the highest RDF intensity reading of 0.37 g(r) at 298K for water, and 2.20 g(r), for CuO NCs in water system at 318K. As the temperature was increased, the highest simulated intensities were similar for a particular system. This might be because there was not enough temperature difference to generate the observable intensity difference.

The water system RDF results interpretations demonstrate better dispersing capability when temperature is increased, whereas the CuO NC water system proves better dispersion at low temperatures. This difference between the water and water with NP system can be explained by kinetic molecular theory i.e. as the temperature is increased the molecular collision increases and this provides a chance for the water molecules to expand, thereby low peak RDF intensities are recorded at higher temperature. However, NPs water system shows high intensity RDF at high temperature that can be explained by the heat conduction of NP; which dissipates the incoming heat homogeneously within the NP itself, ultimately causing the aggregation to increase. This increasing aggregation shows high peak intensities at high temperatures.

4.5 Comparison of Thermo-physical and Rheological Properties from Simulation and Experiment of CuO Nanoparticle Dispersion in Alkanes

Alkane liquids is widely used for heat transfer applications (Sonawane et al., 2012). However, the thermal transfer capability of paraffin is very low due to the monomer nature (i.e. C₂₀H₄₂). The implementation of CuO NPs in paraffin is expected to improve its heat transfer capability, and enhance the thermal stability properties.

4.5.1 Experimental and MD Viscosity Analysis of CuO Nanoparticle Dispersion in Alkanes

The major fluidic property that is also affected by adding NPs to the system is the viscosity. Viscosity can be tested and also simulated as part of the experimental and simulation strategy. The contrast has been made between the pure alkane and alkane with NPs system.

The experimental analysis was conducted to investigate the viscosity of the uncertain alkane liquid Dodecane. The original viscosity of the alkane is found to be 0.83 - 1.40 mPas at room temperature, 297K. This was conducted to investigate the change in viscosity of alkane based nanofluid. Based on previous simulations, the properties of heat transferability, thermal diffusion of alkane are all affected by the viscosity of the system. In turn, the viscosity in biological and energy systems is affected by NP additives as shown in **Figure 4-11**.

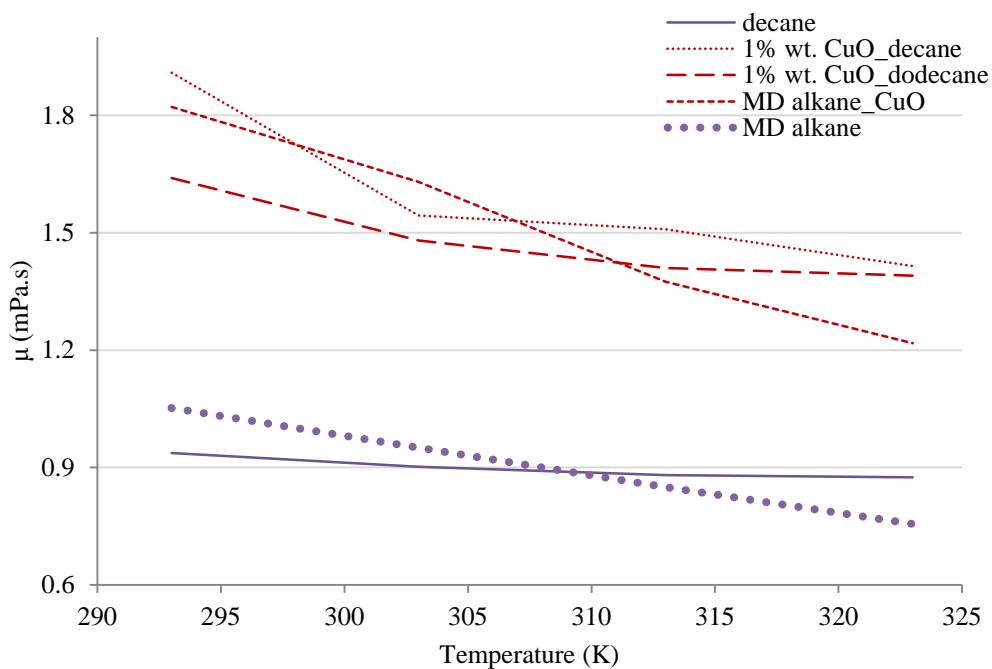


Figure 4-11 Experimental and simulation viscosity of pure alkanes (purple) and alkane with CuO nanoclusters (red) additives against temperature rise

4.5.2 Viscosity of Alkanes

MD simulations were also performed to calculate the viscosity of the system by Green-Kubo formulation method. The results of the viscosity of alkane with NCs were in good agreement with the results achieved by simulations. However, the correlation function took time to converge and this problem is also illustrated in **Figure 4-11**. This shows viscosities of the alkanes are in good coherence with the data achieved by previous studies (Queimada et al., 2005), as tabulated in **Table 4-2**.

Table 4-2 Viscosity of alkanes from our work and comparison with the work of others

<i>Temperature (K)</i>	<i>μ(mPas) This work</i>	<i>μ (mPas) Ref. Queimada et al., (2005)</i>	<i>μ (mPas) Alkane+CuO (This work)</i>
303	0.951	0.900-0.950	1.630 ($\Delta t= 15.500Ps$)
313	0.750	0.720-0.760	1.375($\Delta t= 13.500Ps$)
323	0.656	0.625-0.680	1.218($\Delta t= 12.300Ps$)

4.5.3 Diffusion Coefficient of Alkane and CuO Nanoparticle Dispersion in Alkanes

The diffusion coefficient of CuO-NCs with alkane at different temperatures shows reasonable effect of diffusion. The data achieved by Ferdous et al. (2012) is in the range of $3.7E-10$ m²/s to $5.70E-13$ m²/s at several concentrations, which are similar to the simulation values achieved in this study. **Figure 4-12b**, shows the dispersion of NCs with alkane interfaces.

When the molecular loading (i.e. the number of atoms) is increased, molecular collision between alkane and NCs becomes more intense and more energy barriers come in the way of diffusion. The governing diffusion coefficient decreases due to intensive collision of molecules.

Coppens et al., (1998) found in their study that lattice Monte Carlo simulations on diffusion depend on the lattice topology. They observed a decrease of diffusion coefficient with increasing concentration. For weakly connected lattice of silicates the self-diffusivity decreases in a non-linear fashion. The same is the case with readings obtained for the diffusion coefficient of alkanes as shown in **Figure 4-12 a**; that is higher

than that of the system with NCs. This is due to the loading of NCs in the system creates collisions to increase, making the diffusion coefficient less.

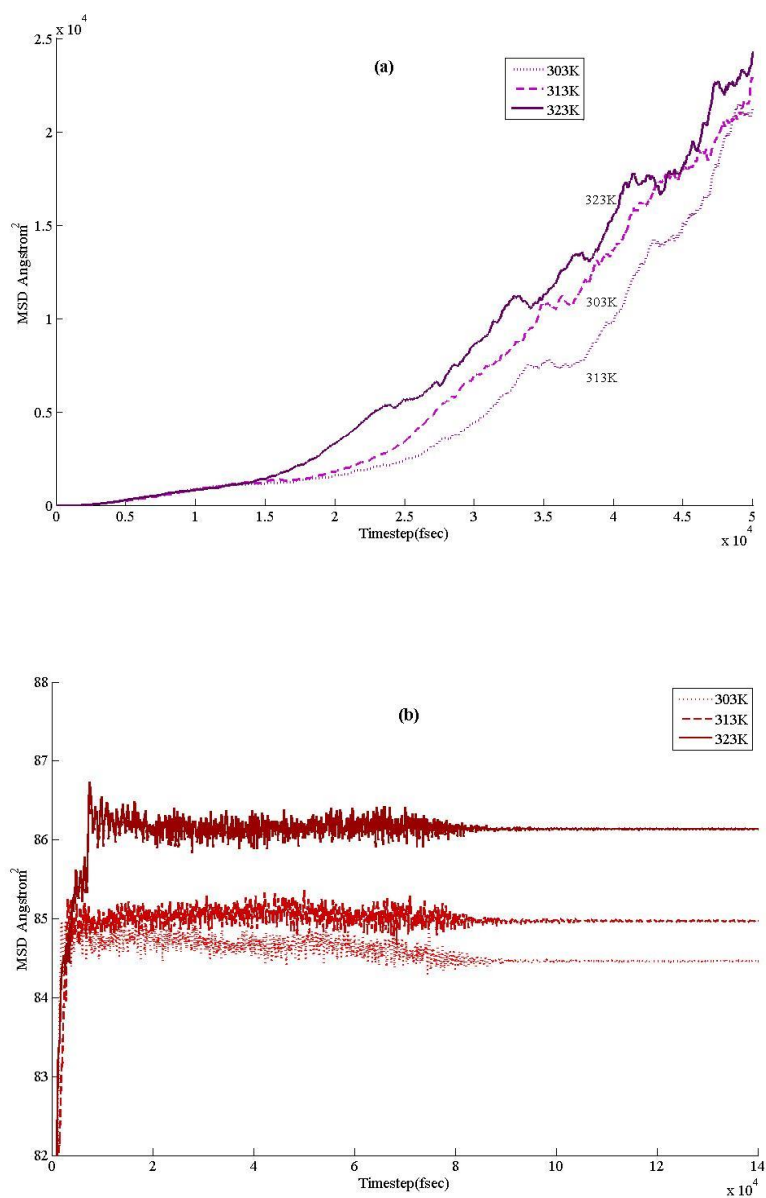


Figure 4-12 Diffusion coefficients; a) diffusion of alkanes at different temperatures. b) diffusion of alkanes with CuO nanoclusters. Values are mostly in the region of $1\text{E-}8$ to $1\text{E-}14$ m^2/s

4.5.4 Thermal Conductivity of CuO Nanoparticle Dispersion in Alkanes

The thermal conductivity of pure alkane was used as a control test. Later, this system was used for comparison with the NCs modified system. Some significant studies carried out before are also collected in alkanes' thermal properties. The thermal conductivity for alkane was found to be around 0.15 W/mK (Rastorguev et al., 1974).

One of the effective properties of heat transfer fluids through the system is thermal conductivity. This is used for specifying the applicability of the hydrocarbons as alkanes in the thermal storage applications. The addition of CuO NCs in hydrocarbon fluid gives a huge rise to the heat transfer capability as shown in **Figure 4-13**. Simulated results demonstrate increase of about 150-200% for thermal conductivity of the nano-modified system.

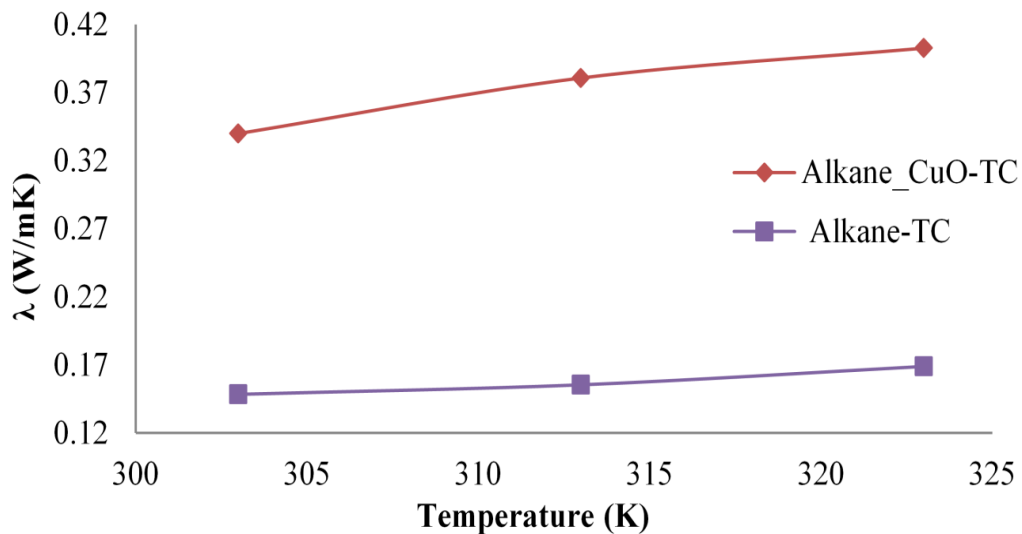


Figure 4-13 Thermal conductivity of alkane with CuO nanoclusters; red line with diamond button is thermal conductivity for CuO with alkane and purple line with square button is for thermal conductivity for pure alkanes

The results of thermal conductivity of the pure alkane in **Figure 4-13** are in good coherence with results achieved by Rastorguev et al., (1974). Moreover, the thermal conductivity of the pure alkane was compared to that of the alkane CuO nanosuspension.

4.5.5 RDF of CuO Nanoparticle Dispersion in Hydrocarbon

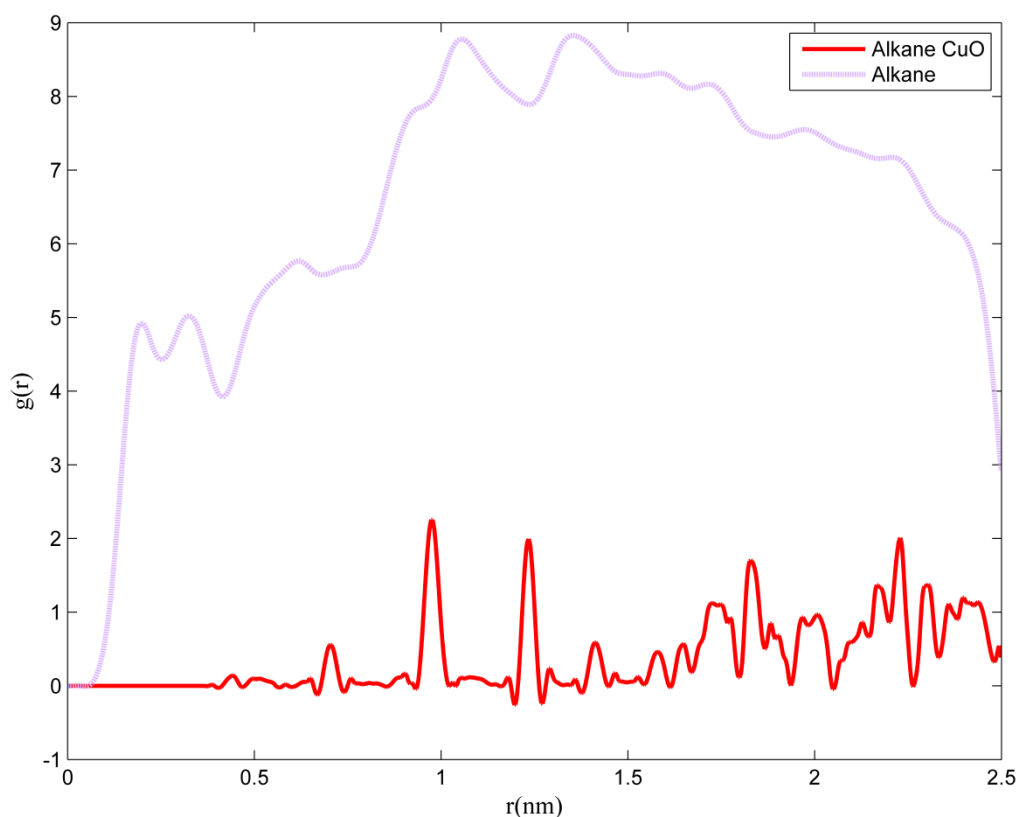


Figure 4-14 RDF figure of alkane CuO nanosuspension and alkane

The RDF of the alkane nanosuspension and alkane system is shown in **Figure 4-14**. The alkane system demonstrates less agglomeration, whereas, the alkane nanosuspension shows high agglomeration. The peaks of the alkane are weak and smooth compared to the peaks of the alkane nanosuspensions. The strong peaks of the alkane nanosuspension indicate that there was high agglomeration present due to the addition of NCs. But when

the particles are not present it does not show agglomerations. The smoothness in the curve is shown at high intensity $g(r)$ for the alkane system. The high intensity is due to the high probability of finding the particles far apart; however, for the alkane-CuO system the probability of finding the particles near to each other is higher. Moreover, this is why the $g(r)$ intensity for the alkane-CuO system is lower and does not show high intensities for smooth peaks as for the case of the alkane system, nevertheless it shows high intensities for the strong peaks.

4.6 Modification of CuO Nanoclusters Using Short Chain Functional Group

The NCs were modified experimentally using a BA functional group; this was also replicated on the simulation platform. This was also simulated to analyse the effect of modifications and predict different dispersion factors. In contrast it was found that modification of CuO NCs has a similar effect on both criteria's when performing experiments. Furthermore, this helped in understanding the diffusion rate in connection with the agglomeration effect. The diffusion of the system with and without a functional group was found to be different and suggested that the diffusion rate decreases due to the attachment of a functional group, this can be seen from **Figure 4-15 a** and **Figure 4-15 b**.

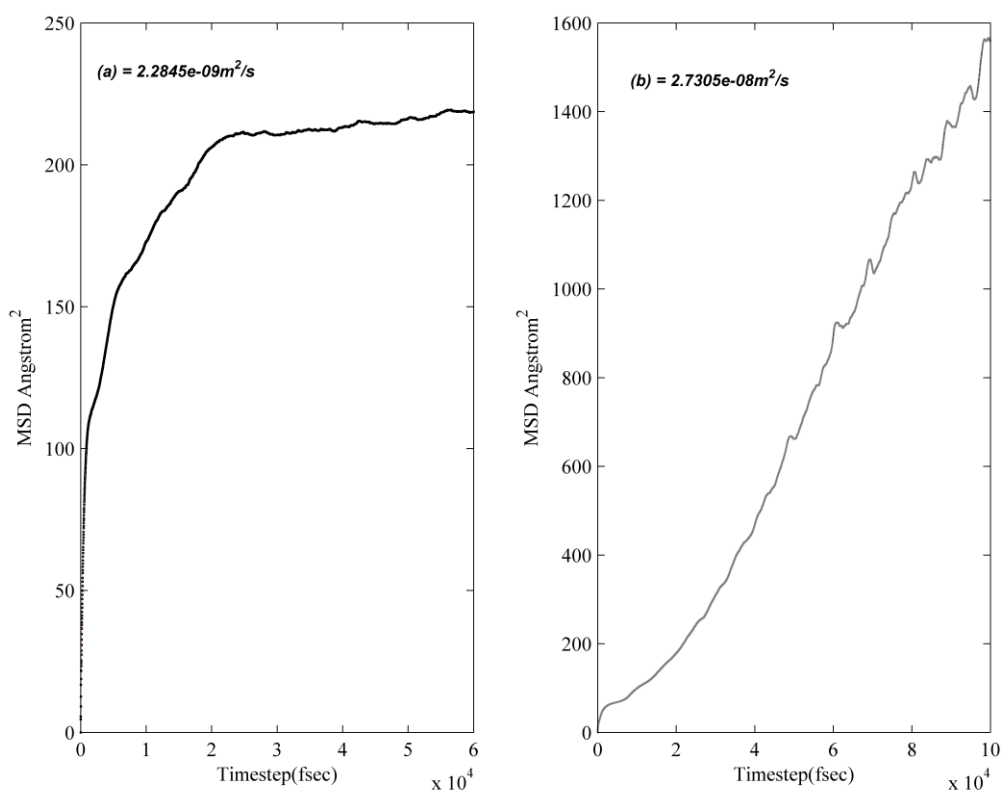


Figure 4-15 Diffusion coefficients; a) diffusion coefficients of CuO nanoclusters in water with butyric acid ($1.517\text{e-}09\text{m}^2/\text{s}$); b) diffusion coefficients of CuO nanoclusters in water ($2.73\text{e-}08\text{m}^2/\text{s}$)

From **Figure 4-15**, it can be seen that the system of the CuO NCs with water has a high rate of diffusion, whereas, the system of NCs with functional group attachment has a low rate of diffusion. This could be due to intensification of agglomeration and the addition of the functional group. The BA functional group attachment to NC causes decrement of the rate of diffusion in the water system because NC population demonstrated coalesces due to functional group moieties. Furthermore, the rate of diffusion is directly related to the effect of agglomeration. Hence, agglomeration causes the rate of diffusion to decrease significantly.

4.7 Summary Outline

Results obtained for the experiments and simulations performed for research work is summarized as follow;

1. The results of different dispersing tools demonstrated that the best device for dispersion of nanoparticle is Ultrasonicator. This tool uses acoustic waves to disperse nanoparticles in fluid. The vibrating sound waves break down the agglomeration of particles. Ultrasonicator homogeneously disperses the particles.
2. The surface modification of CuO nanoparticles using short chain carboxylate functional group i.e. Butyric acid demonstrated three different modification styles a) uni-dentate, b) bi-dentate and c) bridging.
3. ICP outcomes presented more release of ions for 0.1% concentrated CuO nanoparticles than the 0.01% and 0.001% when suspended in water, also, microwave digested particles represented less release of Cu ions.
4. The viscosity estimated using simulation for CuO nanoparticles dispersed in water shows fluctuation of 7-8% to the experimental obtained outcomes.
5. The error difference found between simulation examinations of thermo-physical quantities to experimental study was due to the velocity seeding and pressure fluctuation.
6. The RDF results of CuO nanoparticles water suspension presented aggregation fluctuation through the simulation phase. Whereas the water system was non-aggregative due to uniformity of the molecular system.
7. The diffusion coefficient measured for modified CuO-water system was similar to the water system, i.e. it demonstrated slow diffusion rate to that of the unmodified CuO nanoparticle system. This can be explained further by RDF results, that shows more strong peaks, rather than the unmodified CuO-water system, ultimately accounting for the low diffusive capability of nanoparticles. Further short chain carboxylate functional group attachment causes the particle to act in hydrophobic nature in an aqueous environment; hence causing the diffusivity to decrease.

Chapter 5

Discussions

Chapter 5 Discussions

In this thesis an attempt to explain the necessity and the importance of NPs for thermo-physical, rheological and physiochemical alterations in properties is provided. In this study use of metal oxide and metal NCs (i.e. CuO and CeO₂), through different channels have been further opened in nanotechnology. The results in Chapter 4 show that the studies of NCs dispersion in fluids on the simulative and experimental ground hold their own significance. However, as the experiments are necessary, likewise, the latter predicted results using simulations are also beneficial for the study. Simulations help understanding the mechanisms on the mathematical and numerical aspect. The results achieved from the basic dispersion study are the base conditions for further studies on the simulation and modification experiments. Similarly, due to this reason the experimental results of basic dispersion studies were the foundation of the simulation boundary conditions. Later, these boundary conditions were implemented in a simulation platform using LAMMPS.

The fundamental studies extrapolated the underlying condition of interaction during the dispersion of the NPs in different base fluids. These variables or parameters are hydrodynamic radius, hydrodynamic interactions, hydrodynamic liquid layer, hydrodynamic liquid particle interactions, interaction potentials, dispersion mechanism, Brownian effect, atomic interactions, forces exhibition during interactions and bonding variable. Without the basic studies of NP dispersion, it would have been difficult to define the simulation system. Hence, extrapolating the readings from the simulation system; may have retaliated with the experimental outcomes. Therefore, a basic understanding of the variables and parameters was necessary. Different properties were quantified on experimental and simulation platform. Experimental quantification was done by characterizing equipment. The simulation results were quantified by the convergence of the results.

Throughout the study, BM is the main mechanism behind nanofluid dispersion. BM exhibits four major criteria, a) liquid layering (liquid-particle interface), b) effect of NC agglomeration, c) heat transport through NPs and d) hydrodynamic effect. The liquid layering effect over the NP is due to the interaction with fluid that causes the formation of hydrodynamic layer. The formation of this layer gives a non-realistic size of NP; this size is associated with the hydrodynamic radius formed over the NP surface. This liquid layering is responsible for increasing the true NP size to hydrodynamic particle size as shown in **Figure 5-1**.

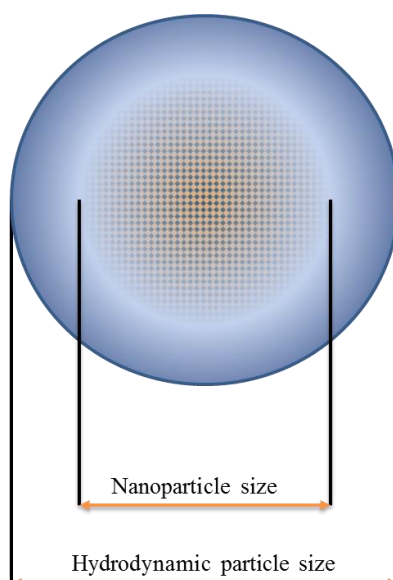


Figure 5-1 Hydrodynamic nanoparticle size

There were two major properties that needed proper quantification a) viscosity change and b) thermal conductivity. Viscosity in the simulation platform is performed using the Green Kubo's method (Lee, 2007). Thermal conductivity is related to the effect of the thermal transport of energy within the system (Lee, 2007). In simulation, there are two major types of autocorrelation functions that define the convergences of the thermo-physical quantities; a) stress autocorrelation function defines the achieved viscosity to be correct on its convergences and b) heat autocorrelation function defines the achieved thermal conductivity to be correct because of its convergence of results. Scaling the

velocity accurately is a good practice and gives a real physical effect that helps the system to reach equilibrium. As indicated in **Figure 5-2**, the heat autocorrelation explores the barriers beyond the experimental boundaries and justifies the obtained simulated results on its convergence.

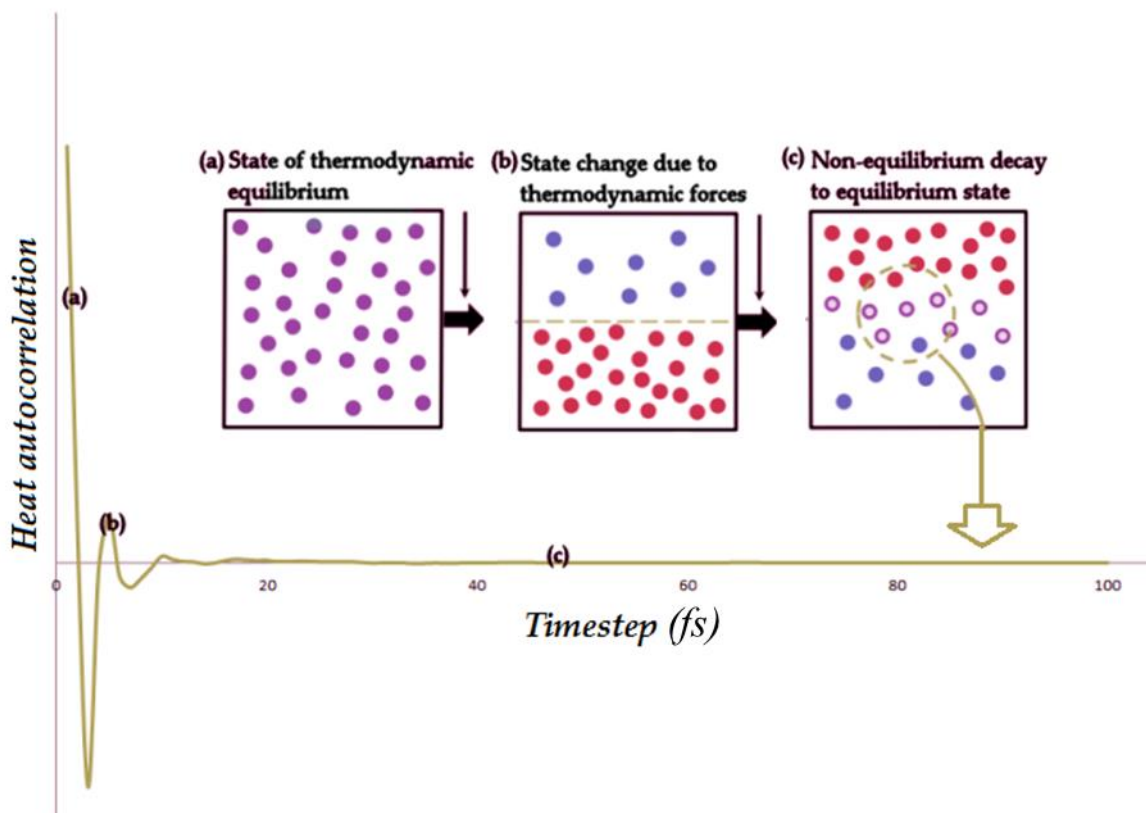


Figure 5-2 Schematic illustration of equilibration convergence of heat autocorrelation

The graphical result in **Figure 5-2** explains the process of the integration of non-equilibrated system to equilibration. At step a) the system starts with a thermo-dynamical equilibrium, however, the system is not at equilibrium state. Step b) the thermo-dynamical conditions are changed due to implementation of the thermal ensemble; consequently the system tends to go towards equilibrium. Step c) the non-equilibrium system moves to the equilibrated level of convergence. This process is followed during the equilibration of the thermo-physical quantities.

The convergence time steps depend on the volume and quantity of the atoms in that system. For the larger system, a large number of computational powers and time step will be required for convergence of results. Additionally, the diffusion constant helps understanding the system dispersion and aggregation status. Diffusion constant also predicts the accurate results of viscosity. Furthermore, in this study of MD simulations, NPT ensemble was used. This ensemble assists in controlling the temperature and pressure of the system.

5.1 Basic Dispersion Study

The study of the NP dispersion was carried out to understand the dispersion phenomenon. Subsequently, these parameters were considered for simulation purposes for the nanofluid dispersion system. The readings that were considered for simulations were mostly related to particle size and zeta-potential. These values were primarily used to understand the underlying hydrodynamic effects of the system.

Figure 4-1, represents sonication of NPs in different beakers that can affect the hydrodynamic particle sizes of the NP. The NP sizes in the small beaker of 60 ml have biggest particle sizes of approximately 2400nm at 0.001% concentration level. Due to the heat dissipation being low, the suspension in 60 ml beaker boils up quickly, causing crossing of the saturation limit, and finally re-agglomeration takes place as stated in a previous study (Mandzy et al., 2005). In contrast to a 500 ml beaker, a totally different effect by varying concentrations from 0.001-0.1% was found, giving a good range of particle size of around 200-160-nm distribution with a similar sonication time as used for 60 ml beaker. For 500 ml beaker; heat dissipation is high due to a large beaker diameter and no agglomeration can be detected.

The second parameter that has a huge effect on particle size is sonication power and sonication time in **Figure 4-2**. The variation of hydrodynamic particle sizes due to the change in sonication power and sonication time is shown. The results show that as the

sonication power is increased, the particle size shows a decreasing trend where the lowest value achieved is around 160nm. However, the increment in time has an opposite effect; with increasing time the particle size decreases. This can be due to less agglomeration is found when the power is increased, as the breaking down of the agglomeration is high. Whereas, when the power is decreased to 150 watts, it gives the highest particle size at the lowest time period which is due to less de-agglomeration of the particles.

In **Figure 4-3**, the effect of dispersion of three different dispersing devices and their effect on the particle sizes are shown. It could be evaluated from the **Figure 4-3** that the best hydrodynamic particle sizes achieved is with an ultrasonic device. The ultrasonic device gives the best hydrodynamic size since it uses acoustic sound waves to break down particles and this is more homogeneous than the other devices that use shear forces to break down the lumps of particles. Finally, from basic dispersion studies it can be concluded that the ultrasonic device shows a high level of dispersion and agglomeration break down.

5.2 Experimental Modification of CuO Nanoparticles

Experimentally, the CuO NPs were modified to alter the properties of the NPs. For the modification studies carboxylate group was used for the surface modification of NPs. As the study is to alter the properties of the fluid using NPs, sometimes it cannot be achieved until the NPs are homogeneously dispersed in the fluid, therefore surface modification is necessary. The modification helps to alter the material property and enhances the stability of the dispersed particles by changing the surface charges.

Similarly, the CuO NPs were modified using short-chain carboxylate group, i.e. BA modification. This modification was confirmed using FTIR results that predicted the surface modification of the NPs. The peaks that indicate carboxylate modification are between the ranges of $1300 - 1750 \text{ cm}^{-1}$. Additionally, peak differences were considered within this particular range. Out of these peaks, three strong peak's differences were

taken and their interpretation revealed useful attachment chemistry. The attachment styles that were revealed were uni-dentate, bi-dentate and bridging attachment.

5.2.1 CuO Modification for 2Hours Butyric Acid pH 5.5

In **Figure 5-3**, the attachment of BA at pH 5.5 on CuO NPs is shown. To interpret the attachment chemistry regarding uni-dentate, bi-dentate and bridging attachments of carboxylate group it requires to take peak differences of two consecutive peaks. Thereby, it is known that if the peak difference is less than 110 cm^{-1} it signifies a bi-dentate attachment. If it is more than 200 cm^{-1} , it is an uni-dentate attachment and if the range is between $140 - 200\text{ cm}^{-1}$, it is a bridging ligand (Jiang et al., 2010, Zhang et al., 2006, Huang et al., 2007). **Figure 5-3** represents the difference of the peaks from $1667 - 1609\text{ cm}^{-1}$ is around 58 cm^{-1} that shows bi-dentate attachment to the CuO NPs, on the other hand, it also shows the uni-dentate attachment; when the difference of two peaks, from $1609 - 1410\text{ cm}^{-1}$ is approximately 200 cm^{-1} , this shows uni-dentate attachment to the CuO NPs. Therefore, the predicted structure for both attachments are shown in **Figure 5-4 a** and **Figure 5-4 b** respectively.

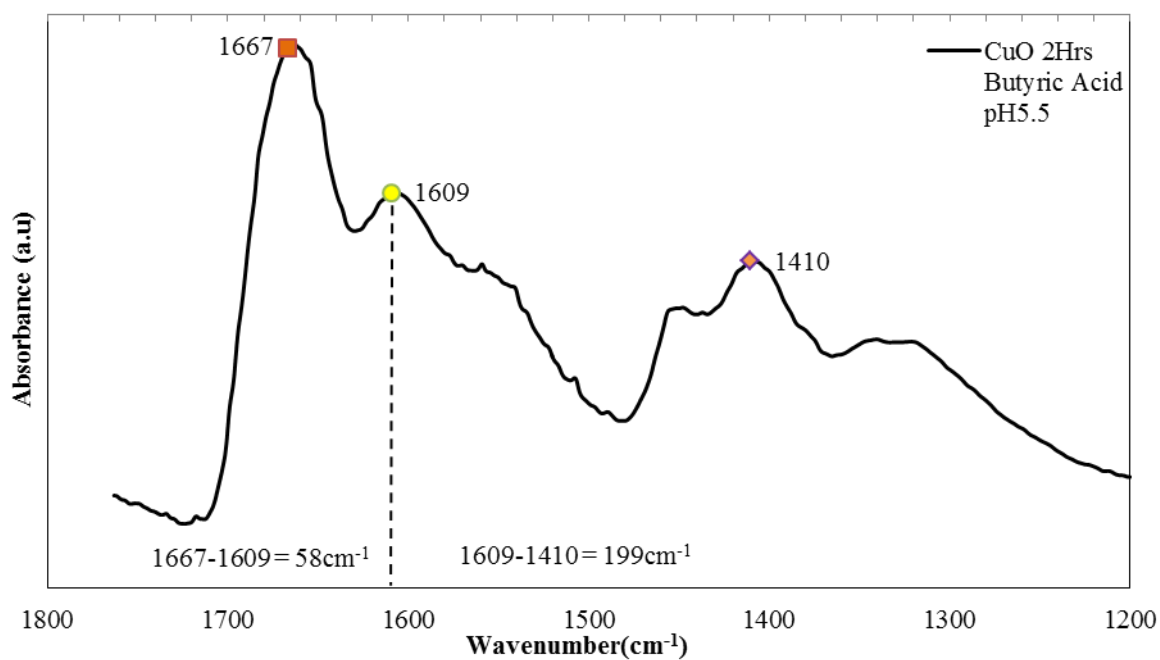


Figure 5-3 Butyric acid surface modified CuO nanoparticles using reagent at pH5.5 and reaction time of 2 hours

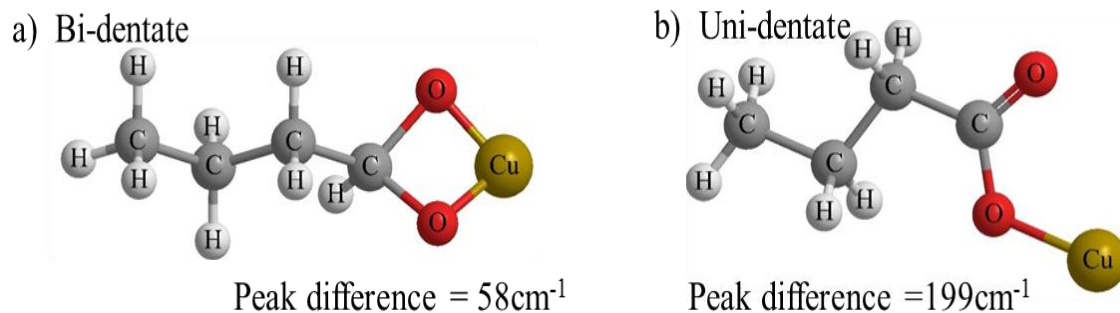


Figure 5-4 Butyric acid surface modified CuO nanoparticles prediction of chemical composition; a) bi-dentate attachment structure; b) uni-dentate attachment structure

5.2.2 CuO Modification for 2Hours Using Butyric Acid at pH 7.0

Figure 5-5, represents the difference of the peaks from $1456 - 1352 \text{ cm}^{-1}$ is around 103 cm^{-1} that shows bi-dentate attachment to the CuO NP. It also shows the uni-dentate attachment, when the difference of two peaks; from $1669 - 1456 \text{ cm}^{-1}$ is approximately 213 cm^{-1} . The predicted structures for both attachments are shown in **Figure 5-6 a** and **Figure 5-6 b** respectively.

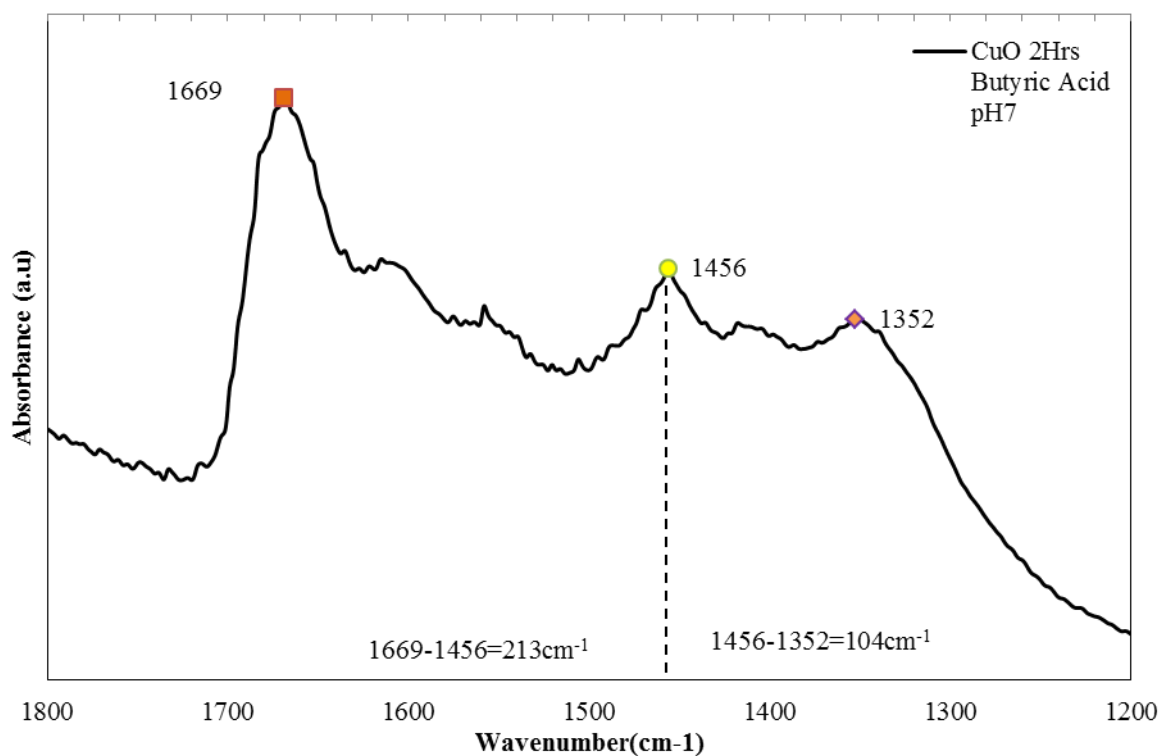


Figure 5-5 Butyric acid Surface modified CuO nanoparticles using reagent at pH7 and reaction time of 2 hours

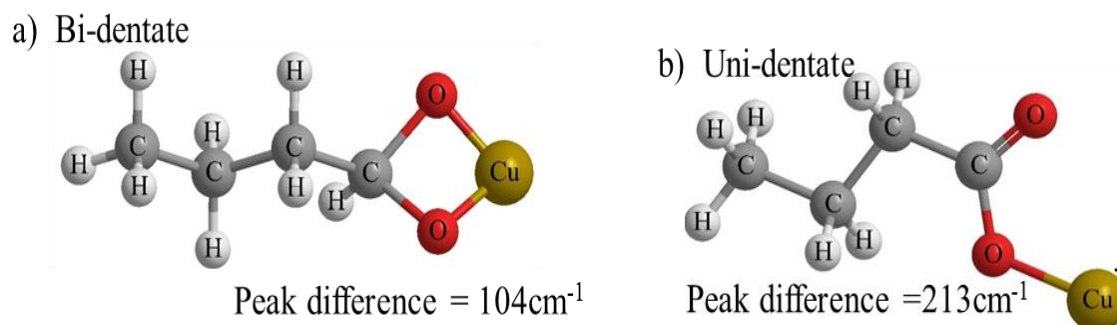


Figure 5-6 Butyric acid surface modified CuO nanoparticles predicted chemical composition; a) bi-dentate attachment structure; b) uni-dentate attachment structure

5.2.3 CuO Modification for 24Hours Using Butyric Acid at pH 7.0

Figure 5-7, shows the difference of the peaks from $1555 - 1410\text{ cm}^{-1}$ is around 145 cm^{-1} . This peak difference shows bridging attachment to the CuO NPs, but at the same time, it also shows the bi-dentate attachment. Moreover, when the difference of two peaks from $1668\text{ cm}^{-1} - 1557\text{ cm}^{-1}$ is approximately 110 cm^{-1} , this shows uni-dentate attachment to the CuO NPs. These predicted structures for both attachments are shown in **Figure 5-8 a** and **Figure 5-8 b** respectively.

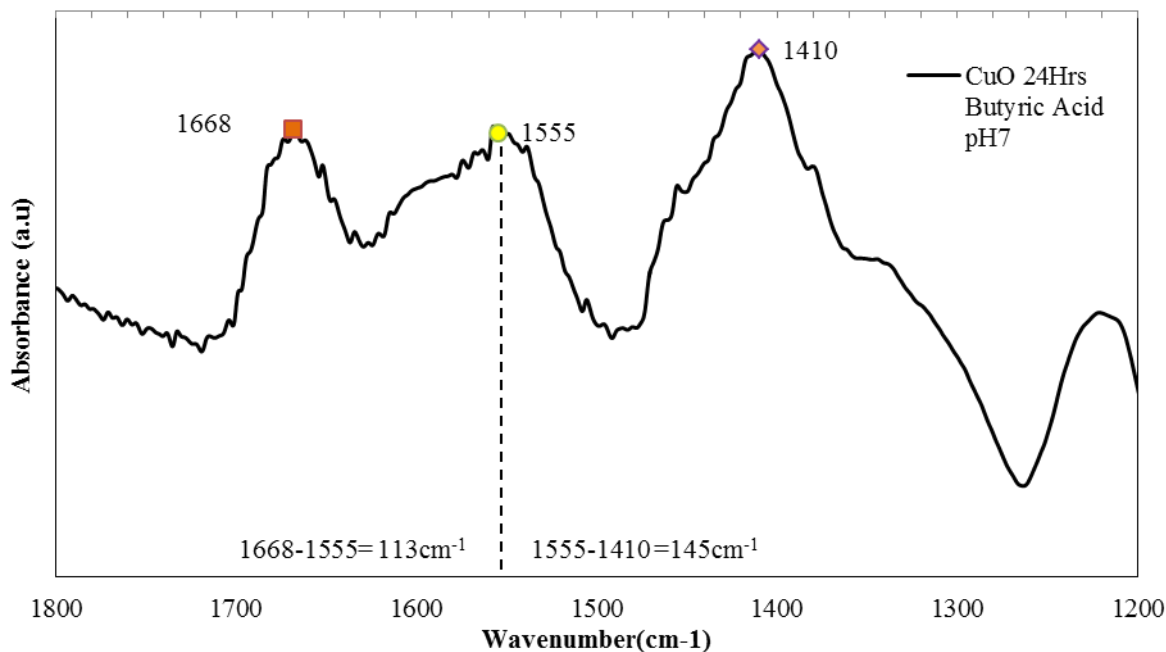


Figure 5-7 Butyric acid surface modified CuO nanoparticles using reagent at pH7 and reaction time of 24 hours

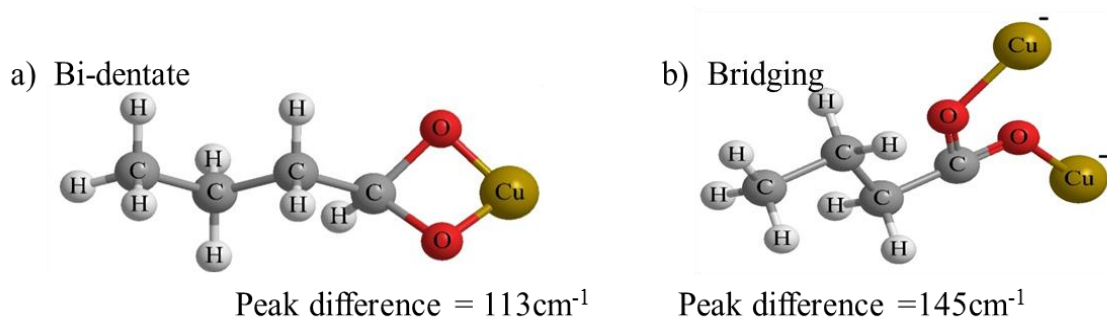


Figure 5-8 Butyric acid surface modified CuO nanoparticles predicted chemical composition; a) bi-dentate attachment structure; b) bridging attachment structure.

Subsequently, the results of section 4.6 are mimicking the work done in section 4.2, and both systems predict the agglomeration of NPs because of BA surface modification on CuO NPs. However, NPs did not lose their hydrophilic nature in water and they were dispersing in an agglomerated state.

5.3 Simulation of Nanofluids

The simulations were also performed using LAMMPS MD package. Two major potentials were used for nanofluid simulation; a) DPD and b) SPH. The DPD implemented the discrete particle dynamics in the system, which is a mimicked method of the BM (random forces movement). The second potential SPH had emphasis on the system hydrodynamic effect (hydrodynamic layering). However, COMPASS force field was used in the simulation. By doing so, good agreements have been achieved under the experimental and simulative conditions.

The most important study that was carried out in this dispersion simulation work was the simulation of metal oxide NCs i.e. CuO (CuO-NC) in water. This study's results have been presented in section 4.4. This was based on the initial experimental dispersion studies of CuO diffusion in water. Results achieved in section 4.4 displayed the effect of dispersion of CuO NCs in water and the change of the thermo-physical properties have been contrasted to the water system. Moreover, significant differences have been observed on RDF, diffusion coefficients and thermo-physical properties.

The time allocated for efficacious convergence of autocorrelation function of thermo-physical quantities is established by iterative process. The time allocated for CuO-water system was around 145-150 picoseconds, CuO-alkane system was setup around 550-650 picoseconds, however their counterparts i.e. base fluids took less time to converge i.e. for Water system it took 122 femtosecond and for alkane as base fluid system it took 200-250 picosecond time for convergence. The difference between the convergence times of nanofluid to base fluid was due to the nanoparticles dispersion increases the number of atoms in the system, which equivalently increase the time of convergence. Addition of nanoparticles also changes the system from homogeneous to inhomogeneous style ultimately causing increment in convergence time period.

The viscosity data obtained through MD is in 6-8% contrast to experimental trends as shown in **Figure 5-9**. In contrast to water MD viscosity results 4% of discrepancies are noted to experimental results. Moreover, 7% of discrepancies were recorded when comparing CuO water nanofluid MD viscosity to experimental results. The discrepancies found between experimental and simulation results were because simulation uses different pair potentials, pressure fluctuation theorems and ensembles, which causes a certain amount of invariance to the experimentally justified results. Furthermore, during the process of simulation equilibration the ensemble cause the velocity to fluctuate and this indecorous controlling of the velocity seeding number cause variation in analytical perturbation, consequently, which leads to certain amount of error.

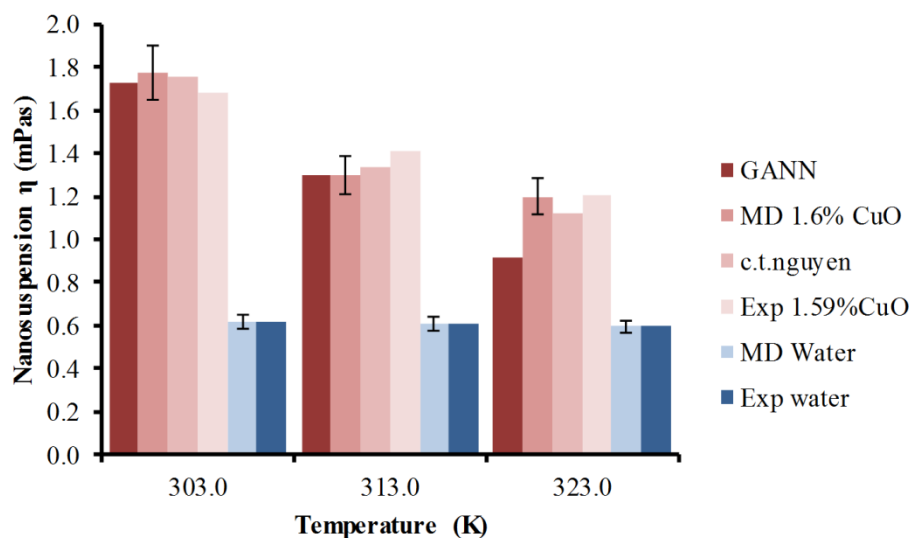


Figure 5-9 Comparison between experimental and MD achieved viscosities for water (blue coloured bars); comparison between experimental and MD achieved viscosities for CuO-water nanofluid (red coloured bars)

Thermal conductivity values ($0.71 \text{ Wm}^{-1}\text{K}^{-1}$ at 300K) from MD is also in excellent agreement with experimental values ($0.70 \text{ Wm}^{-1}\text{K}^{-1}$ at 300K) as investigated in previous research of Karthik et al.,(2012). Moreover, the study incorporates the analysis of the diffusion constant of water-based systems with and without CuO NCs. The diffusion

coefficient value from MD of CuO NCs in water ($1.87 \times 10^{-8} \text{ m}^2/\text{s}$) is in a good agreement with experimental values ($2.31 \times 10^{-7} \text{ m}^2/\text{s}$ at 298K), which were compared to video holographic analyser data (Cheong and Grier, 2010).

Moreover, the log of diffusion coefficient was calculated using the Stoke-Einstein equation of diffusion coefficient. By calculating this, the contrast was made with the simulation achieved values of diffusion coefficient and it was found that the diffusion rate in both cases have small discrepancies.

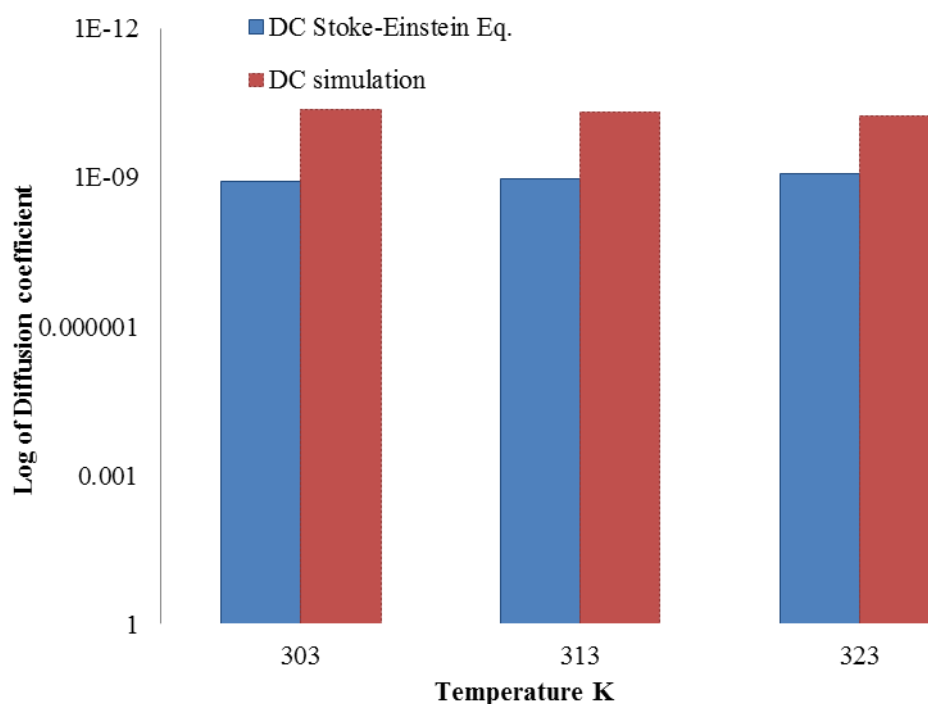


Figure 5-10 A Log diffusion coefficient of simulation and the log diffusion coefficient of calculated by using Stoke-Einstein method

The log diffusion coefficient in **Figure 5-10**, shows the clear resemblance between the two values of diffusion coefficients; one was calculated with the Stoke-Einstein equation and other worked out by using simulations. The difference in two values can be explained

by applied pair potentials and forcefield. In the simulation the pair potentials and forcefield are considered, but Stoke-Einstein equation does not consider these parameters of interactions as carried out using MD simulations. This creates the large amount of discrepancies between two results. Hence, the reliability of diffusion coefficient is greater with simulation obtained value than by the Stoke-Einstein's equation.

Further RDF was used to explain the nature of particle aggregation on various peak intensities. It was found that the intensities of the TIP3P water system were less than 1 a.u, with stretched peaks at different temperatures. However, the intensities acquired from the CuO-H₂O system had intensities higher than 1 a.u and strong peaks were dominating throughout the simulation of this system. However, this molecular interaction and NP inter kinetic in fluids can be further comprehended.

Table 5-1 Water diffusion blocks

Block	Diffusion coefficient- 298K (m ² /s)	Diffusion coefficient- 308K (m ² /s)	Diffusion coefficient- 318K (m ² /s)
1	6.09E-09	6.01E-09	6.14E-09
2	1.48E-09	1.07E-09	1.58E-09
3	8.95E-10	1.84E-09	2.18E-09
4	8.44E-10	1.74E-09	6.73E-10
5	7.25E-10	8.46E-10	2.68E-10
6	9.24E-10	2.42E-10	7.97E-10
7	1.81E-09	1.78E-09	-1.27E-10
8	2.79E-09	7.86E-10	1.38E-09
9	-2.66E-10	1.79E-09	9.76E-10
10	9.52E-10	1.18E-09	9.15E-10
Average	1.62E-09	1.73E-09	1.48E-09

The diffusion coefficient was measure by taking the slope of the mean square displacement. The MSD was broken into ten blocks for more precise slope calculation, since the graph of the MSD is non-linear so it is hard to use linear regression for estimating the correct diffusion coefficient value. Thus multiple slope gradients were taken for the outcomes of the MSD; which in turn provided the individual slope for a particular block as also suggested by (Loya et al., 2014a, Fan et al., 2006). After taking diffusion coefficients for ten blocks the average was calculated for diffusion coefficient; table 5-1 shows calculated average diffusion coefficient for the water system.

Table 5-2 Water + CuO diffusion blocks

Block	Diffusion coefficient- 298K (m ² /s)	Diffusion coefficient- 308K (m ² /s)	Diffusion coefficient- 318K (m ² /s)
1	8.14E-09	9.86E-09	8.53E-09
2	9.15E-09	1.35E-08	1.19E-08
3	1.41E-08	2.09E-08	1.39E-08
4	1.50E-08	2.68E-08	1.65E-08
5	1.80E-08	3.47E-08	2.24E-08
6	1.74E-08	3.62E-08	3.37E-08
7	2.74E-08	2.82E-08	2.88E-08
8	3.20E-08	3.62E-08	2.10E-08
9	2.08E-08	2.20E-08	4.32E-08
10	2.32E-08	3.54E-08	3.89E-08
Average	1.85E-08	2.64E-08	2.39E-08

The table 5-2 demonstrate the diffusion coefficient for ten blocks of the CuO-water system; this was also calculated in the similar manner as carried out for the water system. However, the diffusion coefficient was higher than the water system. The increment in the diffusion is due to addition of nanoparticles, which alters the Brownian motion in the system; consequently changing the rate of diffusion. Furthermore, this diffusion result

can be correlated with the CeO_2 diffusion in water as investigated by Loya et al. (2014a). In their study they calculated the diffusion coefficient to be $1.218\text{E-}08\text{m}^2/\text{s}$, which is in high agreement with the values achieved for the simulated system in this study.

The model presented many dominating peaks that represent agglomeration due to the attraction of CuO-NC's as shown in **Figure 5-11 a1, 5-11 b1 and 5-11 c1**. These RDF results presented the interactions of the CuO NCs in a water-based system; demonstrating the different characteristics of aggregations under different temperatures. As shown in **Figure 5-11 (a1, a2, a3), 5-11 (b1, b2, b3) and 5-11 (c1, c2, c3)**, the aggregations under different cut-off distances were clearly levelled giving the most aggregated system at the temperature of 308K, whereas; at the temperature of 318K the aggregation was observed to be less due to the temperature increment. Initially the superimposed peak of 318K in **Figure 4-10**, shows that there was a high degree of agglomeration but as the temperature settled at equilibrium level, the degree of agglomeration was decreased giving weak peaks after 1.2 nm.

The kinetic energies of the CuO-NC's increase with respect to the environmental temperatures. The coagulation of two particles will not occur after collision, since the kinetic energy of the particles is higher than their interaction attraction potential. Especially, the influence of the potential well will be low in respect of the kinetic energy at high temperatures. It implies that at 318K; most of the colliding particles have enough energy or pulling force to break them up from the potential well, hence remain un-coagulated. This could also be seen from the RDF signal (**Figure 5-11 c1**), where the stretched peaks at 0.25nm and 0.5 nm were observed. The agglomeration was less affected at lower environmental temperature (i.e. **298K**) observed by several peaks as in **Figure 5-11 a1 and Figure 5-11 b1**.

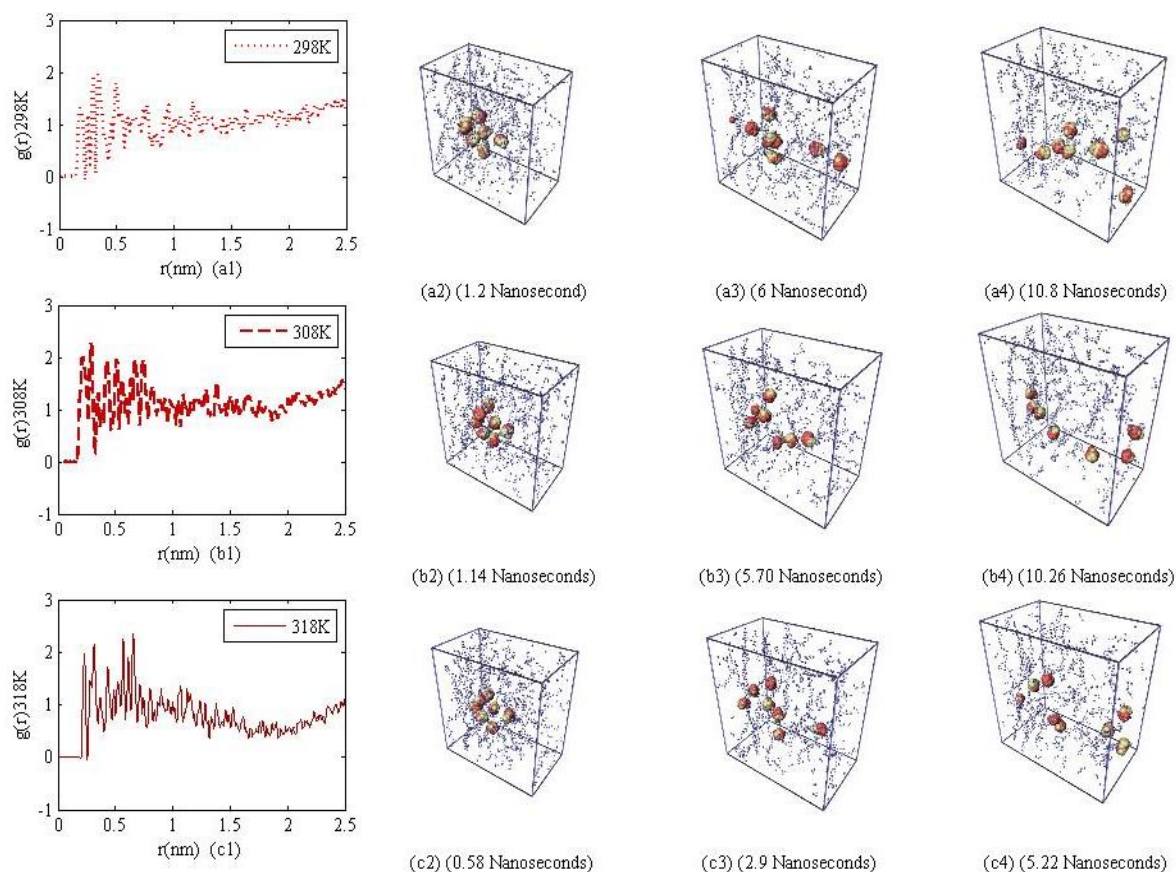


Figure 5-11 The Radial distribution function (RDF) of CuO nanoclusters in water in this work: a1) RDF for 298K; b1) RDF for 308k; c1) RDF for 318k; a2) RDF simulated representation at 298k; b2) RDF simulated representation at 308k; and c2) RDF simulated representation at 318K; a3) RDF simulated representation at 298k; b3) RDF simulated representation at 308k; and c3) RDF simulated representation at 318K; a4) RDF simulated representation at 298k; b4) RDF simulated representation at 308k; and c4) RDF simulated representation at 318K

A third study was based on the dispersion of CuO-NC in hydrocarbon based fluids. These experiments were performed by the use of alkane liquids. During simulations the Eicosane alkane chain (i.e. $C_{20}H_{42}$) was used. The CuO-NC particles in alkane show slow diffusion (i.e. $4.3E-11m^2/s$) than the water based system (i.e. $1.8E-7m^2/s$) at a similar temperature and it can solely due to the viscosity of the alkane being higher than water. This diffusion predicts the NP effect in the different lubrication medium, giving an overview of the thermo-physical properties of the hydrocarbon nanofluids.

Table 5-3 Alkane diffusion blocks

Block	Diffusion coefficient-	Diffusion coefficient-	Diffusion coefficient-
	303K (m^2/s)	313K (m^2/s)	323K (m^2/s)
1	9.79E-08	1.07E-07	1.06E-07
2	1.97E-07	1.84E-07	1.85E-07
3	1.34E-07	9.76E-08	1.97E-07
4	1.58E-07	1.42E-07	6.20E-07
5	5.16E-07	2.71E-07	7.89E-07
6	1.16E-06	6.76E-07	1.03E-06
7	1.21E-06	1.20E-06	8.62E-07
8	1.15E-06	8.45E-07	1.17E-06
9	1.42E-06	1.58E-06	4.34E-07
10	1.49E-06	2.53E-06	1.83E-06
Average	7.52E-07	7.63E-07	7.22E-07

The diffusion coefficients tabulated in table 5-3 for the alkane system was calculated in similar way as calculated for the CuO-water nanofluid and water system. It was found that the diffusion of the alkane system shows high rate of diffusion as compared to the water system, this can be explained by viscosity of the alkane is higher than the water system. This viscosity causes the molecules to be intact together, subsequently causing the molecular collision to

occur more frequently, conversely in the water system the molecules are far apart and the viscosity of the system is very low, ultimately causing the molecular collision to decrease directly effecting the diffusion to decrease.

Table 5-4 CuO-Alkane diffusion blocks

Block	Diffusion coefficient- 303K (m ² /s)	Diffusion coefficient- 313K (m ² /s)	Diffusion coefficient- 323K (m ² /s)
1	4.65E-10	4.73E-10	5.26E-10
2	1.78E-12	4.74E-13	-9.85E-13
3	-5.18E-12	4.89E-12	1.23E-12
4	5.19E-13	6.21E-13	1.26E-11
5	-1.91E-13	-4.65E-13	9.02E-14
6	3.59E-14	2.71E-14	-5.61E-14
7	-1.04E-14	1.46E-14	8.04E-15
8	6.72E-15	1.67E-14	5.60E-14
9	-5.99E-16	6.35E-15	-1.67E-14
10	-1.30E-14	-1.73E-14	-2.34E-14
Average	4.62E-11	4.79E-11	5.39E-11

The diffusion coefficient calculation for CuO-alkane system tabulated in table 5-4 was calculated using the technique used earlier for water and CuO-water system. The non-linear regression was again take for the MSD graph, The diffusion values measured for CuO-alkane were the lowest of all the systems throughout the research work, this is because the viscosity of this system is higher than the other systems, measure throughout this research. Furthermore, the diffusion of CuO seizes in alkanes due to the greater number of molecular intermingling.

The simulation viscosity of the alkane based nanofluid and alkane fluids had similar trends to the experimental achieved values as shown in **Figure 4-11**. The simulation viscosity of the alkane was quantified using the stress autocorrelation function; where monotonic decay was found with time correlation. Furthermore, alkane-NC system presented monotonic decay for only one stress tensor; however, other two stress tensors were trying to converge at the cost of longer time limit. In conclusion, estimation of viscosity in simulation is better carried out at lower correlation times. For simulation estimated viscosity caution needs to be taken for the estimation of correlation time.

Furthermore, the thermal conductivity of CuO-alkane nanofluid system was validated using heat and current auto correlation functions (HACF) as represented in **Figure 5-12 (a), (b) and (c)**.

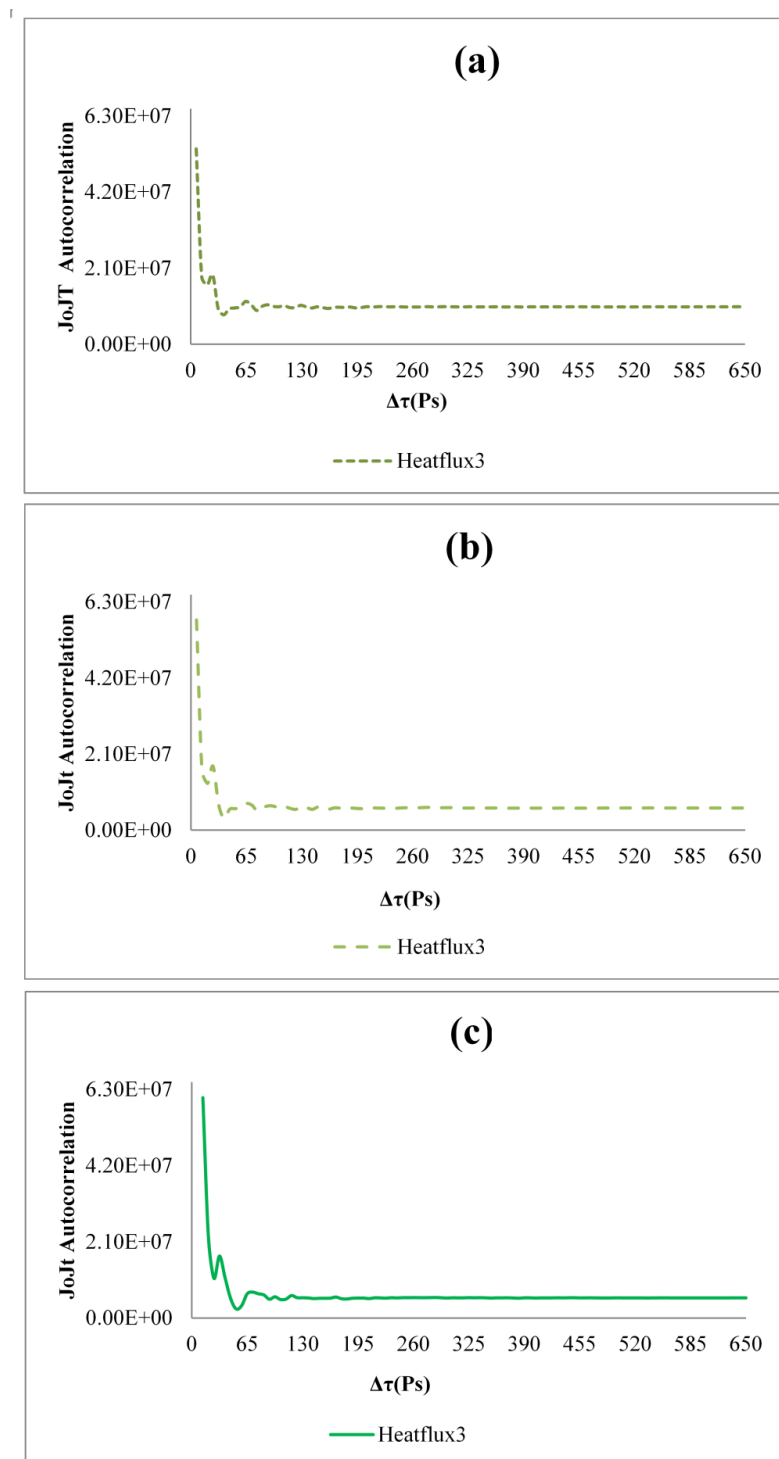


Figure 5-12 HACF for pure alkanes; a) 303K alkane with CuO nanofluid heat autocorrelation convergence result. b) 313K alkane with CuO nanofluid heat autocorrelation convergence result. c) 323K alkane with CuO nanoparticle nanofluid heat autocorrelation convergence result

The HACF results of thermal conductivity of alkanes showed similar coherence to the one presented for alkanes NP system in **Figure 5-12**. The result of HACF in **Figure 5-12 (a), (b) and (c)** represents the heatflux calculation with respect to time correlation function. As the system is equilibrated, the peak seems to decrease. Afterwards the system starts to decay and this convergence to zero frequency level represents that simulated results have achieved equilibrium. It could be seen from **Figure 5-12 (a), (b) and (c)** that at different temperatures the convergence time changes. This could be due to the interatomic collision level mediation as the temperature is changed. It causes the convergence time and equilibration time to increase.

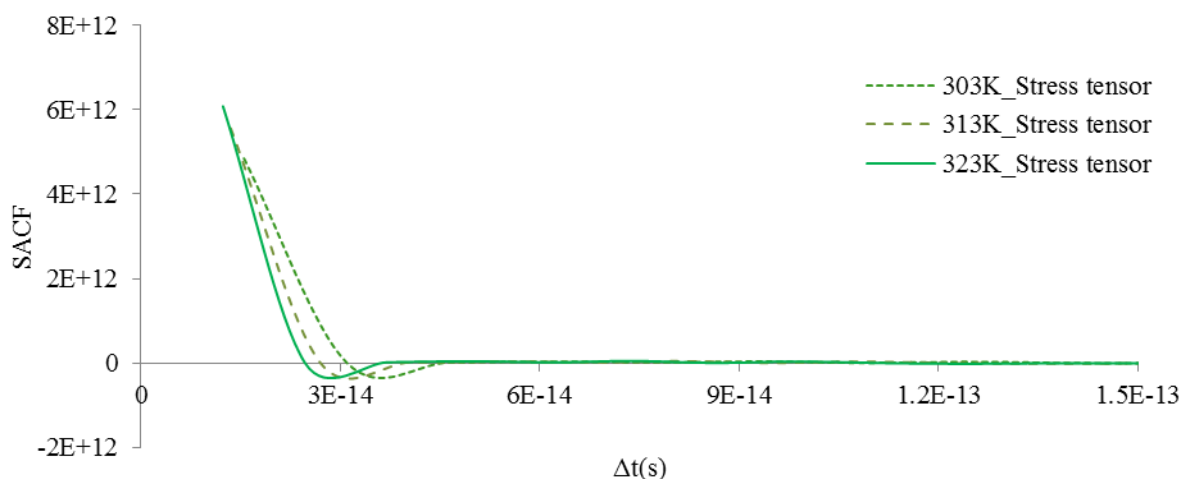


Figure 5-13 Stress autocorrelation function of molecular dynamic simulations of alkanes with CuO nanoclusters (Loya et al., 2015)

SACF convergence of the CuO-alkane nanofluid took longer time to converge. This simulation was performed on a non-equilibrium dynamics. Due to this, the convergence time used was of lower time step intervals. To investigate the macroscopic shear viscosity at zero frequency level of convergence, in this study the estimation of Δt (the duration between intervals) values used are given in **Table 5-1**. These estimate the number of durations approached within two consecutive interval steps, thereby, this duration was short because the convergence was not possible at higher values of Δt . The computational time was increasing

without the convergence of the properties specially for SACF. As the Δt is lowered; the simulation starts to converge significantly as illustrated in **Figure 5-13**.

If the time period is short for the simulation being carried out, the SACF will not converge, giving statistical error of the viscosity estimation. On the other hand, if the time taken for viscosity is too long it will increase the noise in pressure correlation function, finally high fluctuation will be observed in viscosity estimation. However, the optimal selection of time period will solely depend on the system configuration.

An exciting observation was perceived, related to the decay of SACF for each nanosuspension to that of base fluid. In a homogeneous pure system such as water or alkane; monotonic decay is observed. The decaying trend for the nanosuspension revealed monotonic decay too, however, at the cost of a longer time duration. From this study, it was observed that nanosuspensions SACF tensor's decaying trends were not converging monotonically as shown in **Figure 5-14**.

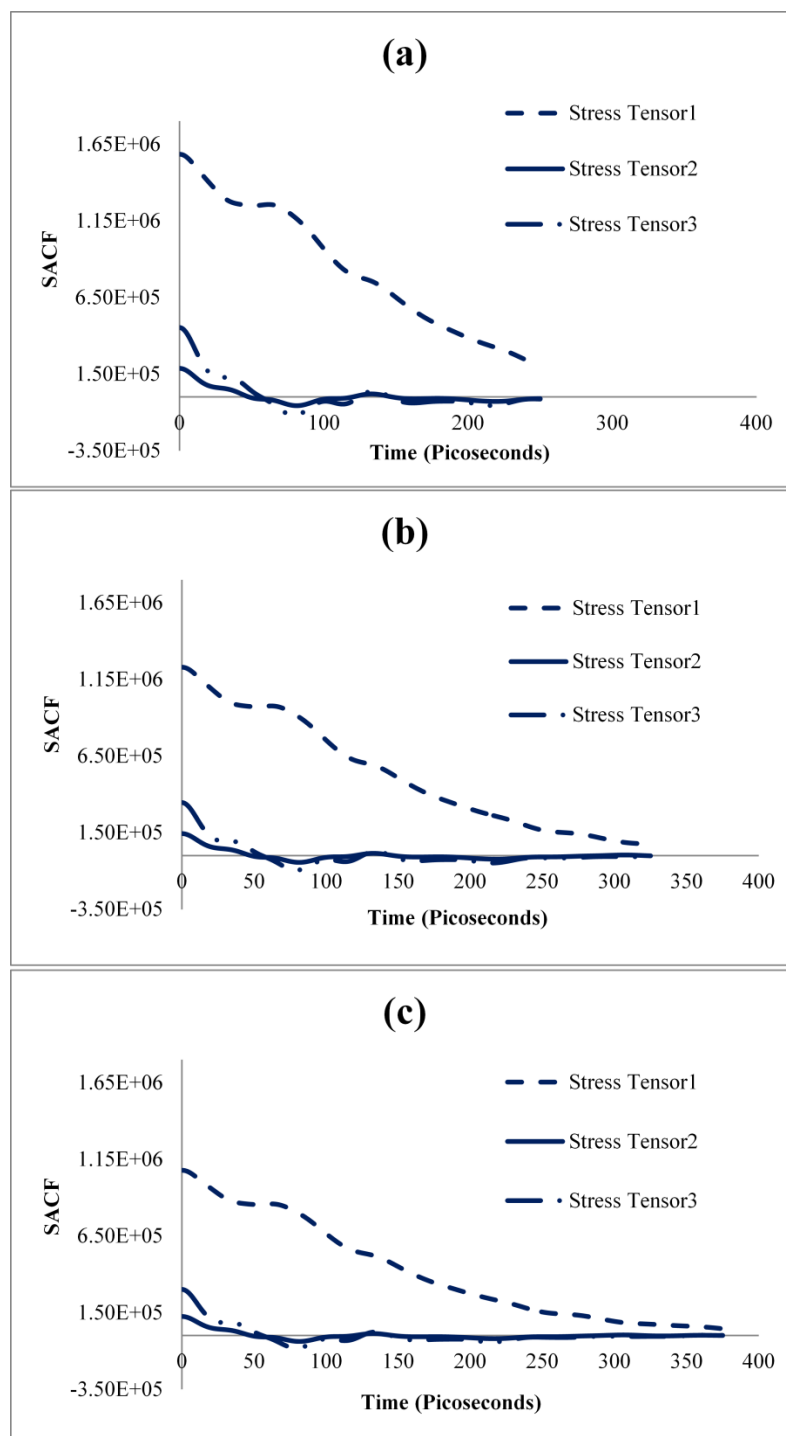


Figure 5-14 Stress autocorrelation function of alkanes at different temperatures; (a) 303K SACF of alkanes; (b) 313K SACF of alkanes; (c) 323K SACF of alkanes (Loya et al., 2015)

The SACF results equilibration time for pure alkane system are shown in **Table 5-1** and **Figure 5-14**, this confirms that the equilibration time taken for the results to converge is reasonable; when comparing with the results of Harris and Wang (1992). They approached the similar equilibration time limit for integration of the results i.e. 500-600 Picoseconds around 300-400K respectively, of n-eicosane MD. For the case of the alkanes-nanoclusters systems, it was hard to identify the detailed viscosity convergence, due to the limited computational power and high time required for computation. However, the results prediction using SACF convergence demonstrated high coherence with the calculated viscosity.

Table 5-5 Time taken by each simulation to evaluate viscosity of alkanes

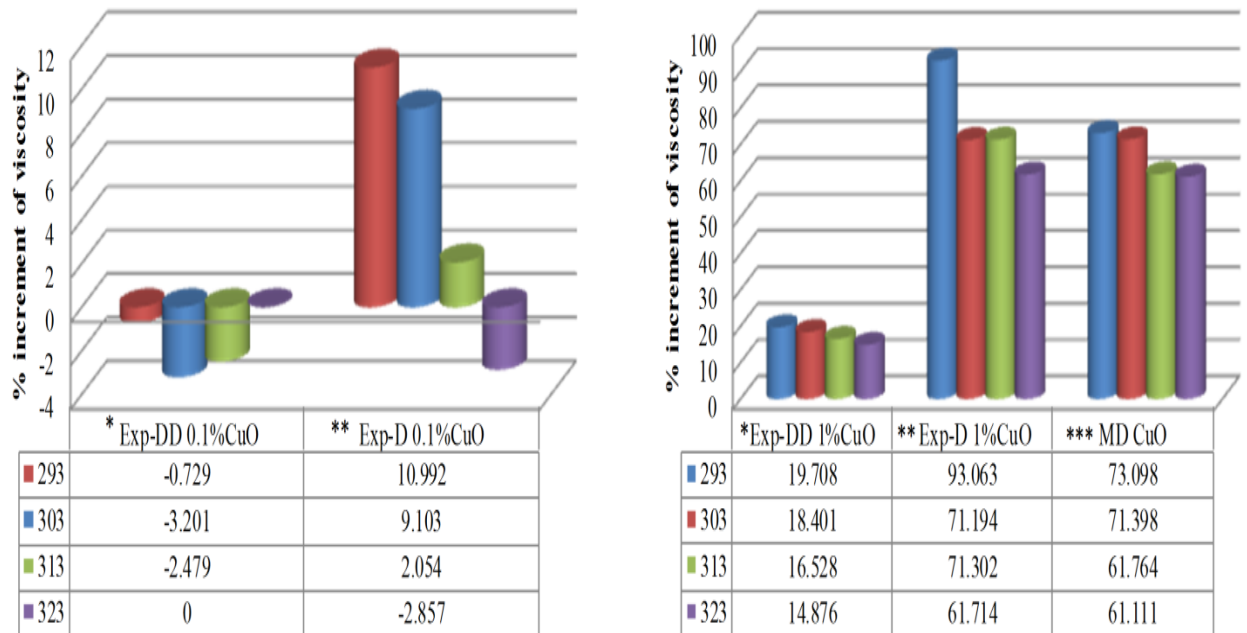
<i>Temperature (K)</i>	<i>τ_e (Picoseconds)</i>
303	250
313	325
323	375

Further, the relative percentage error of experimental work and MD were calculated. The **equation 5-1** shows the method of calculating relative percentage error. This is known as percentage error because it is a difference of optimised viscosity of the base fluid using nanoparticle to the base fluid actual viscosity.

$$i = \frac{v_i - v_0}{v_0} \times 100 \quad (5-1)$$

Where, i is the relative percentage increment of viscosities at respective temperatures. v_i is the viscosity of the paraffin with NCs and v_0 is the viscosity of pure paraffin.

Table 5-2 Relative percentage increments of nanofluid viscosity to base fluid at respective temperatures (for alkanes with CuO nanoclusters to pure alkane)



* Exp-DD = Dodecane experiment

** Exp-D = Decane experiment

*** MD-CuO = MD simulation

Figure 5-15 % increment of viscosity of nanofluid from original alkane.

The addition of NCs to the experimental and MD system of alkane's causes rise in the system viscosity as shown in **Figure 5-15** and **Table 5-2**. This upsurge is associated mainly with the volume fractions of NCs in the system. The viscosities incremented with 1% volume fraction of NCs coincide with the MD system of NCs. When comparing experimental viscosity of CuO-alkane nanofluid to the viscosity of 0.1% volume fraction CuO-alkane MD system, it was found that the size does not matter for viscosity increment.

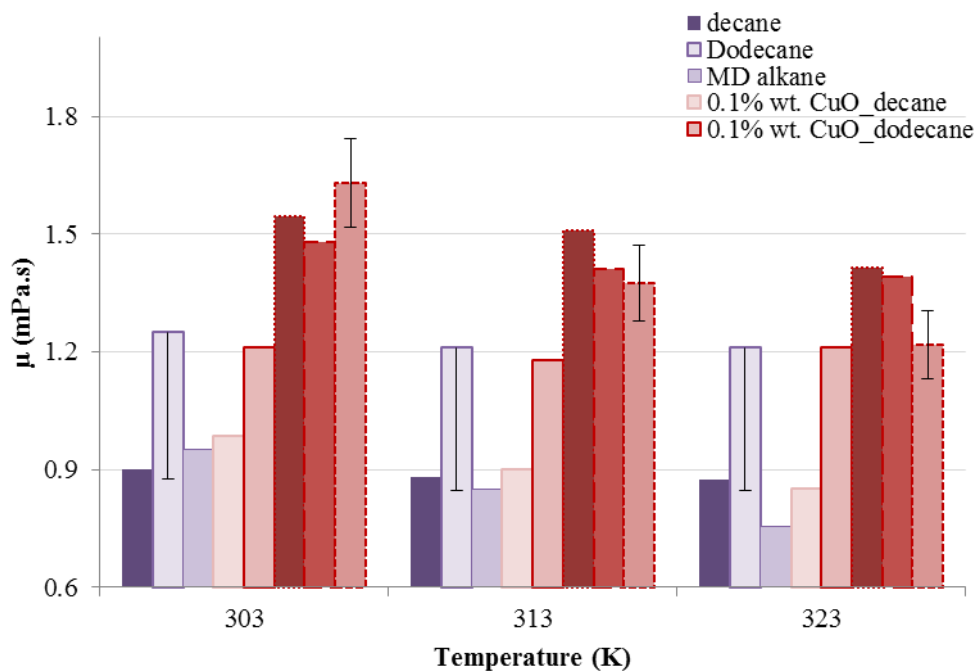


Figure 5-16 Discrepancies between alkane and CuO-alkane nanofluid

Furthermore, when NCs were dispersed in the hydrocarbon nanofluid discrepancies between the experimental alkane and MD alkane viscosity was found to be 30% greater as demonstrated in **Figure 5-16** and this is due to the alkane that was simulated being of 20 carbons chain. Whereas, the experimental alkane used was of 10-12 carbons chain. Consequently, the MD viscosity of alkane was found to be higher than the experimental ones. Moreover, discrepancies between the CuO-alkane MD viscosity results to experimental ones were within 6-8% as shown in **Figure 5-16**. The discrepancies obtained between simulation and experimental results for CuO-alkane system are because of using different number of carbon atoms for alkane for both the cases. Furthermore, the discrepancies for alkane system are not significant as compared to the CuO-alkane system since the addition CuO nanoparticles increases the viscosity and the molecular loading (i.e. number of atoms in the system) in both the cases.

5.3.1 Drawback of Estimating the Thermo-physical Quantities by Particle Size

The NP size was neglected for the viscosity and thermal conductivity calculation by MD, since volume fraction in the simulation domain has larger effects on the outcomes. Volume fraction of NPs is an important property that contributes to the increment of viscosity when compared to the pure system. On the other hand, NP volume is related to its size; however the simulation domain is restricted by the current power of computers to simulate more than 10nm particles. When the comparison of volume concentration is done with respect to NP size, effect on viscosity results will not be significant enough to equate for the thermo-physical calculations. Additionally, the NP dispersion in a pure system is mostly dependent on the volume fraction of the particle concentration rather than the size.

The size affects thermo-physical quantities, but the MD level is not powerful enough to simulate a system with several particles over 10 nm since most particles are above this range. This drawback creates discrepancies with the results expected. Therefore, in our simulation relative trends were compared to the results rather than the absolute values. A comparison has been carried out based on a volume fraction rather than size.

5.3.2 Precise Approach to Approximate the Thermo-physical Quantities

According to Nguyen et al., (2007); their investigation showed that the particle concentration plays a significant role in changing the viscosity. It was investigated that the viscosity increases with the particle volume fraction and decreases with a temperature increase. This is the general behaviour exhibited by NPs in fluids. The importance of particle size effect on viscosity was also investigated and it was found that; at high particle concentrations of more than 5-10%, the size shows significant effect. However, at low concentrations particle sizes do not show any significant effect. Later, Zhao et al., (2009) also investigated the dependence of the SiO₂ particle size on viscosity and discovered that the particle volume concentration is a major factor in changing the viscosity of the nanofluid when the particle sizes are

smaller(0.1-15nm). This is why in this study the dominant effect in the system is the particle volume fraction rather than size.

Further research shows the effect of particle size on viscosity is an ongoing debate among researchers but no definite conclusions have yet been established. Some studies also show that the particle size has negligible effect over the viscosity (Prasher et al., 2006), while others suggest that a decrease in the particle size, leads to an increase of the viscosity (Chevalier et al., 2007, Namburu et al., 2007, Pastoriza-Gallego et al., 2011, Lu and Fan, 2008) and vice versa for other researchers (Nguyen et al., 2007, He et al., 2007, Nguyen et al., 2008). It can be concluded that in this simulation study, the impact is far greater due to volume fraction rather than particle size.

5.4 Simulative Modification of Nanofluid

As discussed earlier about the experimental surface modification of CuO NPs; likewise, surface modification of CuO NCs using short chain carboxylate group was mimicked on the simulation platform, in section 4.6. The findings exhibited that the modification of NPs during simulation gave similar agglomeration mechanisms as observed experimentally. The simulation showed a complex style of agglomeration due to the viscous nature and Van der Waal interactions as shown in **Figure 5-17**. However, the correct prediction and interpretation of agglomeration in a system is, therefore, important for understanding the mechanism of particle transport and Brownian interactions of colloidal particles.

Table 5-6 BA-CuO-water diffusion blocks

Block	Diffusion coefficient- 303K (m ² /s)
1	2.61E-08
2	6.75E-09
3	4.66E-09
4	2.79E-09
5	-5.46E-11
6	5.83E-10
7	5.90E-10
8	-2.25E-10
9	4.98E-10
10	2.36E-10
Average	4.19E-09

The diffusion coefficient calculated for the modified CuO-water system demonstrated decreasing rate of diffusion, this decrease is related to the increase in the viscosity due to the addition of functional group in the system that causes the agglomeration to increase consequently causing the diffusion to decrease. However, when comparing the diffusion of modified CuO-water system to CuO-water system it can be found that the diffusion of CuO-water system is higher than the diffusion of the modified system. No agglomeration found in CuO-water system is the cause of higher diffusion rate for this system.

Perspective

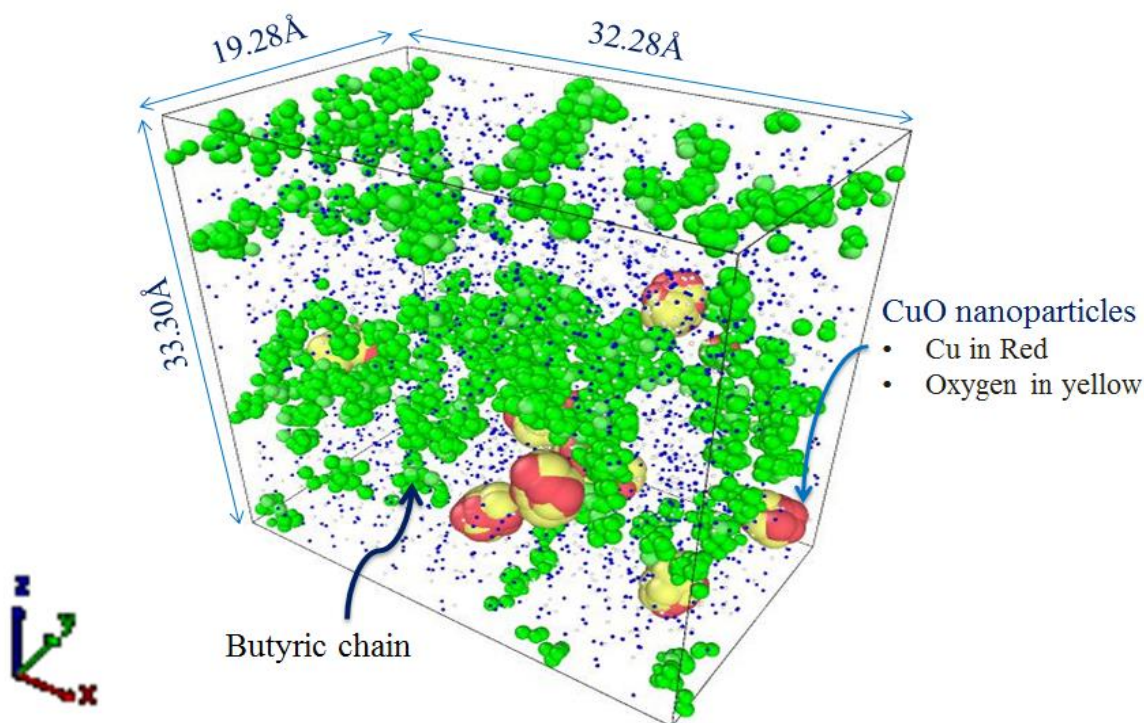


Figure 5-17 Simulated visualization of the surface modification of CuO nanoclusters using butyric acid functional group in water system; a) Green particles are the alkyl chain; b) Dark navy blue colour represents Hydrogen group and white ones represent oxygen particles; c) Yellow and red particles bonded together are CuO nanoclusters

In **Figure 5-17**, the CuO NP's have been represented by yellow and red colour, whereas, the white and blue atoms represent water and green ones represent functional group attachment. From **Figure 5-17**, the green coloured atoms over the surface of the yellow atoms represent the point where the functional group attachments are possibly present. Their attachments are related to the carboxylate group since the carboxylate chain, COO^- has been coloured green for the sake of rationalizing from other molecules.

Additionally, from the RDF results of the BA surface modified CuO NCs shown in **Figure 5-18** demonstrates NCs are not agglomerated but in the later version of **Figure 5-18**

agglomerations can be figured. This system, i.e. **Figure 5-18 a** has just started to equilibrate and it has not reached the desired equilibration time. Likewise, as the simulation is carried out for more time steps, i.e. several picoseconds, the system starts to show high levels of agglomeration due to the surface functionalized BA, which tends to create Van der Waal forces of attractions between NCs. Due to this, electrostatic repulsion is decreased; causing the attraction to dominate and a net potential energy barrier is hard to be overcome. Subsequently, the agglomeration between NCs is increased. This agglomeration, is mostly caused by the addition of surfactants, this depends on the nature of surfactant and the bonding mechanism between the NP and the surfactant.

The previous mechanism could be applied to other metal oxide particles for application in biomedical field as stated by Leuba et al. (2013); that super magnetic iron oxide NPs functionalized using carboxylate group highly dislocated biofilms and inhibited the growth of *S. aureus* compared to untreated biofilms (by over 35% after 24 hours). Therefore, the functionalizing of the metal oxide NPs can highly improve the biodegradability and antibacterial activity by carboxylate, amine and isocyanate modification.

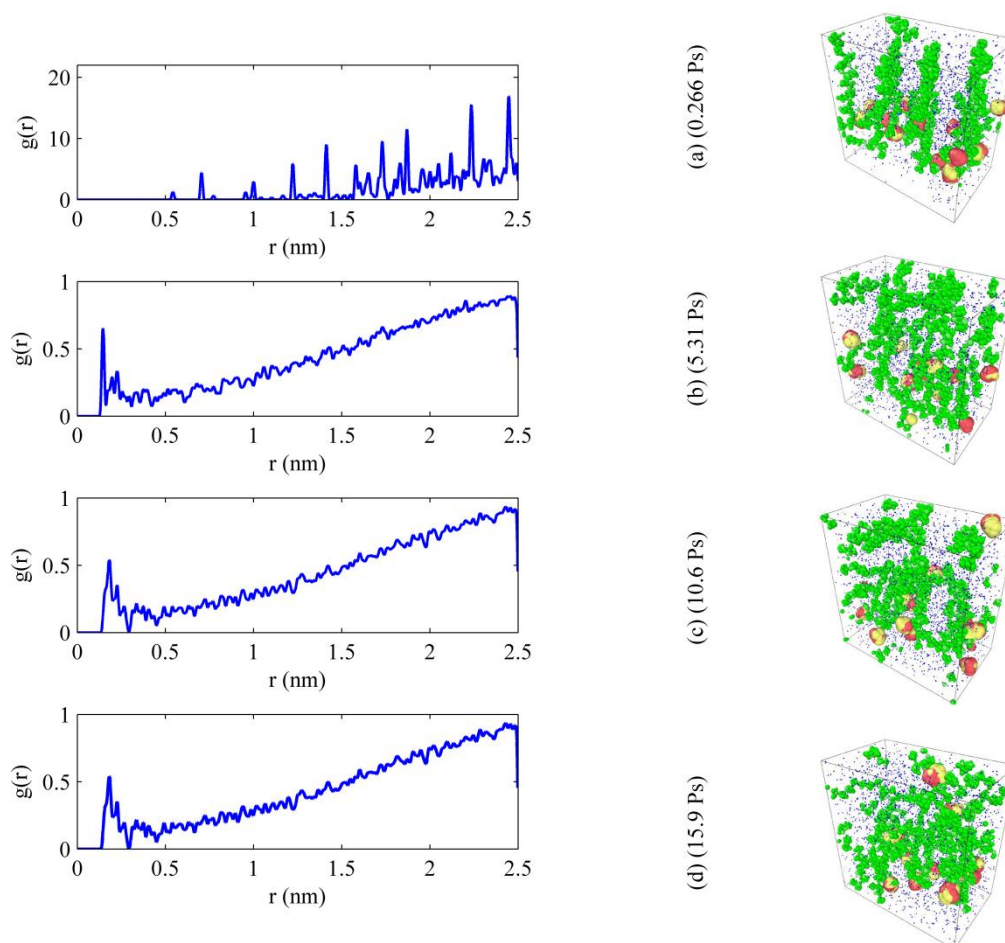


Figure 5-18 Radial distribution function of CuO nanoclusters with butyric acid in water system

From **Figure 5-18**, it can be predicted that the attachment of the CuO and butyric chain has caused high agglomeration in the system, since the spacing between the molecules is less. Furthermore, it is strongly peaking at 0.1-0.15 nm from **Figure 5-18 b, c and d**. Further after 2nm, small but stretched peak can be seen. This can be due to some distant molecules in the system.

Additionally, the diffusion coefficient shows a decreasing trend because of surface modification of NCs, since surface modification increases viscous drag that is created by the attachment of surfactant. In contrast to the diffusion coefficient of basic CuO-NC water

system, the surface functionalized NC system shows slow diffusion rate of $2.7E-7m/s^2$ to $1.5E-8m/s^2$.

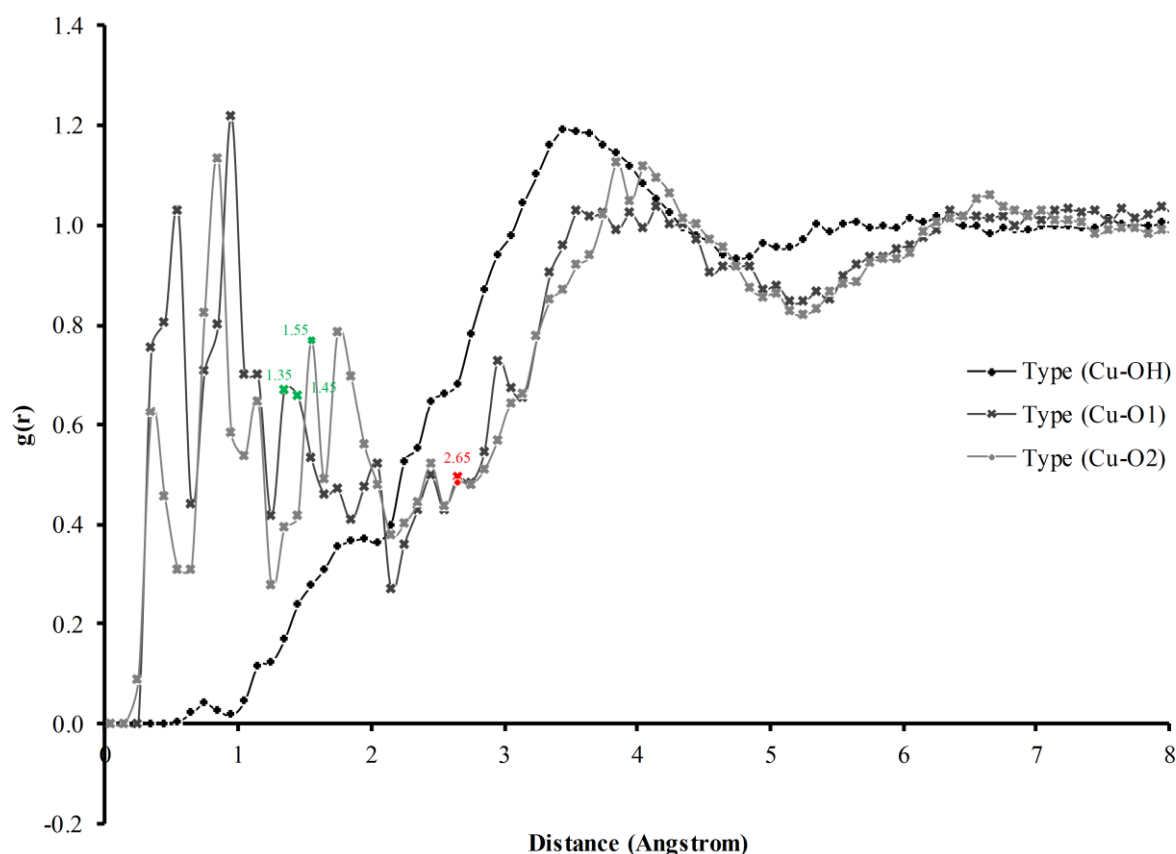


Figure 5-19 Radial distribution function of butyric acid functional group moieties attachment to CuO nanoclusters in a water system

The RDF of Type (Cu-O1) and Type (Cu-O2) shows a peak at 2.6-2.7 Å in **Figure 5-19** (peak coloured in red), this peak represents the attachment of the COO^- group oxygen to the metal surface. This attachment style is interpreted as a bridging attachment; as stated by Raj (2010) that Cu-Cu shows bridging style at 2.6 Å. This bridging attachment is also known as paddle wheel formation. Furthermore, the BA functional group was attached to CuO NCs by experimentation and further, the figures specify of FTIR spectra show different chelation coordination formation. The carboxylate attachment to CuO surface showing bridging ligand

arrangement to two metal centres, leads to formation of metal – carboxylate bond. This Cu-Carboxylate bond that shows bridging arrangement is known as binuclear compounds.

Moreover, the NPs demonstrated a combination of Cu bonding to carboxylate group in water, predictably forming $[\text{Cu}(\text{C}_2\text{O}_2)_2(\text{H}_2\text{O})_2]^{2-}$. This formation is also predicted and investigated by Raj (2010) with a distance between Cu—O—M as 1.28 Å. Furthermore, the simulation RDF results in **Figure 5-19** show some peaks colored in green from at 1.28 – 1.55 Å, these peaks are possibly representing these moieties attachment to Cu.

Furthermore, the black line shows the attachment of Cu with hydroxyl group. This is proposed in the study of metal – ligand correlation carried out by Nimmermark et al., (2013), where they studied different metal oxides attachment to carboxylate group of acids and hydroxyl moieties of water. In their study they found that the Cu - (OH) shows bonding distance of approximately 2.68 Å, however, in our case the black line in **Figure 5-19** shows bond distance of 2.7 – 3 Å. This stretch is due to the use of pair potentials during simulation and further random seeding of velocity through the system.

However, the predictions of results estimate that there were different bonding styles, as discussed were present during different phases of simulation. In contrast to experimental work this simulation is beneficial in further explaining the agglomeration with the help of RDF and diffusion coefficient.

5.5 Summary Outline

The thesis has elucidated the methodology to perform the molecular dynamics of metal oxide nanoparticles; moreover this technique can also be implemented for other kind of nanoparticles and fluidic systems. The research work presented thermo-physical and thermo-mechanical quantification. Quantifications were carried out using LAMMPS. The simulation results were highly coherent to the experimental achieved results and trends, but with a small amount of error difference.

1. The basic dispersion study carried out demonstrated that the fundamental analysis of the properties is important; as from the thesis it can be portrayed, that to achieve better dispersion with low hydrodynamic size of nanoparticle it is better to disperse them in bigger size beaker with a large head diameter.
2. The basic dispersion study also elucidated that increasing sonication time has direct effect on the size of the particles. In the similar manner the sonication power is directly related to the particle sizing. Furthermore, the ultrasonicator is the best tool for dispersing the nanoparticles rather than the shearing mixers.
3. Experimental surface modification carried out on the nanoparticle caused the particles to aggregate in the aqueous suspension. The experimental modification was quantified and characterized using the FTIR analysis, where three different carboxylate attachment styles were found; a) uni-dentate, b) bi-dentate and c) bridging.
4. Simulation of the modified and unmodified water based nanofluids estimated the diffusion coefficient with the range of $1\text{E-}9\text{ m}^2/\text{s}$ to $1\text{E-}7\text{m}^2/\text{s}$.
5. The CuO-alkane nanofluid experimental and simulation viscosity results were highly concurrent with a 6% error difference. The diffusion rate of CuO-alkane system was lower than the alkane system, this is due to the viscosity of the fluid is enhanced due to the addition of nanoparticles, causing the diffusivity of the nanofluid to decrease.
6. The molecular dynamics mimicking of the functional group attachment to the CuO-nanoparticle surface demonstrated similar attachment styles as estimated by experimental FTIR analysis.
7. The nanofluid dispersion simulations were performed for different number of iterations, because the monotonic decay was necessary to achieve for successful convergence of the thermo-physical quantities. For different set of simulation different number of time convergence was used.

Chapter 6

Conclusions

Chapter 6 Conclusion

In this work, the dispersion of CuO NPs was studied in water and alkanes. In addition, these fluids were mostly aqueous and hydrocarbons based. The experiments were carried out to support the parameters obtained from the later simulations performed. For the understanding of the mechanism of dispersion, it was first necessary to understand the reality of the dispersion system. The dispersion mechanism was investigated before the modification of NPs was carried out, using different modifying agents. In this research the modifying agent used was butyric acid.

The simulative predictions of MD results of the transport, thermal and rheological coefficients of the NC system highly correlate with practical works. The confirmation of the results achieved for the viscosity and thermal conductivity were further predicted by the heat flux and the stress autocorrelation functions. It was seen that the predicted results of the simulation at particular temperatures were in good coherence with the experimental based system. The convergences of the autocorrelation functions were highly stable. The nano-system properties (viscosity and thermal conductivity) from the experimental data were mimicked over the MD simulation using LAMMPS. The properties and the mechanism were taken in consideration before successfully running the simulation.

The conclusions that could be drawn from the studies done in this research are first based on the dispersion of the NPs in water on experimental basis. It was observed that the dispersion in 500 ml beaker is better than a 60 ml beaker, since the hydrodynamic particle size achieved for 500 ml was 160.4 nm at 0.1% concentration. Whereas, for a 60 ml beaker a NP size of 712 nm was obtained at a similar concentration. The second experimental test showed that the most appropriate particle size of different sonication time achieved was at 500watts for 10 minutes; 174.6 nm. On the contrary, 150 watts at 10 minutes had higher value of 197.6 nm. The third experimental test advanced the study regarding the best device that is good for dispersion of NPs in water is sonication device. The particle size achieved by this device at

299 watts is 173.6 nm, whereas, mechanical mixer is far higher giving 3725 nm particle size at similar concentration, 0.1% w/w.

After the basic dispersion studies the NPs were modified using carboxylate group attachment, of BA. Later, the characterization helped in proving the modification of NPs. The carboxylate modification can be found under the range of 1300 – 1750 cm^{-1} . Three different modification experiments using BA were carried out and all the experiments showed modification of carboxylate group to NP surface by FTIR analysis. The first one was 2 hour reaction time using BA at pH 5.5, showing bi-dentate and uni-dentate attachments. The second one was a 2 hour reaction time using BA at pH 7.0, showing bi-dentate and uni-dentate attachments. The third and last modification was for 24 hours reaction time using BA at pH7.0, showing bi-dentate and bridging attachments. Conclusion that can be made from the modification of NPs is that all of them displayed agglomeration while in aqueous solution.

Later, ICP experiments were also carried out to evaluate the release of Cu ions in water, it was noticed that the ion release in deionized water is related in linear fashion to the natural log of concentrations. The ICP concentration of microwave digestion was found to be 8mg/L that is higher than the 0.001% and 0.01% ionic release during CuO dispersed in water for 3 days, whereas, for 0.1% the ion release was found to be 10 mg/L.

After carrying on various experiments; the MD simulations were also carried out to quantify some of the results. First simulation was on the TIP3P water model by which the viscosity and thermal conductivities were analysed. The values achieved from MD for viscosity (0.59mPas) was in good agreement with the experimentally calculated value of 0.321 mPas at 298 K. Later, CuO NCs were dispersed in the solution and excellent agreements of the viscosity were analysed, the simulative value was found to be 1.76 mPas and the experimental value is 1.79mpas at 303K. The thermal conductivity values of TIP3P water model was $0.597\text{Wm}^{-1}\text{K}^{-1}$ at 298 K, however, it was also in excellent agreement with the value achieved experimentally of $0.5971\text{Wm}^{-1}\text{K}^{-1}$. Whereas, the modified CuO water nanofluid also revealed concurrent results with simulation results; i.e. $0.712\text{Wm}^{-1}\text{K}^{-1}$ for MD and $0.71\text{Wm}^{-1}\text{K}^{-1}$ for

experimental at 298 K. The third variable that was analysed was diffusion coefficient. This was analysed to compare the water based diffusion rate to the CuO nanofluid diffusion rate. It was seen that the CuO nanofluid exhibited higher diffusion rate than the simple TIP3P model and this is most likely due to the kinetic heat conduction and higher collision of molecules due to the addition of NPs in the system.

A second major study that was carried experimentally was analysis of the properties of the alkane liquid. It was analysed that the viscosity of liquid alkanes Decane and Dodecane obtained from Sigma Aldrich had 0.83 – 1.37 mPas from 303 – 323 K. Later, after doing these experiments the simulations were also done on eicosane (C₂₀H₄₂) alkane to measure their viscosity and thermal conductivity. Pure alkane provided concurrent viscosity for MD 0.951 mPas and experimental 0.95 mPas at 303 K. Furthermore, thermal conductivity value for MD was 0.15 Wm⁻¹ K⁻¹, which was in concurrent agreement with experimental value of 0.15 Wm⁻¹ K⁻¹, however, this experimental reading, was found from literature. Later CuO NCs were dispersed in n-alkanes and simulated, then the viscosity of 1.63 mPas and thermal conductivity 0.33-41 Wm⁻¹K⁻¹ from 303 – 323 K were recorded.

Diffusion coefficients were also measured for alkanes based nanofluid and base fluid. It was noticed that the pure alkane diffuses faster than the nanofluid based on alkane, thus giving the diffusion constant of around 7.37E-6 m²/s and alkane nanofluid around 4.3 E-11m²/s. The slower diffusion has been noticed for alkane based nanofluid compared to that of water based. This is due to the more viscous drag in alkane as compared to water based nanofluidic system.

The last simulation performed during this phase of work was the modification of CuO NPs using the carboxylate group of BA chain. The diffusion constant of the modified nanofluid was compared with the un-modified system of nanofluid. It was recorded that the modified CuO nanofluid showed a slower rate of diffusion of 1.5178E-8 m²/s and CuO nanofluid showed 2.37 E-7 m²/s.

6.1 Future Work

This research has shown different approaches for simulating metal oxide nanoparticles in fluids. There is still further work that can be carried out; both on experimental as well as on simulations. Further experimental study on modifications of metal oxide and metal NPs can be carried out using other modifying groups such as amine group and silanes. Moreover, these modifications can also be mimicked on simulation packages to analyse the properties of the system and further agglomeration and dispersion can be identified.

Further simulative investigations can be proposed on CuO NCs modified by amine modification in aqueous solutions. Currently as it is known, fluids contain bubbles; therefore bubble dynamics can be a perspective study. Changing the size of the NC, and enhancing the computational capabilities to simulate on a large scale will be beneficial. Different NPs and fluid system can be further analysed with the same techniques. Changing force field and checking differences on that basis can be a useful technique. Further work suggests more simulations on NPs with varied particle sizes. Moreover, the diffusion of nanoparticle can further be analysed as a heat transfer flowing liquid through the channels using Poiseuille law. This liquid flow is highly applicable in industrial applications for heat convection and heat dissipation.

Later, the gold NPs can also be beneficial if simulated as these particles are expensive. The simulations can be beneficial to understand their dispersion in water based systems. This could help to know the diffusion rate and other properties of gold NPs. These studies can further give an understanding regarding the nature of gold NPs interaction with polar solvents.

6.2 Recommendations

From the present work, some important facts can be established and a valuable contribution to science for further knowledge and understanding is made.

- 1) The research showed that the best device for dispersing is no other than the Ultrasonic device. This is due to its versatility and easy nature of use. NP dispersion can become un-agglomerated within minutes, depending on the NP concentration and the medium of dispersion.
- 2) The research has shown the importance of modifying NPs for stability and for enhancing the properties of NPs.
- 3) Moreover NP dispersion and stability can be altered using the pH level rather than using surfactant, however, the difference in pH level in different mediums is sometimes hard to maintain for longer duration.
- 4) Dispersion of NPs in fluid exhibits Brownian diffusion. Brownian diffusion is controlled by other environmental factors of suspension. The physiochemical stability can seize the BM at a certain level, but then again this level was not of concern through this research. However, this can be beneficial for future considerations.
- 5) NP properties such as viscosity and stability improvement can be carried out using, modifying agents, nevertheless, this can cause adverse effects.
- 6) NPs volume fraction plays a greater part in improving various thermo-physical properties rather than the size. Quantification of the size of the NP is hard to be obtained by differential light scattering. This size quantification method does not measure the true size of the NPs; it rather provides a hydrodynamic size. Thereby, TEM can be considered in future for size analysis.
- 7) Zeta potential is dependent on the solution charges, thus the surface modification can be replaced by adopting pH levelling .i.e. to stabilize the zeta potential.
- 8) Size is not a crucial parameter for claiming the viscosity change, but rather the volume fraction should be taken in consideration.

- 9) The variation of viscosity is linearly dependent on the temperature profile.
- 10) During the simulation runs, the correct estimation of the random seed number for velocity profile is necessary to obtain correct kinetic movements through the system.

6.3 List of Publication

L. REN, J. CHONG, **LOYA A.**, J.L. STAIR, Q. KANG, L. NAN, G. REN. 2015. Determination of Cu²⁺ ions release rate from the antimicrobial copper-bearing stainless steel by joint analysis using ICP-OES and XPS, Materials Technology, *Advanced Performance Materials*.

LOYA, A., STAIR, J. L., JAFRI, A. R., YANG, K. & REN, G. 2015. A molecular dynamic investigation of viscosity and diffusion coefficient of nanoclusters in hydrocarbon fluids. *Computational Materials Science*, 99, 242-246.

LOYA, A., STAIR, J. & REN, G. 2014a. Simulation and experimental study of rheological properties of CeO₂-water nanofluid. *International Nano Letters*, 1-7.

LOYA, A., STAIR, J. L. & REN, G. 2014b. The Approach of using Molecular Dynamics for Nanofluid Simulations. *International Journal of Engineering Research & Technology*, 3, 1236-1247. **LOYA, A.**, STAIR, J. L. & REN, G. 2014c. The Study of Simulating Metaloxide Nanoparticles in Aqueous Fluid. *International Journal of Engineering Research & Technology*, 3, 1954-1960.

ZHAO, C., CHEN, Y. K., JIAO, Y., **LOYA, A.** & REN, G. G. 2014. The preparation and tribological properties of surface modified zinc borate ultrafine powder as a lubricant additive in liquid paraffin. *Tribology International*, 70, 155-164

References

- AHUJA, A. S. 1982. Thermal design of a heat exchanger employing laminar flow of particle suspensions. *International Journal of Heat and Mass Transfer*, 25, 725-728.
- ALDER, B. J., GASS, D. M. & WAINWRIGHT, T. E. 1970. Studies in Molecular Dynamics. VIII. The Transport Coefficients for a Hard-Sphere Fluid. *The Journal of Chemical Physics*, 53, 3813-3826.
- ALLEN, M. P. & TILDESLEY, D. J. 1989. *Computer simulation of liquids*, Oxford University Press.
- ANANDAN, D. & RAJAN, K. 2012. Synthesis and stability of cupric oxide-based nanofluid: A novel coolant for efficient cooling. *Asian Journal of Scientific Research*, 5, 218-227.
- AQIL, A., SERWAS, H., DELPLANCKE, J. L., JÉRÔME, R., JÉRÔME, C. & CANET, L. 2008. Preparation of stable suspensions of gold nanoparticles in water by sonoelectrochemistry. *Ultrasonics Sonochemistry*, 15, 1055-1061.
- BARBIER, D., BROWN, D., GRILLET, A.-C. & NEYERTZ, S. 2004. Interface between End-Functionalized PEO Oligomers and a Silica Nanoparticle Studied by Molecular Dynamics Simulations. *Macromolecules*, 37, 4695-4710.
- BOOTHROYD, R. G. H., H. 1971. Fully developed heat transfer to a gaseous suspension of particles flowing turbulently in duct of different size. *J. Mech. Eng. Sci.*, 12, 191-200.
- BORN, M. & GREEN, H. S. 1946. A General Kinetic Theory of Liquids. I. The Molecular Distribution Functions. *Proceedings of the Royal Society of London. Series A. Mathematical and Physical Sciences*, 188, 10-18.
- BOWLES, R. S., KOLSTAD, J. J., CALO, J. M. & ANDRES, R. P. 1981. Generation of molecular clusters of controlled size. *Surface Science*, 106, 117-124.
- BROWN, D. P., CHUNG, J. N. & CROWE, C. T. 1992. A Numerical Simulation of Nanocluster Formation in Supersonic Expansion Flows. *Micromechanical Systems, ASME DSC 40*, 211-225.
- BUNTE, S. W. & SUN, H. 2000. Molecular Modeling of Energetic Materials: The Parameterization and Validation of Nitrate Esters in the COMPASS Force Field. *The Journal of Physical Chemistry B*, 104, 2477-2489.
- CANOR, T. & DENOËL, V. 2011. Transient Fokker-Planck Equation solved with SPH. Proceedings of the 5th International Conference on Advanced Computational Methods in Engineering.

- CAO, A.-M., MONNELL, J. D., MATRANGA, C., WU, J.-M., CAO, L.-L. & GAO, D. 2007. Hierarchical nanostructured copper oxide and its application in arsenic removal. *The Journal of Physical Chemistry C*, 111, 18624-18628.
- CHEN, D.-R., PUI, D. Y. & KAUFMAN, S. L. 1995. Electro spraying of conducting liquids for monodisperse aerosol generation in the 4 nm to 1.8 μm diameter range. *Journal of Aerosol Science*, 26, 963-977.
- CHEN, J., ZHANG, G. & LI, B. 2010. How to improve the accuracy of equilibrium molecular dynamics for computation of thermal conductivity? *Physics Letters A*, 374, 2392-2396.
- CHENG, S. & GREY, G. S. 2012. Structure and diffusion of nanoparticle monolayers floating at liquid/vapor interfaces: A molecular dynamics study. *The Journal of Chemical Physics*, 136, 214702.
- CHEONG, F. C. & GRIER, D. G. 2010. Rotational and translational diffusion of copper oxide nanorods measured with holographic video microscopy. *Optics Express*, 18, 6555-6562.
- CHEUNG, D. L. 2010. Molecular simulation of nanoparticle diffusion at fluid interfaces. *Chemical Physics Letters*, 495, 55-59.
- CHEVALIER, J., TILLEMENT, O. & AYELA, F. 2007. Rheological properties of nanofluids flowing through microchannels. *Applied physics letters*, 91, 233103-233103.
- CHOI, S. U. 2009. Nanofluids: from vision to reality through research. *Journal of Heat Transfer*, 131, 033106.
- COOKE, D. J. & ELLIOTT, J. A. 2007. Atomistic simulations of calcite nanoparticles and their interaction with water. *Journal of Chemical Physics*, 127, 104706-104706.
- COPPENS, M.-O., BELL, A. T. & CHAKRABORTY, A. K. 1998. Effect of topology and molecular occupancy on self-diffusion in lattice models of zeolites—Monte-Carlo simulations. *Chemical Engineering Science*, 53, 2053-2061.
- DEGEN, A. & KOSEC, M. 2000. Effect of pH and impurities on the surface charge of zinc oxide in aqueous solution. *Journal of the European Ceramic Society*, 20, 667-673.
- EASTMAN, J., CHOI, U., LI, S., THOMPSON, L. & LEE, S. 1996. Enhanced thermal conductivity through the development of nanofluids. MRS Proceedings. Cambridge Univ Press, 3.
- EASTMAN, J., CHOI, U., LI, S., THOMPSON, L. & LEE, S. 1997. Enhanced thermal conductivity through the development of nanofluids. volume 457 of Materials Research Society Symposium-Proceedings, 3-11. *Materials Research Society, Pittsburgh, PA, USA, Boston, MA, USA*.

- EISENBERG, D. & KAUZMANN, W. 1969. The structure and properties of water, Clarendon. Oxford.
- EL-TRASS, A., ELSHAMY, H., EL-MEHASSEB, I. & EL-KEMARY, M. 2012. CuO nanoparticles: Synthesis, characterization, optical properties and interaction with amino acids. *Applied Surface Science*, 258, 2997-3001.
- ERMAK, D. L. 1975. A computer simulation of charged particles in solution. I. Technique and equilibrium properties. *The Journal of Chemical Physics*, 62, 4189-4196.
- ERMAK, D. L. M., J. A. 1978. Brownian dynamics with hydrodynamic interactions. *Journal of Chemical Physics*, 69, 1352-1360.
- ESFARJANI, K., CHEN, G. & STOKES, H. T. 2011. Heat transport in silicon from first-principles calculations. *Physical Review B*, 84, 085204.
- ESPAÑOL, P. & WARREN, P. 1995. Statistical mechanics of dissipative particle dynamics. *EPL (Europhysics Letters)*, 30, 191.
- EYETT, M. 1990. Small, smaller, smallest - report on the iop conference on nanotechnology. *F&M-Feinwerktechnik & Messtechnik*, 98, 397-398.
- FAN, H. B., CHAN, E. K. L., WONG, C. K. Y. & YUEN, M. M. F. 2006. Moisture diffusion study in electronic packaging using molecular dynamic simulation. Electronic Components and Technology Conference, 2006. Proceedings. 56th. 4 pp.
- FEDELE, L., COLLA, L., BOBBO, S., BARISON, S. & AGRESTI, F. 2011. Experimental stability analysis of different water-based nanofluids. *Nanoscale Research Letters*, 6, 300.
- FERDOUS, S., IOANNIDIS, M. & HENNEKE, D. 2012. Effects of temperature, pH, and ionic strength on the adsorption of nanoparticles at liquid-liquid interfaces. *Journal of Nanoparticle Research*, 14, 1-12.
- FEYNMAN, R. P. 1959. Plenty of Room at the Bottom.
- FLANAGAN, T. P. 1990. 1989 Nanotechnology forum - 13 September 1989, London, UK. *Precision Engineering-Journal of the American Society for Precision Engineering*, 12, 112-113.
- GAO, L., SHILLCOCK, J. & LIPOWSKY, R. 2007. Improved dissipative particle dynamics simulations of lipid bilayers. *The Journal of Chemical Physics*, 126, 015101-8.
- GILJOHANN, D. A., SEFEROS, D. S., DANIEL, W. L., MASSICH, M. D., PATEL, P. C. & MIRKIN, C. A. 2010. Gold Nanoparticles for Biology and Medicine. *Angewandte Chemie International Edition*, 49, 3280-3294.

- GINGOLD, R. A. & MONAGHAN, J. J. 1977. Smoothed particle hydrodynamics: theory and application to non-spherical stars. *Monthly notices of the royal astronomical society*, 181, 375-389.
- GINGOLD, R. A. & MONAGHAN, J. J. 1982. Kernel estimates as a basis for general particle methods in hydrodynamics. *Journal of Computational Physics*, 46, 429-453.
- GONÇALVES, P., ARAÚJO, J., PINHO, M. & MARTEL, F. 2009. Modulation of butyrate transport in Caco-2 cells. *Naunyn-Schmiedeberg's Archives of Pharmacology*, 379, 325-336.
- GONZALEZ, M. A. & ABASCAL, J. L. F. 2010. The shear viscosity of rigid water models. *The Journal of Chemical Physics*, 132, 096101-2.
- GRANQVIST, C. G. & BUHRMAN, R. A. 1976. Ultrafine metal particles. *Journal of Applied Physics*, 47, 2200-2219.
- GREEN, M. S. 1952. Markoff Random Processes and the Statistical Mechanics of Time-Dependent Phenomena. *The Journal of Chemical Physics*, 20, 1281-1295.
- HAN, B., SU, T., WU, H., GOU, Z., XING, X.-H., JIANG, H., CHEN, Y., LI, X. & MURRELL, J. C. 2009. Paraffin oil as a “methane vector” for rapid and high cell density cultivation of *Methylosinus trichosporium* OB3b. *Applied Microbiology and Biotechnology*, 83, 669-677.
- HARRIS, J. G. & WANG, Y. 1992. Molecular Dynamics Simulations and Theory of Interfaces of Oligomers. MRS Proceedings. Cambridge Univ Press, 585.
- HASSAN, M. S., AMNA, T., YANG, O. B., EL-NEWEHY, M. H., AL-DEYAB, S. S. & KHIL, M.-S. 2012. Smart copper oxide nanocrystals: Synthesis, characterization, electrochemical and potent antibacterial activity. *Colloids and Surfaces B: Biointerfaces*, 97, 201-206.
- HE, Y., JIN, Y., CHEN, H., DING, Y., CANG, D. & LU, H. 2007. Heat transfer and flow behaviour of aqueous suspensions of TiO₂ nanoparticles (nanofluids) flowing upward through a vertical pipe. *International Journal of Heat and Mass Transfer*, 50, 2272-2281.
- HERNÁNDEZ BATTEZ, A., GONZÁLEZ, R., VIESCA, J. L., FERNÁNDEZ, J. E., DÍAZ FERNÁNDEZ, J. M., MACHADO, A., CHOU, R. & RIBA, J. 2008. CuO, ZrO₂ and ZnO nanoparticles as antiwear additive in oil lubricants. *Wear*, 265, 422-428.
- HEYES, D. M., NUEVO, M. J., MORALES, J. J. & BRANKA, A. C. 1998. Translational and rotational diffusion of model nanocolloidal dispersions studied by molecular dynamics simulations. *Journal of Physics: Condensed Matter*, 10, 10159.
- HILL, P., WITTING, H. & DEMETRI, E. 1963. Condensation of metal vapors during rapid expansion. *Journal of Heat Transfer*, 85, 303-314.

- HOANG, V. V. 2007. Diffusion in simulated SiO₂ nanoparticles. *Nano*, 2, 301-303.
- HOOGERBRUGGE, P. & KOELMAN, J. 1992. Simulating microscopic hydrodynamic phenomena with dissipative particle dynamics. *EPL (Europhysics Letters)*, 19, 155.
- HOSSEINI, S. M., GHASEMI, E., FAZLALI, A. & HENNEKE, D. 2012. The effect of nanoparticle concentration on the rheological properties of paraffin-based Co₃O₄ ferrofluids. *Journal of Nanoparticle Research*, 14, 1-7.
- HU, M., POULIKAKOS, D., GRIGOROPOULOS, C. P. & PAN, H. 2010. Recrystallization of picosecond laser-melted ZnO nanoparticles in a liquid: A molecular dynamics study. *The Journal of chemical physics*, 132, 164504.
- HUANG, X., BRONSTEIN, L. M., RETRUM, J., DUFORT, C., TSVETKOVA, I., ANIAGYEI, S., STEIN, B., STUCKY, G., MCKENNA, B., REMMES, N., BAXTER, D., KAO, C. C. & DRAGNEA, B. 2007. Self-Assembled Virus-like Particles with Magnetic Cores. *Nano Letters*, 7, 2407-2416.
- HWANG, N. & BARRON, A. R. 2011. BET Surface Area Analysis of Nanoparticles. *The Connexions project*, 1-11.
- IJIMA, M. & KAMIYA, H. 2009. Surface modification for improving the stability of nanoparticles in liquid media. *KONA Powder and Particle Journal*, 27, 119-129.
- JESUMATHY, S., UDAYAKUMAR, M. & SURESH, S. 2012. Experimental study of enhanced heat transfer by addition of CuO nanoparticle. *Heat and Mass Transfer*, 48, 965-978.
- JIANG, W., WU, Y., HE, B., ZENG, X., LAI, K. & GU, Z. 2010. Effect of sodium oleate as a buffer on the synthesis of superparamagnetic magnetite colloids. *Journal of Colloid and Interface Science*, 347, 1-7.
- JORGENSEN, W. L., CHANDRASEKHAR, J., MADURA, J. D., IMPEY, R. W. & KLEIN, M. L. 1983. Comparison of simple potential functions for simulating liquid water. *The Journal of Chemical Physics*, 79, 926-935.
- KANARAS, A. G., KAMOUNAH, F. S., SCHAUMBURG, K., KIELY, C. J. & BRUST, M. 2002. Thioalkylated tetraethylene glycol: a new ligand for water soluble monolayer protected gold clusters. *Chem Commun (Camb)*, 2294-5.
- KANG, H., ZHANG, Y., YANG, M. & LI, L. 2012. Nonequilibrium molecular dynamics simulation of coupling between nanoparticles and base-fluid in a nanofluid. *Physics Letters A*, 376, 521-524.
- KARAKOTI, A., HENCH, L. & SEAL, S. 2006. The potential toxicity of nanomaterials—The role of surfaces. *JOM Journal of the Minerals, Metals and Materials Society*, 58, 77-82.

- KARIMI, H., YOUSEFI, F. & RAHIMI, M. 2011. Correlation of viscosity in nanofluids using genetic algorithm-neural network (GA-NN). *Heat and Mass Transfer*, 47, 1417-1425.
- KARTHIK, R., HARISH NAGARAJAN, R., RAJA, B. & DAMODHARAN, P. 2012. Thermal conductivity of CuO-DI water nanofluids using 3- ω measurement technique in a suspended micro-wire. *Experimental Thermal and Fluid Science*, 40, 1-9.
- KENNEL, P. & ROBINSON, D. W. 1990. UK National Initiative on Nanotechnology: opportunities for collaborative research within the LINK Nanotechnology Programme. 370-376.
- KIDA, T., OKA, T., NAGANO, M., ISHIWATA, Y. & ZHENG, X.-G. 2007. Synthesis and Application of Stable Copper Oxide Nanoparticle Suspensions for Nanoparticulate Film Fabrication. *Journal of the American Ceramic Society*, 90, 107-110.
- KIRKWOOD, J. G. 1935. Statistical Mechanics of Fluid Mixtures. *The Journal of Chemical Physics*, 3, 300-313.
- KIRKWOOD, J. G., MAUN, E. K. & ALDER, B. J. 1950. Radial Distribution Functions and the Equation of State of a Fluid Composed of Rigid Spherical Molecules. *The Journal of Chemical Physics*, 18, 1040-1047.
- KOELMAN, J. & HOOGERBRUGGE, P. 1993. Dynamic simulations of hard-sphere suspensions under steady shear. *EPL (Europhysics Letters)*, 21, 363.
- KOWSARI, M. H., ALAVI, S., ASHRAFIZAADEH, M. & NAJAFI, B. 2008. Molecular dynamics simulation of imidazolium-based ionic liquids. I. Dynamics and diffusion coefficient. *The Journal of Chemical Physics*, 129, 224508-13.
- KRAYNOV, A. & MÜLLER, T. E. 2011. Concepts for the Stabilization of Metal Nanoparticles in Ionic Liquids. *Application of Ionic Liquids in Science and Technology*.
- KRUYT, H. R. 1952. In Colloid Science I. *Colloid Science*, 128-132.
- KUBO, R. 1957. Statistical-Mechanical Theory of Irreversible Processes. I. General Theory and Simple Applications to Magnetic and Conduction Problems. *Journal of the Physical Society of Japan*, 12, 570-586.
- KUMAR, A., MANDAL, S., PASRICHA, R., MANDALE, A. B. & SASTRY, M. 2003. Investigation into the Interaction between Surface-Bound Alkylamines and Gold Nanoparticles. *Langmuir*, 19, 6277-6282.
- KUMAR, D. H., PATEL, H. E., KUMAR, V. R. R., SUNDARARAJAN, T., PRADEEP, T. & DAS, S. K. 2004. Model for Heat Conduction in Nanofluids. *Physical Review Letters*, 93, 144301.

- KUROSAKI, Y., MURASAKI, T., SATOH, I. & KASHIWAGI, T. 1986. Study on heat transfer mechanism of a gas-solid suspension impinging jet (effect of particle size and thermal properties). *Proc. 8th Int. Heat Transfer Conf.* 2587-2592.
- L. XUE, P. K., S.R. PHILLPOT, S.U.-S. CHOI, J.A. EASTMAN 2004. Effect of liquid layering at the liquid–solid interface on thermal transport. *Int. J. Heat MassTransfer*, 47, 4277-4284.
- LEE, S. H. 2007. Molecular dynamics simulation study of the transport properties of liquid argon: The green-kubo formula revisited. *BULLETIN-KOREAN CHEMICAL SOCIETY*, 28, 1371.
- LEPRI, S., LIVI, R. & POLITI, A. 2003. Universality of anomalous one-dimensional heat conductivity. *Physical Review E*, 68, 067102.
- LEUBA, K. D., DURMUS, N. G., TAYLOR, E. N. & WEBSTER, T. J. 2013. Short communication: carboxylate functionalized superparamagnetic iron oxide nanoparticles (SPION) for the reduction of *S. aureus* growth post biofilm formation. *International journal of nanomedicine*, 8, 731.
- LI, D., XIE, W. & FANG, W. 2011. Preparation and properties of copper-oil-based nanofluids. *Nanoscale Research Letters*, 6, 373.
- LI, L., ZHANG, Y., MA, H. & YANG, M. 2008. An investigation of molecular layering at the liquid-solid interface in nanofluids by molecular dynamics simulation. *Physics Letters A*, 372, 4541-4544.
- LI, Y., ZHOU, J. E., TUNG, S., SCHNEIDER, E. & XI, S. 2009. A review on development of nanofluid preparation and characterization. *Powder Technology*, 196, 89-101.
- LIN, Y.-S., HSIAO, P.-Y. & CHIENG, C.-C. 2012. Thermophysical characteristics of ethylene glycol-based copper nanofluids using nonequilibrium and equilibrium methods. *International Journal of Thermal Sciences*, 62, 56-60.
- LIU, G.-R. & LIU, M. B. 2003. *Smoothed particle hydrodynamics: a meshfree particle method*, World Scientific.
- LOYA, A., STAIR, J. & REN, G. 2014a. Simulation and experimental study of rheological properties of CeO₂–water nanofluid. *International Nano Letters*, 1-7.
- LOYA, A., STAIR, J. L., JAFRI, A. R., YANG, K. & REN, G. 2015. A molecular dynamic investigation of viscosity and diffusion coefficient of nanoclusters in hydrocarbon fluids. *Computational Materials Science*, 99, 242-246.
- LOYA, A., STAIR, J. L. & REN, G. 2014b. The Approach of using Molecular Dynamics for Nanofluid Simulations. *International Journal of Engineering Research & Technology*, 3, 1236-1247.

- LOYA, A., STAIR, J. L. & REN, G. 2014c. The Study of Simulating Metaloxide Nanoparticles in Aqueous Fluid. *International Journal of Engineering Research & Technology*, 3, 1954-1960.
- LU, W.-Q. & FAN, Q.-M. 2008. Study for the particle's scale effect on some thermophysical properties of nanofluids by a simplified molecular dynamics method. *Engineering Analysis with Boundary Elements*, 32, 282-289.
- LUCY, L. B. 1977. A numerical approach to the testing of the fission hypothesis. *The astronomical journal*, 82, 1013-1024.
- LUO, M., MAZYAR, O. A., ZHU, Q., VAUGHN, M. W., HASE, W. L. & DAI, L. L. 2006. Molecular Dynamics Simulation of Nanoparticle Self-Assembly at a Liquid-Liquid Interface. *Langmuir*, 22, 6385-6390.
- LV, J., BAI, M., CUI, W. & LI, X. 2011. The molecular dynamic simulation on impact and friction characters of nanofluids with many nanoparticles system. *Nanoscale Research Letters*, 6, 1-8.
- MAEDA, A. & MUNAKATA, T. 1995. Lattice thermal conductivity via homogeneous nonequilibrium molecular dynamics. *Physical Review E*, 52, 234-239.
- MALEVANETS, A. & KAPRAL, R. 2000. Solute molecular dynamics in a mesoscale solvent. *The Journal of Chemical Physics*, 112, 7260-7269.
- MANDZY, N., GRULKE, E. & DRUFFEL, T. 2005. Breakage of TiO₂ agglomerates in electrostatically stabilized aqueous dispersions. *Powder Technology*, 160, 121-126.
- MANIMARAN, R., PALANIRADJA, K., ALAGUMURTHI, N., SENDHILNATHAN, S. & HUSSAIN, J. 2014. Preparation and characterization of copper oxide nanofluid for heat transfer applications. *Applied Nanoscience*, 4, 163-167.
- MARKOVITCH, O. & AGMON, N. 2008. Reversible geminate recombination of hydrogen-bonded water molecule pair. *The Journal of Chemical Physics*, 129, 084505-13.
- MERGOS, J. A., ATHANASSOPOULOU, M. D., ARGYROPOULOS, T. G. & DERVOS, C. T. 2012. Dielectric properties of nanopowder dispersions in paraffin oil. *Dielectrics and Electrical Insulation, IEEE Transactions on*, 19, 1502-1507.
- MINELLI, R., SERPE, L., PETTAZZONI, P., MINERO, V., BARRERA, G., GIGLIOTTI, C., MESTURINI, R., ROSA, A., GASCO, P. & VIVENZA, N. 2012. Cholesteryl butyrate solid lipid nanoparticles inhibit the adhesion and migration of colon cancer cells. *British journal of pharmacology*, 166, 587-601.
- MOHEBBI, A. 2012. Prediction of specific heat and thermal conductivity of nanofluids by a combined equilibrium and non-equilibrium molecular dynamics simulation. *Journal of Molecular Liquids*, 175, 51-58.

- MONAGHAN, J. J. 2005. Smoothed particle hydrodynamics. *Reports on Progress in Physics*, 68, 1703.
- MONTEIRO-RIVIERE, N. A. & TRAN, C. L. 2007. *Nanotoxicology: Characterization, Dosing And Health Effects*, Informa Healthcare.
- MORALES, J., SÁNCHEZ, L., MARTÍN, F., RAMOS-BARRADO, J. R. & SÁNCHEZ, M. 2005. Use of low-temperature nanostructured CuO thin films deposited by spray-pyrolysis in lithium cells. *Thin Solid Films*, 474, 133-140.
- MUDUNKOTUWA, I. A. & GRASSIAN, V. H. 2011. The devil is in the details (or the surface): impact of surface structure and surface energetics on understanding the behavior of nanomaterials in the environment. *Journal of Environmental Monitoring*, 13, 1135-1144.
- MURTHY, P. S., VENUGOPALAN, V. P., SAHOO, P., DHARA, S., DAS, A., TYAGI, A. K. & SAINI, G. 2011. Gallium oxide nanoparticle induced inhibition of bacterial adhesion and biofilm formation. *Nanoscience, Engineering and Technology (ICONSET)*. 490-493.
- NAMBURU, P. K., KULKARNI, D. P., DANDEKAR, A. & DAS, D. K. 2007. Experimental investigation of viscosity and specific heat of silicon dioxide nanofluids. *Micro & Nano Letters, IET*, 2, 67-71.
- NGUYEN, C. T., DESGRANGES, F., GALANIS, N., ROY, G., MARÉ, T., BOUCHER, S. & ANGUE MINTSA, H. 2008. Viscosity data for Al₂O₃-water nanofluid—hysteresis: is heat transfer enhancement using nanofluids reliable? *International Journal of Thermal Sciences*, 47, 103-111.
- NGUYEN, C. T., DESGRANGES, F., ROY, G., GALANIS, N., MARÉ, T., BOUCHER, S. & ANGUE MINTSA, H. 2007. Temperature and particle-size dependent viscosity data for water-based nanofluids – Hysteresis phenomenon. *International Journal of Heat and Fluid Flow*, 28, 1492-1506.
- NIMMERMARK, A., ÖHRSTRÖM, L. & REEDIJK, J. 2013. Metal-ligand bond lengths and strengths: are they correlated? A detailed CSD analysis. *Zeitschrift für Kristallographie-Crystalline Materials*, 228, 311-317.
- ORBAEK, A. & BARRON, A. R. 2009. ICP-AES analysis of nanoparticles. *Connexions module: m22058* <http://cnx.org/content/m22058/1.18>.
- PALABIYIK, I., MUSINA, Z., WITHARANA, S. & DING, Y. 2011. Dispersion stability and thermal conductivity of propylene glycol-based nanofluids. *Journal of Nanoparticle Research*, 13, 5049-5055.
- PASTORIZA-GALLEGO, M. J., CASANOVA, C., LEGIDO, J. L. & PIÑEIRO, M. M. 2011. CuO in water nanofluid: Influence of particle size and polydispersity on volumetric behaviour and viscosity. *Fluid Phase Equilibria*, 300, 188-196.

- PETERSEN, M. K., LECHMAN, J. B., PLIMPTON, S. J., GREY, G. S. & SCHUNK, P. 2010. Mesoscale hydrodynamics via stochastic rotation dynamics: Comparison with Lennard-Jones fluid. *The Journal of chemical physics*, 132, 174106.
- PIKE, J., CHAN, S.-W., ZHANG, F., WANG, X. & HANSON, J. 2006. Formation of stable Cu₂O from reduction of CuO nanoparticles. *Applied Catalysis A: General*, 303, 273-277.
- PLIMPTON, S. 1995. Fast Parallel Algorithms for Short-Range Molecular Dynamics. *J Comp Phys*, 117, 1-19.
- PRASHER, R., SONG, D., WANG, J. & PHELAN, P. 2006. Measurements of nanofluid viscosity and its implications for thermal applications. *Applied Physics Letters*, 89, 133108.
- QUE, Y., LIU, C. & CHEN, Q. 2010. Molecular Dynamics Simulation of Phase Change in Heptadecane-Pentadecane Binary System. *Materials Review*, 8, 028.
- QUEIMADA, A. J., MARRUCHO, I. M., COUTINHO, J. A. P. & STENBY, E. H. 2005. Viscosity and Liquid Density of Asymmetric n-Alkane Mixtures: Measurement and Modeling. *International Journal of Thermophysics*, 26, 47-61.
- RAJ, G. 2010. *Advanced Inorganic Chemistry: Volume II*, Krishna Prakashan.
- RAJABPOUR, A., AKIZI, F., HEYHAT, M. & GORDIZ, K. 2013. Molecular dynamics simulation of the specific heat capacity of water-Cu nanofluids. *International Nano Letters*, 3, 58.
- RAO, Z., WANG, S. & PENG, F. 2013. Self diffusion and heat capacity of n-alkanes based phase change materials: A molecular dynamics study. *International Journal of Heat and Mass Transfer*, 64, 581-589.
- RASTORGUEV, Y. L., BOGATOV, G. F. & GRIGOR'EV, B. A. 1974. Thermal conductivity of higher n-alkanes. *Chemistry and Technology of Fuels and Oils*, 10, 728-732.
- REIA DA COSTA, E. F. & SKORDOS, A. A. 2012. Modelling flow and filtration in liquid composite moulding of nanoparticle loaded thermosets. *Composites Science and Technology*, 72, 799-805.
- REN, G., HU, D., CHENG, E. W. C., VARGAS-REUS, M. A., REIP, P. & ALLAKER, R. P. 2009. Characterisation of copper oxide nanoparticles for antimicrobial applications. *International Journal of Antimicrobial Agents*, 33, 587-590.
- ROSICKA, D. & SEMBERA, J. 2013. Changes in the nanoparticle aggregation rate due to the additional effect of electrostatic and magnetic forces on mass transport coefficients. *Nanoscale Research Letters*, 8, 20.

- RUDYAK, V., KRASNOLUTSKII, S. & IVANOV, D. 2011. Molecular dynamics simulation of nanoparticle diffusion in dense fluids. *Microfluidics and Nanofluidics*, 11, 501-506.
- SANKAR, N., MATHEW, N. & SOBHAN, C. B. 2008. Molecular dynamics modeling of thermal conductivity enhancement in metal nanoparticle suspensions. *International Communications in Heat and Mass Transfer*, 35, 867-872.
- SARKAR, S. & SELVAM, R. P. 2007. Molecular dynamics simulation of effective thermal conductivity and study of enhanced thermal transport mechanism in nanofluids. *Journal of applied physics*, 102, 074302.
- SATISH, G., REDDY, K. H. V., RAMESH, K., KARNAKAR, K. & NAGESWAR, Y. V. D. 2012. Synthesis of 2-N-substituted benzothiazoles via domino condensation-heterocyclization process, mediated by copper oxide nanoparticles under ligand-free conditions. *Tetrahedron Letters*, 53, 2518-2521.
- SHEN, M.-Y. & FREED, K. F. 2002. Long Time Dynamics of Met-Enkephalin: Comparison of Explicit and Implicit Solvent Models. *Biophysical Journal*, 82, 1791-1808.
- SHIMA, P. D., PHILIP, J. & RAJ, B. 2010. Influence of aggregation on thermal conductivity in stable and unstable nanofluids. *Applied Physics Letters*, 97, 153113-3.
- SHIN, D. & BANERJEE, D. 2011. Enhancement of specific heat capacity of high-temperature silica-nanofluids synthesized in alkali chloride salt eutectics for solar thermal-energy storage applications. *International Journal of Heat and Mass Transfer*, 54, 1064-1070.
- SOHN, C. W. & CHEN, M. M. 1981. Microconvective thermal conductivity in disperse two-phase mixtures as observed in a low velocity couette flow experiment. *Journal Name: J. Heat Transfer; (United States); Journal Volume: 103:1, Medium: X; Size: Pages: 47-51.*
- SONAWANE, S. S., KHEDKAR, R. S., WASEWAR, K. L. & RATHOD, A. P. 2012. Dispersions of CuO Nanoparticles in Paraffin Prepared by Ultrasonication: A Potential Coolant. *International Proceedings of Chemical, Biological & Environmental Engineering*, 46.
- SPAETH, J. R., KEVREKIDIS, I. G. & PANAGIOTOPOULOS, A. Z. 2011. A comparison of implicit- and explicit-solvent simulations of self-assembly in block copolymer and solute systems. *The Journal of Chemical Physics*, 134, 164902-13.
- STARR, F. W., SCHRÖDER, T. B. & GLOTZER, S. C. 2002. Molecular Dynamics Simulation of a Polymer Melt with a Nanoscopic Particle. *Macromolecules*, 35, 4481-4492.
- STUKOWSKI, A. 2010. Visualization and analysis of atomistic simulation data with OVITO—the Open Visualization Tool. *Modelling and Simulation in Materials Science and Engineering*, 18, 015012.

- SUN, C., LU, W.-Q., LIU, J. & BAI, B. 2011. Molecular dynamics simulation of nanofluid's effective thermal conductivity in high-shear-rate Couette flow. *International Journal of Heat and Mass Transfer*, 54, 2560-2567.
- SUN, H. 1998. COMPASS: An ab Initio Force-Field Optimized for Condensed-Phase Applications Overview with Details on Alkane and Benzene Compounds. *The Journal of Physical Chemistry B*, 102, 7338-7364.
- SUN, H., REN, P. & FRIED, J. R. 1998. The COMPASS force field: parameterization and validation for phosphazenes. *Computational and Theoretical Polymer Science*, 8, 229-246.
- SYMEONIDIS, V., EM KARNIADAKIS, G. & CASWELL, B. 2005. Dissipative Particle Dynamics Simulations of Polymer Chains: Scaling Laws and Shearing Response Compared to DNA Experiments. *Physical Review Letters*, 95, 076001.
- THOMPSON, S. J. P. A. A. P. 2012. Computational Aspects of Many-body Potentials,. *MRS Bulletin*, 37, 513-521.
- TIAN, Y., HE, Y., YU, L., DENG, Y., ZHENG, Y., SUN, F., LIU, Z. & WANG, Z. 2008. In situ and one-step synthesis of hydrophobic zinc borate nanoplatelets. *Colloids and Surfaces A: Physicochemical and Engineering Aspects*, 312, 99-103.
- TRETIAKOV, K. V. & SCANDOLO, S. 2004. Thermal conductivity of solid argon from molecular dynamics simulations. *The Journal of Chemical Physics*, 120, 3765-3769.
- VILA, M., DÍAZ-GUERRA, C. & PIQUERAS, J. 2010. Optical and magnetic properties of CuO nanowires grown by thermal oxidation. *Journal of Physics D: Applied Physics*, 43, 135403.
- WANG, H., JUNGHANS, C. & KREMER, K. 2009. Comparative atomistic and coarse-grained study of water: What do we lose by coarse-graining? *The European Physical Journal E*, 28, 221-229.
- WOLLOWSKI, I., RECHKEMMER, G. & POOL-ZOBEL, B. L. 2001. Protective role of probiotics and prebiotics in colon cancer. *The American journal of clinical nutrition*, 73, 451-455.
- WU, D., ZHU, H., WANG, L. & LIU, L. 2009. Critical issues in nanofluids preparation, characterization and thermal conductivity. *Current Nanoscience*, 5, 103-112.
- WU, Y., TEPPER, H. L. & VOTH, G. A. 2006. Flexible simple point-charge water model with improved liquid-state properties. *The Journal of Chemical Physics*, 124, 024503-12.
- WU, Y. Y., TSUI, W. C. & LIU, T. C. 2007. Experimental analysis of tribological properties of lubricating oils with nanoparticle additives. *Wear*, 262, 819-825.

- XIANG, H., LONG, Y., YU, X., ZHANG, X., ZHAO, N. & XU, J. 2011. A novel and facile method to prepare porous hollow CuO and Cu nanofibers based on electrospinning. *CrystEngComm*, 13, 4856-4860.
- XU, L.-J., ZHAO, J.-X., ZHANG, T., REN, G.-G. & YANG, Z. 2009. In vitro study on influence of nano particles of CuO on CA1 pyramidal neurons of rat hippocampus potassium currents. *Environmental Toxicology*, 24, 211-217.
- XUAN, Y. & LI, Q. 2000. Heat transfer enhancement of nanofluids. *International Journal of heat and fluid flow*, 21, 58-64.
- XUAN, Y. A. L., Q. 2000. Heat transfer enhancement of nanofluids. *International Journal of Heat and Fluid Transfer*, 21, 58-64.
- YANG, Z., LIU, Z., ALLAKER, R., REIP, P., OXFORD, J., AHMAD, Z. & REN, G. 2010. A review of nanoparticle functionality and toxicity on the central nervous system. *Journal of the Royal Society Interface*, 7, 411-422.
- YATSUYA, S., HAYASHI, T., AKOH, H., NAKAMURA, E. & TASAKI, A. 1978. Magnetic Properties of Extremely Fine Particles of Iron Prepared by Vacuum Evaporation on Running Oil Substrate. *Japanese Journal of Applied Physics*, 17, 355.
- ZHANG, B. & YAN, B. 2010. Analytical strategies for characterizing the surface chemistry of nanoparticles. *Analytical and Bioanalytical Chemistry*, 396, 973-982.
- ZHANG, L., HE, R. & GU, H.-C. 2006. Oleic acid coating on the monodisperse magnetite nanoparticles. *Applied Surface Science*, 253, 2611-2617.
- ZHAO, C., CHEN, Y. & REN, G. 2013. A study of tribological properties of water-based ceria nanofluids. *Tribology Transactions*, 56, 275-283.
- ZHAO, C., CHEN, Y. K., JIAO, Y., LOYA, A. & REN, G. G. 2014. The preparation and tribological properties of surface modified zinc borate ultrafine powder as a lubricant additive in liquid paraffin. *Tribology International*, 70, 155-164.
- ZHAO, J.-F., LUO, Z.-Y., NI, M.-J. & CEN, K.-F. 2009. Dependence of Nanofluid Viscosity on Particle Size and pH Value. *Chinese Physics Letters*, 26, 066202.
- ZHAO, L., LIU, L. & SUN, H. 2007. Semi-ionic Model for Metal Oxides and Their Interfaces with Organic Molecules. *J Phys Chem C Nanomater Interfaces*, 111, 10610-10617.
- ZHU, H.-T., LIN, Y.-S. & YIN, Y.-S. 2004. A novel one-step chemical method for preparation of copper nanofluids. *Journal of Colloid and Interface Science*, 277, 100-103.

- ZHU, H., LIU, S., XU, L. & ZHANG, C. 2007. Preparation, characterization and thermal properties of nanofluids. *Leading Edge Nanotechnology Research Developments*, 5-38.

Appendix A – Dynamic and static model of nanoparticle dispersion

1) Equation and formulation

Static particle model

The static particle model has got two parallel routes of heat flow. First is by liquid conduction of heat and the other is heat conducted by the NPs. Therefore, for the Static particle model the total heat transfer is a one dimensional heat transfer system i.e. expressed in "Q". By this, the theoretical effective thermal conductivity can be calculated.

$$Q = q_m + q_p \quad (\text{A-1})$$

Where "q" is;

$$q = -\lambda_m A_m \left(\frac{dT}{dx} \right)_m - \lambda_p A_p \left(\frac{dT}{dx} \right)_p \quad (\text{A-2})$$

where variables are

Table A-0-1 Variables of equation (A-2)

Variables	Stands for	Variable	Stands for
Q	Total heat flow	$\left(\frac{dT}{dx}\right)$	Temperature gradient of the respective medium (base fluid).
λ	Thermal conductivity	m	Liquid medium
A	Heat transfer area	p	Particle phase

The ratio of the total heat transfer area can be taken into proportion of total surface area of the nanoparticles (S_p) and the liquid as the (S_m) per unit volume of the suspension, further each variable is explained in **Table A-1**.

Assuming both particles i.e. liquid particle and NP as spherical shape so radius of these particles can be represented as r_p and r_m respectively. This help in calculating the effective surface area of particles. This furthers, undermines the amount of functional group that can possibly get attached to surface can be measured.

The total surface area could be determined by multiplying the number of particles n and the surface volume fraction of the NPs as the V , and the volume fraction of liquid will be $(1-\epsilon)$, the number of particles for the two constitutes can be determined by **equation A-3** and **A-4**:

$$n_m = \frac{1-V}{\left(\frac{4}{3}\right) * \pi r_m^3} \quad (\text{A-3})$$

$$n_p = \frac{V}{\left(\frac{4}{3}\right) * \pi r_p^3} \quad (\text{A-4})$$

Thereby corresponding surface area to the number of nanoparticle and number of liquid particle is given by **equation A-5** and **A-6**.

$$S_m = n_m 4\pi r_m^2 = 3 \frac{(1-\varepsilon)}{r_m} \quad (\text{A-5})$$

$$S_p = n_p 4\pi r_p^2 = 3 \frac{\varepsilon}{r_p} \quad (\text{A-6})$$

Now after obtaining the above surface area equation, equating $\frac{S_m}{S_p} = \frac{A_m}{A_p}$ and now substituting the equation (6 and 7) into heat transfer equation (3), we get:

$$q = -\lambda_m A_m \left(\frac{dT}{dx} \right) \left[1 + \frac{\lambda_p \varepsilon r_m}{\lambda_m (1-\varepsilon) r_p} \right] = -\lambda_{\text{eff}} A_m \left(\frac{dT}{dx} \right) \quad (\text{A-7})$$

Where effective thermal conductivity i.e. λ_{eff} is expressed as

$$\lambda_{eff} = \lambda_m \left[1 + \frac{\lambda_p V r_m}{\lambda_m (1-V) r_p} \right] \quad (A-8)$$

Now the dimensionless form of heat transfer is expressed as:

$$q^* = \frac{q}{-\lambda_m A_m \left(\frac{dT}{dx} \right)} = 1 + \frac{\lambda_p V r_m}{\lambda_m (1-V) r_p} = \frac{\lambda_{eff}}{\lambda_m} \quad (A-9)$$

The **equation A-9** deduces that the thermal conductivity enhancement is directly related to the ratio of the conductivities and also to the volume fraction i.e. V . This proportionality has been taken by the investigated study of thermal conductivity enhancement of nanofluids based on concentration of 4nm Au nanoparticles in Toluene (Kumar et al., 2004). However, this enhancement is inversely related to the radius of the nanoparticles.

Dynamic particle model

There is a strong dependence of nanoparticle suspension thermal conductivity to increase with temperature increment. This also effect, the viscosity of the fluid as given by Shima et al., (2010), this effect accounts for variation of velocity leading to change in thermal conductivity and temperature. This is due to the MD and collision of particle i.e. it represents as a colloidal system. According to the kinetic theory the rise in temperature is directly proportional to the increase in velocity where the Kinetic energy is represented as:

$$K.E_p = \frac{1}{2} m_p v_p^2 \quad (\text{A-10})$$

Where m_p is the mass of the nanoparticle and V is the average velocity of the particle so Kinetic energy can be determined by **equation A-10**. Since we know that the thermal conductivity of particle is directly proportional to Velocity of the particle which is given by **equation A-11** and **A-12**

$$K.E_p \propto \bar{V}_p \quad (\text{A-11})$$

Therefore

$$K_p = c \bar{V}_p \quad (\text{A-12})$$

c is the constant of thermal conductiveness due to the effect of velocity. As thermal conductivity is directly proportional to the velocity, this is also directly proportional to the size of NPs where size refers to particle radius. In **equation A-15** where \bar{V}_p is the average particle velocity of NP, now combining **equation A-8** and **A-12**, the complete model for calculating the varying effective thermal conductivity with respect to temperature is obtained as **equation A-13**. Over here BM can be expressed with thermal conductivity enhancement as **equation A-14**

$$\lambda_{eff} = \left[\frac{c \bar{V}_p V r_m}{(1-V) r_p} \right] + \lambda_m \quad (\text{A-13})$$

Thereby;

$$\text{enhancement of conductivity} \propto \bar{V}_p \left[\frac{V}{1-V} \right] \frac{1}{r_p} \quad (\text{A-14})$$

Now finalized average velocity of nanoparticle due to BM at a particular temperature in the suspension condition can be expressed by Stokes-Einstein mean velocity of NP i.e.

$$\bar{V}_p = \frac{2K_b T}{\pi \eta d_p^2} \quad (\text{A-15})$$

Table A-0-2 Variables of equation (A-15)

<i>Variables</i>	<i>Stands for</i>
K_b	Boltzmann Constant
T	Temperature
μ	Dynamic viscosity of the fluid medium
d_p	Diameter of particle

Now c can be evaluated with help of kinetic theory i.e. shown in **equation A-16**.

$$c \cong \frac{\sqrt{Vl\bar{c}_v}}{3} \quad (\text{A-16})$$

Where

Table A-0-3 Variables of equation (A-16)

<i>Variables</i>	<i>Stands for</i>
\bar{c}_v	Specific heat per particle
l	Mean free path

V

Volume fraction

Where the specific heat per particle can be calculated **equation A-17** with help of Debye's Model for the particle i.e.

$$\bar{c}_v = 3NK_B \quad (\text{A-17})$$

Where N is the number of atoms and k is the Boltzmann constant. Hence

Value of c is approximately unity i.e. shown in **equation A-18**.

$$c = \frac{3 * 10^{18} 10^{-2} 10^{-16}}{3} = 1 \quad (\text{A-18})$$

Where $N = 10^6$, $n = 10^{18}$, $l = 10^{-2}$, $\bar{c}_v = 10^{-16}$

Finally, by above mentioned equations it will be easy to calculate the effect of BM of NP in the suspension form. Hence, computing this all, can help in simulating phenomena of NP suspension using BM. This formula computation helped in simulating the Brownian effect for dispersion of NPs in fluids.

COMPASS Force Field computation paramters:

Equations A-19 and **A20** are used for *compass forcefield* calculation during simulations are:

$$E_{total} = \sum bond + \sum \theta + \sum \phi + \sum x + E_{UB} \quad (\text{A-19})$$

Table A-0-4 Description of variables on total potential energy for equation (A-19)

Symbols	Abbreviations
\sum_{bond}	Summation of All bonds
$\sum\theta$	The covalent bond stretching energy terms
$\sum\phi$	Summation of all angles
$\sum x$	The bond angle bending energy terms,
E_{UB}	Summation of all torsions
$E_{crossterms}$	The torsion angle rotation energy terms
$E_{Nonbond}$	Summation of all out of plane angles
E_{H-Bond}	This is a harmonic function.
	$E_{crossterms} + E_{Nonbond} + E_{H-Bond}$
	Cross interacting terms include the dynamic variation among the bond stretching, bending, and torsion angle rotation.
	Deals with Vander Waals forces and Columbic electrostatic force.
	Hydrogen bonding term.

$$E_{Non\ bond} = \sum_{i>j} \left[\frac{A_{ij}}{r_{ij}^9} - \frac{B_{ij}}{r_{ij}^6} \right] + \sum_{i>j} \left[\frac{q_i q_j}{\epsilon r_{ij}} \right] + E_{H-Bond} \quad (A-20)$$

Where q is the atomic charge, ϵ is the dielectric constant, and r_{ij} is the i-j atomic separation distance.

A_{ij}, B_{ij} all are from quantum mechanics. Later implemented by discover module of Material studio.

DPD phenomena further connected equations explained from **equation A-21 to A-25:**

$$r < r_c$$

$$F^C = A\omega(r) \quad (A-21)$$

$$F^D = -\gamma \omega^2(r) (\mathbf{r}_{ij} \cdot \overline{\mathbf{v}_{ij}}) \quad (\text{A-22})$$

$$F^R = \sigma \omega(r) \alpha(\Delta t)^{\frac{1}{2}} = \sqrt{2K_b T} \omega(r) \alpha(\Delta t)^{\frac{1}{2}} \quad (\text{A-23})$$

$$\omega(r) = 1 - \frac{r}{r_c} \quad (\text{A-24})$$

R_{ij} is a unit vector in the direction $R_i - R_j$, V_{ij} is the vector difference in velocities of the two atoms = $V_i - V_j$, α is a Gaussian random number with zero mean and unit variance, d_t is the timestep size, and $\omega(r)$ is a weighting factor that varies between 0 and 1. R_c is the cut-off. σ is set equal to $\sqrt{2K_b T}$, where K_b is the Boltzmann constant and T is the temperature parameter in the pair-style command.

$$W(R, h) = \alpha_d \begin{cases} (1+3R)(1-R)^3, & \text{if } R \leq 1 \\ 0, & \text{if } R > 1 \end{cases} \quad (\text{A-25})$$

With $R = r/h$ and where α_d is dependent on dimension n of the state space and its values are listed in **Table A-5**.

Table A-0-5 Dimension and their state space values.

<i>Dimensions</i>	<i>State space</i>
1-D	$5/4h$
2-D	$5/\pi h^2$
3-D	$105/16\pi h^3$

Appendix B – ICP methodology

ICP methodology for investigating Cu^{+2} ion release from NPs in water nanofluid suspension.

Consideration of apparatus and equipment before ICP examination is carried out.

For the experiments you need to acid wash everything you think you will need. This takes into consideration all glass pipettes, containers and volumetric flasks you will use.

For example;

- If you do a hot plate digestion, you will need to wash a 150ml tall beaker and watch glass per sample
- If you do a microwave digestion you will need to wash the Teflon digestion tube set per sample
- You will need 1 x 5ml glass bulb pipette to transfer high purity acid for digestion
- Depending on how much copper you think is in your sample, you will need to wash either a 25 ml or 50 ml volumetric flask per sample
- You will need to wash a set of volumetric flasks in order to make your calibration standards
- Also the set of bulb pipettes for making your calibration standards
- For the volume of 2% HNO_3 you will need to make up (for blanks, calibration standards etc) and you will need a large volumetric flask (e.g. 500ml or 1L)

Appendix C – LAMMPS input script

```
# =====  
  
# LAMMPS input script for Viscosity of CeO2 in water  
  
# Unit & Variable definition  
  
# =====  
  
units      real  
  
variable  T equal 323  
  
variable  V equal vol  
  
variable  dt equal 1e-3  
  
variable  p equal 100 # correlation length  
  
variable  s equal 10 # sample interval  
  
variable  d equal $p*$s # dump interval  
  
# =====  
  
# Convert from LAMMPS real units to SI  
  
# =====  
  
variable  kB equal 1.3806504e-23 # (Boltzmann Constant)  
  
variable  atm2Pa equal 101325.0 # (atmospheric to Pascal)  
  
variable  A2m equal 1.0e-10 # (Angstrom to meters)  
  
variable  fs2s equal 1.0e-15 # (Femtosecond to seconds)  
  
variable  convert equal ${{atm2Pa}}*${atm2Pa}*${fs2s}*${A2m}*${A2m}*${A2m}
```

```
# =====  
  
# Dimension settings and Reading atom file supplied by material studio  
  
# =====  
  
dimension 3 # (3D)  
  
boundary p p p # (Periodic assumption)  
  
atom_style full # (Atom setting all inclusive)  
  
read_data data.wce01pv # (Reads the initial configuration file)  
  
  
# =====  
  
# Create groups  
  
# =====  
  
group Ce1 type 1 # (Grouping atoms of same type)  
  
group H type 2  
  
group O type 3  
  
group O2 type 4  
  
group O3 type 5
```

```
# =====  
  
# Potential Parameters  
  
# =====  
  
pair_style hybrid/overlay sph/heatconduction dpd/tstat 1.0 1.0 2.5 34387 ## ( Pair potential settings)  
  
pair_coeff * * sph/heatconduction 2.0e-9 2.0e-9  
  
pair_coeff * * dpd/tstat 1.0  
  
bond_style harmonic  
  
bond_coeff 1 493.8480 0.9600 # Setting bonding coefficients  
  
thermo $d # (Number of steps for between each interval)  
  
# =====  
  
# Velocity, fixes, equilibration and thermalization  
  
# =====  
  
communicate single vel yes  
  
fix 1 all viscosity 100 x z 60  
  
velocity all create $T 4928459 rot yes dist gaussian  
  
fix 2 all npt temp $T $T 20 aniso 1.0 1.0 1000  
  
fix 3 all thermal/conductivity 100 z 20
```

```
# =====  
  
# Viscosity calculation  
  
# =====  
  
variable pxy equal pxy  
  
variable pxz equal pxz  
  
variable pyz equal pyz  
  
fix SS all ave/correlate $s $p $d &  
  
v_pxy v_pxz v_pyz type auto file S0St.dat ave running # (Stress autocorrelation command)  
  
variable scale equal ${convert}/(${kB}*${T})*V*$s*${dt}  
  
variable v11 equal trap(f_SS[3])*$ {scale}  
  
variable v22 equal trap(f_SS[4])*$ {scale}  
  
variable v33 equal trap(f_SS[5])*$ {scale}  
  
#variable v_v equal (v11+v22+v33)/3  
  
thermo_style custom step temp press v_pxy v_pxz v_pyz v_v11 v_v22 v_v33
```

```
# =====
```

Neighbouring settings for inter-collision

```
# =====
```

```
neighbor 2.5 bin
```

```
neigh_modify delay 0
```

```
thermo_style custom step temp press vol pe
```

```
thermo_modify norm no flush yes
```

```
# =====  
  
# Computer and fix different properties  
  
# =====  
  
#=====MSD=====  
  
compute msd all msd com yes  
  
fix msd all ave/time 1 10 10 c_msd[4] file water_CeO2_308.msd  
  
#=====RDF=====  
  
compute myRDF all rdf 1000  
  
fix myRDF all ave/time 1 10 100 c_myRDF file tmp_CeO2_308.rdf mode vector  
  
#=====Density=====  
  
# Compute density in g/cm^3  
  
variable dens equal atoms*${watMoleculeMass}/(vol*${A3 in cm3})  
  
fix dens all ave/time 1 10 100 v_dens file wat_CeO2.dens  
  
# =====  
  
# screen dumps visualization  
  
# =====  
  
dump waterdump all atom 1000 Viscosity_CeO  
  
restart 1000 Viscosity_ceO
```

```
# =====  
  
# Run Simulation  
  
# =====  
  
timestep 0.156  
  
run      20000  
  
# =====  
  
# Printing the required quantity  
  
# =====  
  
variable  v equal (v_v11+v_v22+v_v33)/3.0  
  
variable  ndens equal count(all)/vol  
  
print    "average viscosity: $v [Pa.s/ @ $TK, ${ndens} /A^3"
```

Appendix D – Published Study 1

The paper presented in appendix C is a published study on CuO nanoparticles in water; this study explains the thermo-physical properties of CuO nanofluid and how the molecular dynamics of it can be performed using LAMMPS.

International Journal of Engineering Research & Technology (IJERT)
ISSN: 2278-0181
Vol. 3 Issue 4, April - 2014

The Study of Simulating Metaloxide Nanoparticles In Aqueous Fluid.

Adil Loya
School of Engineering and
Technology
University of Hertfordshire
Hatfield, UK

Jacqueline L. Stair
School of Pharmacy
University of Hertfordshire
Hatfield, UK

Guogang Ren
School of Engineering and
Technology
University of Hertfordshire
Hatfield, UK

Abstract— Dynamics of nanoparticle dispersion in engineering fluids has a significant impact on the quality and performance of liquid based fluidic systems; such as in biomedical fluids, contaminated water system and its purifications. The dispersion dynamics of metaloxide nanoparticles in an aqueous fluidic system, was studied using large-scale Atomic/Molecular Massively Parallel Simulator (LAMMPS) in this paper by using CuO particles as a targeting material in water (H₂O) fluid system. Two major calculation parameters were selected for evaluating the system in the simulation: a) discrete particle dynamics (DPD), and b) smoothed particle hydrodynamics (SPH). Comparing experimental with the molecular dynamics (MD) simulation results show good correlations with the MD viscosity as 1.44 mPas at 313K and diffusion coefficient of metaloxide nanoparticle-H₂O system was obtained as $1.03 \times 10^{-8} \text{ m}^2/\text{s}$.

Keywords – Nanoparticle dispersion in fluids • Molecular dynamics • Diffusion simulations • Copper oxide • LAMMPS

I. INTRODUCTION

Nanoparticles provides large surface area to their volume ratio, which may reduce or enhance their diffusion capabilities in a fluidic system, and specifically controlling of this diffusion proved to be a challenging task [1, 2]. Several studies have focused on nano particle dispersion and stabilization in a base fluid such as water, to establish an effective methodology for a thorough dispersion of nano particles in fluidic systems [3-5]. The metal oxide nano particles (M₂O_n) are the widely used in biomedical devices, environmental and water contamination research due to their environmental stability, functionality [6], thermo-mechanical [7-9] and physio-chemical properties [10, 11]. These types of nanoparticles including CuO, ZnO, MgO, CaO, and many others, are increasingly used in applications such as biomedical fluidic and water purification [12-14], as antibacterial additives and components and mostly the medical devices surface coating [6, 12, 15, 16]. Especially, in the water purification processes and biomedical applications, it is involving the releases of Cu²⁺, Zn²⁺ and ionic particles that may result in disinfection of contaminations from bacteria pathogens [12-14]. As the metal oxides such as CuO nanoparticles (CuO-NPs) are common atomic structures and thermally and physically stable and cost-effective,

therefore, this study concentrated on investigating the CuO nanoparticle's dispersibility in water fluid system using molecular dynamics which is not yet reported [3, 4].

Simulations as a major prediction of the mechanism of nanoparticles dispersion in engineering liquids, is a fast and cost-effective alternative parallel to the experimental works. A number of diffusion simulations of polymeric, ionic and mineral nanoparticles have been extensively reported [17-19]. The major particle diffusion phenomena in these studies have been carried out is based on the Brownian dynamics (BD), targeting the random motion of the nanoparticle in a water fluidic system. One of the most accepted simulation parameters for the dispersion of metal oxide nanoparticles in a water system is the discrete particle dynamic (DPD) potential, which is used for assessing the power to disperse nanoclusters reflecting the phenomena of the Brownian dynamics [20, 21]. Studies using DPD for complex fluidic systems [22-24] shown that the dispersion of nanoparticles in water exhibits complex properties in simulation.

An initial selection of boundary conditions is carried out with a molecular dynamic simulator [25], working on cluster particle sizes, their force field interactions, diffusion in solvent, and physiochemical properties [26, 27]. Within the simulation system, force field is a mathematical parameter that governs the energies and potentials between interactive atoms controlled by the pair potentials between atoms. The physiochemical settings of the system referred to the thermal, chemical and physical properties of the system such as initial temperature settings, charges and dynamics of the system.

3 Materials

The CuO nanoparticles were prepared by thermal plasma forming technology (Tescmia™) by QinetiQ Nanomaterial Ltd (Farnborough, UK). The bulk density of CuO-NPs is 6.3-6.49 g/cm³. The measurement of the CuO-NP average crystal size mixture is 22.6 nm.

The simulated CuO-NP configuration of crystal lattice was α is 90°, β is 99.54° and γ is 90° with a space group of C2/c that was generated on a Material Studio software by Accelry Ltd.

4 Methodology

Experimental viscosity was measured in this work by using TA 1500Ex. The TA Instruments AR1500ex Rheometer is an advanced analyzer for measuring properties of rheology such as viscosity, shear rate, stress and strain. The experimental viscosity of CuO-water nanofluid system was measured to compare and support the MD results. The mixture of nanoparticles in the experiments were measured and calculated with a volumetric fraction of ~2% vol.

1.3 Simulation conditions: nanoparticles dispersed in water fluids

Metal oxide nanoparticles in water fluidic media were simulated by using COMPASS force field on condensed-phase optimized molecular Potential [26-29]. The COMPASS force field was used for computational energy calculations. This force field has been implemented for different molecular interactions from organics, inorganics, monomers, and polymers, to metals, metallic ions and metal oxides [26-29]. Green-Kubo formulation was also used shown in Equation 5 to extrapolate the system viscosity, which is a well-established method of computing the viscosity by autocorrelation functions equation 6. Later the results of the viscosity achieved through simulation are validated using stress autocorrelation function as shown in Fig.3.

The Interactive parameters for the fluidic system used in this simulation are DPD and SPH potential for composing the diffusion model of the CuO-NP-water fluidic system. The DPD factor is explained by Equation 1, which composes of 3 force components, accounting for the particle random movement and momentum through the system.

$$\vec{f} = (F^C + F^D + F^R) \hat{r}_{ij} \quad (1)$$

These three forces (i.e. F^C , F^D and F^R) are comprised in DPD pair-style to execute the DPD action to perform the desired motion. The influence of the forces in particular directions is handled by \hat{r}_{ij} .

1.4 Simulation

The dispersing nanoparticles in water was simulated by using LAMMPS [30-32] composed of 80000 transferable intermolecular potential (TIP3P) water molecules [33]. The nanoparticles used in this study are in 80000 TIP3P water molecular system. The system was simulated with SPH and DPD potential in an imaginary orthogonal box (i.e., 100 Angstrom x 100 Angstrom x 100 Angstrom) shown in Fig.1. The initial simulation system was setup by using 3320 CuO molecules, which were represented by 2 nanoclusters each carrying 1660 molecules bonded by compass force field. Therefore, the simulated particles in this work are in the nanometre scale between 4-6 nm. This is due to the limitations of current lab-based computers, which are impractical for simulating particles larger than 10nm with particle volume fraction between 1.5-2% equivalent to the volume fraction used in the experiments. Simulation trajectories were visualized using OVITO the code free available by Alexander Stukowski [34].

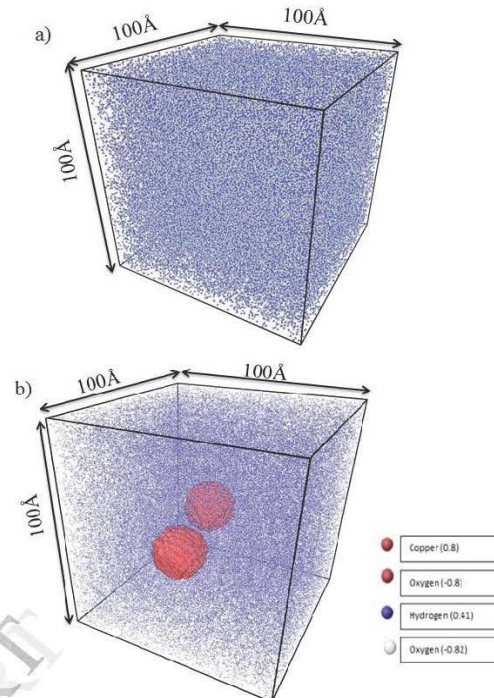


Fig.1 Molecular system comparison with and without CuO-NPs: a) simulation results (control) of pure water molecules in an Orthogonal box of 100 Angstrom x 100 Angstrom x 100 Angstrom, the box contained 80000 TIP3P water molecules, where white is oxygen and blue is hydrogen. b). Molecular system of 80000 TIP3P water molecules with 2 CuO-NPs of 4nm in an Orthogonal box of 100 Angstrom x 100 Angstrom x 100 Angstrom, where white is oxygen, blue is hydrogen and red is representing CuO-NP, under NPT (NPT ensemble enables the system to keep the pressure constant but the volume is varied) conditions i.e. 1 bar pressure at the temperature of 303K.

5 Results and Discussion

The simulations were carried out by resembling the nanoparticle simulation in the water fluidic system. Although the particulate did not reach the actual nanoscale size in the simulation, the results still proved valuable as it showed temperature effects on the system's viscosity and particle diffusion efficiency, which is mostly effected by the particle volume fraction [35]. The diffusion coefficient is a measure of the number of atoms movement with the change in position; it is dependent on the viscosity, size and shape of molecules. However, viscosity is a measure of resistance to the fluid flow and depends on the gradual deformation of shear stress. The equations used for calculating these variables, shown in Table 1 are the bases for analyzing and comparing the results with the experimental trends. The properties analysed using the MD simulation were dependent on the statistical mechanical calculation implemented by Green-Kubo. However, images shows a constant volume, whereas, during

the simulation due to implementation of NPT ensemble caused the volume of simulation box to vary. The variable definition and further statistical formula has been presented in Table

1. Where n is the number of atoms, T is the temperature, t is timeperiod, v_i is velocity of particle i and p is the shear stress in Table 1.

Table 1 Diffusion coefficient and viscosity variables, definitions and the statistical mechanical formula, and their equations.

Property	Variable	Definition	Statistical Mechanical formula (Green-Kubo)
Diffusion Coefficient	D	$\dot{n} = -D \frac{\partial \phi}{\partial x}$ (2)	$D = \frac{1}{6} d \langle (r_i(t) - r_i(0))^2 \rangle / dt$ (4)
Viscosity	μ	$F = \mu \frac{\partial U}{\partial x}$ (3)	$\mu = \frac{V}{3k_B T} \int_0^\infty \left\langle \sum_{x \neq y} P_{xy}(t) P_{xy}(0) \right\rangle dt$ (5)

Where \dot{n} is the diffusion flux, D is the diffusion coefficient and $\frac{\partial \phi}{\partial x}$

$\frac{\partial \phi}{\partial x}$ is the concentration at a particular position as shown in equation 1; μ (mPa s) is viscosity for the system V is the

Brownian volume fraction (\AA^3) of particles in the system, $\frac{\partial U}{\partial x}$ Velocity in x direction, F is the magnitude of force in equation

3; $r_i(t)$ radius of particle i at time t and $r_i(0)$ radius of particle i at starting time in equation 4; T is the temperature (K) of the system and P_{xy} is the stress component for atoms (atm), t is time (ps), K_B Boltzmann constant in equation 5.

Viscosity

The simulated viscosity of CuO-NP dispersed in water is coherent to the experimental values. The Green Kubo method utilizes stress tensor to analyse the viscosity. This stress tensor P_{xy} is the stress component between molecules of the x-y direction.

The viscosity from the TIP3P water model is decreasing with increasing temperature as shown in Figure 2. These simulation values are in good correlations with H.L. Tepper and Gonzalez results [36, 37], which were shown at temperatures around 298-300K giving the viscosity of TIP3P model as 0.321-0.311 mPas, whereas the experimental value obtained in this work was around 0.59 mPas. These values can further be compared with Min-yi Shen and Karl F. Freed's [38] achieved similar viscosity around 0.5 mPas at 300K using simulation technique of Langevin dynamics. The viscosity values obtained in this work were slightly higher due

to the higher heat conduction through the system and dissipative particle dynamics potential.

A decrease was seen for the viscosity of the TIP3P water model with the increasing temperature of the system. This is a usual phenomenon for any liquid when temperature is increased while molecules started to expand which leads to anomalous decrease in viscosity shown in Figure 2.

High concurrent trend of experimental viscosity results [29] of dispersing CuO-NPs in deionized water were compared with the algorithm-neural network (GANN) method [39], which are shown in Fig. 2 to the trend of molecular dynamic simulation results. Some studies relate that particle size shows negligible effect over the viscosity [40] while others suggest that a decrease in particle size gives a viscosity increase [41-44] and vice versa for other researchers [35, 45, 46]. The results of the system are averaged over the N number of particles in the system.

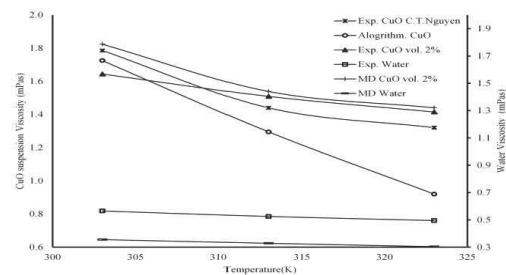


Fig. 2 Viscosity (mPa.s) comparison of the fluidic systems of experimental, MD simulation of CuO-water system, pure water, and the algorithm results [39] and experimental [35].

This size dependent system causes an increase in the number of runs and equilibration time. Later improvement of the statistical precision is achieved by three off diagonal element of the stress tensor.

Stress Autocorrelation function (SACF)

The molecular dynamic viscosity was measured using the Green-Kubo method. This method uses an autocorrelation function to validate the results of viscosity. The viscosity validation is carried out using the stress autocorrelation function. This function uses three off-diagonal terms to analyse the system viscosity. These terms are P_{xy} , P_{yz} and P_{zx} related to pressure fluctuations in different directions. The stress tensors in between the angular brackets as shown in equation 6 compute's averages of large number of samples. Where term P_{xy} computes the stress in x-y direction. The sample quantities consist of duration the MD simulation will run for, Δt , and N number of particles in the system.

$$C_{xy}(t) = \left\langle \sum_{x < y} P_{xy}(t) P_{xy}(0) \right\rangle \tag{6}$$

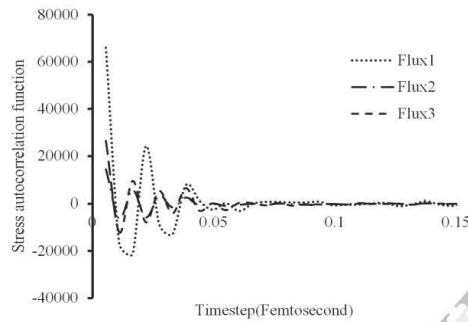


Fig.3 Stress autocorrelation function graphs for validation of achieved viscosity of CuO.NPs in water from MD simulation at 303k.

Further, the monotonic decay of the SACF relates to the successful achievement of rheological quantity i.e. viscosity in our case. The SACF took 0.07 fs to completely settle for 303k viscosity reading, whereas, for other two temperature readings of 313k and 323k took 0.07-0.09 fs.

1.5 Mean Square Displacement (MSD)

Diffusion coefficient was measured for analyzing the diffusion rate of the CuO in water using Equation4, where D is diffusion coefficient (m^2/s^2), r is the distance between consecutive particles and t is time (s).

The diffusion rate was calculated by the slope measurement of trend lines using one-sixth of the slope which gives the self-diffusion coefficient. The calculated MSD is shown in Fig. 4, by using the slope of these lines, the diffusion coefficient of CuO-NPs in water suspension at different temperatures of 303K, 313K and 323K was found. Table 2 lists particular diffusion coefficients of CuO-NP water suspension and pure water system. Later, Fig. 4 shows the CuO-NP water suspension MSD at different temperatures. The diffusion coefficient results obtained for this suspension model is similar with the result of CuO nano-rods diffusion coefficient in water by Cheong F.C et al. [47], they measured diffusion coefficient of CuO nano-rods with holographic video microscopy and obtained the value of $2.31E-7 m^2 s^{-1}$ at 298K. However, there is a slight difference, this can be due to temperature and heat conduction through the system that causes the Brownian effect to change and consequently altering the diffusion.

In Figure 4 there is a linear increase in the diffusion coefficient (m^2/s) of the water with temperature increase and this has been correlated by other studies of TIP3P water molecules [48]. This study investigated TIP3P water molecular diffusion coefficient at 320 K is $2.272E10^{-9} m^2/s$, which is in a good agreement with achieved value in this work as shown in table 2, together with other experimental value obtained from previous literature [49]. It is also known that by implementation of DPD helped in decreasing the computing time step for equilibrium convergence and higher accuracy [50].

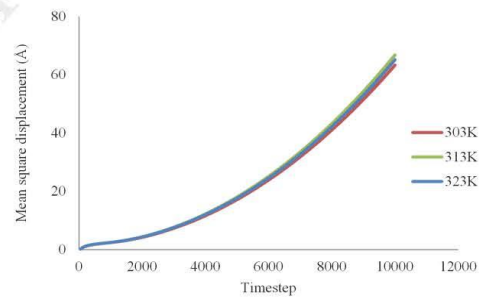


Fig.4 MSD of CuO nanoparticles in water suspension a)303K, b)313K, c)323k.

Table 2 Simulated diffusion coefficients of nanoCuO-water system and pure water system.

Temperature (K)	Diffusion Constant (m^2/s^2)	
	CuO-water system	Water system
303	1.033×10^{-8}	9.000×10^{-9}
313	1.150×10^{-8}	9.060×10^{-9}
323	1.051×10^{-8}	9.1066×10^{-9}

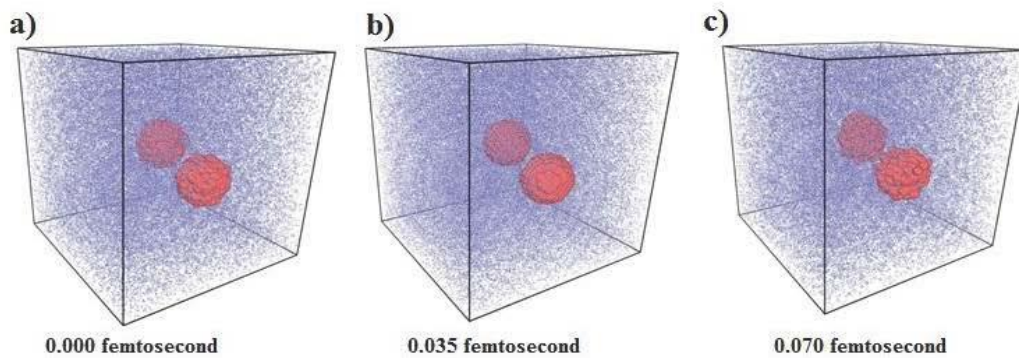


Fig.5 CuO-NPs water suspension system at 303K; 5a) 0.000 femtoseconds; 5b) 0.035 femtoseconds; and 5c) 0.070 femtoseconds.

Finally, the Fig.5 illustrates the simulation screen dumps of CuO water suspension at 303K. The Fig. 5a shows the screen dump at 0fs, the initial condition when simulation was just started, no atomic movement can be found. Later Fig. 5b demonstrates the simulation at an interval of 0.035fs. Here the simulation is approaching the equilibrium level of convergence as shown in Fig.3 of S.ACF. Further, Fig. 5c shows the simulation at final stage's or the time when the simulation has gained the equilibrium convergence. It can be seen in Fig. 5c that the nanoparticles structural shape has changed, this is due to the influence of hydrodynamic

boundary layer that forms around the nanoparticles while in a nanofluidic dispersion state. However, Brownian motion cannot be neglected here, since this influence on nanoparticles micro motions i.e. responsible for rotation and vibration of the particles in suspension.

The viscosity trends obtained through molecular dynamics simulation is in 4-6% contrast with experimental obtained values. The CuO-NPs simulated results of diffusion coefficient is found to be $1.033 \times 10^{-8} \text{ m}^2/\text{s}$ at 303K, this can be correlated with the data found from literature [47].

CONCLUSIONS

This study has demonstrated a simulative model prototype development, which can be used for different metal oxide nanoparticle's dispersion in aqueous fluid in terms of the viscosity and diffusion coefficients. Reproductions of self-diffusion constant of TIP3P water model in the system has been given to provide a comparative base for the system with CuO nanoparticles in diffusion interactions. However, concurrent trends and results have been achieved under the experimental and simulative conditions. It is investigated that the viscosity increment is dependent on

the volume fraction of particles rather than its size. It was seen that the molecular dynamic of 2% CuO nanoparticle suspension shows similar trend as 2% vol. of experimentally setup mechanism.

This study excavated the interactive dispersion mechanism of nanoparticles at molecular level in order to exploit the lab-based computersimulation capabilities towards the nanoparticles-water system in reflecting of some larger sized potential particles and multiple particle system for future considerations.

REFERENCES

- [1] M.I.a.H. Kamiya, Surface Modification for Improving the Stability of Nanoparticles in Liquid Media, KONA Powder and Particle Journal No.27 (2009).
- [2] T. Kida, T. Oka, M. Nagano, Y. Ishiwata, X.-G. Zheng, Synthesis and Application of Stable Copper Oxide Nanoparticle Suspensions for Nanoparticle Film Fabrication, Journal of the American Ceramic Society, 90 (2007) 107-110.
- [3] D.a.K.S.R. Anandan, Synthesis and stability of cupric oxide-based nanofluid A novel coolant for efficient cooling., Asian J. Sci. Res., 5: 218-227. (2012).
- [4] L. Fedele, L. Colla, S. Bobbo, S. Barison, F. Agresti, Experimental stability analysis of different water-based nanofluids, Nanoscale Research Letters, 6 (2011) 300.
- [5] I. Palabiyik, Z. Musina, S. Witharana, Y. Ding, Dispersion stability and thermal conductivity of propylene glycol-based nanofluids, J Nanopart Res, 13 (2011) 5049-5055.

- [6] G. Ren, D. Hu, E.W.C. Cheng, M.A. Vargas-Reus, P. Reip, R.P. Allaker, Characterisation of copper oxide nanoparticles for antimicrobial applications, *International Journal of Antimicrobial Agents*, 33 (2009) 587-590.
- [7] J.A. Mergos, M.D. Athanassopoulou, T.G. Argyropoulos, C.T. Dervos, Dielectric properties of nanopowder dispersions in paraffin oil, *Dielectrics and Electrical Insulation, IEEE Transactions on*, 19 (2012) 1502-1507.
- [8] S. Jesumathy, M. Udayakumar, S. Suresh, Experimental study of enhanced heat transfer by addition of CuO nanoparticle, *Heat Mass Transfer*, 48 (2012) 965-978.
- [9] A. Hernández Battez, R. González, J.L. Viesca, J.E. Fernández, J.M. Díaz Fernández, A. Machado, R. Chou, J. Riba, CuO, ZrO₂ and ZnO nanoparticles as antiwear additive in oil lubricants, *Wear*, 265 (2008) 422-428.
- [10] R.S.K. Shiram S. Sonawane, Kailas L. Wasewar and Ajit P. Rathod Dispersions of CuO Nanoparticles in Paraffin Prepared by Ultrasonication: A Potential Coolant 3rd International Conference on Biology, Environment and Chemistry, IPCBEE vol.46 (2012) © (2012) IACSIT Press, Singapore (2012).
- [11] Y.Y. Wu, W.C. Tsui, T.C. Liu, Experimental analysis of tribological properties of lubricating oils with nanoparticle additives, *Wear*, 262 (2007) 819-825.
- [12] Y. Yang, C. Zhang, Z. Hu, Impact of metallic and metal oxide nanoparticles on wastewater treatment and anaerobic digestion, *Environmental Science: Processes & Impacts*, 15 (2013) 39-48.
- [13] M.A.A. K. A. Al-Saad, D. T. Hadi, R. S. Arar, M. M. AL-Sulaiti, T. A. Abdulmalik, N. M. Alshamary, J. C. Kwak, Iron oxide nanoparticles: applicability for heavy metal removal from contaminated water, *Arab Journal of Nuclear Sciences and Applications*, 45 (2012) 335-346
- [14] V.D.N.M.S. K.L.P. Palanisamy, The utility of magnetic iron oxide nanoparticles stabilized by carrier oils in removal of heavy metals from waste water, *International Journal of Research in Applied, Natural and Social Sciences*, 1 (2013) 15-22.
- [15] M.A. Vargas-Reus, K. Memarzadeh, J. Huang, G.G. Ren, R.P. Allaker, Antimicrobial activity of nanoparticulate metal oxides against peri-implantitis pathogens, *International Journal of Antimicrobial Agents*, 40 (2012) 135-139.
- [16] M.A.V.-R. R.P. Allaker, Guogang Ren, Nanomaterials as antimicrobials, *Antimicrobial Polymers Book*, (2012).
- [17] D.J. Cooke, J.A. Elliott, Atomistic simulations of calcite nanoparticles and their interaction with water, *The Journal of Chemical Physics*, 127 (2007) 104706-104709.
- [18] V.V. HOANG, Diffusion in simulated SiO₂ nanoparticles, *Nano*, 02 (2007) 301-303.
- [19] M.H. Kowsari, S. Alavi, M. Ashrafzaadeh, B. Najafi, Molecular dynamics simulation of imidazolium-based ionic liquids. I. Dynamics and diffusion coefficient, *The Journal of Chemical Physics*, 129 (2008) 224508-224513.
- [20] P.J.H.a.J.M.V.A. Koelman, Simulating microscopic hydrodynamic phenomena with dissipative particle dynamics, *Europhys.Lett.*, 19:155-160, (1992).
- [21] J.M.V.A.K.a.P.J. Hoogerbrugge., Dynamic simulations of hard-sphere suspensions under steady shear, *Europhysics Letters*, 21(3):363-368. , (1993).
- [22] J.R. Spaeth, I.G. Kevrekidis, A.Z. Panagiotopoulos, A comparison of implicit- and explicit-solvent simulations of self-assembly in block copolymer and solute systems, *The Journal of Chemical Physics*, 134 (2011) 164902-164913.
- [23] V. Symeonidis, G. Em Karniadakis, B. Caswell, Dissipative Particle Dynamics Simulations of Polymer Chains: Scaling Laws and Shearing Response Compared to DNA Experiments, *Physical Review Letters*, 95 (2005) 076001.
- [24] L. Gao, J. Shillcock, R. Lipowsky, Improved dissipative particle dynamics simulations of lipid bilayers, *The Journal of Chemical Physics*, 126 (2007) 015101-015108.
- [25] S. Cheng, G.S. Grest, Structure and diffusion of nanoparticle monolayers floating at liquid/vapor interfaces: A molecular dynamics study, *The Journal of Chemical Physics*, 136 (2012) 214702.
- [26] S.W. Bunte, H. Sun, Molecular Modeling of Energetic Materials: The Parameterization and Validation of Nitrate Esters in the COMPASS Force Field, *The Journal of Physical Chemistry B*, 104 (2000) 2477-2489.
- [27] L. Zhao, L. Liu, H. Sun, Semi-ionic Model for Metal Oxides and Their Interfaces with Organic Molecules, *J Phys Chem C Nanomater Interfaces*, 111 (2007) 10610-10617.
- [28] H. Sun, COMPASS: An ab Initio Force-Field Optimized for Condensed-Phase Applications Overview with Details on Alkane and Benzene Compounds, *The Journal of Physical Chemistry B*, 102 (1998) 7338-7364.
- [29] H. Sun, P. Ren, J.R. Fried, The COMPASS force field: parameterization and validation for phosphazenes, Computational and Theoretical Polymer Science, 8 (1998) 229-246.
- [30] S. Plimpton, Fast Parallel Algorithms for Short-Range Molecular Dynamics, *J Comp Phys*, 117, 1-19, (1995).
- [31] S.J.P.a.A.P. Thompson, Computational Aspects of Many-body Potentials., *MRS Bulletin*, 37, 513-521. , (2012).
- [32] J.B.L. M. K. Petersen, S. J. Plimpton, G. S. Grest, P. J. in't Veld, P. R. Schunk, Mesoscale Hydrodynamics via Stochastic Rotation Dynamics: Comparison with Lennard-Jones Fluid, *J Chem Phys*, 132, 174106, (2010).
- [33] W.L. Jorgensen, J. Chandrasekhar, J.D. Madura, R.W. Impey, M.L. Klein, Comparison of simple potential functions for simulating liquid water, *The Journal of Chemical Physics*, 79 (1983) 926-935.
- [34] A. Stukowski, Visualization and analysis of atomistic simulation data with OVITO—the Open Visualization Tool, *Modelling and Simulation in Materials Science and Engineering*, 18 (2010) 015012.
- [35] C.T. Nguyen, F. Desgranges, G. Roy, N. Galanis, T. Maré, S. Boucher, H. Angue Mints, Temperature and particle-size dependent viscosity data for water-based nanofluids – Hysteresis phenomenon, *International Journal of Heat and Fluid Flow*, 28 (2007) 1492-1506.
- [36] Y. Wu, H.L. Tepper, G.A. Voth, Flexible simple point-charge water model with improved liquid-state properties, *The Journal of Chemical Physics*, 124 (2006) 024503-024512.
- [37] M.A. Gonzalez, J.L.F. Abascal, The shear viscosity of rigid water models, *The Journal of Chemical Physics*, 132 (2010) 096101-096102.
- [38] M.-y. Shen, K.F. Freed, Long Time Dynamics of Met-Enkephalin: Comparison of Explicit and Implicit Solvent Models, *Biophysical Journal*, 82 (2002) 1791-1808.
- [39] F.Y. Hajir Karimi, Mahmood Reza Rahimi, Correlation of Viscosity in Nanofluids using Genetic Algorithm-neural Network (GA-NN), *World Academy of Science, Engineering and Technology* 49 (2011).
- [40] R. Prasher, D. Song, J. Wang, P. Phelan, Measurements of nanofluid viscosity and its implications for thermal applications, *Applied Physics Letters*, 89 (2006) -.
- [41] J. Chevalier, O. Tillement, F. Ayela, Rheological properties of nanofluids flowing through microchannels, *Applied Physics Letters*, 91 (2007) 233103-233103-233103.
- [42] P.K. Namburu, D.P. Kulkarni, A. Dandekar, D.K. Das, Experimental investigation of viscosity and specific heat of silicon dioxide nanofluids, *Micro & Nano Letters, IET*, 2 (2007) 67-71.
- [43] M.J. Pastoriza-Gallego, C. Casanova, J.L. Legido, M.M. Piñeiro, CuO in water nanofluid: Influence of particle size and polydispersity on volumetric behaviour and viscosity, *Fluid Phase Equilibria*, 300 (2011) 188-196.
- [44] W.-Q. Lu, Q.-M. Fan, Study for the particle's scale effect on some thermophysical properties of nanofluids by a simplified molecular dynamics method, *Engineering Analysis with Boundary Elements*, 32 (2008) 282-289.
- [45] Y. He, Y. Jin, H. Chen, Y. Ding, D. Cang, H. Lu, Heat transfer and flow behaviour of aqueous suspensions of TiO₂ nanoparticles (nanofluids) flowing upward through a vertical pipe, *International Journal of Heat and Mass Transfer*, 50 (2007) 2272-2281.
- [46] C.T. Nguyen, F. Desgranges, N. Galanis, G. Roy, T. Maré, S. Boucher, H. Angue Mints, Viscosity data for Al₂O₃-water nanofluid—hysteresis: is heat transfer enhancement using nanofluids reliable?, *International Journal of Thermal Sciences*, 47 (2008) 103-111.
- [47] F.C.G. Cheong, David G., Rotational and translational diffusion of copper oxide nanorods measured with holographic video microscopy, *Opt. Express*, 18 (2010) 6555-6562.
- [48] O. Markovitch, N. Agmon, Reversible geminate recombination of hydrogen-bonded water molecule pair, *The Journal of Chemical Physics*, 129 (2008) 084505-084513.
- [49] W.K. D Eisenberg, The structure and properties of water, Clarendon Press, Oxford, (1969).
- [50] P. Español, P. Warren, Statistical Mechanics of Dissipative Particle Dynamics, *EPL (Europhysics Letters)*, 30 (1995) 191.

Abbreviation Table and their units

Symbols	Meanings
CuO	Copper Oxide
CuO-NP/s	Copper Oxide Nanoparticle/s
H ₂ O	Water
DPD	Discrete particle dynamics
MD	Molecular dynamics
BD	Brownian Dynamics
SPH	Smoothed Particle hydrodynamics
°K	Degree Kelvin (Temperature unit)
Å	Angstrom
mPa.s	Milli Pascal second (Viscosity unit)
m/s ²	Meter per second square (Diffusion coefficient unit)
COMPASS	Condensed-phase Optimized Molecular Potential for Atomistic Simulation studies
r_{ij}	i-j atomic separation distance.
\vec{f}	Total force
F ^c	Conservative force linked to momentum
F ^D	Dissipative force
F ^R	Random force
\hat{r}_{ij}	Force in particular directions
Δt	Timestep size
K_B	Boltzmann constant
T	Temperature
t	Timeperiod
F	Magnitude of Force
$\frac{\partial U}{\partial x}$	Velocity in x-direction
\dot{n}	Diffusion flux
D	Diffusion Coefficient
$\frac{\partial \phi}{\partial x}$	Molar concentration in x-direction
$r_i(t)$	radius of particle <i>i</i> at time t
$r_i(0)$	radius of particle <i>i</i> at starting time
C_v	SACF Function
P_{xy}	Stress tensor in x-y direction
LAMMPS	Large-scale Atomic/Molecular Massively Parallel Simulator
TIP3P	Transferable intermolecular potential 3P
TEM	Transmission Electron Microscope
μ	Viscosity
α, β, γ	Lattice parameters
MSD	Mean Square Displacement
SACF	Stress autocorrelationfunction

Appendix E – Published Study 2

The draft of paper, presenting simulation and experimental study of rheological properties of CeO₂ nanoparticles in water, which is published in International journal of nanoletters.

Simulation and experimental study of rheological properties of CeO₂-water nanofluid.

Adil Lova^{1*}, Jacqueline L. Stair², and Guogang Ren¹

¹Department of Engineering, University of Hertfordshire, Hatfield, UK

²Department of Pharmacy, University of Hertfordshire, Hatfield, UK

* a.lova2@herts.ac.uk

Abstract

Metaloxide nanoparticles offer great merits over controlling rheological, thermal, chemical and physical properties of solutions. The effectiveness of a nanoparticle to modify the properties of a fluid depends on its diffusive properties with respect to the fluid. In this study, rheological properties of aqueous fluids (i.e. water) were enhanced with the addition of CeO₂ nanoparticles. This study was characterized by the outcomes of simulation and experimental results of the nanofluids. The movement of nanoparticles in the fluidic media was simulated by a large-scale molecular thermal dynamic program (i.e. LAMMPS). The COMPASS force-field was employed with smoothed particle hydrodynamic potential (SPH) and discrete particle dynamics potential (DPD). However, this study develops the understanding of how the rheological properties are affected due to the addition of nanoparticles in a fluid and the way DPD and SPH can be used for accurately estimating the rheological properties with Brownian effect. The rheological results of the simulation were confirmed by the convergence of the stress autocorrelation function, whereas experimental properties were measured using a rheometer. These rheological values of simulation were obtained and agreed within 5 % of the experimental values, they were identified and treated with a number of iteration and experimental tests. The results show that the CeO₂ nanoparticle dispersion in water has a viscosity of 2.0 – 3.3 mPas.

Keywords: Metaloxide nanoparticles; CeO₂; LAMMPS; Rheology.

1. Introduction:

The thermophysical applications is creating opportunity for a wide use of nanoparticles in fluids. The use of the CeO₂ nanofluids for enhancing the thermophysical and rheological properties has shown importance in applications such as plate heat exchanger, fuel cells, tribology[1], heat transfer[2], coolant material[2], metal polishing, UV absorbent [3] and filters, etc. The dependencies on nanoparticles is increasing due to their characteristics of high surface area to volume ratio, size, and stability. Where different nanoclusters show diffusive and thermophysical enhancements[4-6], likewise, CeO₂ nanoclusters have capabilities of promoting different properties when dispersed in various fluids. It has been seen by researchers that CeO₂ nanoparticle stability in water is less[1], whereas, the stability can still be enhanced by the use of modifying agents.

By improving the dispersibility of CeO₂ nanoparticles with the surfactant Sorbitan monostearate in water, a contribution to friction reduction was shown [1, 7]. The application of this additive was able to reduce the friction coefficient of the water based lubricant effectively i.e. good for tribology applications. Later, wear scar depth observed with water based CeO₂ nanofluid presented less enhanced antiwear properties rather than the CeO₂ modified with Sorbitan

monostearate as investigated by Zhao et al. [7]. Later, ceria based water nanofluids showed improvements in convective heat transfer applications; this nanofluids is capable of enhancing the heat transfer coefficient to about 39-40% in a plate heat exchanger [2].

However, the CeO₂ simulations were carried to study the phase separation and particle aggregation as Conesa investigated the CeO₂ surface structural stability analysis simulations using molecular mechanics. Their simulation through molecular mechanics were 10% in contrast with experimental results for bulk modulus of CeO₂[8].

Moreover, the metal oxides nanoparticles of silica (SiO₂), ceria (CeO₂), and alumina (Al₂O₃) nanofluids at low concentrations with a particle size of 10 nm and 20 nm in pool boiling have been analyzed. When these particles do not deposit on the wire, the nanofluid with metal oxides suspension increases critical heat flux by about 50% irrespective of the type of the oxide particle and its size[9].

Furthermore, Baudin et al. discussed the structural energies and surface properties over different orientations of the CeO₂ by molecular dynamics using NPT ensemble[10-12].

Apart from nanofluid's simulations, all these simulations that are mostly related to the structural analysis of CeO₂ nanoparticle is beneficial and easily available. On the contrary the dispersion simulation of CeO₂ also holds a great importance, due to the use of this in many different fluidic applications.

This is why, due to the greater importance of this, we have initiated the investigation on the dispersion CeO₂ particles in water based nanofluids. However, in our study, we have discussed about the rheological properties and diffusive properties of nanoparticle in aqueous medium since the nanoparticles hold greater effect on altering the rheological regime of the solution. Moreover, we have solved analytically the full interactive system integrals to evaluate the viscosity through the Green-Kubo formula and compared it with the results of the experimental approximation. Furthermore, the viscosity of the CeO₂ nanoparticles in water system has not yet been known, since there is less research with respect to the viscosity calculation of this nanoparticle. There are other researches available for viscosity analysis of CuO nanoparticle[13, 14] and Al₂O₃ nanoparticles dispersed in water[15, 16]. Thereby, the necessity of this research can be understood from our previous statement, since in this research experimental results trend have been compared with the simulative achieved results.

2. Methodology:

CeO₂ nanoparticles of 10-40nm diameters and 99.9% purity (Shandong Yitong, China) were first dispersed in water by ultrasonication device for 3 minutes at 200 watts using Heilshcers US200 ultrasonicator . Later, the nanofluids viscosity was measured using a rheometer i.e. TA instrument 1500Ex. The measurement was taken from 293K -323K.

Moreover, simulations were performed on CeO₂ nanoparticles dispersed in TIP3P water using Large-scale Atomic/Molecular Massively Parallel Simulator (LAMMPS) [17]. CeO₂ nanoparticles was formed using Material studio from Accelrys Ltd UK. Later, both nanoparticle and water was introduced in one system. Charges on the atoms was assigned using COMPASS force field[18]. Moreover, two pairpotentials i.e. Discrete ParticleDynamics (DPD) and Smoothed Particle Hydrodynamics (SPH)[19] in hybrid style were used to execute the hydrodynamics and Brownian motion in the system. There were 40 CeO₂ nanoparticle of 1 nm in size, within 8000 TIP3P water molecular system as shown in Figure1. The first system consisted of around 10% volume fractions of particles. The second system consisted of 4 CeO₂ nanoparticle of 1 nm that hold approximately 1% of volume fractions. The system was equilibrated for three different temperature settings that were between 293- 323K.

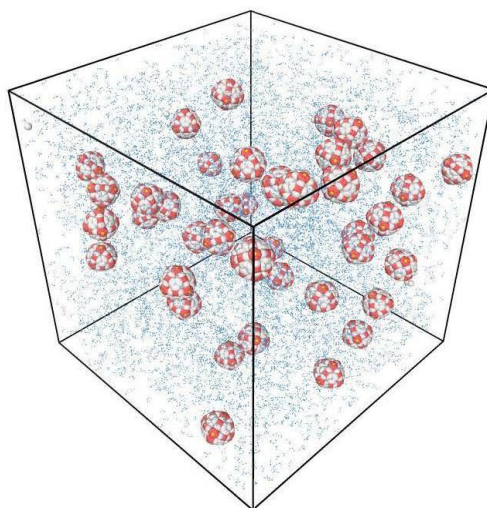


Figure 1. 40 CeO₂ (1nm) nanoparticles in 8000TIP3P water molecular system; blue coloured atoms are of TIP3P water and nanoparticles are in white and red colour..

3. Results:

The viscosity of CeO₂ nanoparticle dispersion was analysed by a TA 1500Ex instrument. The experimental viscosity trends were gathered and compared with the simulation obtained results. As the nanoparticles were similar in their volumetric concentrations, some probable trends were achieved and were compared. The data from the simulation were quantified for their accuracy by stress autocorrelation functions (SACF).

The time taken to simulate depends on the number of atoms in the system and the statistical analysis required to be performed. The correct selection of the timestep is necessary for computation. Since this correlates with the decaying of the SACF, it is necessary for the SACF to decay monotonically to analyse the real statistical observation of average viscosity. Therefore, the results of the viscosity achieved through simulation are convincing till the SACF decay monotonically to zero as shown in Figure 6, that was the case found with our simulation results as shown in Figure 2.

Furthermore, the analysis also used radial pair distribution functions. This function mathematically helps to determine the atomic pair distance between two consecutive atoms. This function is approached for agglomeration and dispersibility analysis.

3.1 Viscosity:

The experimental viscosity was calculated using a TA 1500Ex rheology instrument. The simulation viscosity calculation carried out in this study was done using the Green-Kubo method noted in equation 1. This method performs non equilibrium molecular dynamics. The results of the viscosity measured by experiment and simulation are presented in Figure 2.

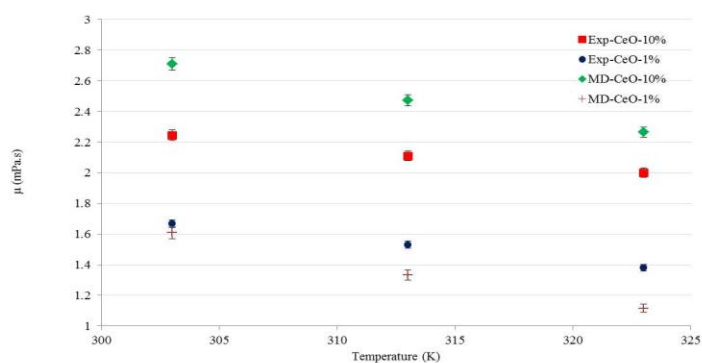


Figure 2. Measured viscosities of CeO₂ nanoparticles in water from temperatures 300-325K.

Nonequilibrium methods have become increasingly popular for calculating the viscosity of liquids. The application of nonequilibrium methods is often simplified by the concept of pressure fluctuation-based equilibrium methods as shown by equation 1, such as those using the Green-Kubo.

$$\eta = \frac{V}{3k_B T} \int_0^{\infty} \left\langle \sum_{x < y} P_{xy}(t) P_{xy}(0) \right\rangle dt \quad \text{Equation 1}$$

Molecular dynamics simulations were carried out to calculate the viscosity of the system by - Kubo formulation. The results of the viscosity of water with nanoparticles were in a good agreement with the results obtained from simulations, but the correlation function took a lot of time to converge and this problem is also shown in Figure 6.

Later, the Stress tensor is used to validate the accuracy of achieved viscosity reading by integrating the stress tensor with respect to time correlation as presented in section 4.3.

3.2 Diffusion coefficient

The diffusion coefficient was also calculated to analyse the system aggregation and viscous regime. However, the diffusion in the CeO-water system is due to the layering of nanoparticles with water molecules and nanoparticle-nanoparticle layering forming a stabilized system. Hydrodynamic layering also effects the diffusion, especially in our case, as we are using water, the effect of hydrodynamic layering can not be neglected. The TIP3P water self-diffusion coefficient is roughly 0.5-0.7E-9 m²/s as investigated [20]. This shows that the results which are achieved in this study are realistic[21, 22].The diffusion coefficient was calculated by Eq. 2 and are presented in Figure 3.

$$D = \frac{1}{6} d \langle (r_i(t) - r_i(0))^2 \rangle / dt \quad \text{Equation 2}$$

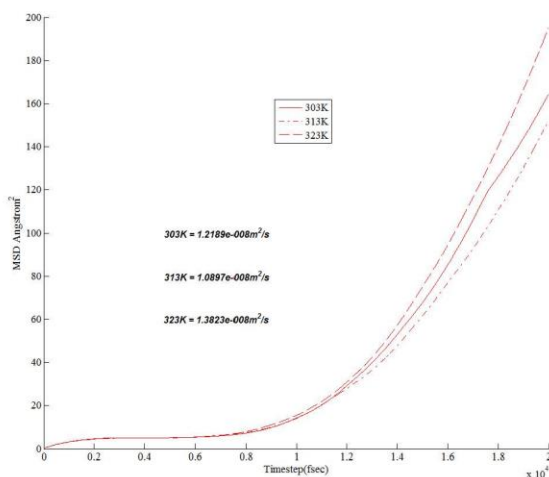


Figure 3. Diffusion graphs of CeO₂ nanoparticles in water for temperatures 300-325K.

4. Discussion

In the nanoparticle-water system, important factors that contribute towards the particle-particle interactions and changing the dispersibility of the system are diffusion coefficient and viscosity, that have been already discussed in the results section. Later, the viscosity achieved from the simulation can be further validated using the stress autocorrelation function. Whereas, radial distribution function has also been discussed to understand the aggregation nature of the CeO₂ nanoparticle system.

4.1 Radial Distribution Function

Radial distribution function, also known as the pair distribution function, are the essential link between macroscopic thermodynamic properties and intermolecular interactions of fluids and fluid mixtures. RDF theories were effective in describing the behavior of simple liquids and liquid mixtures. Ce atoms in water system show less aggregation as seen from Figure 4. At 0.3 – 0.4 nm a strong peak is observed due to the Ce-Ce interaction within the nanoparticle bond. Whereas, the peaks after 2 nm shows weak peaks with lower intensities, these peaks relate to the distance between Ce atom of one nanoparticle to another nanoparticle.

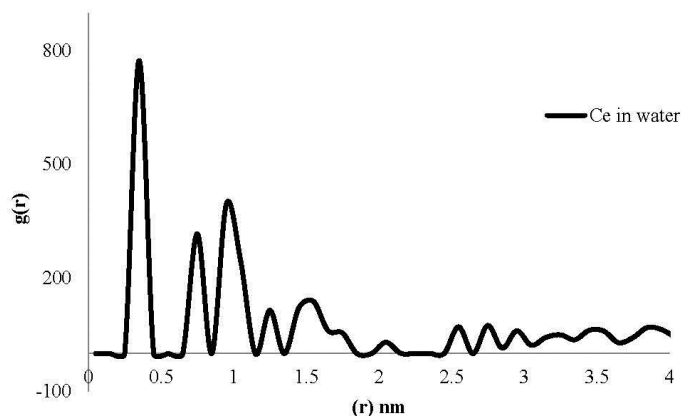


Figure 4. Radial distribution function of Ce in water.

Further, RDF is used for understanding the self-assembly (i.e. aggregation) of nanoparticles, that can be concerned as a fundamental question and this is also dependent on atom to atom shearing stress i.e. the viscosity of the system. In this way, the interactions involved in controlling the self-assembly and aggregation mechanism can be understood. However, the experimental determination of these forces still remains a challenging task. On the other hand, theoretical methodologies such as radial distribution function in MD can be used to help understand the atomic interactions.

4.2 Density:

Later, the density was analysed through MD simulation as shown in Figure 5 and compared with the experimental and theoretical density. The theoretical density was calculated using Eq. 3. Whereas experimental density was found to be around 1.02 kg/m^3 , theoretical density was calculated to be around 1.06 kg/m^3 . The difference between the theoretical and MD density is low. This shows that the system was properly configured.

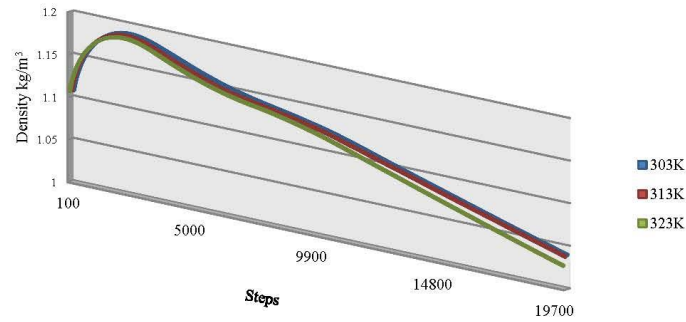


Figure 5. Density of CeO₂ nanoparticles in water from MD simulation.

$$\rho_{nf} = (1 - \varphi) \rho_f + \varphi \rho_p$$

Equation 3

4.3 Stress Autocorrelation Function

Validation of the measured viscosity is carried using the stress tensors. The stress tensor equation Eq. 4 [23] has three components for controlling the stress in a particular direction. This formulae can be used with molecular dynamics simulations. However, alternative formulations based on particle displacement require translational invariance, an assumption violated in MD simulations utilizing periodic boundary conditions. The summation within the angle brackets in Eq. 4 implies averaging of a ‘adequately large’ number of samples [24]. The specified term P_{xy} in Eq. 4 is the tensor for x-y direction, whereas, there are other independent terms of the shear viscosity that are used as off-diagonal components of the stress. These terms are P_{xz} and P_{yz} . To implement Eq.4, the optimal way is to use with specific quantities. These quantities include the duration of the MD simulation, Δt . Another quantity is the number of particles, N .

$$C_{xy}(t) = \left\langle \sum_{x < y} P_{xy}(t) P_{xy}(0) \right\rangle$$

Equation 4

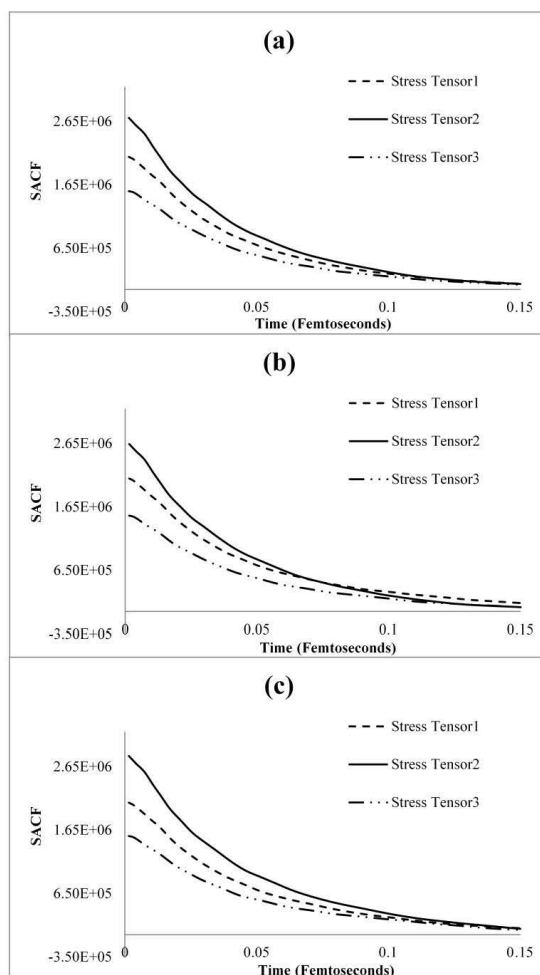


Figure 6. Stress autocorrelation function graphs for validation of achieved viscosity of CeO_2 nanoparticles in water from MD simulation; a) SACF for 303K, b) SACF for 313K and c) SACF for 323K.

The monotonic decay of stress autocorrelation function for the CeO₂-water nanoparticle system presented different timestep for various temperatures, i.e. for 303 K, the system decayed in 0.125 fs, whereas, for 313 K it decayed in 0.135 fs and 323K decayed in 0.15fs. Further the SACF showed that the decaying function relies on the viscosity validation. The viscosity validation is achieved when the SACF reaches a monotonic decaying trend.

5. Conclusion

In the present work, we have used the MD method to simulate nanoparticle dispersion at an atomistic level in aqueous solution. We have chosen the cerium oxide (CeO₂) nanoparticle as a model because this metal oxide has several important applications, such as fuel cell electrolyte, catalyst, polishing materials, insulators, gas sensor, and UV blockers. Although we have used a small size and number of nanoparticles, it shows advancement in the understanding of nanoparticles aggregation and dispersibility at atomic level. Moreover, this study is necessary for the development and to achieve initial parameters for further implementation on future simulations for various nanoparticles-fluid system.

References

1. Zhao, C., Y.K. Chen, and G. Ren, *A Study of Tribological Properties of Water-Based Ceria Nanofluids*. Tribology Transactions, 2013. **56**(2): p. 275-283.
2. Tiwari, A.K., P. Ghosh, and J. Sarkar, *Performance comparison of the plate heat exchanger using different nanofluids*. Experimental Thermal and Fluid Science, 2013. **49**(0): p. 141-151.
3. Ngoc Nhiem, D., et al., *UV absorption by cerium oxide nanoparticles/epoxy composite thin films*. Advances in Natural Sciences: Nanoscience and Nanotechnology, 2011. **2**(4): p. 045013.
4. Hernández Battez, A., et al., *CuO, ZrO₂ and ZnO nanoparticles as antiwear additive in oil lubricants*. Wear, 2008. **265**(3-4): p. 422-428.
5. Shriram S. Sonawane, R.S.K., Kailas L. Wasewar and Ajit P. Rathod *Dispersions of CuO Nanoparticles in Paraffin Prepared by Ultrasonication: A Potential Coolant* 3rd International Conference on Biology, Environment and Chemistry, 2012. **IPCBE vol.46 (2012) © (2012)IACSIT Press, Singapore**
6. Jesumathy, S., M. Udayakumar, and S. Suresh, *Experimental study of enhanced heat transfer by addition of CuO nanoparticle*. Heat and Mass Transfer, 2012. **48**(6): p. 965-978.
7. Zhao, C., et al., *The preparation and tribological properties of surface modified zinc borate ultrafine powder as a lubricant additive in liquid paraffin*. Tribology International, 2014. **70**(0): p. 155-164.
8. Conesa, J.C., *Computer modeling of surfaces and defects on cerium dioxide*. Surface Science, 1995. **339**(3): p. 337-352.
9. Milanova, D., et al. *Heat transfer behavior of oxide nanoparticles in pool boiling experiment*. 2006. ASME.
10. Gotte, A., K. Hermansson, and M. Baudin, *Molecular dynamics simulations of reduced CeO₂: bulk and surfaces*. Surface Science, 2004. **552**(1): p. 273-280.
11. Gotte, A., et al., *Molecular dynamics study of oxygen self-diffusion in reduced CeO₂*. Solid State Ionics, 2007. **178**(25): p. 1421-1427.
12. Herschend, B., M. Baudin, and K. Hermansson, *Oxygen vacancy formation for transient structures on the CeO (110) surface at 300 and 750 K*. The Journal of Chemical Physics, 2007. **126**: p. 234706.
13. Karimi, H., F. Yousefi, and M. Rahimi, *Correlation of viscosity in nanofluids using genetic algorithm-neural network (GA-NN)*. Heat and Mass Transfer, 2011. **47**(11): p. 1417-1425.
14. Nguyen, C.T., et al., *Temperature and particle-size dependent viscosity data for water-based nanofluids – Hysteresis phenomenon*. International Journal of Heat and Fluid Flow, 2007. **28**(6): p. 1492-1506.
15. Duan, F., D. Kwek, and A. Crivoi, *Viscosity affected by nanoparticle aggregation in Al₂O₃-water nanofluids*. Nanoscale Research Letters, 2011. **6**(1): p. 248.
16. Nguyen, C.T., et al., *Viscosity data for Al₂O₃-water nanofluid—hysteresis: is heat transfer enhancement using nanofluids reliable?* International Journal of Thermal Sciences, 2008. **47**(2): p. 103-111.
17. Plimpton, S., *Fast Parallel Algorithms for Short-Range Molecular Dynamics*. J Comp Phys, 117, 1-19, 1995.
18. Sun, H., *COMPASS: An ab Initio Force-Field Optimized for Condensed-Phase Applications Overview with Details on Alkane and Benzene Compounds*. The Journal of Physical Chemistry B, 1998. **102**(38): p. 7338-7364.
19. R.A. Gingold and J.J. Monaghan, *"Smoothed particle hydrodynamics: theory and application to non-spherical stars,"*. Mon. Not. R. Astron. Soc, 1977. **Vol 181, pp. 375–89**.

20. Mark, P. and L. Nilsson, *Structure and Dynamics of the TIP3P, SPC, and SPC/E Water Models at 298 K*. The Journal of Physical Chemistry A, 2001. **105**(43): p. 9954-9960.
21. Allen, M.P. and D.J. Tildesley, *Computer simulation of liquids*1989: Oxford University Press.
22. Alder, B.J., D.M. Gass, and T.E. Wainwright, *Studies in Molecular Dynamics. VIII. The Transport Coefficients for a Hard-Sphere Fluid*. The Journal of Chemical Physics, 1970. **53**(10): p. 3813-3826.
23. Kubo, R., *Statistical-Mechanical Theory of Irreversible Processes. I. General Theory and Simple Applications to Magnetic and Conduction Problems*. Journal of the Physical Society of Japan. **12**(Copyright (C) 1957 The Physical Society of Japan): p. 570.
24. Rapaport, D.C., *The Art of Molecular Dynamics Simulation*2004: Cambridge University Press.